A Study of Magnetic Helicity in Decaying and Forced 3D-MHD Turbulence

von

Shiva Kumar. Malapaka

geboren am 28.04.1977 in Secunderabad, Indien

ॐ शुक्लाम्बरधरम विष्णुम शशीवर्ण चर्तुभुजम
प्रसन्नवदनम ध्यायेत सर्वविघ्नोपशान्तये ||1

गुरुर्ब्रह्मः गुरुर्विष्णुः गुरुर्देवो महेश्वरः
गुरुरसाक्षात पर् ब्रह्मा तस्मै श्रीगुरवे नमः||2

सरस्वति नमस्तुभ्यं वरदे कामरूपिणी
विद्यारंभं करिष्यामि सिद्धीर्भवतु में सदा ||3

वागर्थाविव सम्प्रुक्तौ वागर्थप्रतिपत्तये
जगतः पितरौ वन्दे पार्वती परमेश्वरौ ||4

To
My Parents
Smt.Sathya Vani. Malapaka
Sri.Agasteshwara Rao. Malapaka
&
To my late Grand Father
Sri. Lakshmana Rao. Gorugantu

Abstract

This thesis presents a numerical study of a property of three dimensional magnetohydrodynamic (3D-MHD) turbulence, namely, inverse cascade (spectral transport from small scales to large scales) of magnetic helicity. Magnetic helicity is defined as the volume integral of the dot product of the magnetic field and the magnetic vector potential. It characterizes the linkage and twists of the magnetic field lines. The inverse cascade is believed to be one of the causes of large-scale magnetic structure formation in the universe.

This numerical studies is aimed at understanding how the inverse cascade of magnetic helicity effects other quantities of the turbulent flow. Two setups, namely, forced turbulence and decaying turbulence are studied. In the forced case, the numerical simulation setup consists of an initial energy distribution and a forcing localized in the small scales. The decaying setup consists of an initial energy distribution in the intermediate scales, which is allowed to decay naturally. The analysis of the results shows that several quantities in the turbulent flow, show self-similar behavior in their spectra, giving rise to power laws, which were hitherto unknown. Some of the quantities which are known to show power law behaviors exhibit different values to the power law exponents. These power law behaviors are analyzed together with the dimensional analysis of the eddy damped quasi normal Markovian (EDQNM) approximation equations, to attain a new relation which explains the evolution of large-scale magnetic structures in both the turbulent setups. The results are substantiated by the analysis of structure functions, probability density functions and correlation functions. Visualization of real space structures is also carried out. A mechanism to achieve large-scale magnetic structures from random small-scale magnetic fluctuations involving both the forced and decaying turbulences, is suggested.

Zusammenfassung

Das Ziel dieser Arbeit ist die Untersuchung des Einflusses der inversen Kaskade der magnetischen Helizität auf Größen der dreidimensionalen magnetohydrodynamischen Turbulenz. Die Untersuchungen stützen sich auf die Ergebnisse direkter numerischer Simulationen mit Auflösungen von bis zu 1024^3 Gitterpunkten. Ein bereits bestehender 3D-MHD Pseudospektralcode wird hierfür um die Möglichkeit eines kleinskaligen Turbulenzantriebs erweitert.

Zwei Fälle (bzw. Anordnungen) sind zu unterscheiden. Im ersten Fall basiert getriebene Turbulenz auf Anfangsbedingungen mit einer Konzentration der Energieverteilung und des Antriebs bei hohen Wellenzahlen ($k > 100$). Diese Bedingungen werden mit dieser Arbeit erstmals betrachtet. Vorausgegangene Untersuchungen waren sowohl durch kleinere Auflösungen als auch durch Lokalisierung des Antriebs und der Energieverteilungen bei moderaten Wellenzahlen ($k \leq 30$) beschränkt. Dieser erste Fall dient auch der Überprüfung des k^{-2} Potenzgesetzes der inversen Kaskade der magnetischen Helizität in dreidimensionaler MHD-Turbulenz, welches in numerischen Simulationen der EDQNM-Näherungen beobachtet wird.

Der zweite Fall beschäftigt sich mit der inversen Kaskade der magnetischen Heliziät in zerfallender Turbulenz. Hierbei werden die Anfangsbedingungen so gewählt, dass die Energieverteilung ein Maximum bei moderaten Wellenzahlen ($k = 70$) besitzt. In allen numerischen Simulationen wird zusätzlich Hyperviskosität verwendet. Dadurch soll gewährleistet werden, dass die Skalen des Inertialgebiets und des Dissipationsgebiets möglichst weit voneinander getrennt werden. Der numerische Kniff der Hyperviskosität bringt allerdings Nachteile mit sich. Zum einen zeigen die Energiespektren ein ausgeprägtes Flaschenhals-Phänomen ("bottle-neck"-Effekt), zum anderen macht es die Verwendung der Hyperviskosität unmöglich, dem System eine eindeutige Reynoldszahl, zuzuordnen.

Anhand der numerischen Ergebnisse wird der Einfluss der inversen Kaskade der magnetischen Helizität auf die spektralen Eigenschaften einiger Größen der MHD Turbu-

lenz berichtet. Durch den Antrieb bei relativen hohen Wellenzahlen bilden sich zwei getrennte Bereiche mit ungefährem Skalierungsverhalten aus (Ein Skalierungsbereich wird dann zu einem Inertialgebiet, wenn entsprechende Größe einen konstanten Fluss aufweist). Ein Skalierungsbereich zeigt sich bei kleinen Wellenzahlen (zwischen 7 und 40). Im Fall zerfallender Turbulenz tritt ein Inertialgebiet bei kleinen Wellenzahlen auf. Das Inertialgebiet bei kleinen Wellenzahlen zeigt in beiden Fällen das bekannte $k^{-5/3}$ Potenzgesetz des Energiespektrums. Im Falle getriebener Turbulenz wird das Spektrum bei hohen Wellenzahlen vom Flaschenhalsphänomen überlagert. Über den gesamten Wellenzahlenbereich ist die magnetische Energie größer als die entsprechende kinetische Energie. Die beobachteten Potenzgesetze der Helizität stimmen nicht mit den Vorhersagen durch die EDQNM Simulationen überein. Die magnetische Helizität weist stattdessen mehrere neue Intertialgebiets-Potenzgesetze auf. Auch einige andere Größen zeigen bisher nicht beobachtete Skalierungsgesetze im Inertialgebiet niedriger Wellenzahlen in beiden Fälle. Hierbei ist zu erwähnen, dass nicht alle Größen, die ein Potenzgesetz aufzeigen, auch ideale Invariante der 3D-MHD Tubulenz sind. Das Potenzgesetz-Verhalten von vier der Größen wird zusammen mit der Dimensionsanalyse der EDQNM-Gleichungen untersucht. Dies führt zu einen neuen Zusammenhang zwischen den vier Größen. Dies betrifft die magnetische Helizität (H_k^M), die magnitsche Energie (E_k^M), die kinetische Helizität (H_k^V) und die kinetische Energie (E_k^V). Der sich ergebende Zusammenhang lautet: $E_k^M \sim k^2 \frac{H_k^M E_k^V}{H_k^V}$. Dieser Zusammenhang zeigt sich in allen Intertialgebieten der beiden Fälle. Die Relation impliziert, dass es über den gesamten spektralen Berich zu nichtlinearen Modeninteraktionen zwischen dem Geschwindikeitsfeld ($\mathbf{v}$) und dem Magnetfeld ($\mathbf{b}$) kommt, welche sich für die inverse Kaskade der magnetischen Helizität verantwortlich zeigen, und hierdurch den Anstieg der magnetischen Energie bewirken. Der bereits bekannte Zusammenhang zwischen der Gesamtenergie und der Residualenergie ist in beiden Inertialgebieten und in beiden Fälle ebenfalls bestätigt. Die beobachteten Skalierungsgesetze der anderen Größen entsprechen keiner Vorhersage aus Dimensionsanalyse oder Phänomenologie. Diese Potenzgesetze können wahrscheinlich nur im Rahemen einer neuen mathematischen Beschreibung verstanden werden.

Als nächstes wird der Einfluss der inversen Kaskade der magentischen Helizität auf die räumlichen Strukturen des Magnetfelds untersucht. Zunächst kann gezeigt werden, dass ein Antrieb bei hohen Wellenzahlen die Ausbildung von großskaligen räumlichen Strukturen nicht unterstützt. Es wird im Gegenteil beobachtet, dass eben dieser Antrieb bei hohen Wellenzahlen die sich bildenden großskaligen Strukturen zerstört.

Im Ortsraum werden die großskaligen Strukturen von den kleinskaligen Strukturen überlagert. Daher wird ein Tiefpassfilter mit Abschneidewellenzahl $k = 70$ verwendet, um die kleinskaligen Strukturen auszublenden. Zur Analyse der großskaligen Strukturen werden zunächst die Strukturfunktionen herangezogen. Des weiteren wird hierzu die erweiterte Selbstähnlichkeit (extended self similarity, ESS) und das Log-Poisson-Intermittenzmodell der Skalierungsexponenten der Strukturfunktionskurven genutzt. Durch die Analyse der Strukturfunktionen und die Modellierung der Intermittenz der gefilterten Ausgabe des getriebenen Falls wird hervorgehoben, dass die sich bildenden magnetischen Strukturen nicht ein- oder zweidimensional, sondern fraktaler Dimension sind. Wendet man diese Analyse auf den zerfallenden Fall an, so zeigen sich hier zweidimensionale Strukturen. Da eines der Hauptaugenmerke dieser Arbeit die Bildung großskaliger Strukturen ist, wird hierfür ein neues Vorgehen gewählt. Der Antrieb wird hierin zu drei unterschiedlichen Zeitpunkten ausgesetzt und der damit eintretende Zerfall der Turbulenz beobachtet. Die Strukturen treten so deutlicher hervor. Die Wahrscheinlichkeitsdichtefunktionen (PDFs) und Strukturfunktionen wurden auch in dieser Anordnung ausgewertet. Diese weisen auf den intermitttenten Charakter des Magnetfelds und des Geschwindigkeitsfelds hin. Die Form der Exponenten der Strukturfunktionskurven und der Wahrscheinlichkeitsdichtefunktionen weist darauf hin, dass im getriebenen Fall nichtzusammenhängende Substrukturen das System dominieren. Im zerfallenden Fall dominieren hingegen die zusammenhängenden Strukturen. In dieser speziellen Anordung kann demnach die Entwicklung von dominanten Substrukturen zu zusammenhängenden Strukturen untersucht werden. In allen drei Fällen bzw. Anordnungen zeigen sich zunehmende Korrelationslängen für viele der beobachteten Größen. Dies ist ein Hinweis auf die Ausbildung großskaliger Strukturen im Verlauf der Simulationen.

Die Strukturen im Ortsraum werden mit Softwarepaketen wie AMIRA und Visit visualisiert. Diese Visualisierungen belegen und bekräftigen die Resultate aus der Analyse der Strukturfunktionen. Im angetriebenden Fall sind die Flächen gleicher Magnetfeldstärke weder ein- noch zweidimensional. Der Charakter der fraktalen Dimension, welcher sich bereits in der Analyse der Strukturfunktionen zeigt, kann hiermit bestätigt werden. Es zeigt sich zudem eine große Anzahl von Magnetfeldkonzentrationen ohne definierter Ausbildung von Struktur. Dies weist auf die Auswirkungen des Antriebs bei hohen Wellenzahlen hin. Im Fall der zerfallenden Turbulenz bilden sich mit der Zeit großskalige Strukturen des Magnetfelds aus. Während die Turbulenz zerfällt nimmt die Intensität dieser Strukturen ab und die Ausdehnung der Strukturen nimmt zu.

Bei Aussetzung des Antriebs hängt die Ausdehnung und Entwicklung der Magnetfeld-
strukturen vom gewählten Zeitpunkt der Abschaltung des Antriebs ab. Da in dieser
Anordung drei verschiedene Zeitpunkte für das Abschalten untersucht wurden, zeigen
sich einmal großskalige Strukturen (bei Ausschalten des Antriebs zu einem späten Zeit-
punkt), einmal mittelgroße (bei Abschalten des Antriebs zu einem mittleren Zeitpunkt)
und einmal kleinskalige Strukturen des Magnetfelds (bei Abschalten des Antriebs nach
kurzer Zeit). Gemeinsam ist den drei Fällen der Anordnung mit der Aussetzung des
Antriebs und dem zerfallenden Fall die Anwesenheit von Regionen magnetischer Re-
konnektion. Die Anzahl dieser Rekonnektionsgebiete ist dann hoch, wenn viele kleine
magnetische Strukturen vorliegen. Deutlich weniger Rekonnektionsgebiete zeigen sich
hingegen bei großen und wenigen magnetischen Strukturen.

Zusammenfassend kann der Einfluss der inversen Kaskade der magnetischen Helizi-
tät wie folgt beurteilt werden: Es zeigen sich Potenzgesetze bei einigen Observablen
der MHD Turbulenz, insbesondere auch bei Größen, die keine Invarianten der MHD
Turbulenz sind. Eine neue Relation, welche sich auf die EDQNM-Theorie stützt, lie-
fert eine Erklärung für das Zusammenspiel maßgeblicher Größen bei der Ausbildung
großskaliger Magnetfeldstrukturen. Des weiteren zeigt sich, dass der Antrieb bei hohen
Wellenzahlen die großskaligen Magnetfeldstrukturen zertört. Der Zerfall der Turbulenz
und die magnetische Rekonnektion sind wichtige Einflussfaktoren auf die Ausbildung
von Magnetfeldstrukturen.

Contents

Introduction

Turbulence is a constantly encountered natural phenomenon. Fluids, when set into intense motion tend to develop turbulence. The turbulent structures formed in the flow are called eddies. These eddies span length scales of kilometers down to a few centimeters as in oceanic and atmospheric turbulences. Electrically conducting fluids in addition to the turbulent motions are associated with magnetic field fluctuations. Turbulence in conducting fluids is not normally felt in day-to-day life. Reversed-field pinch fusion experiments and dynamo experiments using liquid metals are some of the places where this specific type of turbulence is seen in laboratories. In common life, the chance of encountering this turbulence is almost zero. But plasma i.e. ionized gas, the most natural electrically conducting fluid, contributing to almost 99% of the visible material in the universe, shows this type of turbulent motions. Hence turbulent motions seen in Sun or stars, interstellar media (ISM), planetary cores and the intergalactic medium (IGM) are some of the examples where turbulence is seen in plasma. Here, the size of turbulent structures at the higher end span many light years as in ISM or IGM, while on the lower end they might be of kilometer size or even less, as in sub-structure of the plasma in stars or cores of planets.

The physical properties of plasma are studied from various aspects. In principle two approaches stand out, the particle approach and the fluid approach. In the former, the plasma is treated as the collection of individual particles and statistical methods are applied to understand the behavior of the systems. In the fluid approach, the plasma is studied using single fluid or multi fluid approximations. In the context of this work, single fluid approximation is used for simplicity.

The branch of fluid dynamics which deals with electrically conducting fluids is called magnetohydrodynamics (MHD). The equation set for studying MHD principally consists of three equations. The first equation looks similar to hydro-dynamical Navier-Stokes equation, with an additional term specifying the interactions of velocity field and the associated magnetic field. Second is the induction equation which signifies that

the magnetic field lines are anchored to the plasma. Finally there is the solenoidality condition for the magnetic field. This equation set is called MHD equations and they have to be simultaneously solved to get an understanding of MHD flows. The equation set is nonlinear and in general can not be solved analytically. It is characterized by two non-dimensional parameters, the magnetic and kinetic Reynolds numbers. The value of the Reynolds numbers gives an idea of the type of flow. There exists a critical Reynolds number beyond which the flow is termed as turbulent. Reynolds numbers also determine the smallest possible scales in the flow. The larger the value of Reynolds number, the greater is the range of scales in the flow. Turbulence is characterized by a broad range of spatial scales, extending down to very small eddies, if the Reynolds number is large [1]. The Reynolds numbers associated with astrophysical system are of the order of 10^{12} to 10^{20}. In the laboratory experiments the Reynolds numbers achieved are of the order of 10^6 [2].

Their exist some phenomenological models to Navier-Stokes and MHD equations, which enable in enhancing the understanding of turbulent flows. These models assume different mechanisms through which the structures in the fields act and build-up or destroy turbulence. The Kolmogorov phenomenology (K41) is based on interaction of eddies of several sizes. Under the influence of some energy input, the larger sized eddies break into smaller and smaller sized ones and ultimately dissipate completely. In this setup their exists a range of spatial scales, where the system exhibits self-similar behavior and is independent of either the energy input or the dissipation. This particular range over which such a behavior is seen is called 'inertial range'. Here the energy spectrum of the flow shows a power law behavior of $k^{-5/3}$. This phenomenology is valid for the hydrodynamic case. For the magnetohydrodynamic case, two other phenomenologies, namely, Iroshnikov-Kraichnan (IK) and Goldreich-Sridhar (GS) are prominent. In IK phenomenology, the main interaction mechanism is through Alfvén waves propagating along the magnetic field. Here a power law behavior of $k^{-3/2}$ is predicted for the total energy. However this does not account for the anisotropic nature of the MHD flows due to the presence of mean magnetic fields. The Goldreich-Sridhar phenomenology takes into account this anisotropy and through a principle called 'critical balance', predicts two power laws one for the turbulent fluctuations traveling parallel to magnetic field and other for the ones moving perpendicular to it. Some new modifications have been put-in, in recent times to refine IK and GS phenomenologies.

There are several methods of solving the MHD equations approximately. The eddy damped quasi normal Markovian (EDQNM) approximation, large eddy simulations

and direct numerical simulations (DNS) are some of the methods. The aim of these methods is to get a solution which closely resembles the systems in nature. However, the Reynolds numbers mentioned above are not achievable numerically, with the current best computing facilities. Nevertheless with the available supercomputing facilities, Reynolds number of the order of 10^3 in MHD turbulence and $\sim 10^4$ in case of hydrodynamic turbulence, have been regularly attained. The results from these methods, although, far from what is seen in nature, in terms of Reynolds numbers, do give insights into the physical aspects of the turbulent flows. Of these methods, DNS suffers from the least amount of errors as they do not use any approximations to the equations, but solve them as they are, using some simple physical assumptions. The methods mentioned here are also used to verify the power law behaviors predicted by the different phenomenologies.

Magnetic helicity, which represents the linkage and twist of field lines in the turbulent flows, was first reported by K.Moffatt in 1969 [3]. It is defined as the volume integral of the dot product of the magnetic field and its vector potential, for the volume under consideration. It was also realized that in an ideal three dimensional flow (i.e. flow with no dissipative effects), this quantity is an invariant. This invariance property is useful in plasma fusion research, specifically in the reversed field pinch (RFP) devices. In RFP devices, it has been shown that because of the invariance property of magnetic helicity, the magnetic field changes its topology and relaxes into a characteristic state. These relaxation phenomena are a fundamental process determining both the formation and sustainment of the so called RFP magnetic distribution as well as plasma particle and energy confinement [4].

Pouquet et al. in 1975 [5], showed that magnetic helicity exhibits an inverse cascade (spectral transfer from small scales to large scales) in 3D-MHD turbulence, similar to the kinetic energy inverse cascade predicted by Kraichnan in 1967 [6] for 2D-hydrodynamic turbulence. A year later, through the numerical simulations of EDQNM equations of forced 3D-MHD turbulence, for the first time the inverse cascade was clearly shown in the spectra of magnetic helicity [7]. A mechanism for this inverse cascade; different from the kinetic energy inverse cascade mechanism in 2D-hydrodynamic turbulence; was also suggested. It was also shown that the spectrum has an inertial range, which shows a power law behavior of k^{-2}. It was reported that this inverse cascade of magnetic helicity results in large-scale magnetic structure formation [7]. Several low to moderate resolution direct numerical simulations have been performed to verify the inverse cascade. But in all the previous DNS trials, the initial scales were

not sufficiently small and the forcing scale was also in small to moderate wavenumber region (k=3 to 30) [8, 9, 10, 11]. Hence the number of Fourier modes through which the inverse cascade was progressing were only a few. Apart from the forced 3D-MHD turbulence, there are reports on numerical studies of decaying 3D-MHD turbulence (i.e. turbulence without any forcing) [12, 13, 14], but in these works the inverse cascade of magnetic helicity was not studied.

In order to see a spectral transfer from extremely small scales in the forced turbulence and to verify or confirm the k^{-2} spectral law for magnetic helicity in that case and to study the inverse cascade of magnetic helicity in decaying turbulence, this thesis work was initiated. Also the problem of large-scale magnetic structure formation, which was paid less attention to in previous works, is taken up here. To understand the influence of the inverse cascade of magnetic helicity on various other quantities of turbulent flow and to find out mechanism(s) for large-scale magnetic structure formation(s), form the main motivations of this work. For this purpose high resolution DNS of 3D-MHD equations, for both forced and decaying turbulence cases, are performed using a pseudo-spectral MHD code and the results are discussed.

For this, the work is divided into five chapters. In the first chapter, the basic equations and properties of MHD turbulence are described. Important assumptions needed for the simplification of the equations are mentioned. The mathematical background of some of the important properties of magnetic helicity like invariance and inverse cascade is established. In the second chapter, the numerical setup which includes the exact process of generating the initial conditions and the forcing mechanism is described. Hyperviscosity is also introduced into the simulation setup. The two cases that will be studied i.e. decaying turbulence and forced turbulence are explained.

In the third chapter phenomenologies explaining the spectral and spatial properties for hydrodynamical turbulence and 3D-MHD turbulence, are summarized. As already mentioned, these phenomenological concepts explain the properties of turbulence with the help of some simple power laws. These power laws play an important role in understanding the properties of 3D-MHD turbulence. Also included in this chapter is a brief introduction and discussion of EDQNM concepts. These phenomenologies and EDQNM form the theoretical basis for the results obtained in the next two chapters. The spectral properties of 3D-MHD turbulence under the influence of the inverse cascade of magnetic helicity, are studied in the fourth chapter. The fifth chapter, reports the spatial properties of 3D-MHD turbulence under the same influence. From the results of these two chapters, a plausible explanation for large-scale structure formation

in some celestial bodies like planets and ISM is given. In the end a summary of the work, which includes suggestions for further studies is provided.

Chapter 1

3D-MHD Turbulence and Magnetic Helicity

In this chapter first the basic concepts of turbulence and magnetohydrodynamic (MHD) turbulence and their salient properties and features are introduced. Next the concept of magnetic helicity is defined and its important properties: invariance in ideal 3D-MHD, inverse cascade and their importance in nature, are discussed.

1.1   Turbulence and MHD

Turbulence is a phenomenon seen in nature and is generally associated with fluids. It can be described as a disorderly state of a physical system both in space and time. A flow is said to be turbulent if it is able to mix transported quantities much more rapidly than if only molecular diffusion processes were involved. More formally, following Lesieur [15], a flow is turbulent if:

- it is unpredictable in the sense that a small uncertainty as to its knowledge at a given initial time, will amplify, so as to render *impossible* a precise *deterministic prediction* of its evolution i.e. highly nonlinear in time,

- it satisfies the increased mixing property and

- it involves a wide range of spatial scales i.e. nonlinear in space.

Turbulent flows may possess different dynamics depending on their spatial dimensionality and may exhibit well-organized structures or otherwise [15]. Atmospheric or ocean currents, planetary cores, magnetospheres of planets, interiors of stars, interplanetary media, interstellar media and galaxies are some of the systems where turbulence is seen

over large-scale ranges [15, 1]. Turbulent flows also arise in aeronautics, hydraulics, nuclear and chemical engineering; in this context they are much smaller in scale relative to the settings mentioned earlier. Turbulence is often studied in physical systems mainly to understand its appearance so that an attempt is made to avoid it, where its emergence causes unwanted phenomenon and some times even destruction. But there are many technical applications, where its mixing properties are desirable [15].

Turbulence is extensively studied in plasma(s): a macroscopically electrically neutral substance containing many interacting free electrons and ions which exhibit collective behavior due to long range Coulomb forces. Plasmas are abundant in extraterrestrial world with close to 99% of the visible matter believed to be in this state. Plasma properties can be accurately described by particle distribution functions in phase space. The spatial and temporal evolution of these distribution functions are governed by the Boltzmann-Maxwell equations, which are partial differtial equations in 7-dimensional space [16]. This set of complicated equations are difficult to solve, although they describe the microscopic and macroscopic properties of the plasma very well. In many cases, the interest lies in understanding the macroscopic quantities like density, temperature and pressure to name a few, and their time and space evolutions [16]. A simpler approach can be taken that can give almost the same amount of information on macroscopic properties. In this simple approach these macroscopic quantities are obtained as moments of distribution functions. It is simpler to investigate their evolution than that of the full distribution function, owing to the number of dimensions that are to be dealt with. The macroscopic moments are quantities that have been studied in fluid and gas dynamics, and fall into the realm of fluid theory [16]. Thus plasma is studied as a fluid. Since material in the plasma is electrically conducting, it exhibits electromagnetic properties too. Thus, turbulence in plasma is more complicated than in normal fluids as both electromagnetic and fluid dynamic influences on its evolution have to be understood simultaneously. Magnetohydrodynamics (MHD) is one of the important tools used for the studies of plasma turbulence and thus the name MHD turbulence. It is believed that the large-scale magnetic structures and magnetic fields associated with celestial bodies can often be understood as a consequence of MHD turbulence and its properties. The primary interest of this study is to understand some of the important properties of MHD turbulence. In the following part of the section, the equations used in studying these properties are introduced.

1.1.1 MHD Equations

Plasma, as already stated, is matter in an ionized state, thus contains both positively and negatively charged ions typically kept apart by the high average energies they possess. But the size of the dynamical regions and associated time scales of interest for studying turbulence are huge in comparison to the effective mean free paths and frequencies associated with these plasma particles. For example, the convective motions in the solar convection zone have length scales of 10^3 to 10^7 m, whereas the Debye length of solar plasma is only 10^{-4}m. The time scales for the convective motions are of the order of 10^2 to 10^3 s, while the gyro motion time scale in solar plasma is of the order of 10^{-10} s [17]. For simplicity, plasma is assumed to be consisting of singly charged ions and electrons only. Further, since the turbulent motions occur on larger time scales when compared to the short collisional time scales among these species, the ions and electrons can be assumed to be strongly coupled, forming one single electrically conducting fluid (see [17, 18] and the references there of). MHD turbulence comprises of dynamics of many interacting degrees of freedom and thus, this relatively simple single fluid description of MHD would form a good starting point. Additional properties like gravity, radiation, rotation, convection etc. are neglected in this work as the emphasis is on understanding an inherent property of the MHD turbulence: magnetic helicity (introduced in the next section). For additional simplicity the mass density ρ of the plasma or magnetofluid is assumed to be a constant, ($\rho = \rho_0 = 1$) in time and spatially uniform. Note that as ρ is set to unity, it will not be mentioned further in the equations below. Relativistic effects are neglected and fluid velocities are assumed to be significantly smaller than the magnetosonic speeds in the plasma (see [18]). The flow is thus incompressible [19]. With this condition the continuity equation

$$\frac{d\rho}{dt} + \rho \nabla \cdot \mathbf{v} = 0 \tag{1.1}$$

imposes a solenoidality constraint on the velocity field $\mathbf{v}$, $\nabla \cdot \mathbf{v} = 0$. With these assumptions in place and using the conservation laws of momentum and electrical charge in combination with Maxwell's equations, the MHD equations can be derived and are stated below in Gaussian units (see [1, 16]).

$$\nabla \cdot \mathbf{v} = 0 \tag{1.2}$$

$$\partial_t \mathbf{v} + (\mathbf{v} \cdot \nabla)\mathbf{v} = -\nabla p - \frac{1}{4\pi}\mathbf{b} \times (\nabla \times \mathbf{b}) + \mu \mathbf{\Delta v} \tag{1.3}$$

$$\nabla \cdot \mathbf{b} = 0 \tag{1.4}$$

$$\partial_t \mathbf{b} = \nabla \times (\mathbf{v} \times \mathbf{b}) + \eta \mathbf{\Delta b} \tag{1.5}$$

Here $\mathbf{b}$ is the magnetic field, p is the thermodynamic pressure, μ is the kinematic viscosity and η is the magnetic diffusivity of the fluid. The pressure p is not an independent variable as incompressibility condition holds in the system [20, 17]. It is calculated through the divergence of the equation (1.3):

$$\mathbf{\Delta} p = \nabla \cdot [-(\mathbf{v} \cdot \nabla)\mathbf{v} + \frac{1}{4\pi}\mathbf{b} \times (\nabla \times \mathbf{b})]. \tag{1.6}$$

Here it is advantageous to work with non-dimensional form of the above set of equations. So a series of mathematical operations are performed to make them non-dimensional.

The mean magnetic field is assumed to be zero [20, 17]. The pressure term is eliminated altogether, from the equations by writing the equation (1.3) in terms of vorticity i.e. $\boldsymbol{\omega} = \nabla \times \mathbf{v}$. The quantities are written in non-dimensional form, in terms of the characteristic length scale L_0 and velocity V_0 of the configuration under consideration as:

$$\mathbf{r}' \equiv \frac{\mathbf{r}}{L_0}, \quad \mathbf{v}' \equiv \frac{\mathbf{v}}{V_0}, \quad t' \equiv \frac{V_0}{L_0}t, \quad \mathbf{b}' \equiv \frac{\mathbf{b}}{\sqrt{4\pi}\,V_0} \qquad \text{and} \qquad p' \equiv \frac{p}{V_0^2} \quad . \tag{1.7}$$

With these two operations the set of equations (1.2)- (1.5) now becomes:

$$\partial_t \boldsymbol{\omega} - \nabla \times (\mathbf{v} \times \boldsymbol{\omega} + S_B \mathbf{j} \times \mathbf{b}) = Re^{-1}\mathbf{\Delta}\boldsymbol{\omega} \tag{1.8}$$

$$\partial_t \mathbf{b} = \nabla \times (\mathbf{v} \times \mathbf{b}) + Rm^{-1}\mathbf{\Delta b} \tag{1.9}$$

$$\boldsymbol{\omega} = \nabla \times \mathbf{v} \tag{1.10}$$

$$\mathbf{j} = \nabla \times \mathbf{b} \tag{1.11}$$

$$\nabla \cdot \mathbf{v} = \nabla \cdot \mathbf{b} = 0. \tag{1.12}$$

Note that the quantities are now written without their respective primes (i.e. $\mathbf{v}'$ as $\mathbf{v}$ and so on) and this notation is continued for the rest of the work. The above set contains three dimensionless parameters S_B, Re and Rm which characterize the system. S_B is defined as $S_B = \frac{V_A^2}{V_0^2}$ where V_A is characteristic Alfvén velocity (the phase velocity of Alfvén wave, given by $\frac{\mathbf{b}}{\sqrt{4\pi}V_0}$ [1, 18]). This parameter determines the relative dynamical importance of velocity compared to magnetic field and is set to unity for the rest of the work. This means the magnetic field is measured in units of the characteristic Alfvén velocity. Re and Rm are related to the dissipation coefficients μ and η through the characteristic length L_0 and velocity V_0 as

$$Re = \frac{L_0 V_0}{\mu} = \hat{\mu}^{-1}, Rm = \frac{L_0 V_0}{\eta} = \hat{\eta}^{-1} \tag{1.13}$$

and are called kinetic Reynolds number and magnetic Reynolds number respectively. These Reynolds numbers are rough estimates of the strength of the nonlinearities compared to the dissipative terms (described next) in the equations (1.8) and (1.9). With the above set of operations, the final form of the non-dimensional MHD equations look as (1.14 - 1.16), which will be used in the rest of the work.

$$\partial_t \boldsymbol{\omega} = \nabla \times (\mathbf{v} \times \boldsymbol{\omega} - \mathbf{b} \times \mathbf{j}) + \hat{\mu}\boldsymbol{\Delta\omega} \tag{1.14}$$

$$\partial_t \mathbf{b} = \nabla \times (\mathbf{v} \times \mathbf{b}) + \hat{\eta}\boldsymbol{\Delta}\mathbf{b} \tag{1.15}$$

$$\nabla \cdot \mathbf{v} = \nabla \cdot \mathbf{b} = 0 \tag{1.16}$$

$\hat{\mu}$ and $\hat{\eta}$ are now the dimensionless dissipation coefficients.

An equivalent formulation of the equations is also possible by introducing Elsässer fields $\mathbf{z}^{\pm} = \mathbf{v} \pm \mathbf{b}$ as:

$$\partial_t \mathbf{z}^{\pm} = -\mathbf{z}^{\mp} \cdot \nabla \mathbf{z}^{\pm} - \nabla(p + \frac{b^2}{2}) + \frac{Re^{-1} + Rm^{-1}}{2}\boldsymbol{\Delta}\mathbf{z}^{\pm} + \frac{Re^{-1} - Rm^{-1}}{2}\boldsymbol{\Delta}\mathbf{z}^{\mp} \tag{1.17}$$

$$\nabla \cdot \mathbf{z}^{\pm} = 0 \tag{1.18}$$

From the definition of turbulence, it is clear that it is highly nonlinear, hence like many nonlinear processes, is difficult to understand, characterize or predict. There are a number of ways in which a nonlinear process could be understood; within the bounds of error. Numerical modeling, stochastic analysis, stability analysis are some of the methods that have been useful in improving the understanding of turbulent flows. As

seen from the set of equations (1.14 to 1.16), this notion of nonlinearity is justified for MHD turbulence too. Although stochastic and other approximation methods exist (see [21, 22]), in the context of this study the concentration is mainly on 3D- direct numerical simulations (DNS) and modeling of the turbulent flow.

Numerical simulations of a turbulent flow involves solving simultaneously the above set (equations (1.14 to 1.16)) of nonlinear differential equations involving various quantities that constitute the flow. In 3D-MHD, the equations in their current form are termed as resistive MHD equations and if the dissipation coefficients are set to zero, they are called ideal MHD equations. It is also important to note that in the Maxwell's equations the displacement current is neglected. Thus the current density in the system is divergence-free. It is the dominance of the nonlinear terms in these equations that actually leads to the onset of turbulence in the flows.

1.1.2   Significance of the Terms of the Equations

The first equation (1.14) is the vorticity equation which also represents the balance of momentum, in the system, in this vorticity formulation. In this equation the first part of the first term on the r.h.s. determines the advection by the velocity field. The second part of this term is the Lorentz force. This term signifies the influence of magnetic field on the velocity dynamics. It is responsible for energy transfer from magnetic field to velocity field or vice versa resulting in driving or suppression of velocity fluctuations [17].

The equation (1.15) is the induction equation. The first term on the r.h.s. is the term that signifies the nonlinear interaction between velocity and the magnetic field, which influences the evolution of the magnetic field fluctuations. It is a counterpart to the Lorentz force term of the equation (1.15). This term not only exchanges the energy between both the fields but also redistributes this energy over different spatial scales of the magnetic field [17].

The non-dimensional dissipation coefficients $\hat{\mu}$ and $\hat{\eta}$ are related to the Reynolds numbers by the equation (1.13). In the case of the kinetic Reynolds number Re, a critical Reynolds number $Re > Re_{crit}$ is necessary to generate turbulence. This is because its inverse, the normalized kinematic viscosity, has a damping effect on turbulent fluctuations. The critical kinetic Reynolds number depends on the geometry of the flow and typically $Re_{crit} \sim 10^2$ [1]. In the hydrodynamic case, it determines the transition to turbulence at low Re and properties of the turbulence itself at high Re. In addition to this parameter there is the magnetic Reynolds number Rm. Very low Rm implies the

domination of the magnetic dissipation whereas very high Rm means that the magnetic flux through a surface moving with the fluid remains almost constant i.e. the 'frozen-in' property [1]. Reynolds numbers determine the ratio of large and dissipation scales in a flow and thereby their separation (for discussion on various scales in turbulence see chapter 3). Turbulent flows are characterized by large Reynolds numbers. Typically, the Reynolds numbers range from 10^6 for laboratory plasmas to 10^{12-20} or more in the case of astrophysical systems [17]. These large Reynolds number regimes are not achievable in direct numerical simulations with the current computational capabilities. Nevertheless the computations that are being performed are believed to give a reliable impression of the inherent properties of these systems to a large extent. Another parameter, namely, the magnetic Prandtl number is introduced which is the ratio of the two Reynolds numbers. Here it is defined as:

$$Pr_m = \frac{Rm}{Re}. \tag{1.19}$$

This parameter measures the relative importance of viscous and Ohmic dissipation. The typical values range from as low as 10^{-10} to 10^{-5} in the exteriors of certain celestial bodies and their interiors respectively, to as high as 10^2 for fusion plasma and 10^{14} for interstellar medium [17]. However in this work the magnetic Prandtl number is always set to unity to achieve a formally symmetric configuration with regard to **v** and **b** [18]. Which means only the case where both the kinetic and magnetic diffusivities are equal is considered.

The terms in the equation (1.16) signify the fact that both the velocity and magnetic fields are solenoidal. In addition the $\nabla \cdot \mathbf{b} = 0$ condition ensures that there are no magnetic monopoles.

The equations (1.17) and (1.8) contain Elsässer fields, which are more fundamental quantities than **v** and **b** in incompressible MHD as these equations are symmetric in nature [20, 1]. Ideal invariants (see next section) and some properties like residual energy can also be expressed in terms of these fields (e.g. see [1]). Also as seen in equation (1.17), there is no self coupling in the nonlinear term but a cross coupling of $\mathbf{z}^+$ and $\mathbf{z}^-$ [1]. This forms the basis of the Alfvén effect, which describes a fundamental nonlinear interaction process (see section 3.2.2. of chapter 3 for details). They assume more significance in the phenomenological models of the MHD, which will be described in the chapter 3.

1.1.3   Ideal Invariants

In any system characterized by a nonlinear set of equations like MHD, it is difficult to characterize the system fully. But it has been identified that there exist three important quadratic invariants [20] in the ideal 3D-MHD case, which give a fair idea of the large-scale dynamics of the system. These ideal invariants are 1)total energy, 2)cross helicity and 3)magnetic helicity.

1) Total energy: It is the sum of the kinetic energy and the magnetic energy of the system and is given by:

$$E = \frac{1}{2} \int_V dV (v^2 + b^2).$$ (1.20)

2) Cross helicity: The dot product of the velocity field and magnetic field is called cross helicity and is given by:

$$H^C = \frac{1}{2} \int_V dV \mathbf{v} \cdot \mathbf{b}.$$ (1.21)

2) Magnetic helicity: The volume integral of the dot product of the magnetic vector potential and the magnetic field is called magnetic helicity and is given by:

$$H^M = \frac{1}{2} \int_V dV \mathbf{A} \cdot \mathbf{b}.$$ (1.22)

Here $\mathbf{A}$ is the magnetic vector potential which is related to the magnetic field by $\mathbf{b} = \nabla \times \mathbf{A}$ and V is the volume of the system under consideration.

The invariance property means $\dot{E} = \dot{H}^C = \dot{H}^M = 0$ in the ideal MHD case ($\hat{\eta} = \hat{\mu} = 0$), where the dot represents the time derivative. In the resistive MHD case, these derivatives are given as

$$\dot{E} = -D^E = -\int_V dV (\hat{\mu}\omega^2 + \hat{\eta}j^2)$$ (1.23)

$$\dot{H}^C = -D^{H^C} = -(\hat{\mu} + \hat{\eta}) \int_V dV \mathbf{j} \cdot \boldsymbol{\omega}$$ (1.24)

$$\dot{H}^M = -D^{H^M} = -2\hat{\eta} \int_V dV \mathbf{j} \cdot \mathbf{b}$$ (1.25)

The derivation of these dissipation relations in equations (1.23 - 1.25) is given in [1]. It is to be noted that invariance of magnetic helicity necessarily depends on the boundary conditions of the system (see section 1.2.1). Total energy of the system and its dissipative relation give an idea of the nature of the scales involved in the flow. Cross helicity is an indication of the degree of alignment between the velocity and magnetic

fields. Magnetic helicity is a measure of linkage and twist in the magnetic field. This is the primary physical quantity of this studies because it shows a particular feature called the 'inverse cascade' (to be discussed in detail in section 1.2) in turbulent flows.

Other Quantities of Interest

There are few more important quantities of interest which need to be studied when looking at 3D-MHD turbulent system. They are kinetic helicity, residual energy and residual helicity. Kinetic helicity represents the twist of vortex lines and is the volume integral of the dot product of vorticity and velocity fields:

$$H^V = \frac{1}{2} \int_V dV \, \mathbf{v} \cdot \boldsymbol{\omega}. \tag{1.26}$$

Residual energy is the difference of magnetic energy and kinetic energy whereas residual helicity is the difference of magnetic and kinetic helicities.

Kinetic helicity is an ideal invariant in 3D-hydrodynamics (HD). According to the Kelvin-Helmholtz theorem (which shows the invariance of kinetic helicity in ideal 3D-HD), for a perfect fluid (either barotropic or of uniform density), vortex surfaces, filaments and tubes are *material* and move with the fluid particles they contain [15]. From the 3D-DNS results of isotropic turbulence in hydrodynamic case, it has been established that the turbulent structures are *in fact* thin tubes of high vorticity due to vortex stretching[1] (see [15] and references there of). In 2D-HD turbulence, vortex stretching is not present but since vorticity is conserved[2] it leads to inverse cascade of kinetic energy [1]. In MHD turbulence, however, this phenomenon of vortex stretching is inhibited, because of the presence of the magnetic field. It is to be noted that in 3D-MHD turbulence, magnetic helicity is an ideal invariant and is responsible for the inverse cascade of magnetic helicity (which represents the twists in the magnetic field). Kinetic helicity is important in the interiors of many celestial objects like stars, planet cores and is believed to be responsible for the generation of their magnetic fields through dynamo action i.e. the self-sustained generation of magnetic fields by the motion of the conducting fluid [23].

The value of residual energy determines which energy component is dominant in the system. Three possibilities exist here: a) kinetic energy is greater than magnetic energy:

---

[1]The term $\boldsymbol{\omega}.\nabla\mathbf{v}$ derived from the first term of r.h.s. of equation (1.14) with no magnetic field, indicates to the fact that if a thin vortex tube is embedded in turbulent flow, it is both stretched by turbulence as well as diffused by molecular viscosity. This is the phenomenon of vortex stretching.

[2]since only diffusive decay is present and no source term to give the vortex stretching effect.

this is the case in the initial stage of turbulent dynamo configurations mentioned earlier, b) kinetic energy and magnetic energy are equal or almost equal and c) kinetic energy is smaller than the magnetic energy. The last two cases are of interest in this work and often it is seen that the dominant component of the energy budget comes from the magnetic energy.

Residual helicity determines which of the two fields is responsible for the structure formation in the flow and is the true motor of the turbulent fluctuations in the system [7]. The quantities mentioned above are not studied normally in real space but in spectral space. The importance of these quantities is described in more depth, when discussing the MHD turbulence properties in spectral space, in chapters 3 and 4. Before proceeding any further, magnetic helicity in real space and its importance is discussed more elaborately.

1.2   Magnetic Helicity

As defined by the equation (1.22) the magnetic helicity in a given volume, is the volume integral of the dot product of magnetic vector potential ($\mathbf{A}$) and the magnetic field. As the curl of a vector measures its rotation around a point, this relation gives how much $\mathbf{A}$ rotates around itself times its own modulus i.e. like a helix. The name helicity is thus appropriate as it gauges the relative curling or braiding of the lines of $\mathbf{A}$ and $\mathbf{b}$ (i.e. to what degree they resemble helixes). This could be termed as the curliness of the field [24]. Several types of magnetic fields including twisted, kinked, knotted or linked magnetic flux tubes, sheared layers of magnetic flux and force-free fields, all possess magnetic helicity. As magnetic helicity quantifies various aspects of the magnetic field structure, it allows the comparison of models of fields in different geometries, avoiding the use of parameters specific to the model [25].

Thus it is a topological property of the magnetic field and can be measured as follows: consider three flux tubes T_1, T_2 and T_3 with fluxes ϕ_1, ϕ_2 and ϕ_3 respectively, interlinked as shown in the figure 1.1. Here flux ϕ of a magnetic field $\mathbf{b}$ is defined as the surface integral $\int_S \mathbf{b}.d\mathbf{S}$ across a surface $S(t)$ bounded by a closed curve $l(t)$, which is moving with the plasma. Sweeping the boundary curve l along the field defines a flux tube [1]. From this configuration, magnetic helicity is determined using the Gauss linking number $L(T_i, T_j)$ or simply L_{ij}[3] [25] between any two flux tubes T_i and T_j, of any N

---

[3]Gauss linking number determines the twist between two flux tubes. and in equation (1.27) the term $2L_{ij}\phi_i\phi_j$ determines the mutual helicity between the two flux tubes. When $i = j$, the term determines the self helicity with L_{ii} representing an average twist T_i within a flux tube.
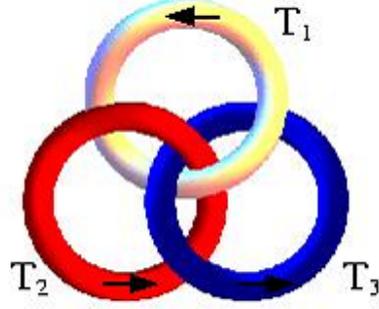
Figure 1.1: Schematic of linking of the flux tubes. Shown are three flux tubes T_1, T_2 and T_3 interlinked together, with their respective fluxes ϕ_i, i=1-3. Adapted from [3].

flux tubes, from [3] as

$$H^M = 2 \sum_{i=1}^{N} \sum_{j=1}^{N} L_{ij} \phi_i \phi_j \tag{1.27}$$

If now $N \to \infty$ with $\phi_i \to 0$ then equation (1.22) is got back with the following mathematical operations shown below for two flux tubes, as in [25, 3]. Let σ parameterize the curve 1 and τ parameterize the curve 2, with points $\mathbf{x}(\sigma)$ and $\mathbf{y}(\tau)$ on the each of the curves respectively. Let $\mathbf{r} = \mathbf{y} - \mathbf{x}$. From the definition of Gauss linking number:

$$L_{12} = -\frac{1}{4\pi} \oint_1 \oint_2 \frac{d\mathbf{x}}{d\sigma} \cdot \frac{\mathbf{r}}{r^3} \times \frac{d\mathbf{y}}{d\tau} d\tau d\sigma$$

Combining this equation and equation (1.27),

$$H^M = -\frac{1}{4\pi} \int \int \mathbf{b}(\mathbf{x}) \cdot \frac{\mathbf{r}}{r^3} \mathbf{b}(\mathbf{y}) d^3 x d^3 y.$$

Simplifying the calculations using Coulomb gauge for the vector potential ($\nabla \cdot \mathbf{A} = 0$):

$$\mathbf{A}(\mathbf{x}) = -\frac{1}{4\pi} \int \frac{\mathbf{r}}{r^3} \mathbf{b}(\mathbf{y}) d^3 y,$$

H^M reduces to

$$H^M = \int \mathbf{A} \cdot \mathbf{b} \, d^3 x,$$

which is same as equation (1.22).

1.2.1 Ideal Invariance of Magnetic Helicity

From the definitions in equations (1.22) and (1.26), which have similar type of terms, for helicities, it might be tempting to declare magnetic helicity as an ideal invariant in 3D-MHD, like kinetic helicity in 3D-HD. The vector potential, is a gauge dependent quantity, therefore the magnetic helicity is also gauge dependent. In order that magnetic helicity be an ideal invariant, it needs to be gauge invariant.

In order to prove the gauge invariance of magnetic helicity, the notation used so far is slightly modified as follows, closely in the lines of [24]. Let a divergence-free magnetic field $\mathbf{B}(\mathbf{r})$ be given in a region $\mathbf{D}$, which may be either bounded or not. Its magnetic helicity when $\mathbf{B} = \nabla \times \mathbf{A}$, is defined as

$$h(\mathbf{B}, \mathbf{D}) = \int_{\mathbf{D}} \mathbf{A} \cdot \mathbf{B} d^3 r \qquad (1.28)$$

Here $\mathbf{A}$ is the magnetic vector potential. It is necessary to assign boundary conditions to $\mathbf{B}$. It will be assumed that the magnetic field $\mathbf{B}$ is parallel to the surface $\partial \mathbf{D}$ that bounds $\mathbf{D}$. If now $\mathbf{n}$ is a unit vector normal to $\partial \mathbf{D}$, then it is seen that $\mathbf{B} \cdot \mathbf{n} = 0$ in $\partial \mathbf{D}$. As the configuration consists of only finite energy fields, $\mathbf{B} = 0$ in any part of $\partial \mathbf{D} \to \infty$. For the same reason a gauge transformation is considered as follows:

$$\mathbf{A}' = \mathbf{A} + \nabla f. \qquad (1.29)$$

With the boundary conditions stated above and $\nabla \cdot \mathbf{B} = 0$, it is found that

$$h' - h = \int_{\mathbf{D}} \mathbf{B} \cdot \nabla f d^3 r = \oint_S f \mathbf{B} \cdot \mathbf{n} dS = 0. \qquad (1.30)$$

It is necessary that f be single valued in $\mathbf{D}$ for the above relation to be true. Hence magnetic helicity is a property of the transverse or solenoidal part of $\mathbf{A}$. It does not depend on the longitudinal part of the magnetic vector potential ($\mathbf{A}_{\|}$) (as $\mathbf{A}$ is expressed as the gradient of a potential which is single valued in $\mathbf{D}$). If it were not so, then Gauss theorem could not be applied to $\int_D \nabla f. \mathbf{b} d^3 r$, the change in helicity under gauge transformation for equation (1.29) [24].

For gauge invariance the normal component of $\mathbf{B}$ i.e. $\mathbf{B}_n$ must vanish at the boundary surface since function f is arbitrary. Only in special cases, for example if periodic boundary conditions are used, then a finite $\mathbf{B}_n$ is possible. Many magnetic configurations of interest in astrophysics are either open with field lines extending upto infinity

or bounded by surfaces crossed by field lines. In such cases magnetic helicity is no longer gauge invariant. In order to overcome this situation an alternative formulation is needed [1]. Hence following [1] let

$$h_{alt} = \int_V dV(\mathbf{A} + \mathbf{A}_0) \cdot (\mathbf{B} - \mathbf{B}_0) \quad \text{where} \quad \mathbf{B}_0 = \nabla \times \mathbf{A}_0 \quad \text{is a reference field.}$$
(1.31)

The reference field is chosen suitably. In an open system this reference field may be a static field with the same asymptotic properties as $\mathbf{B}$. In a bounded system the normal components of both the fields should be equal. To show that h_{alt} is indeed gauge invariant even under separate gauge transformations of $\mathbf{A}$ and $\mathbf{A}_0$, consider the conservation law for the magnetic helicity. The gauge is chosen such that the scalar potential vanishes, $\mathbf{E} = -\partial_t \mathbf{A}/c$, where c is the velocity of light. Applying Faraday's law

$$\partial_t \mathbf{B} = -c \nabla \times \mathbf{E}$$
(1.32)

to get

$$\int \partial_t(\mathbf{A} \cdot \mathbf{B})dV = \int (\mathbf{B} \cdot \partial_t \mathbf{A} + \mathbf{A} \cdot \partial_t \mathbf{B})dV = -2c \int \mathbf{E} \cdot \mathbf{B}dV + c \oint (\mathbf{A} \times \mathbf{E}) \cdot d\mathbf{S}$$
(1.33)

When Ohm's law

$$\mathbf{E} + \frac{1}{c}\mathbf{v} \times \mathbf{B} = \frac{1}{\sigma}\mathbf{j},$$
(1.34)

is inserted into equation (1.33), and the boundary condition $\mathbf{B}_{n=0}$ is applied, then the second term in the equation (1.33) becomes:

$$-\oint (\mathbf{A} \cdot \mathbf{B})\mathbf{v} \cdot d\mathbf{S} \qquad .$$
(1.35)

Here σ is the electrical conductivity of the medium, and it is related to the dimension less magnetic diffusivity $\hat{\eta} (= Rm^{-1})$ through $\eta = c^2/4\pi\sigma$ which is $\eta/L_0 V_0$ (see equation (1.13)). From the above equations the time variation of h is obtained as in equation (1.36) by using the equation (1.37) which represents the change in h due to change in dV of the volume.

$$\frac{dh}{dt} = \int \partial_t(\mathbf{A} \cdot \mathbf{B})dV + \oint (\mathbf{A} \cdot \mathbf{B})\mathbf{v} \cdot d\mathbf{S} = -\frac{2c}{\sigma} \int dV \mathbf{j} \cdot \mathbf{B} \quad \text{as} \qquad (1.36)$$

$$\oint (\mathbf{A} \cdot \mathbf{B})\mathbf{v} \cdot d\mathbf{S}dt = \int_{dV} \mathbf{A} \cdot \mathbf{B}dV \tag{1.37}$$

Hence the helicity is conserved in the ideal limit $\sigma \to \infty$ or $\hat{\eta} \to 0$. In a similar manner it can be shown that h_{alt} is also conserved.

First term on the r.h.s. of equation (1.33) and the r.h.s. of equation (1.36) are the two terms that depict the variation of helicity, with respect to time. These two terms represent the nonlinear helicity transmission and dissipation respectively, constituting the helicity flux and hence will be used in chapter 4 in their Fourier transformed forms.

Importance of the Invariance Property

From the above discussion, it can be inferred that the magnetic helicity is conserved in ideal MHD and is approximately conserved during magnetic reconnection (A process in which there is a change of magnetic connectivity of plasma elements due to the presence of a localized diffusion region where ideal MHD breaks down. [26]). In a confined volume, widespread reconnection may reduce the magnetic energy of a field while approximately conserving its magnetic helicity [4]. As a result, the field relaxes to a minimum energy state, often called the Taylor state, where the current is parallel to the force free field [4]. Such relaxation processes are important to both fusion (especially in reversed field pinch devices) and astrophysical plasmas [25]. The derivative of magnetic helicity obtained in the equation (1.33) has two terms, a dissipative and a transport term. The dissipative term represents the effect of twisting motions on the boundary while the second transport term represents the bulk transport of helical field across the boundary. From these two terms some astronomical observations e.g. hemispheric specific sign of helicity[4], production of solar coronal mass ejections[5]; could be interpreted [27, 28]. The constraint of magnetic helicity preservation implies that a dynamo (the mechanism whereby electric currents within an celestial body generate a magnetic field) is more easily produced if the electric potential varies in the surface of the dynamo [29, 30].

The invariance constraint also infers that with external forcing or with any kind of agitations to the system, only scale changes could be achieved in the system but the magnetic helicity cannot be destroyed. Thus in order that this constraint be fulfilled, the magnetic field topology in a system must change significantly, while the total magnetic helicity of the system remains invariant or approximately invariant. This feature

---

[4]In the Sun, observations of magnetic helicity indicate that it has a positive sign in the southern hemisphere and a negative sign in the northern hemisphere

[5]Huge violent ejections of plasma coming out of the Sun's outer surface i.e. corona.

paves wave to large-scale magnetic structure formation through a process called 'inverse cascade' (see [30, 11, 31]). In the next section this property is discussed.

1.3   Inverse Cascade of Magnetic Helicity

Transformation of Flow Equations into Spectral Domain

Inverse cascade of magnetic helicity is best explained in the spectral domain. Hence the flow equations (1.14 - 1.16) are Fourier transformed. For example a quantity like vorticity $\boldsymbol{\omega}$ is transformed into the spectral domain as:

$$\boldsymbol{\omega}(\mathbf{r}, t) = \int d^3k\, \tilde{\boldsymbol{\omega}}(\mathbf{k}, t) e^{-i\mathbf{k}\cdot\mathbf{r}} \tag{1.38}$$

here, the l.h.s. is the real space quantity and on the r.h.s. $\tilde{\boldsymbol{\omega}}(\mathbf{k}, t)$ is its Fourier space counterpart, $e^{-i\mathbf{k}\cdot\mathbf{r}}$ is the basis function for the Fourier space and $\mathbf{k}$ is the spectral wave vector, with $\mathbf{r}$ and $\mathbf{k}$ being the Fourier transform pair $\mathbf{r} = 2\pi/\mathbf{k}$. For simplicity of notation, the quantities will be generally referred without their respective variables as: $\boldsymbol{\omega}(\mathbf{r}, t)$ and $\tilde{\boldsymbol{\omega}}(\mathbf{k}, t)$ as $\boldsymbol{\omega}$ and $\tilde{\boldsymbol{\omega}}$ respectively. With this formulation the set of the equations (1.14 - 1.16) will now read as:

$$\partial_t\tilde{\boldsymbol{\omega}} = i\mathbf{k} \times [\widetilde{\mathbf{v} \times \boldsymbol{\omega}} - \widetilde{\mathbf{b} \times (\nabla \times \mathbf{b})}] - \hat{\mu}k^2\tilde{\boldsymbol{\omega}} \tag{1.39}$$

$$\partial_t\tilde{\mathbf{b}} = i\mathbf{k} \times \widetilde{\mathbf{v} \times \mathbf{b}} - \hat{\eta}k^2\tilde{\mathbf{b}} \tag{1.40}$$

$$\mathbf{k} \cdot \tilde{\mathbf{v}} = \mathbf{k} \cdot \tilde{\mathbf{b}} = 0 \tag{1.41}$$

Here the symbol $\widetilde{(...)}$ means the convolution integral *Viz*.

$$\widetilde{(\mathbf{v} \times \boldsymbol{\omega}(\mathbf{k}))} = \int d^3k' \tilde{\mathbf{v}}(\mathbf{k}') \times \tilde{\boldsymbol{\omega}}(\mathbf{k} - \mathbf{k}') \qquad . \tag{1.42}$$

In this formulation the three ideal invariants stated in equations (1.20 - 1.22) read:

$$E_k = \frac{1}{2}\int d^3k(|\tilde{\mathbf{v}}|^2 + |\tilde{\mathbf{b}}|^2) \tag{1.43}$$

$$H_k^C = \frac{1}{2}\int d^3k\tilde{\mathbf{v}}^* \cdot \tilde{\mathbf{b}} \tag{1.44}$$

$$H_k^M = \frac{1}{2} \int d^3k \, \tilde{\mathbf{A}} \cdot \tilde{\mathbf{b}}^*. \tag{1.45}$$

Here * is the usual complex conjugate notation. In the relations (1.43) and (1.44) the symmetry property of the Fourier transforms for the real-valued functions e.g. $f(-k) = f^*(k)$ has been used. Using these flow equations in the Fourier space, the process of 'inverse cascade' is described below.

1.3.1   Realizability Condition and Inverse Cascade

In this work the 3D-MHD turbulence is described by statistical averages of physical quantities. Fully periodic boundary conditions ensure that the viscous boundary layers are not present in the system, so approximate statistical homogeneity of the turbulent system is preserved [17]. Isotropy of the system is also assumed. Next the three quantities of equations (1.20 - 1.22) are represented in their statistically averaged forms. With the above assumptions in place and without assuming invariance under planar reflexions, following the arguments given in [5] for a non-helical turbulence,the realizability condition for magnetic helicity is obtained, which is reproduced here:

$$|H^M(k)| \leq E^M(k)/k \leq E(k)/k. \tag{1.46}$$

Here E^M and E are magnetic and total energies respectively. Suppose that an initial state of maximal helicity is confined to two wavenumbers $\mathbf{p}$ and $\mathbf{q}$ with $(p < q)$ and let this excitation be entirely transferred to the wave number $\mathbf{k}$. From the conservation of total energy and magnetic helicity it is seen that

$$E(k) = E(p) + E(q) \tag{1.47}$$

$$H^M(k) = H^M(p) + H^M(q) = E(p)/p + E(q)/q. \tag{1.48}$$

Using the realizability condition, and performing few simple manipulations, the above equations are written as

$$k \leq \frac{p|H^M(p)| + q|H^M(q)|}{|H^M(p)| + |H^M(q)|}. \tag{1.49}$$

The expression on the r.h.s. of the above equation is a weighted mean of p and q and thus

$$min(p,q) \leq \frac{p|H^M(p)| + q|H^M(q)|}{|H^M(p)| + |H^M(q)|} \leq max(p,q) \tag{1.50}$$

Therefore $k \leq max(p, q)$. Thus simultaneous up-transfer of total energy and magnetic helicity is not possible. Also the invariance of magnetic helicity holds only under the assumption that $\mathbf{b}(\mathbf{r}, t)$ vanishes at infinity, in the statistically homogeneous case or that the mean magnetic field vanishes. Hence the transfer of magnetic helicity takes place from large wavenumbers to small wavenumbers and this is known as 'inverse cascade'. A more detailed version of this process and the physics involved will be discussed in chapter 3.

Importance of Inverse Cascade of Magnetic Helicity

Inverse cascade of magnetic helicity in 3D-MHD turbulence, is believed to be one of the processes responsible for the formation of large-scale magnetic structures in the universe, as the movement of this quantity is towards smaller wavenumbers or large scales. In the celestial bodies with rotation, it is believed that the difference of kinetic helicity (twists in the velocity field) and magnetic helicity (twists in the magnetic field) results in the so called α-dynamo, where kinetic helicity injection results in enhancement of the magnetic field [1], but not necessarily lead to stable large-scale magnetic structure formation. The relation deduced from equation (1.48) i.e. equation (1.50), suggests that the magnetic helicity always moves to large scales. Thus in all probability, 'inverse cascade' of magnetic helicity might be an important process for the formation of the stable large-scale magnetic structures seen in the celestial atmospheres and their vicinities. Currently no clear evidence of magnetic helicity transfer from comparatively very small scales to very large scales, has been put forward. In this work an attempt to gather such an evidence is being made using DNS. Two cases: forced turbulence and decaying turbulence are reported. In the following chapters the numerical method is described first and then data analysis of the simulations is presented followed by a discussion on the findings from this work.

Chapter 2

Direct Numerical Simulations of 3D-MHD Turbulence

In this chapter the numerical methods employed for the simulation of 3D-MHD turbulence are described. First the spectral scheme used for this purpose is discussed along with the aliasing error problem and its solution. Next the integration scheme followed by initial conditions is discussed. The forcing mechanism used for the simulations is explained next. The concept of hyperviscosity is mentioned along with a short discussion on Reynolds number. Finally the software and hardware that make these simulations work are mentioned, as well as the diagnostics from these simulations.

2.1 Motivation for Direct Numerical Simulations (DNS) and Equation Set

The inverse cascade of magnetic helicity is best understood in the spectral domain. It is noteworthy that not only this property but many other properties of MHD turbulence demonstrate interesting characteristics in the spectral domain. Of these characteristics, the most important one is the so called 'inertial range' of wavenumbers (discussed in detail in chapter 3) exhibited by the spectra of certain quantities of MHD turbulence like total energy. In the inertial range the spectra show self-similar power law behavior, which is a predictable property of a randomly fluctuating system. The investigation of inertial ranges and the universality of the power laws forms one of the important aspects of turbulence studies. Numerical simulations of turbulence in the spectral domain are performed using several methods like large eddy simulations (LES), shell models or direct numerical simulations (DNS) [15]. LES methods and

shell models approximate the nonlinear terms of equations (1.39 - 1.41) in one or other form (see for e.g. [32, 22]), whereas DNS methods do not use any such approximations and deal with the equations in their true form. Thus methods other than DNS usually involve additional assumptions. If the equation set is studied without any additional physical approximations, a better understanding of the turbulent flows could be obtained. The DNS methods stay closest to the underlying differential equations describing the turbulent systems although they are computationally expensive. With appropriate choice of numerical methods however the computational overhead can be reduced.

In studying the equation set (1.39 - 1.41) in the Fourier domain, the spatial derivatives are transformed into simple multiplications with wave vectors. Here the time evolution of the equations directly yields the spectra of the physical quantities. Although the Fourier methods have several advantages, they also have a major drawback, namely, the Gibbs phenomenon. The Gibbs phenomenon manifests itself as characteristic oscillations of Fourier series near steep gradients. By assuming incompressibility, such discontinuities of physical quantities are excluded [17]. For incompressible flows, spectral methods are more accurate than finite difference schemes as they require less discretization points for achieving the same accuracy (see [33] for a detailed description of different numerical schemes).

This study aims at a better understanding of nonlinear inertial range dynamics of two types of MHD turbulent flows: forced MHD turbulence and decaying MHD turbulence in three dimensions. For this purpose the set of equations (1.39 - 1.41) is actually written in the following manner:

$$\partial_t \tilde{\boldsymbol{\omega}} = i\mathbf{k} \times [\widetilde{\mathbf{v} \times \boldsymbol{\omega}} - \widetilde{\mathbf{b} \times (\nabla \times \mathbf{b})}] - \hat{\mu}k^2\tilde{\boldsymbol{\omega}} + \mathbf{F_v} \tag{2.1}$$

$$\partial_t \tilde{\mathbf{b}} = i\mathbf{k} \times \widetilde{\mathbf{v} \times \mathbf{b}} - \hat{\eta}k^2\tilde{\mathbf{b}} + \mathbf{F_b} \tag{2.2}$$

$$i\mathbf{k} \cdot \tilde{\mathbf{v}} = i\mathbf{k} \cdot \tilde{\mathbf{b}} = 0 \tag{2.3}$$

where $\mathbf{F_v}$ and $\mathbf{F_b}$ are the forcing terms for the velocity and magnetic fields respectively. Thus, if $\mathbf{F_v}$ and $\mathbf{F_b}$ are set to zero, the equation set represents a decaying turbulence case and if they are non-zero, it is a forced turbulent system. In this set of equations, the nature of forcing very much influences how the turbulent flow and its characteristics evolve. In the forced system studied here a random forcing is employed, which is discussed in the section 2.4.2.

Fully periodic boundary conditions are chosen so that influence of the boundary on the system remains minimum. This also ensures that the turbulence remains approximately statistically homogeneous. Therefore inherent properties of MHD turbulence in the system can be studied, with considerable detachment from the influence of the boundary.

2.2 Pseudospectral Scheme

The equation set (2.1 - 2.3) is solved in the Fourier space in a regular cubic box of linear size 2π, discretized with N points in each direction. This corresponds to the Fourier wavenumber range $\frac{-N}{2} + 1 \leq k \leq \frac{N}{2} - 1$. All physical quantities are approximated by truncated Fourier series, e.g. for the Fourier counterpart of the real quantity $\boldsymbol{\omega}(\mathbf{x}_j, t)$, $\hat{\boldsymbol{\omega}}_k(t)$ as

$$\hat{\boldsymbol{\omega}}_k(t) = \frac{1}{N^3} \sum_j \boldsymbol{\omega}(\mathbf{x}_j, t) e^{-i\mathbf{k}\cdot\mathbf{x_j}} \quad \text{where} \quad x_j = \frac{2\pi j}{N} \quad j = 0, ..., N-1 \text{ for each direction.} \tag{2.4}$$

The mode $\mathbf{k} = (0, 0, 0)$ of all physical quantities, i.e. their spatial average, is set to zero. As already mentioned in section 1.3, the physical quantities are real valued and satisfy symmetry $(\hat{\boldsymbol{\omega}}_{-k}(t) = \hat{\boldsymbol{\omega}}_k^*(t))$ in Fourier space, hence it is enough to only store one half of Fourier modes. This symmetry property helps in reducing the memory requirement and also speeds up the calculations. The convolution terms in the equations (2.1) and (2.2) may in general be represented as

$$\widetilde{\overline{[a\ b]_\mathbf{k}}} = \sum_{\mathbf{k=p+q}} \widetilde{\overline{a_\mathbf{p}}}\ \widetilde{\overline{b_\mathbf{q}}} \quad \text{where} \quad |\mathbf{k}|, |\mathbf{p}|, |\mathbf{q}| \leq \frac{N}{2} - 1. \tag{2.5}$$

A simple calculation shows that numerically evaluating such an expression in three dimensions requires $O(N^6)$ operations. This fact limits the application of spectral methods to small Fourier data sets [34]. In order to overcome this limitation, the variables in the relation are first transformed into real space. A multiplication is performed here and the value retransformed into the Fourier space. This mathematical operation is facilitated by the fact that a convolution in Fourier domain is a multiplication in real space. The method explained here is the 'pseudospectral scheme' [34]. This method reduces the complexity of the order of operations performed to $O(N^3 log_2 N)$, which is only possible with FFT (Fast Fourier Transform). But this method suffers from 'aliasing error' caused by the finite discretization, shown in equation (2.4).

2.2.1   Treatment of Aliasing Errors

The aliasing error of the pseudospectral scheme is removed by a truncation technique known as dealiasing. This technique utilizes the calculation of extended Fourier fields of size $M \geq \frac{3N}{2}$ instead of the original size of N. For this, equation (2.5) is written considering only a one-dimensional convolution as:

$$\widetilde{\overline{[a \; b]}}_k = \sum_{k=p+q} \widetilde{\overline{a_p}} \; \widetilde{\overline{b_q}} + \sum_{k \pm N = p+q} \widetilde{\overline{a_p}} \; \widetilde{\overline{b_q}}. \tag{2.6}$$

Now if original Fourier variables are padded with zeros in the extra wavenumber range $\frac{M}{2} - 1 \geq |p|, |q| \geq \frac{N}{2} - 1$, the second term in the equation (2.6) vanishes and the exact result of the convolution is obtained. This is the *3/2* dealiasing rule. However, the number of operations performed here is higher than the normal pseudospectral calculation. In one dimension the truncation technique requires $\sim 50\%$ more numerical operations. The computational effort increases with number of dimensions as many finally discarded modes that do not carry any physical information have to be included and evaluated (see [17] and reference thereof).

The dealiasing step performance can be improved by reducing the number of extra modes by the introduction of spherical truncation of the Fourier variables in three dimensions. In this dealiasing method, a sphere of physical Fourier modes is assumed that are padded to a cubic shape. The aliasing error due to the modes in this sphere was empirically found to be of the order of discretization error, and is neglected. In this way the number of additional calculations are reduced by a factor of more than $\frac{2}{3}$ compared to the full $\frac{3}{2}$ dealiasing [20, 17].

2.3   Leapfrog Integration

The equation set (2.1 - 2.3) is evolved in time using a leapfrog scheme. The leapfrog scheme is a fast explicit two-step algorithm that uses a constant time step. The scheme is implemented as second order accurate, and is suitable for non-dissipative problems. However, the algorithm is unstable in the presence of diffusion terms. An additional modification in the form of an integrating factor, is therefore required to avoid this property. This method treats the linear diffusion term exactly (see [20, 17, 35]). In this method equations (2.1) and (2.2) with the forcing terms set to zero appear as:

$$\partial_t(\tilde{\boldsymbol{\omega}}_{\mathbf{k}} e^{\hat{\mu} k^2 t}) = e^{\hat{\mu} k^2 t} i\mathbf{k} \times [\widetilde{\mathbf{v} \times \boldsymbol{\omega}} - \widetilde{\mathbf{b}} \times (\nabla \times \mathbf{b})] \tag{2.7}$$

$$\partial_t(\tilde{\mathbf{b}}_{\mathbf{k}} e^{\hat{\eta} k^2 t}) = e^{\hat{\eta} k^2 t} i \mathbf{k} \times \widetilde{\mathbf{v} \times \mathbf{b}} \tag{2.8}$$

Here the dissipation term is included implicitly and stability and accuracy properties do not depend anymore on the dissipation term, but only on the non-linear term. With this modification the leapfrog scheme for the equations is:

$$\tilde{\boldsymbol{\omega}}_{n+1} = \tilde{\boldsymbol{\omega}}_{n-1} e^{-\hat{\mu} k^2 \Delta t} + 2\Delta t e^{-\hat{\mu} k^2 \Delta t} [\widetilde{\mathbf{v} \times \boldsymbol{\omega}} - \widetilde{\mathbf{b} \times (\nabla \times \mathbf{b})}]_n \tag{2.9}$$

$$\tilde{\mathbf{b}}_{n+1} = \tilde{\mathbf{b}}_{n-1} e^{-\hat{\eta} k^2 \Delta t} + 2\Delta t e^{-\hat{\eta} k^2 \Delta t} [\widetilde{\mathbf{v} \times \mathbf{b}}]_n \tag{2.10}$$

where n is a time step index and Δt denotes the time interval of one time step. The solution obtained with this scheme is often modified by temporal oscillations with the period $2\Delta t$. These oscillations arise due to the inaccurate approximation of time derivatives. They can be avoided by temporal averaging of the obtained solution over every two subsequent time steps (see [20, 17, 35]). For nonlinear partial differential equations like the ones under consideration there are no clear rules to guarantee the numerical stability of a simulation, and therefore no recipes to indicate how small Δt ought to be. The Courant-Friedrichs-Lewy (CFL) condition, an estimate originally developed for advection, provides the upper bound as:

$$\Delta t \leq \frac{\Delta x}{v_{max}} \sim \frac{\pi}{k_{max} v_{max}} \tag{2.11}$$

where v_{max} is the maximal speed of propagation in the system. As incompressibility was assumed magneto-acoustic waves are excluded. A good estimate for the maximum speed of propagation is $v_{max} = \sqrt{E^{tot}}$. Although equation (2.11), forms a good estimate for stability, the time step additionally can be adjusted in particular simulations for maximum stability [20, 17, 35, 36].

2.4 Initial Conditions and Forcing

2.4.1 Initial Conditions

The simulation is initiated by providing definite amounts of kinetic and magnetic energies, following [20, 13].

Step1 : The initial velocity and magnetic fields are symmetrical Gaussian fluctuations centered around a particular wave number k_m with a functional form $a e^{\frac{-(k-k_m)^2}{(2k_0^2)}}$, with a being the amplitude, k_0 as its width and k the wavenumber.

Step2 : An orthonormal basis of the form $\left\{ \mathbf{e_m} := \frac{\mathbf{k}_m}{|\mathbf{k}_m|}, \mathbf{e}_1, \mathbf{e}_2 \right\}$ is generated with $\mathbf{e}_m \perp \mathbf{k}_m$ and $\mathbf{e}_2 := \mathbf{e}_m \times \mathbf{e}_1$, where $\mathbf{e}_1$ and $\mathbf{e}_2$ are random vectors that are orthogonal to $\mathbf{k}$ and are normalized. This orthonormal basis is generated to preserve solenoidality of the initial magnetic and velocity fields.

Step3 : A random vector potential is now generated using the functions from step-1 and step-2 for a grid point m whose j^{th} component is defined as:

$$\hat{\mathbf{A}}_{m_j} = a e^{\frac{-(k-k_m)^2}{(2k_0^2)}} \left\{ q_+(\phi) \underbrace{(\mathbf{e}_1 + i\mathbf{e}_2)_j}_{=:\gamma^+} e^{i2\pi\alpha_m} + q_-(\phi) \underbrace{(\mathbf{e}_1 - i\mathbf{e}_2)_j}_{=:\gamma^-} e^{i2\pi\beta_m} \right\} \quad (2.12)$$

here α_m and β_m are random numbers in the range $[0, 1]$. $\gamma^\pm$ are the eigenvectors of the rotational operators. Local magnetic helicity is then generated with the help of these eigenvectors, using the relation $H_m = \frac{1}{2}\mathbf{A}_m^* \cdot (i\mathbf{k}_m \times \mathbf{A}_m) = k e^{-\frac{k_m^2}{k_0^2}} [q_+^2(\phi) - q_-^2(\phi)]$.

Note that the parameter $q_\pm(\phi)$ sets the amount of magnetic helicity (H^M) introduced into the initial condition, and can vary between $\pm H_{max}^M$ while $H_{max}^M \cong E^M/k_0$, E^M being the magnetic energy. Here $\phi \in [-1, 1]$ and $q_\pm(\phi)$ is defined by:

$$q_\pm := cos(\frac{\pi}{4}\phi) \pm sin(\frac{\pi}{4}\phi) = \sqrt{2}sin(\frac{\pi}{4}(1 \pm \phi)). \quad (2.13)$$

In the helicity expression above the relation $i\mathbf{k}_m \times \mathbf{A}_m$ is the magnetic field $\mathbf{b}_m$, generated from the already obtained magnetic vector potential. The factor ϕ determines the amount of magnetic helicity in the system; $\phi = 0$ is the state with no magnetic helicity and $\phi = \pm 1$ the state of maximum helicity.

For generating the initial velocity field, the magnetic field is rotated using a set of transformation matrices in the $\mathbf{e}_1, \mathbf{e}_2$- plane:

$$\mathbf{v_m} = \mathbf{D}_{\mathbf{k}_m}^{-1} \mathbf{D}_\varphi \mathbf{D}_{\mathbf{k}_m} \mathbf{b}_m. \quad (2.14)$$

This also sets the cross helicity H^C of the initial state. The transformation matrices are defined using the orthonormal vectors $\mathbf{e}_m, \mathbf{e}_1, \mathbf{e}_2$ as:

$$\mathbf{D}_{\mathbf{k}m} := \begin{pmatrix} \mathbf{e}_m^T \\ \mathbf{e}_1^T \\ \mathbf{e}_2^T \end{pmatrix} \quad (2.15)$$

$$
\mathbf{D}_\varphi := \begin{pmatrix} 1 & 0 & 0 \\ 0 & cos(\varphi) & sin(\varphi) \\ 0 & -sin(\varphi) & cos(\varphi) \end{pmatrix} \tag{2.16}
$$

here $\varphi \in [0, \pi]$. Note that $\varphi \in \{\pi/2, 3\pi/2\}$ actually correspond to a case where local cross helicity is zero and the case $\varphi \in \{0, \pi\}$ correspond to the case of maximum cross helicity. The magnetic field and velocity field are normalized in such a way that the magnitudes of initial kinetic and magnetic energies E^V, E^M, can be set to any required value by appropriate normalization factors. This procedure also ensures that the initial magnetic and velocity fields are divergence free.

An initial condition generated at a low resolution can be used for performing high resolution simulations with the help of some simple numerical operations. In this strategy, the initial setup is padded with the necessary number of additional zeros at time $t = 0$, without disturbing the initial energy budget. This procedure allows the switch from any lower resolution to any wanted higher resolution, without effecting the initial values of the physical quantities.

The table containing the exact initial conditions, is shown in chapter 4, table 4.1. The initial kinetic and magnetic energies for the forced turbulence case are chosen to be small in magnitude, while for decaying case they are chosen to be high. In the forced case, the forcing term contributes to the energy budget and hence to avoid unwanted increases in energies which could violate the CFL criterion or would evolve the system relatively slowly while satisfying the CFL; the initial energies are deliberately kept low. In the decaying case, no such external energy contribution is present, but the initial energy is decreasing with time. Hence, to study the system for a considerable time, in this decaying phase, the initial energy is kept high. The position of the initial velocity and magnetic fields are in the high k to intermediate k regions, to facilitate the study of inverse cascade. In the system, initial cross helicity is zero, while the fraction of magnetic helicity present is set to 0.5.

2.4.2   Forcing

In the forced case i.e. when $((\mathbf{F_v}$ and $\mathbf{F_b}) \neq 0)$ they are generated in a manner very similar to the way the initial conditions were obtained. First as in step-2 above

two orthonormal basis sets $\left\{ \mathbf{e}_{\mathbf{k}_1} := \frac{\mathbf{k}_1}{|\mathbf{k}_1|}, \mathbf{e}_{11/21}, \mathbf{e}_{12/22} \right\}$ are generated. Using these unit vectors the forcing terms are obtained as in equations (2.17 - 2.24). The parameters ϕ_1 and ϕ_2 essentially determine the amount of magnetic helicity and kinetic helicity generated by these forcing terms. ψ_1 and ψ_2 are the amplitudes of these forcing terms respectively. It is important to note that the terms $\mathbf{F_v}$ and $\mathbf{F_b}$ are only limited to a certain wave number region, i.e. the forcing is limited to a band of wave numbers $[k_{st}, k_{end}]$. The random numbers $\alpha_{1/2}$ and $\beta_{1/2}$ are as above in the range [0,1] and are generated every time step. The threshold values ψ_1 and ψ_2 have been decided in such a way that CFL is not violated, after some trial and error.

$$\mathbf{F_b} = \begin{cases} \psi_1 \frac{\mathbf{b_{k_1}}}{|\mathbf{b_{k_1}}|} & \text{if} \quad k_{st} \leq \mathbf{k}_1 \leq k_{end}, \\ 0, & \text{otherwise} \end{cases} \tag{2.17}$$

where

$$\mathbf{b_{k_1}} = \frac{(i\mathbf{k}_1 \times \mathbf{A}_1)}{|\mathbf{k}_1|} \qquad \text{while} \tag{2.18}$$

$$\mathbf{A}_{1_j} = \left\{ q_+(\phi_1)(\mathbf{e}_{11} + i\mathbf{e}_{12})_j e^{i2\pi\alpha_1} + q_-(\phi_1)(\mathbf{e}_{11} - i\mathbf{e}_{12})_j e^{i2\pi\beta_1} \right\} \tag{2.19}$$

and

$$H_1^M = \frac{1}{2}\mathbf{A}_1^* \cdot (i\mathbf{k}_1 \times \mathbf{A}_1) \qquad \text{the generated magnetic helicity} \tag{2.20}$$

$$\mathbf{F_v} = \begin{cases} \psi_2 \frac{\mathbf{v_{k_1}}}{|\mathbf{v_{k_1}}|} & \text{if} \quad k_{st} \leq \mathbf{k}_1 \leq k_{end}, \\ 0, & \text{otherwise} \end{cases} \tag{2.21}$$

where

$$\mathbf{v_{k_1}} = \frac{(i\mathbf{k}_1 \times \mathbf{A}_2)}{|\mathbf{k}_1|} \qquad \text{while} \tag{2.22}$$

$$\mathbf{A}_{2_j} = \left\{ q_+(\phi_2)(\mathbf{e}_{21} + i\mathbf{e}_{22})_j e^{i2\pi\alpha_2} + q_-(\phi_2)(\mathbf{e}_{21} - i\mathbf{e}_{22})_j e^{i2\pi\beta_2} \right\} \tag{2.23}$$

and

$$H_1^V = \frac{1}{2}\mathbf{A}_2^* \cdot (i\mathbf{k}_1 \times \mathbf{A}_2) \qquad \text{the generated kinetic helicity.} \tag{2.24}$$

It is possible, in principal, with this forcing setup, to have varying levels of magnetic and kinetic helicities generated and added to the system, over a small band of wavenumbers. But, here the studies concentrates on two cases: 1) maximum amount of magnetic

helicity being added with the kinetic helicity generated by $\mathbf{F_v}$ set to zero and 2) both of them added at their maximum values. These cases were chosen because primary focus of the studies is to understand how would the system respond to the injection of magnetic helicity alone, (inverse cascade and other parameters), at its maximum value. The secondary focus is to know whether and how this response changes with the injection of both the helicities at their maximum values. The description on the forcing terms is also seen in the table 4.1 of chapter 4. The maximum magnetic helicity that can possibly be added is a factor of unity and this is true for kinetic helicity too. The forcing terms are added in the equations (2.9) and (2.10) on the r.h.s. to the second term in each equation, within the square brackets. They are generated and added on the fly at every integration step, keeping up the random nature of the forcing at every point of time.

Currently existing simulations on the forced MHD turbulence have forcing mechanisms at small to intermediate wavenumbers $k \leq 3$ to 30. The resolutions of these simulations range from moderate (512^3) to small (64^3) values and the forcing mechanisms used are also different from those discussed above [8, 11, 9]. Hence, in this studies, the forcing is concentrated at large wavenumbers (see table 4.1), with an initial condition in the same region [the explanation on small, intermediate and large wavenumbers can been seen in chapter 3] and the simulations are carried out at what can be termed as high resolution i.e. 1024^3. This is the first such attempt in the MHD case to investigate inverse cascade process from extremely small scales to large scales, although many attempts exist on the inverse cascade of kinetic energy in 2D-hydrodynamic turbulence (see e.g. [37, 38]).

For generating the initial conditions, a simple random number generator with moderate repetivity is sufficient. But for generating the forcing, a random number generator with very long repetivity is needed as at every time step, large number of random modes in the range $k_{st} \leq \mathbf{k}_1 \leq k_{end}$, are required by the simulation. Thus two different random number generators are used for these two purposes. For the initial condition, the random number generator available with the Fortran compiler is used. For the forcing, a special random number generator developed by Nishimura and Matsumoto [39] is used.

2.5   Hyperviscosity and Reynolds Number

It has been observed that by using the equations (1.14) and (1.15) in their original form in direct numerical simulations, the needed scale separation in the spectra is not

achieved even at high resolutions. The scale separation (various scales and their defi-
nitions to be described in chapter 3) is necessary to study the so called inertial range,
without any dissipative pollution. Usage of large Reynolds numbers in the simulations
proves to be computationally expensive as linear resolution N and Reynolds number
are related by $N^3 \propto Re^{9/4}$ [40]. So the choice is either to limit the simulations to
low Reynolds numbers or wait for even more powerful computers. There are several
ways out of this problem. One of them is to use hyperviscosity. In this, the Lapla-
cian operator in the equations is replaced by higher order operators, simultaneously
the dissipation coefficients are replaced with the so called 'hyperviscous dissipation
coefficients'. With these two replacements the equations (1.14) and (1.15) now look as:

$$\partial_t \boldsymbol{\omega} = \nabla \times (\mathbf{v} \times \boldsymbol{\omega} - \mathbf{b} \times \mathbf{j}) + (-1)^{n-1} \hat{\mu}_n \nabla^{2n} \boldsymbol{\omega} \qquad (2.25)$$

$$\partial_t \mathbf{b} = \nabla \times (\mathbf{v} \times \mathbf{b}) + (-1)^{n-1} \hat{\eta}_n \nabla^{2n} \mathbf{b}, \qquad (2.26)$$

where n is the level of hyperviscosity. This is the final form of the forced equations
which are transformed into the spectral domain, and are used for the simulations. The
level of hyperviscosity has been chosen to be 8 for both the decaying and forcing 3D-
MHD turbulence simulations. This choice was driven by two reasons: 1) to compare
and extend the results from already existing work on decaying 3D-MHD turbulence
[13, 14], and 2) to achieve necessary scale separation (which was best seen at $n = 8$).
The parameter values used in the simulations can be seen in table 4.1, chapter 4.

The hyperviscosity approach limits the dissipation of the system to a small band of
wavenumbers in the large k region, thus allowing more degrees of freedom to participate
in the nonlinear dynamics of the system [41]. This approach comes with a disadvantage
that the spectra show a feature called 'bottle neck' which will be discussed in chapter
4.

Another problem that exists with this approach is the definition of Reynolds number.
Although there are some definitions of Reynolds numbers which include the effect
of hyperviscosity [20, 42, 40], there is no unique satisfactory definition for Reynolds
numbers in a hyperviscous setup (see chapters 3 and 4).

2.6   Simulation Program and Diagnostics

A highly parallelized FORTRAN 90 simulation code consisting of initial conditions,
integration and some diagnostics for the simulation of decaying 3D-MHD turbulence,
formed the starting point of this work, which is described in [20, 13]. The parallelization

uses the message passing interface (MPI) library [43]. In this code, the initial condition is modified so that it is situated in the large wavenumber region (see table 4.1 chapter 4). A subroutine representing the forcing mechanism described in the section 2.4.2 is included into the program. It is observed that in the forced case, the system feels the effects of the boundary at small wavenumbers, when the physical quantities like magnetic helicity inverse cascade. In order to avoid this unwarranted effect, an energy sink of the form $\alpha \triangle^{-2}$ multiplied with $\boldsymbol{\omega}$ and $\mathbf{b}$ individually, is added appropriately to the vorticity and induction equations. Here $\boldsymbol{\alpha}$ is a free parameter, set to 0.5 in all the forced 3D-MHD turbulence simulations. This sink works effectively for small wavenumbers and is relatively ineffective for larger wavenumbers, thus the boundary effects on the physical quantities are minimized.

All the simulations were run at Rechenzentrum Garching (RZG), in the Max-Planck Institute for Plasma Physics (IPP), Garching, on IBM pSeries super computers. Initially Power4 and Power5 series computers were used to run the programs. The given FORTRAN-90 code was already optimized for these computers. With the advent of the new Power6 series computers, the earlier optimizations to the code were not sufficient. Thus, the code was again optimized to utilize the hardware capabilities of these new machines, to the maximum possible extent. Without compromising on the precision and accuracy of the results, the code was adapted to the new machine and final production runs were run on this machine. There were no significant scaling issues for the code and it worked efficiently on Power4, Power5 and Power6 architectures, without any notable changes.

The output from the main integration program is the vorticity and magnetic fields, written in unformatted double precision mode, in spectral space, at specified intervals of time. Using these two fields, several diagnostics are also evaluated simultaneously. The diagnostics implemented in real space include integrated kinetic energy, magnetic energy, magnetic helicity, cross helicity among various other quantities (see chapter 4 for complete details). These are written out at every time step along with the time value in formatted single precision form. In the spectral space, several quantities are evaluated, kinetic energy, magnetic energy, cross helicity, magnetic helicity and kinetic helicity being some of them. These quantities are written in unformatted single precision form, along with the wavenumber, at each instance of time.

Using the spectral space data, some real space diagnostics like structure functions, PDFs, kurtosis and correlations are calculated by transforming the magnetic field and velocity field into real space and performing the necessary mathematical operations on

them. This part of the diagnostics is generally done as a post processing step and not as a part of the regular simulation. The spectral data and some real space quantities are plotted using 'IDL' and the structures are visualized using either AMIRA (a commercial visualization software) or Visit (an open source visualization software by Lawrence Livermore National Laboratory, USA). In 4th and 5th chapters these diagnostics are reported and interpreted.

Chapter 3

Phenomenologies of Turbulence, EDQNM and Intermittency Models

In this chapter three important phenomenologies existing currently, for the understanding of hydrodynamic and MHD turbulences: Kolmogorov(K41), Iroshnikov-Kraichnan(IK) and Goldreich-Sridhar(GS), are discussed first. The eddy damped quasi normal Markovian (EDQNM) approximation, a statistical closure theory, which uses a phenomenological eddy-damping rate, obtained from the IK phenomenology, as a crucial parameter, is explained next and finally intermittency models which are used in the course of this work are explained.

3.1   Phenomenologies

There are several approaches explaining the way turbulent structures form, nonlinearly interact and dissipate. Each such approach gives rise to a different phenomenological description of turbulent flows. In the context of this work, three phenomenologies are discussed (see next section): Kolmogorov, Iroshnikov-Kraichnan (IK) and Goldreich-Sridhar (GS) phenomenologies. Kolomogorov phenomenology has eddy interactions as the basic idea, where as IK phenomenology has Alfvén wave interactions as the central idea, as is the case with GS. Before these phenomenological ideas are explained, important terms which appear in them are discussed first. While doing so, some of the aspects of these phenomenologies are borrowed beforehand. The concentration of this section is only on defining scales, ranges, interactions and interaction time scales, which will later be used for a smooth description of the phenomenologies.

3.1.1   Terms useful in Understanding the Phenomenologies

Scales and Ranges

From the description of turbulence mentioned in the introduction and from its formal definition in section 1.1, it can be inferred that structures in turbulence i.e. eddies have wide range of sizes. To understand the physical processes in these eddies it is better to first classify them and then understand the interactions among various classes. Since size is a striking feature of these eddies over which they could be classified, they are in fact classified using this factor into large, intermediate and small-scale eddies. Here the word 'scales' approximately represents the wavelength considered in these structures (in turbulence studies the inverse of the wavelength i.e. wave number k is generally used). More formally it could be said that turbulent fluctuations are classified according to their spatial scales. It is to be noted that this classification is highly subjective to the system under consideration. That is for atmospheric turbulence, the large eddies might be of few tens or hundred of kilometers in size and the small-scale eddies may be of few meters, while for a industrial mixing process involving turbulence, the large-scale eddies could be only of few tens of centimeters and small scales restricted to few millimeters [15, 44]. Intermediate eddies would have sizes in between the largest and the smallest scaled eddies. It is the interaction between the eddies of various sizes, spanning over several orders of magnitude (in size), that makes study of turbulences interesting.

In general, energy is injected into the system typically by some large-scale gradient. In the numerical simulations of driven (forced) turbulence, conventionally the driving mechanisms are placed in these scales. Hence the range associated with these scales is termed as the 'drive range'. The large structures break into smaller and smaller structures due to the shear stresses. In this process the structures of intermediate scales are created which in turn under the shear stresses create the small scales, through several steps. Thus in an established turbulent flow, structures of all scales could be observed. In the small scales, dissipative processes like heat generation, radiation are dominant, which dissipate the energy of the structures. So this range is called the 'dissipation range'. During the transition from large scales to small scales and eventual dissipation, the structures exhibit self-similar behavior in some physical quantities, uninfluenced by either energy injection or dissipation. This range over which the self-similar behavior is present in the flow, is called the 'inertial range' where large-scale driving and small-scale dissipation are negligible. This range gets its name from the hydrodynamic

turbulence studies where in this range, the dynamics is supposed to be determined by the (nonlinear) inertia terms of the Navier-Stokes equation [15].

The above discussion can be summed up in the plot of energy spectrum of fig 3.1. Marked on this plot are the three ranges discussed above. Also shown are the scales involved. Additionally the plot has two terms 'direct cascade' with a arrow pointed towards the right and 'inverse cascade' with arrow pointed towards left. Cascade literally means 'flow' and going by it, 'direct cascade' would mean 'direct flow' and 'inverse cascade' an 'inverse flow'. But here in the context of this discussion, it would mean nonlinear 'spectral transport'. In the inertial range, it was observed that certain physical quantities transport down smoothly from large scales to small scales, without the influence of either of these two scales. Such quantities are said to have shown a direct cascade (for example: enstrophy: the surface integral of square of vorticity, in 2D-hydrodynamic turbulence [45, 46]). There exist some other quantities which spectrally transport in the reverse direction i.e. from small scales to large scales once again uninfluenced by either of the scales, in the inertial range. Such quantities are said to show an 'inverse cascade' behavior (for example kinetic energy in 2D-hydrodynamic turbulence). It is to be noted that the cascade is said to have taken place in either direction only if the flux of the quantity remained constant over the range of transport (i.e. the inertial range). This would also mean the ideal invariants discussed in section 1.1.3, would show a cascade by virtue of their invariance (i.e. they possess constant dissipation rates $\sim$ transfer rate), which results in constant flux. From the plot of fig 3.1 it can be seen that the energy in the turbulent structures can span many orders of magnitude between the small and the large scales (here it is close to 12 orders). In the inertial range because of the self-similar behavior of the physical quantity, the observed curve is a straight line with a specific slope in a double logarithmic representation. This constitutes a power law behavior for the cascading quantity (here total energy).

As mentioned above, conventionally the driving range is always present in the large-scale regions, but in this work the driving is placed in small-scale regions to understand the spatial and spectral influences of inverse cascade of magnetic helicity on other quantities of turbulent flow. In chapter 4 it will be shown that certain other quantities which do not show a cascade, also show power law behavior, under the influence of quantities that are cascading.

Often cascade processes are local (explained next) and for any wavenumber k, the range of interaction is within a range $[k/2, 2k]$ [47]. There are works which also state that properties like the magnetic helicity interact both locally and nonlocally as well

[10]. The meaning of local and nonlocal interactions is explained next.
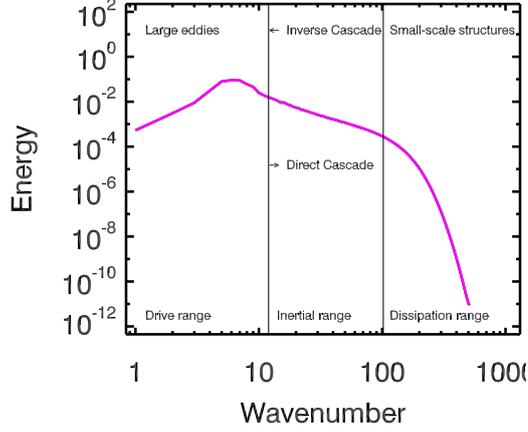
Figure 3.1: Spectrum of wavenumber Vs energy, taken from 1024^3 decaying turbulence simulations. The figure shows all the turbulent scales and ranges. Also shown are the directions of direct and inverse cascades, although the latter occurs only in the turbulent energy of 2D-hydrodynamic turbulence.

Local and Nonlocal Interactions

In section 2.2.1, a method to discretize the MHD equations, in the Fourier domain was shown. This discretization not only is useful in solving the equations numerically but also helps in applying the formalism of equilibrium statistical mechanics to continuum fluid turbulence [1]. In this process, ideal invariants are not strictly conserved. However, quadratic invariants are robust and rugged enough to survive this truncation. This property is based on validity of detailed conservation relation [1]. Before this property can be understood, an important property of the Fourier transform need to be mentioned. For any nonlinear term, e.g. a product of two functions $f(x)g(x)$ in configuration space, there corresponds a convolution integral in the Fourier space

$$\tilde{f} * \tilde{g} = \int \tilde{f}(\mathbf{p})\tilde{g}(\mathbf{k}-\mathbf{p})d^3\mathbf{p} = \int\int \tilde{f}(\mathbf{p})\tilde{g}(\mathbf{q})\delta(\mathbf{k}-\mathbf{p}-\mathbf{q})d^3\mathbf{p}d^3\mathbf{q}$$

where $\int \delta(\mathbf{k})d\mathbf{k}{=}1$, for the Dirac delta function $\delta(\mathbf{k})$. Here $\mathbf{k}$, $\mathbf{p}$, $\mathbf{q}$ are any three wave vectors. In the case of the discrete Fourier transform the convolution integral becomes a convolution sum. Thus nonlinear terms of the MHD equations of section 2.1, make three wavenumbers (i.e. three scales) appear in the Fourier space, defining a triad. By the detailed conservation relation it is meant that for elementary interaction between any triad of wave numbers $\mathbf{k}$, $\mathbf{p}$, $\mathbf{q}$ forming a triangle i.e. $\mathbf{k} + \mathbf{p} + \mathbf{q}{=}0$, a quadratic

invariant e.g. energy ($E_{\mathbf{k}}$) satisfies

$$\dot{E}_{\mathbf{k}} + \dot{E}_{\mathbf{p}} + \dot{E}_{\mathbf{q}} = T(\mathbf{k}, \mathbf{p}, \mathbf{q}) + T(\mathbf{p}, \mathbf{q}, \mathbf{k}) + T(\mathbf{q}, \mathbf{k}, \mathbf{p}) = 0,$$

where the dotted quantity represents the differentiation with respect to time and T represents the nonlinear transfer function. These interactions are called triadic interactions and can be inferred from the nonlinear terms of the MHD equations. These interactions are intrinsically related to the mathematical nature of the MHD equations. They are classified on the basis of the topology of the triangle formed from the three wave vectors, into local and nonlocal types [47](see fig 3.2). Local interactions are the ones occurring between the wave numbers of almost the same size i.e. $1/a \leq max\,\{p/k, q/k\} \leq a$, where $a = O(1)$. The nonlocal interactions are the ones which involve wave vectors of *different* sizes (in general one short wave vector and two long wave vectors), i.e. $k \ll p \sim q$ or $k \sim p \gg q$. The nonlocal interactions thus normally involve both the large and small scales.
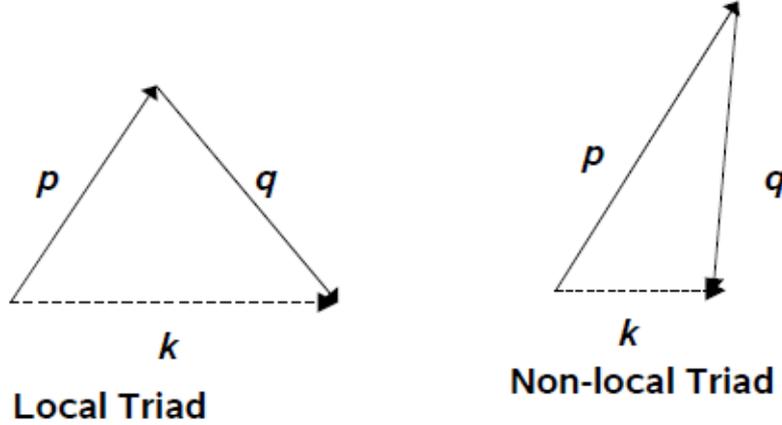
Figure 3.2: Local and Nonlocal triadic interactions adapted from [47].

Fluctuations and Interaction Time

As a result of the discussion on turbulent structures, it was established that the turbulent structures could be of various sizes and that they interact either locally or nonlocally. An attempt is being made to quantify these interactions. For this purpose, various properties of turbulent flow are statistically measured and the interaction time scales quantified based on these measurements. Here the example of velocity field $\mathbf{v}$ is used to illustrate this approach.

The turbulent velocity field is viewed as a superposition of eddies, characterized by a

spatial scale, $\boldsymbol{\ell}$. The associated velocity fluctuation is given by

$$\delta v_\ell \simeq [\mathbf{v}(\mathbf{r} + \boldsymbol{\ell}) - \mathbf{v}(\mathbf{r})] \cdot \boldsymbol{\ell}/\ell \qquad (3.1)$$

On small scales statistical isotropy of the field is often assumed. This assumption is valid because of the random mixing, the fluid forgets the anisotropic way the turbulence is generated [1]. So, the fluctuation in amplitude only depends on ℓ, thus allowing the characteristic eddy velocity to be defined as :

$$v_\ell \sim \left\langle \delta v_\ell{}^2 \right\rangle^{1/2}. \qquad (3.2)$$

In the inertial range, the statistical moments of the two-point probability distribution of the turbulent field, namely, structure function of order p, is defined based on the velocity fluctuations as:

$$S_p^v(\ell) \sim \langle \delta v_\ell \rangle^p \sim \ell^{\zeta_p}, \qquad (3.3)$$

where ζ_p is a constant, p-dependent scaling exponent. This family of constants characterize the intermittency of flow structures, by establishing a connection between inertial range and dissipative range physics (see [1] and section 3.3.2).

With the help of the spatial scale and the characteristic eddy velocity, the eddy turnover time τ_ℓ is now defined as:

$$\tau_\ell \sim \frac{\ell}{v_\ell}, \qquad (3.4)$$

here τ_ℓ is the typical time for a structure of size $\sim \ell$ to undergo a significant distortion due to shear stresses. As incompressibility has been assumed, it is also the time for the transfer of an excitation at one scale to other (i.e. cascade). It is achieved by the changes in the shapes of the structures, in order to preserve incompressibility. Typically in the case of a direct cascade (i.e. physical quantity getting transferred to smaller scales) e.g. for energy, the flux can be defined as:

$$\Pi'_\ell \sim \frac{v_\ell^2}{t_\ell} \sim \frac{v_\ell^3}{\ell} \sim \epsilon. \qquad (3.5)$$

Here ϵ is equivalent to the equation (1.23), the energy dissipation rate. Dimensional considerations were used in deriving the equation (3.5), in Kolmogorov phenomenology (for further details see [48]).

In the MHD case, the energy transfer is driven by shear Alfvén waves (central idea of

IK phenomenology) (see section 3.1.3 for an overview). If $\mathbf{b}_0$ is a magnetic guide field, which is either generated by the large energy-containing eddies or imposed externally, interacting with the eddies of size ℓ, then

$$\tau_A \sim \ell/b_0, \tag{3.6}$$

is the duration of collision of the counter-propagating shear-Alfvén wave packets. Note that since the magnetic field is measured in Alfvén speed units, $|\mathbf{b}_0| = b_0$ is the Alfvén speed as explained in section 1.1.1 τ_A is typically much shorter than τ_ℓ such that the change in amplitude during one scattering event is small and many such events are needed in order to produce a relative change of order unity [1].

In cases where a mean magnetic field is applied, the turbulent system is no longer isotropic, leading to anisotropic MHD turbulence (explained by GS phenomenology). In this case, the excitations are not uniformly transferred, but have a preferred direction. Typically if the wave vector $\mathbf{k}$ is resolved into its parallel and perpendicular components, $k_\parallel$ and $k_\perp$ respectively, small-scale modes are primarily excited perpendicular to the magnetic field [1]. In this set up the time scales corresponding to the two components of $\mathbf{k}$ are different and are defined by

$$\tau_A \sim \ell_\parallel/v_A \tag{3.7}$$

$$\tau_{\ell_\perp} \sim \ell_\perp/z_{\ell_\perp}, \tag{3.8}$$

with $\ell_\parallel$ and $\ell_\perp$ being the length scale ℓ resolved in parallel and perpendicular directions, v_A the Alfvén velocity and $z_{\ell_\perp}$ the Elsässer field in the perpendicular direction. τ_A is called Alfvén time and $\tau_{\ell_\perp}$ the eddy turnover time of the system.

3.1.2 Kolmogorov-Richardson Phenomenology

This model which is abbreviated as K41, is mainly useful in explaining phenomena in hydrodynamic turbulence. Some of the important predictions of this phenomenology appear to be true even for the MHD case, though the interaction mechanisms leading to such results are completely different from the hydrodynamic case and are not well understood. The important aspects of this theory in the hydrodynamic case are described below, following the explanation given in [48].

The turbulent eddies form a spatial hierarchy and the kinetic energy is transferred

to small scales by the unstable eddies which break into smaller fluctuations. Under the assumption of quasi-stationarity condition, the spectral energy flux, in the inertial range is scale-independent and is equal to the rate of energy dissipation as in (3.5). With the help of this relation, the velocity scaling and the 4/5-law [48] (one of the very few exact results in turbulence theory) can now be a determined as

$$v_\ell \sim (\epsilon \ell)^{1/3} \tag{3.9}$$

$$S_3^v(\ell) = -\frac{4}{5}\epsilon \ell. \tag{3.10}$$

Using (3.10), a relation $v_\ell^3 \sim \ell$ is obtained and also the generalized version of (3.10) can now be written as:

$$S_p^v(\ell) \sim (\epsilon \ell)^{p/3}. \tag{3.11}$$

In the spectral space, where $k \sim \ell^{-1}$, for the hydrodynamic case, the angle-integrated energy spectrum E_k is given by

$$E_k = \frac{1}{2} \int d^3 k' \delta(|\mathbf{k'}| - k)|v_{\mathbf{k'}}|^2, \tag{3.12}$$

with $\mathbf{v_{k'}}$ being the Fourier counter part of the velocity $\mathbf{v}$.

With the relation $v_\ell^2 \simeq k E_k$, the scaling exponent of $S_2^v(\ell)$, ζ_2 and the inertial range scaling of $E_k \sim k^{-\alpha}$ can be linked to get a relation between the two exponents as $\alpha = -(1 + \zeta_2)$. This particular relation yields the most important K41-spectrum in incompressible hydrodynamic turbulence

$$E(k) \sim C_K \epsilon^{2/3} k^{-5/3}, \tag{3.13}$$

with $C_K \approx 1.6$ being Kolmogorov constant. It is to be noted that this power law could also be arrived at, using only the dimensional analysis of the relation $E_k \sim \epsilon^\alpha k^\beta$, where α and β are the constants to be determined. This spectral relation has been verified experimentally and also seen in several natural phenomena like atmospheric turbulences and ocean wave turbulences [48].

As seen in figure 3.1, the inertial range is limited to a certain band of wavenumbers. As intermediate range eddies hierarchically break into smaller and smaller eddies, a stage is reached when the self-similar behavior of the system starts to fail and energy dissipation is no longer negligible. A steep gradient of energy dissipation rate is seen in high k

region, marking the beginning of dissipation range. In this range dissipative processes (e.g. heat radiation etc.) slowly take over and dominate the system. The scale at which the dissipation ($\sim v_\ell^2 \hat{\mu}/\ell^2$) starts to dominate over nonlinear transfer(v_ℓ^2/τ_{NL}), marks the beginning of dissipation range and is called Kolmogorov dissipation scale ℓ_D. The kinetic Reynolds number is associated with kinematic viscosity, a parameter characterizing the dissipative effect in a flow. Thus the dissipation scale estimate could be used to define the Reynolds number in a turbulent system following the below set of arguments:

$$\frac{\hat{\mu}}{\ell^2} \sim \tau_{NL}^{-1} = v_\ell/\ell \sim (\epsilon\ell)^{1/3}/\ell \qquad \text{yielding} \tag{3.14}$$

$$\ell_D = \left(\frac{\hat{\mu}^3}{\epsilon}\right)^{1/4} \tag{3.15}$$

as $\hat{\mu} = Re^{-1}$. In the case where hyperviscosity is used, the equation (3.14) is modified as:

$$\ell_D = \left(\frac{\hat{\mu}_n^3}{\epsilon}\right)^{1/(6n-2)}, \tag{3.16}$$

where n is the level of hyperviscosity and $\hat{\mu}_n$ the hyperviscous diffusion coefficient.
The Kolmogorov predictions are restricted to hydrodynamic turbulence, but in many numerical simulations of magnetohydrodynamic turbulence, the energy spectra show a -5/3 power law behavior (see [13, 49, 8, 36]). But the interaction mechanism that allowed the flow to reach this state, where this power law could be seen, is not well understood even after several attempts (see the discussion in Goldreich-Sridhar phenomeonology below).

3.1.3   Iroshnikov-Kraichnan Phenomenology

Magnetohydrodynamic turbulence, apart from the velocity field has additionally a magnetic field too. The flows associated with MHD could not be satisfactorily explained by the K41. Iroshnikov and Kraichnan independently developed a phenomenology, which is called IK phenomenology, which takes into account both the fields, while trying to understand the turbulent flows. The important features of this theory are explained briefly here following [1, 20]. The fundamental fact on which this theory is based is *only oppositely directed Alfvén waves interact* in incompressible MHD. The other important assumptions in this theory are: 1) turbulence is statistically isotropic and 2) the dominant interactions are those which couple three waves, implicitly (triadic interactions).

In this model the energy transfer is driven by Alfvén waves. The energy is redistributed between different length scales by nonlinear scattering of colliding Alfvén-wave packets, along a magnetic field line, traveling in opposite directions. Here the Elsässer quantity z_ℓ is used in defining the major relations. Elsässer variables have a special property that $\mathbf{z}^\pm = \mathbf{0}$ are exact nonlinear solutions of the ideal incompressible MHD equations, representing Alfvén wave pulses on a mean magnetic field. There is no distinction made between $\mathbf{z}^-$ and $\mathbf{z}^+$, [1] as the mean alignment between the magnetic and velocity fields is restricted to small values. The Alfvén effect (generation and attenuation of Alfvén waves through coupling of magnetic and velocity fields), leads to approximate equipartition of magnetic and kinetic energies at small scales. If a magnetic guide field $\mathbf{b_0}$ is present in the system, and if the perturbations δv and δB are small compared to b_0 then it is seen that $\delta v \simeq \pm \delta B$. The interaction time is given by (3.6). The nonmagnetic eddy-distortion time $\tau_\ell \sim \ell/\delta z_\ell$ is much longer than the interaction time τ_A.

With the above inputs, the IK phenomenology follows the same pattern as K41 phenomenology, but with a small difference. The difference is that it distinguishes two dynamic time scales, the Alfvén time and the time for distortion of a wave packet by a counter propagating eddy, both assumed to have same scale ℓ. In general $\tau_A \ll \tau_\ell$. Since the interaction time of two oppositely propagating wave packets is τ_A, the change of amplitude $\triangle \delta z_\ell$ during a single collision of two wave packets is small and is given by

$$\frac{\triangle \delta z_\ell}{\delta z_\ell} \sim \frac{\tau_A}{\tau_\ell} \ll 1.$$

Because of the random nature of the process, the number of elementary interactions needed to produce a relative change in amplitude of order unity is $N \sim (\frac{\delta z_\ell}{\triangle \delta z_\ell})^2$ [1]. Hence the energy transfer time is defined by $\tau_{in} \sim \tau_\ell^2/\tau_A$ and if $\tau_\ell \to \tau_{in}$ then, the dissipation rate here is defined by

$$\epsilon \sim \delta z_\ell^4 \tau_A/\ell^2. \tag{3.17}$$

This leads to the non-intermittent inertial range scaling

$$S_p^z(\ell) \sim (\epsilon b_0 \ell)^{p/4}, \tag{3.18}$$

---

[1]This is possible by restricting to consider MHD turbulence with a small **v-b** alignment, $\sigma = \frac{H^C}{E^K E^M}$ where H^C is the cross helicity, E^M is the magnetic energy and E^K is the kinetic energy.

which in turn leads to the spectral relation for total energy

$$E(k) \sim C_{IK}(b_0 \epsilon^{1/2}) k^{-3/2},$$ (3.19)

with a dissipation length

$$\ell_{IK} = \left(\frac{b_0 \hat{\eta}^2}{\epsilon} \right)^{1/3},$$ (3.20)

here $\hat{\eta} = Rm^{-1}$. For hyperviscous case putting $b_0 \sim v_A$ the dissipation length is given by

$$\ell_{IK} = \left(\frac{\hat{\eta}_n^2 v_A}{\epsilon} \right)^{1/(4n-1)}.$$

The dissipation rate ϵ can also be obtained in an other way through decorrelation time τ_k using dimensional analysis [1] as

$$\epsilon \sim \tau_k E_k^2 k^4,$$ (3.21)

where the decorrelation time occurs on the Alfvén time scale $\tau_k \sim \tau_A \sim (kv_A)^{-1}$, in the MHD case.

The IK phenomenology relies on the isotropic nature of the turbulent fields. But the magnetic field does not satisfy Galilean invariance and hence this assumption is not valid. Although IK phenomenology appears to explain many aspects of the MHD turbulence, the anisotropy that sets in because of the mean magnetic field remains a major challenge. However, the triad interaction assumption, which is fundamental to this phenomenology forms the basis for a stochastic description of 3D-MHD through eddy damped quasi normal Markovian (EDQNM) approximation [7] (to be discussed in the next section).

The IK phenomenology is valid in 2D-MHD turbulence as several numerical simulations confirmed the scaling law for the energy and the dimensions of the level surfaces of current are consistent with equation (3.18) (see section 8.2.3 of [1] for more details).

3.1.4   Goldreich-Sridhar Phenomenology

Goldreich and Sridhar take into account the anisotropic nature of the magnetic field, while formulating the phenomenology for MHD turbulence. Their phenomenology is explained briefly here following [50, 51, 20, 1]. In this phenomenology, turbulence is treated in two variants, namely, strong MHD turbulence and intermediate (weak) MHD turbulence. The wave vector **k** is split into its parallel and perpendicular components

with respect to the magnetic field. The fundamental assumption in this phenomenology is that there exists a *critical balance* between τ_A and τ_ℓ defined as above in IK phenomenology, i.e. $\tau_A \sim \tau_\ell$. Which means that the magnetic field deformations associated with the field-perpendicular turnover time τ_ℓ, propagate with Alfvén speed b_0, over a parallel distance $\lambda = b_0 \tau_A$, in the same time. Also it was deduced that the nonlinear energy flux is much weaker along the direction of the magnetic field.

Thus from the strong and intermediate MHD turbulence arguments, power law behavior similar to the K41 spectra in the perpendicular direction and a new power law behavior in the parallel direction, respectively, were predicted. The derived power law behaviors are stated below

$$E(k_\perp) \sim \epsilon^{2/3} k_\perp^{-5/3} \qquad \text{and} \qquad E(k_{||}) \sim k_{||}^{-2} \qquad (3.22)$$

However it was seen from the numerical simulations of strong MHD turbulence that, this 5/3 law is not observed and instead a 3/2 behavior is seen [52]. This prompted Boldyrev [53] to suggest that an increasingly parallel polarization of Alfvénic fluctuations results in weakening of nonlinear turbulent interaction and this results in the 3/2 power law of the perpendicular spectrum.

Recently, Gogoberidze [54] had modified the IK model for anisotropic incompressible MHD which yields a 3/2 spectrum in the perpendicular direction for the energy spectrum. In the context of this work, neither IK or GS phenomenologies are directly relevant, but due to their importance for MHD turbulence, they have been briefly introduced here. They are also not capable of explaining all the features observed in numerical simulations and observations inspite of the recent modifications, mentioned above. In fact, no unique phenomenological model exists for this purpose. Explaining all the features of 3D-MHD turbulence, using an unique phenomenological model is currently an important area of research.

3.2   EDQNM

Eddy damped quasi normal Markovian approximation (EDQNM) is a quantitative statistical theory on MHD turbulence, described in detail in the seminal work of Pouquet et al..(see [7]). Here a brief overview of this theory, its advantages and disadvantages, using the same notations and symbols as in [7],[15]and [31], are presented in this section.

3.2.1 Assumptions and Equations

General Framework

EDQNM is a stochastic model with two-point closure, since it deals with correlations in two different (points of the space) wave numbers (k, k') in Fourier space, that satisfy $k + k' = 0$ [15]. In the process of adapting EDQNM to MHD, the following assumptions are made: a) magnetic and velocity fields are homogeneous and isotropic (but helical) random fields, b) initial magnetic field is statistical invariant under sign reversals (i.e. **b**= -**b**), so that cross helicity ($< \mathbf{v} \cdot \mathbf{b} >$) is always zero as the MHD equations preserve this invariance.

Let a MHD equation be written symbolically as

$$du/dt = uu$$

where u stands for unknown functions (**v** or **b**) and uu stands for all nonlinear terms. Assuming the first moment $< u >$ to be zero and dropping dissipation and forcing on the ground that they do not pose any specific closure problems, second and third order moments for nonlinear terms can be written as:

$$\frac{d < uu >}{dt} = < uuu >$$

$$\frac{d < uuu >}{dt} = < uuuu > .$$

(3.23)

The idea of the *quasi-normal* approximation is to simply assume that fourth and other higher even order cumulants are zero, without any assumption on the third order moments. This allows to close the problem at fourth order moments, which can now be replaced with corresponding Gaussian values. This results in splitting the fourth order moments into three terms involving second order moments as $< u_1 u_2 >< u_3 u_4 >$ in a cyclic manner, which can be simply represented by $\sum < uu >< uu >$. It was realized that this approximation leads to appearance of negative energy spectra in the energy-containing eddies range, which is an unacceptable fact, from the physics point of view. This behavior was attributed to a build-up of too high third order moments on the l.h.s. of equation (3.23) above.

To overcome this problem, on the l.h.s. of equation (3.23) a damping term proportional

to μ_{kpq} [2], which has dimension of the inverse of time and is a characteristic *eddy-damping rate* of the third order moments associated to the triad $(\mathbf{k}, \mathbf{p}, \mathbf{q})$, is introduced as:

$$\mu_{kpq}\frac{d<uuu>}{dt} = \sum <uu><uu>.$$

For isotropic turbulence, this parameter is given by $\mu_{kpq} = \mu_k + \mu_p + \mu_q$ to give quantitative predictions, where each of the sub-constituents have a specific meaning (see next subsection for the specific description of the terms).

Even at this stage the positiveness for energy spectrum of the energy spectrum is not guaranteed in all situations, which has come to be known as 'realizability' criterion. Thus to achieve this, further modifications to equation (3.23) are made by introducing *Markovianization*. For Markovianization it is assumed that the third moment responds to the instantaneous product of the second moments [31] as opposed to higher order moments. The resultant third moment is substituted back in r.h.s. of equation (3.23) to obtain

$$\frac{d\langle u(t)u(t)\rangle}{dt} = \theta(t)\langle u(t)u(t)\rangle\langle u(t)u(t)\rangle, \tag{3.24}$$

where the triad-relaxation time $\theta(t)$ is defined by

$$\theta(t) = \int_0^t d\tau \exp\left\{-\int_\tau^t \mu_{kpq}(s)ds\right\}. \tag{3.25}$$

τ in the above equation represents a time in the past, indicating memory property of the Markovianization. But for short times $\theta(t) = t + O(t^2)$ and for stationary case, $\theta = \mu_{kpq}^{-1}$ (θ is also represented as θ_{kpq}). The eddy damping operator μ_{kpq} may be obtained either from a phenomenological study or from the analysis of an auxiliary problem. It is very important to find the appropriate μ_{kpq} for MHD turbulence. The realizability (the positivity of energy spectra) is ensured in this approach.

The general form of EDQNM equations with forcing term F (a prescribed forcing tensor), is now written as:

$$d\langle u \otimes u\rangle/dt = 4\theta\left\{L(u,u)(u,u) + L(L(u,u),u) \otimes u + u \otimes L(u,L(u,u))\right\}$$
$$+\langle L_0 u \otimes u\rangle + \langle u \otimes L_0 u\rangle + F, \tag{3.26}$$

---

[2]Please do not confuse this term with kinematic viscosity, which has the same basic symbol μ. Note that it **never** appears in this whole work with any of the subscripts k, p, q. Any other symbol could have been chosen, but since uniformly throughout all the literature, for eddy-damping rate this is the symbol. Hence here too, the same convention is followed.

where $L(.,.)$ collects all the quadratic terms, L_0 represents the linear dissipative terms. The operator $\otimes$ represents the dyadic or outer product of two vectors. Here on the r.h.s., in the first three terms, the inner most two $u's$ have the same moments as does the outer most two $u's$, independently, and hence are linked in pairs. The MHD turbulence is assumed to be homogeneous, isotropic and helical. The cross helicity is assumed to be zero and magnetic Prandtl number is set to unity. With these assumptions in place, the four EDQNM integro-differential equations are for kinetic energy E_k^V, magnetic energy E_k^M, kinetic helicity H_k^V and magnetic helicity H_k^M, and relate these four quantities to several other quantities involved in the turbulent dynamics. A representative of these is given below in some detail.

EDQNM Equation for Magnetic Helicity

The equation for magnetic helicity in the EDQNM frame work is shown below:

$$\left(\frac{\partial}{\partial t} + 2\eta k^2\right) H_k^M = \tilde{F}_k^M + \int_{\triangle k} dp dq \theta_{kpq} \left(T_{V\tilde{M}}^{\tilde{M}} + T_{\tilde{V}M}^{\tilde{M}} + T_{M\tilde{M}}^{\tilde{M}} \right). \tag{3.27}$$

In this equation, on the l.h.s. the first term represents the time evolution of the quantity and the second term represents the dissipation effects on the quantity, with η being the 'magnetic diffusivity'. On the r.h.s., the term $\tilde{F}_k^M$ represents the prescribed injection spectra of magnetic helicity or simply the forcing. It is an element of the set of four forcing terms which satisfy realizability conditions, with their respective counterparts. $\mathbf{k}, \mathbf{p}$ and $\mathbf{q}$ are the three wave vectors which form a triangle, with $\triangle_k$ being a subset of the $p - q$ plane i.e. $(k = p + q)$. The time θ_{kpq} is characteristic of the relaxation of the nonlinear energy flux involving the modes k, p and q and can be approximated as

$$\theta_{kpq} = \frac{t}{1 + \mu_{kpq}}, \tag{3.28}$$

where μ_{kpq} is a phenomenological expression for the damping rate of the flux by higher order moments,with $\mu_{kpq} = \mu_k + \mu_p + \mu_q$, ensuring energy conservation. A straight forward choice for damping rates ensuring the conservation of all the quadratic invariants, is $\mu_{kpq} = \tau_{NL}^{-1} + \tau_A^{-1} + \tau_D^{-1}$, which combines all the three processes that are present in the turbulent dynamics. τ_{NL}^{-1} represents the time scale for deformation of field lines by turbulent motions and is given by $\tau_{NL}^{-1} \sim \ell/\sqrt{v_\ell^2 + b_\ell^2} \sim (k^3 E_k)^{-1/2}$. τ_A represents the interaction time scales of colliding shear Alfvén waves given by (3.6) and finally τ_D^{-1} represent the viscous and joule dissipation time scales, thus $\tau_D \sim (\mu + \eta)^{-1} k^{-2}$. Under the

realistic conditions, diffusion is associated with the longest time scales of the turbulent system. Thus when $t \gg \tau_D$, the estimated value for θ_{kpq} is $\theta_{kpq} \simeq \mu_{kpq}^{-1} \simeq min(\tau_{NL}, \tau_A)$. The interaction terms on the r.h.s. of equation (3.27) are given by:

$$T_{V\tilde{M}}^{\tilde{M}} = kp^{-1}q^{-1}h_{kpq}(k^2 H_p^M E_q^V - p^2 E_q^V H_k^M) \qquad (3.29)$$

$$T_{\tilde{V}M}^{\tilde{M}} = kp^{-1}q^{-1}h_{kpq}(k^2 p^{-2} H_p^V E_q^M - p^2 k^{-2} H_q^V E_k^M) \qquad (3.30)$$

$$T_{M\tilde{M}}^{\tilde{M}} = p^2 k^{-1} e_{kpq} H_q^M E_k^M - kpq^{-1}j_{kpq}E_q^M H_k^M \qquad (3.31)$$

In the above set, terms j_{kpq}, h_{kpq}, e_{kpq} are the geometric coefficients and are defined as:

$$j_{kpq} = pk^{-1}z(1 - x^2) \qquad (3.32)$$

$$h_{kpq} = (p/k)(z + xy) = (1 - y^2) \qquad (3.33)$$

$$e_{kpq} = x(1 - z^2). \qquad (3.34)$$

These geometric coefficients are the directional cosines of the triangle formed by the wave vectors $\mathbf{k}, \mathbf{p}, \mathbf{q}$ and these coefficients also ensure solenoidality of the turbulent fields [18]. In other three EDQNM equations, several such geometric coefficients exist, which are also defined in a similar manner as shown in equations (3.32 - 3.34). The terms like E_q^M, H_p^V etc.. represent the physical quantity at a particular wavenumber, i.e. H_p^V is the kinetic helicity at the wavenumber p. The product terms of these quantities represent the non-linear interactions among them due the assumed triadic interactions of the turbulent fields. The terms on the r.h.s. represent the nonlinear flux density contributions.

The above description was limited to one EDQNM equation, in its totality, for more description and details see [7]. The complexity involved in these equations, prevents easy theoretical investigation, but numerical simulations of these equations can be seen in [7]. The equations's structure allows them to be splitted in such a manner that local and nonlocal effects could be individually studied. This is one of the major advantages of EDQNM method.

3.2.2   Summary of Important Results of 3D-MHD Turbulence Obtained from EDQNM

The unique way in which the MHD equations have been approximated in EDQNM, in terms of physical quantities that are not explicitly seen at first glance from the

original equations, help in the understanding of some important physical phenomenon like the Alfvén effect and inverse cascade of magnetic helicity, to name a few. Some of them are briefly explained here.

Alfvén Effect

Kraichnan [55] noticed that in the presence of large-scale magnetic energy, Alfvén waves can bring small-scale velocity and magnetic energies to equipartition and relax triple correlations (due to triadic interactions) in a time which may be shorter than the local eddy turnover time [7]. This can be illustrated using the EDQNM equations. For this, EDQNM equations are expanded to represent local and nonlocal effects and all the nonlocal effects are ignored. In the next step, only terms that represent large-scale interactions are retained. With these two operations, the effect of random Alfvén waves on the kinetic and magnetic energy spectra can be analyzed. When the Alfvén contribution to the eddy-damping rate dominates the self-distortion and dissipation terms, it will essentially represent the r.m.s. magnetic field (b_0), which is also the typical group velocity of the Alfvén waves. Under the action of random Alfvén waves, it is observed that magnetic and kinetic energy spectra relax to equipartition, in a time of order of $(kb_0)^{-1}$, as predicted by Kraichnan [55]. Also it was observed that the helicity spectra relax to equipartition given by the relation

$$H_k^V = k^2 H_k^M. \tag{3.35}$$

When the energy spectra and helicity spectra deviate from equipartition, the difference between them gives rise to residual energy and residual helicity, given by $E_k^R = E_k^V - E_k^M$ and $H_k^R = H_k^V - k^2 H_k^M$ respectively. When these two differences relax to zero, the effect is called 'Alfvén' effect.

Helicity or α Effect

The above discussion was centered around the large-scale effects alone. Since EDQNM equations allow the study of effects at various scales separately, now only the small-scale effects are considered.

The same treatment of expanding the equations in terms of local and nonlocal effects, retaining only the local terms and finally ignoring the large-scale effects results in a

small-scale phenomenon known as the 'torsality' α_k^R, which is given by:

$$\alpha_k^R = -\frac{4}{3} \int_{k/a}^{\infty} dq \theta_{kpq} H_q^R. \tag{3.36}$$

Thus when α_k^R is known, it is easy to integrate the equations representing the small scale effects (see equations 3.16 and 17 of [7]). This results in the exponential growth (decay) of magnetic energy and magnetic helicity, at a rate given by $k|\alpha_k^R|$. The important conclusion from this study is that the small-scale residual helicity destabilizes the large-scale magnetic energy and magnetic helicity. This is similar to the 'helicity or α effect'. Both the kinetic and magnetic helicities produce a destabilizing effect and it is the difference, as measured by the residual helicity, that acts as a true driver of instability in the flow. This instability is responsible for the 'inverse cascade', of magnetic helicity and eventually the large-scale magnetic structure. The helicity effect could also give a rate of growth of mean magnetic field, when such a field is present. Such an effect is very important for the production of a α dynamo [7].

Inverse Cascade of Magnetic Helicity and Inertial Range

The physics of inverse cascade of magnetic helicity can be explained from the above discussed two effects, in a MHD turbulent system forced at small-scale. It is explained in steps below:

- 1) The helicity injection at a wavenumber say $k \sim k_E$, produces a growth of both magnetic energy and magnetic helicity in a small wavenumber $k \sim (1/2)k_E$, through the 'helicity effect'.

- 2) The growing magnetic energy at this wavenumber, reduces the residual helicity near k_E by the Alfvén effect, while the growing magnetic helicity at $(1/2)k_E$, destabilizes the small wavenumbers.

- 3) It is easily noticeable, that the steps 1 and 2 could go on and on to drive the magnetic helicity spectra into ever smaller wave numbers, resulting in what is called the 'inverse cascade of magnetic helicity'.
  From the numerical simulations of EDQNM equations for forced 3D-MHD turbulence, it was observed that the magnetic helicity shows a k^{-2} power law behavior in its spectra while magnetic energy showed a k^{-1} power law behavior. The verification or conformation of these power law behaviors, in high resolution DNS is

one of the key motivations to perform this study.

Other aspects

Importance of EDQNM

The EDQNM equations are a flexible set having equations and parameters that allow the study of interactions on local and nonlocal scales separately, without disturbing each other. This property also indicates the robustness of the equation set. A dimensional study of these equations together with the results from the direct numerical simulations, can be used to gain further insights into the properties of MHD turbulence. For this purpose stationarity is assumed. Further the analysis is restricted to inertial range thus eliminating the influence of the driving or dissipation scales. Finally a dynamical equilibrium between the local and nonlocal effects (discussed above), which tends to result in an energy equipartition between the velocity and magnetic fields, is also assumed [18]. In [14] using such assumptions, phenomenological description of residual energy has been obtained. Further, numerical simulations of the EDQNM equations could be conducted. In these simulations, very high values for Reynolds numbers could be achieved, larger than what are possible in direct numerical simulations [31]. Using the EDQNM equations, systems like nonlinear turbulent dynamo have been studied [7]. The correlations between velocity and magnetic fields have also been studied using a modified set of EDQNM equations [56, 57]. The set of equations have been used to verify, prove or disprove several aspects of 3D-MHD turbulence for example: a) verification of power law behavior for total energy spectra in 3D-MHD turbulence (through the numerical simulations of EDQNM), b) existence of a power law behavior for quantities like the magnetic helicity and magnetic energy (through numerical simulations and phenomenological arguments) and c) a comment on the scales of the magnetic structures (based on pure theoretical arguments backed by numerical simulations). With all these positives, there do exist few negative aspects for the EDQNM equations.

Shortcomings of EDQNM

The major shortcoming of EDQNM is that the eddy-damping parameter, so crucial to the equations is set from outside the system. As it is also a closure theory it suffers from general weaknesses of closure theories and also suffers from their constraints. Some of these are a) the value of the Kolmogorov constant is not

been determined using this model. b) real space structures and intermittency aspects of the turbulent flow are not explained because of the Gaussian assumption of the fields's fourth and higher order moments. c) Overemphasis is given to the strength of nonlinear interactions, ignoring the fact that the local rearrangements of the fields, often give rise to a depletion of nonlinearity. d) The random character of the turbulence is over emphasized in closure theories. Anisotropic nature of the MHD turbulence is hard to be explained using closure theories, though not impossible [1]. Mean square of the random variable can have a negative value, violating the realizability.

Despite these short comings, the already mentioned flexibility and robustness offered by the EDQNM equations is what is most attractive to work with. The focus of this work will be on applying dimensional analysis to EDQNM equations together with some of the results from DNS studies of MHD equations (see section 4.5) to gain further insights into the properties of MHD turbulence.

3.3   Intermittency Modeling

3.3.1   Structure Functions

The phenomenological models discussed in the section 3.1 explain the spectral properties of the turbulent flows assuming the spatial structures to be self-similar. This assumption implies that the spatial distribution of turbulent structures is space-filling and statistically uniform. It also means that the energy dissipation is homogeneously distributed in space. Observational data of turbulent solar wind, atmospheric turbulence and experiments do not comply with this assumption. The DNS data in hydrodynamic as well as MHD turbulence including the compressible and incompressible cases in the latter, also do not agree with this assumption. Kolmogorov's refined similarity hypothesis tries to explain this deviation from self-similarity by the spatial distribution of dissipative turbulent structures [48]. In this hypothesis the equation (3.11) is written in terms of the local energy dissipation ϵ_ℓ which is assumed to scale self-similarly, in a sphere of radius ℓ and reads as:

$$S_p^v(\ell) \sim < \epsilon_\ell^{p/3} > \ell^{p/3}. \tag{3.37}$$

The equation (3.37), which is a modified form of the equation (3.11), expresses the fact that in a turbulent flow small regions of intense dissipative structures are

embedded into a weakly dissipative environment making the associated spatial distribution intermittent [58]. Hence this modified equation complies with the observations to a large extent. The K41 and IK models predict the isotropic structure function exponents as $\zeta_p^{K41} = p/3$ and $\zeta_p^{IK} = p/4$ respectively, without taking intermittency into consideration. The actual behavior of these exponents is only understood by examining various orders of structure functions. Thus in a plot of order p Vs ζ_p it is observed that the structure function exponents deviate from linearity (a behavior expected from the isotropy assumption of the structure function exponents), as the order of structure function increases. It has also been noticed that the statistical convergence of associated averages, necessary for calculating the structure functions, deviate pronouncedly for higher order structure functions. This is because their reaction to extreme fluctuations is more stronger. Thus the associated statistical noise is so high that it becomes very difficult to ascertain an exponent value to these higher order structure functions. To overcome this, a low order structure function, whose exponent value is known to a greater degree of certainty is used as the base. All other structure functions are now referred to this new base. This process is called 'extended self similarity' approach or ESS (see [1] and references thereof). This approach stems from the idea that structure functions of different order, deviate, qualitatively in the same way from their ideal shape. Hence if S_r is the base or reference structure function with a known scaling exponent ζ_r, then the scaling exponent of any other structure function S_p, can be determined using the following relation:

$$S_p(S_r(\ell)) \sim (\ell^{\zeta_r})^{\zeta_p} \sim \ell^{\xi_{p,r}}, \tag{3.38}$$

which yields the absolute scaling exponent as

$$\zeta_p = \xi_{p,r}/\zeta_r. \tag{3.39}$$

3.3.2 Intermittency Modeling

Physical conclusions can be drawn from the scaling exponents obtained from ESS approach, only if they are compared with phenomenological models and are found to be in good agreement with those model values (see e.g. [1, 14, 18]). A plot of these scaling exponent values with their respective order is drawn. This curve is compared with the model curves of intermittency. Such a comparison helps in

understanding the dimensionality and nature of the structures in the turbulent flow.

Although many intermittency models exist in the hydrodynamic case [48], as of now only one of them, the She - Lévêque (or the Log-Poisson) model, has been successfully adapted to MHD turbulence. In its most general form the equation of this model is given by the equation (3.40).

$$\zeta_p = (1 - x)p/g + C_0(1 - (1 - x/C_0)^{p/g}) \tag{3.40}$$

It has three parameters x, g and C_0 which are determined on physical grounds. The non-intermittent scaling, $< v_\ell > \sim \ell^{1/g}$, is used to determine g (for K41 it is 3 and for IK it is 4). The parameter C_0 can be thought of as co-dimension (see footnote of section 5.3 for an explanation on co-dimension) of a set of singularities of strength ℓ^{τ_∞} which is equivalent to the most singular dissipative structures. The parameter x is related to the dissipation rate in these structures $t_\ell^\infty \sim \ell^x$ and is normally given in terms of g as $x = 2/g$ (see e.g.[1, 14, 18] for more detailed discussion).

Equation (3.40) offers to explore and find the closest model possibly matching the simulation data, thus making it possible to model the intermittent nature of the system. The possibilities that exist are K41 (i.e.$g = 3, x = 2/3$) and IK (i.e. $g = 4, x = 1/2$) with parameter C_0 taking three possible values, in each case. The value of C_0 determines the dimensions of the modeled structures . C_0=1, is indicative of two dimensional structures, C_0=2, is indicative of a filamentary uni-dimensional structures and C_0=1.5 (see foot note of section 5.3) is indicative of fractal dimensional structures. The exponents from the simulation are plotted along with all the possible model plots and it is then determined, to which model the data is closely related to. The results can then be matched with the real space structures, for conformation. In general intermittency analysis offers insight into two aspects of the structures one being the dimensionality of the structures and the second being the mechanism responsible for the formation of these structures (phenomenological model matching with the scaling exponent curve automatically points at the processes involved in formation of those structures. The value of C_0 used determines the dimensionality). Intermittency modeling has been successfully applied in the 2D-hydrodynamic, 3D-HD and 3D-MHD turbulence cases to understand and model the inherent structures [1]. For example: the

velocity field structures in the 3D-HD case are filament like and in 3D-MHD they are sheet like [15, 1]. These features can be confirmed from the intermittency modeling using the log-Poisson model, by choosing the correct set of parameters C_0 and x in each case. In 2D-HD turbulent convection the nature of the temperature fluctuations and structures in the velocity field have been determined using intermittency modeling [1]. Here too the log-Poisson model plays an important part. In the MHD case, the analysis has been carried out for decaying turbulence case [14, 18] for the quantity $\mathbf{z}^+$, to understand the nature of structures formed due to the non-linear interaction of both the magnetic and velocity fields. In chapter 5 of this work, the analysis is further extended to magnetic field alone and further a similar analysis is carried out for forced turbulence case as well (see section 5.3).

Chapter 4

Influence of Inverse Cascade of Magnetic Helicity on Spectral Properties of 3D-MHD Turbulence

In this chapter, spectral properties of 3D-MHD turbulence in both forced and decaying cases are studied. The equations used and the initial conditions are discussed first and then time variation of some of the important quantities in the system are discussed. Difficulties in defining the Reynolds numbers due to the use of hyperviscosity are also mentioned. This DNS study confirms some known spectral properties of 3D-MHD turbulence and also several new properties are reported. These spectral properties are combined with dimensional analysis of EDQNM equations to obtain a new relation, which shows how some of the spectral properties are inter-related. The physics of this new relation is also explained.

4.1   Equations and Initial Conditions

From the discussion on the phenomenologies and the power laws obtained from them, an impression that these power laws reflect basic principles of physics, can be had. Hence these power laws must be valid if only the Reynolds number is sufficiently high [1]. The Kolmogorov spectrum for total energy is observed in diverse conditions, both in experiments and numerical simulations. Significant deviations from this law seem to occur only if special processes dominate the

turbulent dynamics in the inertial range, such as buoyancy forces in thermal convection, which can lead to a steeper energy spectrum [1]. These deviations may or may not dominate the inertial range dynamics, the answer to which can only be obtained from either experiments or numerical simulations. Here DNS is employed with high resolutions. This ensures a clear inertial range power law allowing the associated scaling exponent to be determined reliably. The equations used for DNS have already been discussed in chapter 2. They are recalled once again here, in a form useful for the discussion as shown below

$$\partial_t \boldsymbol{\omega} = \nabla \times (\mathbf{v} \times \boldsymbol{\omega} - \mathbf{b} \times \mathbf{j}) + \hat{\mu}_n (-1)^{n-1} \nabla^n \boldsymbol{\omega} + \mathbf{F_v} + \boldsymbol{\alpha} \triangle^{-2} \boldsymbol{\omega} \qquad (4.1)$$

$$\partial_t \mathbf{b} = \nabla \times (\mathbf{v} \times \mathbf{b}) + \hat{\eta}_n (-1)^{n-1} \nabla^n \mathbf{b} + \mathbf{F_b} + \boldsymbol{\alpha} \triangle^{-2} \mathbf{b} \qquad (4.2)$$

$$\nabla \cdot \mathbf{v} = \nabla \cdot \mathbf{b} = 0. \qquad (4.3)$$

Here $\mathbf{v}$ is the velocity, $\boldsymbol{\omega}$ is the vorticity, $\mathbf{b}$ is the magnetic field and $\mathbf{j}$ is the current of the system under consideration. $\hat{\mu}_n$ and $\hat{\eta}_n$ are the hyperviscous dimensionless dissipation coefficients, of order n. $\boldsymbol{\alpha} \triangle^{-2}$ represents an energy sink used to overcome the boundary effects in the small wave number region, for both the fields, with $\boldsymbol{\alpha}$ being a free parameter (set to 0.5 here). The forcing terms $\mathbf{F_v}$ and $\mathbf{F_b}$ are random in nature, delta correlated in time, and act over a band of wave numbers in the small-scale region, adding a fraction of magnetic helicity and or kinetic helicity to this band. The functional form of these equations has been discussed in section 2.4.2. The initial velocity and magnetic fields are smooth with random phases and fluctuations, having a Gaussian energy distribution, peaked in high to intermediate wavenumbers, in the forced and decaying cases respectively. The two fields have equal initial energies, in both the cases. The initial setup in both the cases is at 512^3 resolution, which is padded with zeros at t $\sim$ 0 (as mentioned in section 2.4.1) to get the initial setup for the resolution at 1024^3 mesh points. The amplitudes for both the forcing terms are also the same. Hyperviscosity of level $n = 8$ is used. The actual values used in the simulations are summarized in the table 4.1 below. Few 512^3 simulation results are also presented in the forced turbulence case. In these, the forcing is for the wavenumbers k=103 - 109, with initial condition peaked at k=106 and dissipation coefficients having a value of 2×10^{-35} each. In the decaying case, the forcing and the sink terms do not exist. Decaying turbulence is studied to understand the system, free of the uncontrolled effects arising from the choice of the forcing. But in the forced case, the forcing

Parameters	Forced turbulence	Decaying turbulence
$\hat{\mu}_n = \hat{\eta}_n$	9e-41	3e-41
n	8	8
Initial $|E_k^M| \sim |E_k^V|$	0.05	1.
$|\mathbf{F_v}| \sim |\mathbf{F_b}|$	0.5	–
Forcing wave numbers	203 - 209	–
Initial amplitudes peaked at wave number	206	70
Resolution N	1024	1024

Table 4.1: Initial conditions and characteristic parameters of the simulations. $\boldsymbol{\alpha}\triangle^{-2}$ is a sink present in forced turbulence with $\boldsymbol{\alpha}$=0.5.

terms maintain the turbulence at a steady average level. In the decaying case, the spectra are not stationary, such that direct time averaging is not possible. Instead self similarity of the spectrum (normalization described below) is used to eliminate the variation of the integral quantities. For an appropriate normalization, the energy spectra do not vary with time apart from the statistical fluctuations [1]. The same procedure is followed even for forced case quasi-stationary spectra, for consistency and reliability.

Motivation

From the above numerical setup it can be inferred that the aim of the simulations is to try and achieve an inverse cascade from very high k to low k regions. Earlier works on inverse cascade of magnetic helicity mainly had the forcing in low k region (see [8, 59, 10, 11]). Thus the transfer of helicity was limited to only few wavenumbers except in the case of experiment 6 of [8], where, the forcing was at k =30, in a resolution domain of 128^3. In all these previous cases the resolution was also limited and hence, only a glimpse of an inverse cascade was seen but never a full fledged inverse cascade which spans at least a decade or more in the spectral space. The power laws obtained from these simulations thus need to be verified. Although the numerical simulations of EDQNM appear to show a considerable inverse cascade [7], since this approach is only an approximation to the original set of equations, the results have to be confirmed using DNS. The above mentioned two factors mainly led to take up this work. Here the resolution can be considered as high and the parameters are carefully chosen so that their

is sufficient scale separations between inertial and dissipative ranges.

The forcing terms chosen in the case of forced MHD turbulence, inject, into a finite band of wavenumbers, a finite amount of magnetic helicity and or kinetic helicity, in the high k region. The resultant fluctuations, are expected to travel towards low k because of magnetic helicity interactions both at local scales as well as at nonlocal scales[1] [10], and thus build up the necessary inverse cascade. Since, the simulation domain here provides for considerable scale separation, the power laws obtained here are less influenced by either the boundary effects or the dissipative effects, as compared to other lower resolution simulations mentioned earlier.

4.2   Time Evolution of the Systems

The main interest of this studies is to look at spectral properties of 3D-MHD turbulence, under the influence of inverse cascade of magnetic helicity. However it is interesting to also see how the quantities of interest evolve in time. Here the time evolution of some of the important quantities is presented. All the plots in this section are integrated values of the quantity under concern, over all the wavenumbers at each time point (see table 4.2).

Helicities

The quantities first discussed are the helicities, both cross and magnetic helicity (see fig. 4.1). It can been seen that the magnetic helicity is quasi-constant in the decaying turbulence case whereas it is monotonically increasing with time in the forced case (fig. 4.1 a and b top). The cross helicity is a positive quasi-constant in the decaying case where as it oscillates around zero in the forced case (fig. 4.1 a and b bottom). The monotonic increase in the magnetic helicity value is due to the amount of magnetic helicity that is being injected at each time step, over a band of wavenumbers, in the forced case. The observation that both cross helicity and magnetic helicity remain fairly constant over a long period of time, once the turbulence develops by about $t \simeq 0.5$, clearly brings out the invariance nature ($\frac{d}{dt} = 0$) of these two quantities in the decaying turbulence case. However the invariance nature is not explicitly seen from the time plots, of the forced case. In general, effects of dissipation are felt in high k regions. But since the magnetic

---

[1]Local and nonlocal interactions referred here are same as the triadic interactions explained in chapter 3 section 3.1.1.

helicity moves towards the low k regions, the dissipation effects are negligible (also see fig. 4.7c), thus the time evolution of magnetic helicity shows either a quasi-constant behavior (as in decaying case) or an monotonic increase (as in forced case), almost independent of dissipation.
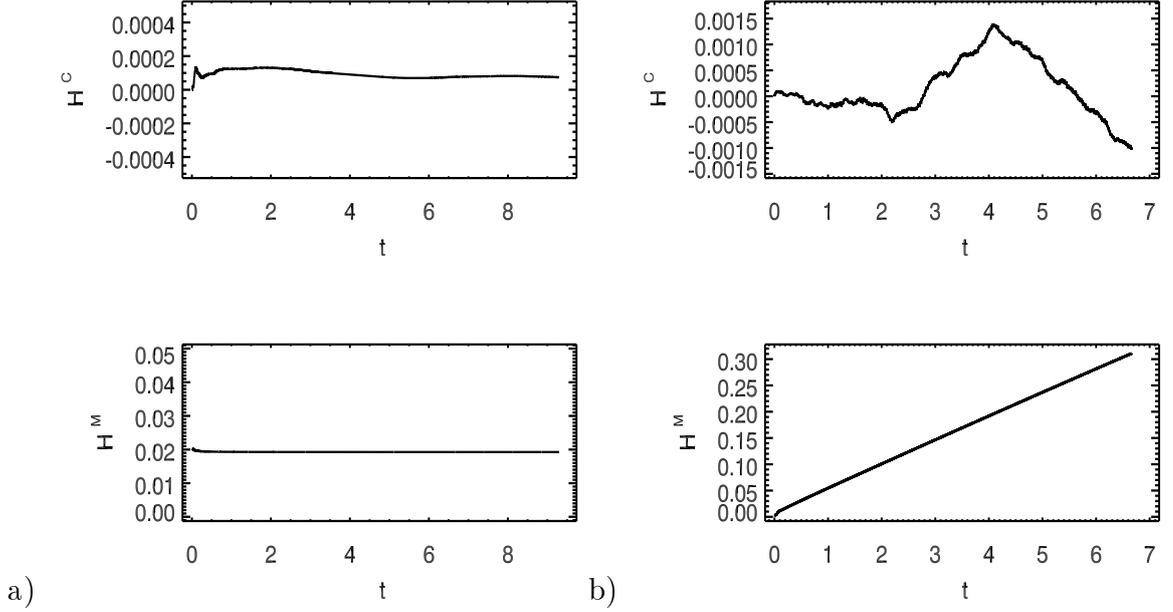
Figure 4.1: Evolution of cross helicity H^C and magnetic helicity H^M in time for a) decaying turbulence and b) forced turbulence.

Energies

The time evolution of total energy, kinetic energy and magnetic energy along with their respective dissipations are discussed next. In the decaying turbulence case, a log-log scale is chosen to represent the quantities, while in the forced case the quantities are plotted on a linear scale. Figure 4.2a represents the total energy and its dissipation. Also seen are the respective reference plots, which help in determining the power law behavior of these quantities (see legend of the figure for more details) and also show the fine deviations from that behavior. From this plot it can be seen that total energy shows an asymptotic fall off of $\sim t^{-0.5}$ as observed in [13]. In addition it is also observed that the dissipation increases up to a maximum, until the turbulence is fully developed ($t \sim 0.5$), and then it also shows an asymptotic fall off with a power law of $\sim t^{-1.5}$. When this energy and dissipation are broken down into individual components i.e. kinetic

(fig. 4.2b) and magnetic (fig. 4.2c) energies and their respective dissipations, some more details emerge. Although the initial kinetic and magnetic energies are equal (here of the order of unity), the kinetic energy shows a sharp fall off of $\sim t^{-0.8}$ instead of the earlier observed t^{-1} power law behavior in [13]. Where as in the case of magnetic energy, the fall off is much more gradual and the nature of this fall can be summed up with the functional form $\sim t^{-0.5}$. The dissipation curves in both the cases follow the same trend as was observed for the total energy dissipation curve and the power law behavior also does not differ and remains at $\sim t^{-1.5}$ in both the cases. It can be seen from the fig. 4.2a, that the total energy dissipation is several times more in its value up to $t \sim 5$ than the total energy and later it becomes smaller than the energy value. Hence for determining the spectral properties, the time range beyond $t \sim 5$ is used in the decaying case.
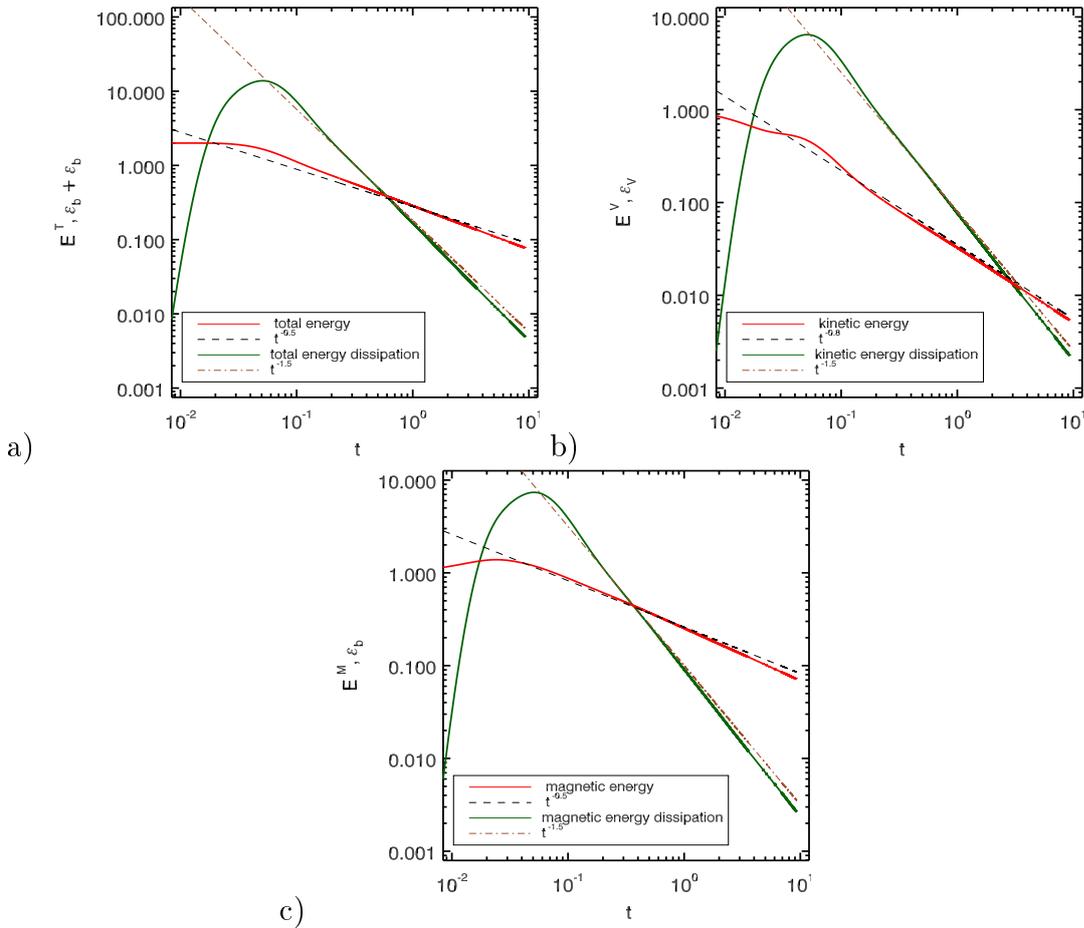
Figure 4.2: Energy and dissipation plots in decaying turbulence. a) total energy b)kinetic energy and c) magnetic energy.

In the case of forced turbulence, the total energy shows a sharp rise initially (up to $t \sim 0.35$), but once turbulence sets in, it falls (up to $t \sim 0.5$) and remains fairly constant throughout, indicating the attainment of a quasi-stationary state (see fig. 4.3a). The same is true for the dissipation of total energy, which is at least 5 times larger in value but has the same trend. But a look at the individual energies shows that although the initial value of both the kinetic (fig. 4.3b) and magnetic (fig. 4.3c) energies are the same, the magnetic energy gains at the expense of kinetic energy in the very initial stages and is far away from equipartition. It reaches a stable state after a small fall off. Here it is at least 3 - 3.5 times higher than the kinetic energy value. However it is interesting to note the shape of the kinetic energy curve which shows a constant growth over the period when turbulence is developing and once in the fully developed turbulent phase, becomes a constant. The initial rise in both the energies and subsequent sustainment of energies at these higher levels, is a result of the forcing. The sustainment of the magnetic energy is attributed to the appearance of dynamo action, which transfers energy to the magnetic field at the expense of the kinetic energy. The dissipation curves here too show a similar trend as was seen in the decaying case. It is not possible to fit a unique curve for all these quantities, like in the decaying case, due to the inherent nature of the curves (i.e. sudden rise and fall in a short span and later being fairly constant throughout).

Quantity evaluated	
Energy:	$E = \frac{1}{2} \sum_k \left(\mathbf{v_k}.\mathbf{v_{-k}} + \mathbf{b_k}.\mathbf{b_{-k}} \right)$
Magnetic helicity:	$H^M = \sum_k i(\mathbf{k} \times \mathbf{b_k}).\mathbf{b_{-k}}/k^2$
Cross helicity:	$H^C = \sum_k \mathbf{v_k}.\mathbf{b_{-k}}$
Dissipation:	$\epsilon_v = \mu(k^2)^n.\frac{1}{k^2}\omega^2, \quad \epsilon_b = \eta(k^2)^n.b^2$

Table 4.2: Quantities evaluated for time evolution. Here $\sum_k$ represents the discretization in configuration space achieved by applying a finite grid or in Fourier space by limiting the number of modes included to a band $k_{min} \leq k \leq k_{max}$. Note that ideal invariants of the continuum system are not strictly conserved in the truncated system, however quadratic invariants are robust to survive this truncation, owing to detailed conservation relation in triadic interactions (see section 5.2 of [1] for more details).

4.3   Consequences of using Hyperviscosity

After the time evolution of some of the important quantities in the system is discussed, the next step should have been the discussion on the spectral properties
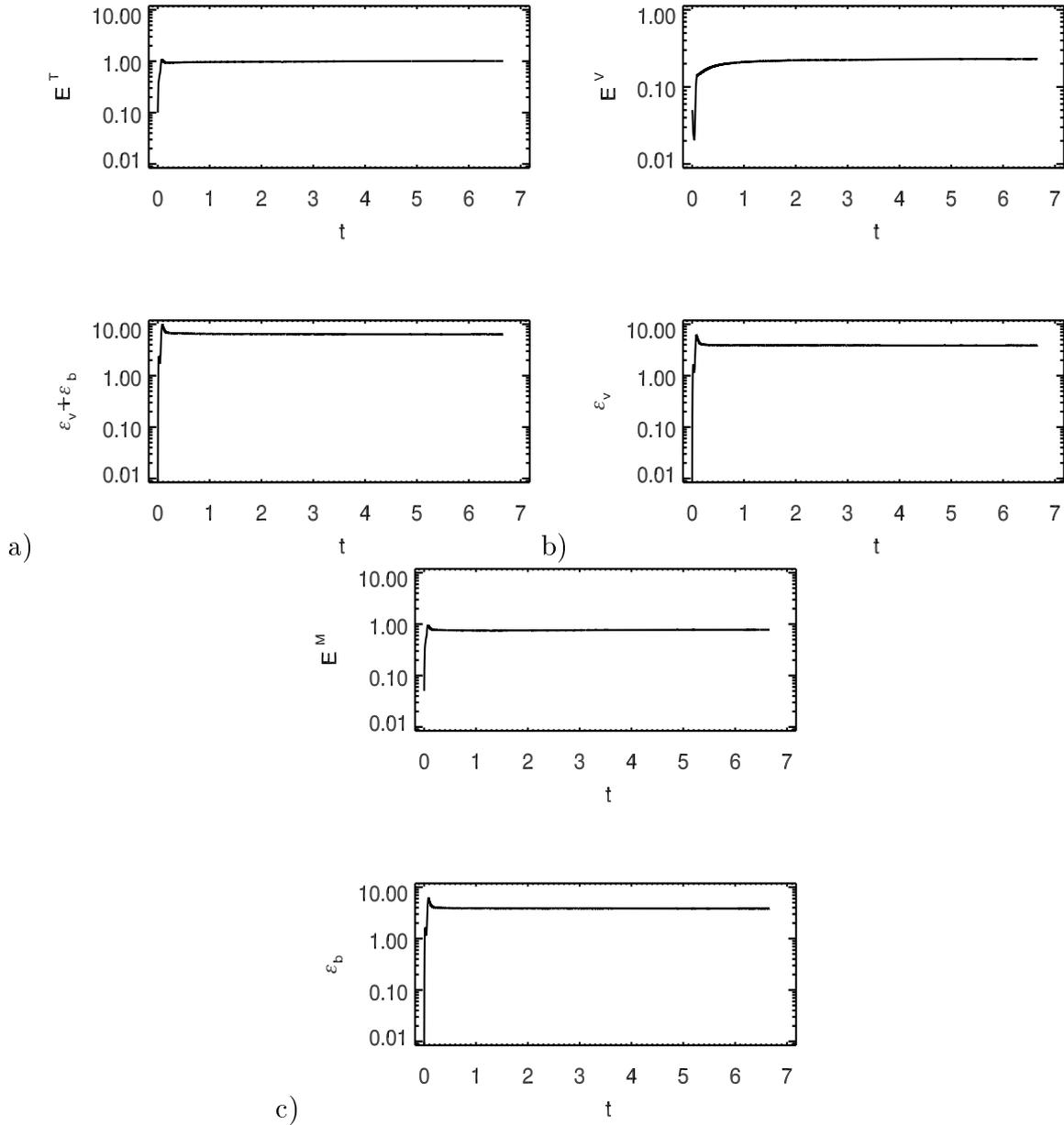
Figure 4.3: Energy plots in forced turbulence a) total energy b) kinetic energy and c) magnetic energy. Shown in each plot at the bottom are the energy dissipation rates.

of the system. But before the spectral properties are discussed, it is interesting to know the difficulties in defining a unique Reynolds number in the hyperviscous systems under consideration. Another important issue that needs to be understood is the bottleneck effect seen in the spectra due to hyperviscosity.

4.3.1 Defining the Reynolds numbers

Reynolds numbers as already mentioned in chapter 1, inversely quantify the dissipative nature of the fluid flow. The simplest definition for the kinetic Reynolds number is $Re = 1/\hat{\mu}$. $\hat{\mu}$ is the non-dimensional kinematic viscosity. The Reynolds numbers in turbulent flows are estimated using several different definitions, which yield several different formulas. Four of these formulas, modified for a hyperviscous turbulent flow are shown in table 4.3. These different formulas for Reynolds numbers, will yield different numbers, with different meanings, for the same flow. In determining the Reynolds numbers, some of these formulas use some unphysical assumptions like 1) the dissipation length l_d being assumed to be the same for all levels of n and 2) the dissipative coefficient being assumed to be the same for all levels of n. These assumptions are unacceptable as the very purpose of using hyperviscosity is to free the inertial range of dissipative pollution by shifting the dissipation to high k range. These assumptions tend to ignore this important fact. Although an estimate on the characteristic length scale l, can be obtained from the quasi-stationary state energy value, it appears that, each of these formulas have at least one parameter, which is totally determined by the afore mentioned unphysical assumptions. The parameter ϵ in column 2, $\hat{\mu}$ in column 3 of the table serve as good examples for this argument. The fourth definition is devoid of any parameters determined from the unphysical assumptions (both the length scales could be directly determined from hyperviscous simulations without any further reductions) and yields very small Reynolds numbers (27 and 140 in the decaying turbulence case and 6 and 14 for forced turbulence case, when l_d from 1) and 2) of table 4.3, are used respectively in each case). These values, however small, support the fact that hyperviscosity shifts the dissipation scales into very high k region, which results in small values for Reynolds numbers. In hydrodynamic turbulence, another method exists, in which Taylor micro scale ($\lambda = \sqrt{5}.v_{rms}/\omega_{rms}$) is used in determining a notional Reynolds number, where v_{rms} and ω_{rms} are the r.m.s. values of velocity and vorticity respectively. The actual value of the Reynolds number is then obtained by multiplying this notional value with an external parameter, obtained from wind tunnel experiments (see [60]). This approach is neither warranted nor is it possible to do some such equivalent adjustment in the case of MHD turbulence.

The small values for Reynolds number obtained, however, do not give an actual impression of the resolution or the computing effort that has gone into this work (as the Reynolds numbers obtained only correspond to the dissipative scales

which any how are small due to hyperviscosity) (also see section 2.5). Hence in their place, the hyperviscous diffusive terms are used *as is*, in this work. However from the experience of others like [37, 61], it can be safely assumed that the Reynolds numbers in this work (if can be defined at small k) will be in the range of 1000 (forced case) to around 4000 (decaying case). But since such a definition currently is not available for the hyperviscous systems, no claim is made on the exact value of Reynolds number, in both the cases. Also note that except for second definition (magnetic Reynolds number), which is based on the Iroshnikov- Kraichnan phenomenology, all other definitions use terms and definitions from the Kolmogorov phenomenology. The dissipation lengths (l_d) obtained from both the phenomenological definitions result in values very close to each other $(\sim 2.5 \times 10^{-3})$ in both forced and decaying cases. Thus this value of (l_d) will be used in the normalization of wavenumber k to obtain $\overline{k}$ $(=l_d k)$, the normalized wavenumber. The eddy turnover time is not defined in the simulations as t_d $(\sim \frac{l_d}{v_d})$, where $v_d = 2 \int_{l_d^{-1}}^{\infty} E_q^V \, dq$, does not give acceptable values, due to the presence of hyperviscosity.

Definition of Reynolds number
1) $Re = 1/\hat{\mu}$ where $\hat{\mu}$ obtained from $l_d = (\frac{\hat{\mu}_n^3}{\epsilon})^{\frac{1}{6n-2}}$
2) $Rm = (\frac{l}{l_d})^{3/2}$ where $l = \frac{E^{3/2}}{\epsilon}$ $v_A = \sqrt{E^M}$ and $l_d = (\frac{\hat{\eta}_n^2 v_A}{\epsilon})^{\frac{1}{4n-1}}$
3) $Re = VL/\mu \sim \frac{1}{\hat{\mu}}$ where $V = \sqrt{E^V}$ and $L \sim l$
4) $Re^{9/4} = \frac{L_0}{l_d}$ where $L_0 \sim l$ and l_d from [1) and 2)] above

Table 4.3: Various ways of determining Reynolds numbers. Here n=8, $\hat{\mu}_n$, $\hat{\eta}_n$ are the non-dimensional hyperviscous diffusive terms used in the simulations, $\hat{\mu}$ is the non-dimensional diffusive term obtained by taking the same l_d and ϵ, from n=8 and then replacing n to unity.

4.3.2   Bottleneck Effect

The first spectrum that is examined, when looking for spectral properties of turbulence, is the energy spectrum. In MHD case it is the sum of the kinetic and magnetic energies. Classically it is expected to show a Kolmogorov like behavior (i.e. a -5/3rd power law) in the inertial range. But a small hump in the energy spectrum is observed near the dissipative wavenumber region. This region is a result of partial reflection of the energy in front of the dissipation range. This is called '*bottle neck*' effect. This effect is prominent in hyperviscous simulations [41, 62, 63, 64, 65, 61], and is considered an 'unwanted guest', one has to live

with. A mathematical interpretation of this effect is related to a property of the Fourier transformation: that a sharply bent structure function in configuration space corresponds to an overshoot in the Fourier spectrum (see [1] and references thereof). Recent work [66], suggests that the advantage of widening the inertial range may be offset by artifacts at bottleneck scales. An incomplete thermalization will bring the statistical properties of such scales closer to Gaussian, thereby reducing the rather strong intermittency which would otherwise be expected [66], and hence further studies is on, to overcome these bottlenecks in energy spectra (see [67]).

In the context of this work, however, it is argued that although bottleneck is present in the 3D-averaged energy spectrum (equation 1.43), a one dimensional spectrum (1D) $(E_{kx} = \int dk_y dk_z E_{\mathbf{k}})$ is free from such an artifact, in line with [13]. This argument is supplemented by the plots in fig. 4.4 a and b. In fig. 4.4a, the total energy spectrum$(E_k = \int_0^\infty E_k dk)$ is normalized with a Kolmogorov spectral relation $(E_k = \epsilon^{2/3} \overline{k}^{-5/3})$ and compensated by $k^{5/3}$. Here $\overline{k}$ is the normalized

a)   b)
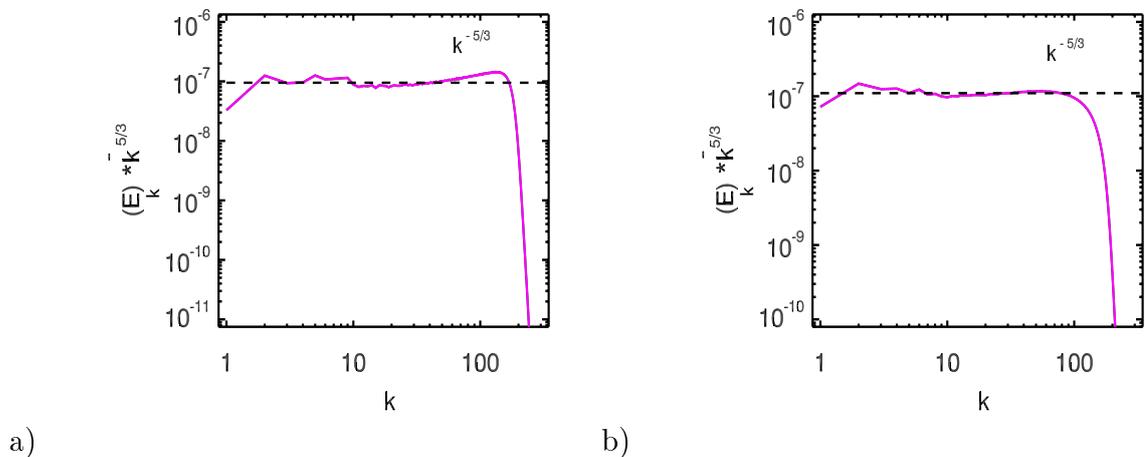
Figure 4.4: Energy spectra in a 512^3 forced simulation at t=9.59. a) 3D- spectra and b) 1D-spectra. Simulation setup: the initial condition: random fluctuations in the shape of a Gaussian peaked at k=6, forcing: to the band of wavenumbers k=3-9, $\hat{\mu}_n = \hat{\eta}_n$ =2e-35. $|E_k^M| \sim |E_k^V|$=0.05, $|\mathbf{F_v}| \sim |\mathbf{F_b}|$= 0.5, n=8.

wave number. This spectrum has a flat region (indicating good compensation) over wave numbers k=10 to k=50. From there it starts showing a deviation, and forms a hump in the high k region. This is the bottleneck. This effect results from the Fourier transform of the correlation function and is more pronounced at

higher levels of hyperviscosity [13]. Figure 4.4b, is the one dimensional spectrum of energy ($E(|k_z|) = E(k_z) + E(-k_z)$ [13, 1]), normalized and compensated the same way as was done for fig. 4.4a. This spectrum does not show the bottleneck behavior, due to the fact that here the transition to the dissipation region is more gentle [13]. In both the spectra, the horizontal line represents the Kolmogorov scaling. From [65], the total energy and one-dimensional energy spectra are related by $E(k) = [\frac{5}{3} - \frac{dln E_{1D}(k)}{dln k}]E_{1D}(k)$. From this relation two things can be inferred: 1) if there is a finite interval where the Kolmogorov scaling holds for the one-dimensional spectrum, then the same scaling will hold for the three-dimensional spectrum and vice-versa. 2) If one-dimensional energy spectrum shows a bottleneck effect, the three dimensional energy spectrum also shows a bottleneck effect, but vice versa *may not be true*. Thus, the relation discussed, supports the observations of fig. 4.4. Hence in the course of this work, the spectral powers obtained for various parameters in the bottleneck region are also presented and discussed (see next section). It is also shown that even with a bottleneck present in the energy spectrum, the spectral powers of various quantities, hold on to the same physical relation satisfied in the proper inertial range region (see section 4.5).

4.4 Spectral Properties

Here, the spectral properties of several quantities of interest are discussed in both forced and decaying cases, starting with magnetic helicity. In the forced case, the discussion is centered around only the injection of maximum magnetic helicity by the forcing terms, with no injection of kinetic helicity, unless other wise stated. When the spectra are compensated, *two inertial ranges (one at high k and one at low k) are observed in the forced case* and one in the decaying case for some quantities. Here it need to be emphasized that, although, there was a prediction of possibility of two inertial ranges, in 3D-MHD turbulence [13], it was never reported. In this respect, this work uniquely shows the two predicted inertial ranges. However due to the limitations in the resolution, the high k inertial range is very small and in order to resolve this inertial range clearly further high resolution simulations are necessary. It also need to be noted that in 2D-hydrodynamics, there are published reports of clearly resolved two inertial ranges from very high resolution simulations (see e.g. [37, 68]). Another interesting fact

that emerges from this studies is that several quantities in 3D-MHD turbulence, show two approximate scaling ranges and power law behaviors, in the forced case and a lone approximate scaling range with a power law behavior in the decaying case. Although the power law values are determined for both the scaling ranges in the forced case, importance is attached to the measurements in the low k inertial range. The performed analysis on this low k scaling range is found to be valid even for the high k scaling range for most of the quantities, although this range is not very well resolved.

The data sets used for plotting the compensated spectra in all the spectra below, are at t=6 for forced case and t=10 for the decaying case.

4.4.1   Spectral Behavior of Magnetic Helicity

As discussed in section 1.2, magnetic helicity is one of the important ideal invariant of the system and hence its spectral behavior helps in gaining some insight into the MHD turbulent flow. Normalized magnetic helicity spectra for both the decaying case and the forced case are shown below (fig. 4.5). Here it is observed that the initial helicity present in high k region, moves to low k region, with the progress of time It was realized in this work that the power law exponent does not satisfy the k^{-2} power law for the inverse cascade of magnetic helicity but varies in the two cases studied here significantly (see next section and table 4.4). In view of this, the prefactor ϵ_{H_d} also is dropped as the whole expression (see footnote below) [2] goes together and cannot be separated out. Hence a normalization factor of k^{α} is used, where α is the actual power law exponent obtained for each case by trial and error (taking the value at which the spectra gets compensated the best). The figure below i.e. fig. 4.5 represents the set of such normalized curves that depict the 'inverse cascade of magnetic helicity', first seen in the numerical simulations of EDQNM equations [7]. Although the same affect was observed in several DNS methods [10, 8, 69, 9], never in any of these works a transfer from such a high k to low k was reported. However in 2D-hydrodynamics, such transfers over a vast region, are seen in the inverse cascade of energy e.g.[37]. The compensated spectra show inertial ranges, the horizontal line here indicating the

---

[2]The normalization factor that should have been used here is $\epsilon_{H_d}^{2/3}\overline{k}^{-2}$, with ϵ_{H_d} the dissipation of magnetic helicity. The suggested power law of k^{-2} is the one obtained from numerical simulations of EDQNM equations [7] and the power law to ϵ_{H_d} is obtained from dimensional analysis [1]. This dimensional analysis is reproduced in Appendix A for academic interest.

compensated spectral power. In the forced case, the power law exponents are
-3.3 and -1.7 for low k (7 - 30) and high k (250 - 400) inertial ranges respectively
(see fig. 4.6 and table 4.4). The inertial range in the low k region, is close to
the Kolmogorov type scaling. While for decaying case the power law exponent

a)   b)
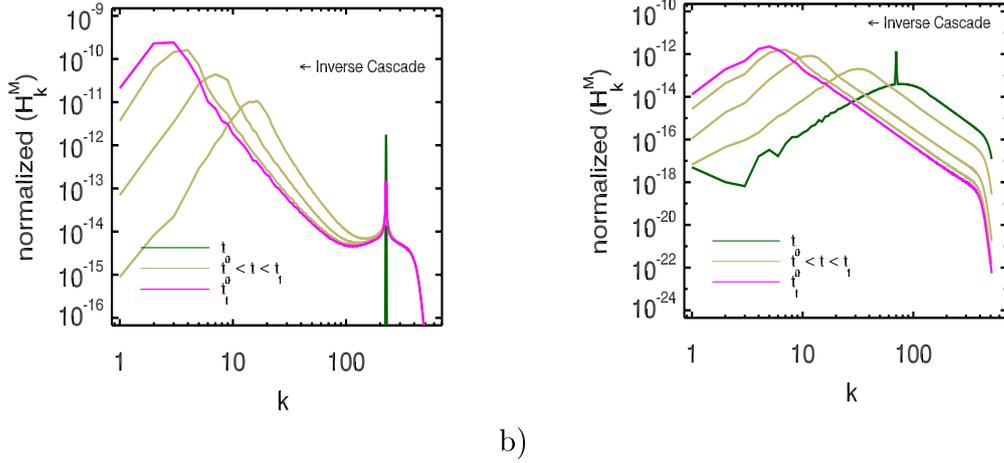
Figure 4.5: Normalized magnetic helicity spectra in a 1024^3 simulation. a) forced case and b) decay
case. Forced case t=0 to 6.9. Decay case t= 0.03 to 10. Inverse cascade is clearly seen in both the
cases. Note that in the decaying case, the initial condition shown here is at a time slightly away
from t=0 (i.e. at t=0.03), where already the initial spectrum (which was limited to a band of wave
numbers) is stretched over the entire spectral width available to the system. But the majority of the
energy is still contained in the initial band of wavenumbers which is making the initial state shown
here look like a spectrum from the forced case. Normalization of the type k^α is used where α is the
power law exponent, in both the cases.

has a value of -3.6. It is interesting to note that exponents in any case do not
satisfy the prediction of EDQNM (power law exponent of -2)(see [7]). The dis-
sipation region lies beyond the second inertial range in the forced case and the
only inertial range in the case of decaying turbulence. The cascade regions seen
in the above figures can be well understood by looking at the flux of magnetic
helicity. To obtain the flux of magnetic helicity, the first term on the r.h.s. of
the equation (1.33) and r.h.s. of the equation (1.36) are Fourier transformed
after accounting for the hyperviscosity, in their non-dimensional form, to obtain
$\dot{H}^M(\mathbf{k}) = \underbrace{2\mathbf{Re}\left\{\tilde{\mathbf{b}}^*.\widetilde{\mathbf{v}\times\mathbf{b}}\right\}}_{H^M_{Tr}(\mathbf{k})=\pi_{HM}} - \underbrace{\frac{2k^6}{Rm}\tilde{\mathbf{b}}^*\tilde{\mathbf{j}}}_{H^M_{Di}(\mathbf{k})}$. In this equation, the first term on the
r.h.s. is the nonlinear transfer term and second is the dissipation term of mag-
netic helicity. The plots below (fig. 4.7 a and b), show the transmission spectra
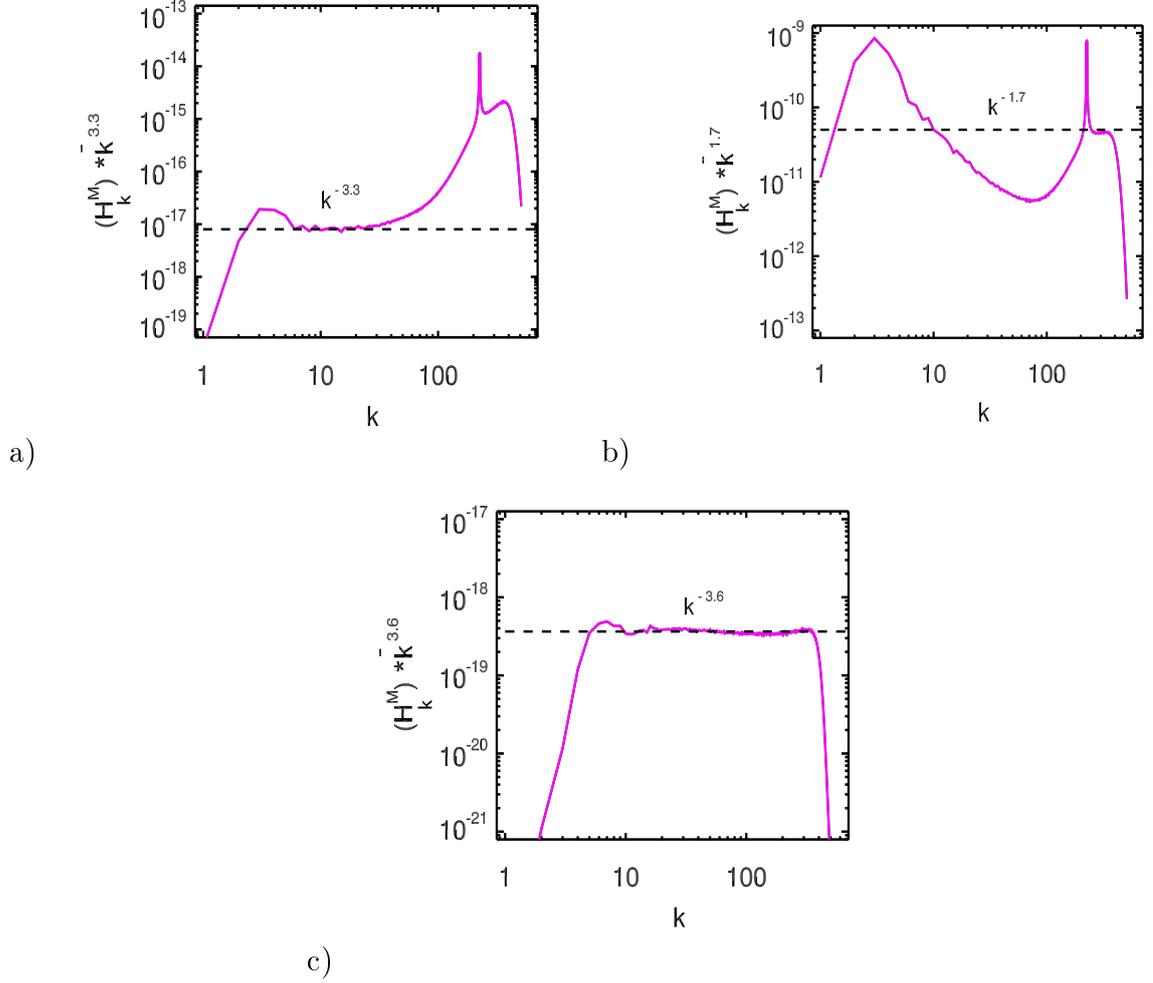
Figure 4.6: Compensated magnetic helicity spectra in a 1024^3 simulation. a) low k inertial range for forced case b) high k inertial range for forced case and c) inertial range for decay case.

of magnetic helicity $(\Pi_{HM}(k) = \int_0^k d^3k' 2\mathbf{Re}[\widetilde{\mathbf{b}}^* . \widetilde{\mathbf{v} \times \mathbf{b}}])$, over all wavenumbers for both the cases. This quantity represents the conservative flux of magnetic helicity as is seen in the figures. These plots have two regions. A region of positive flux and other a region of negative flux. The negative flux (absolute of the negative flux is plotted in 'magenta') is the flux moving *in* towards the smaller wavenumber shells (inverse cascade), while the positive flux (plotted in 'blue') is the flux moving *out* towards the large wavenumber shells (normal direct cascade). In the forced turbulence case, the fluxes are constant over a large wavenumber region for both inverse and direct cascades. This constant flux is a indicator of a

sustained cascade process, maintained by the input of magnetic helicity through the forcing of a band of wavenumbers at high k ($k = 203$ - 209). Here magnetic helicity is moving towards the low k regions, while dissipation is concentrated in the high k regions. Thus the magnetic helicity experiences very low dissipation and is transmitted towards the low k regions. In the decaying case, though, there is an established inverse transfer process, the flux is not a constant as there is no active injection of magnetic helicity. In the high k regions, the inverse cascade is not present and here in general, the direct energy cascade process dominates, thus only a direct downward cascade is seen, in both forced and decay cases. It can be seen that the contribution to the flux is mainly due to the transmission term alone. This is because of the negligible values of the dissipation term, in comparison to the transmission term. This fact is true for both the decaying and forced cases and thus a spectrum representative of this fact is only shown (see fig. 4.7c).

4.4.2 Magnetic Energy Spectrum

As the inverse cascade of magnetic helicity progresses, it may influence the spectral properties of other quantities of interest. One such very important quantity to look for is the magnetic energy spectrum as magnetic energy and magnetic helicity are spectrally related ($E_k^M \sim k H_k^M$). It is indeed observed that as the magnetic helicity inverse cascades, so does the magnetic energy, but with a less steeper (approximate) power law [7]. Here, the same trend continues albeit the difference in power laws is slightly different from that of [7], in the forced case and the deviation is much larger in the decaying case. Once again in the forced case, there are two approximate scaling ranges, while in the decaying case there is one approximate scaling range. This is depicted in the fig. 4.8 a,b and c below, here too the horizontal line in the spectra is representative of the power laws. It is seen that in the low k region (7 - 30) of the magnetic energy spectrum, the power law exponent has a value of -2.1, while in the high k (250 - 400) region it is -0.6. In the decaying case it is once again -2.1. The flux of magnetic energy

$$\Pi_{jb+vb}(k) = \int_0^k d^3k' [(\mathbf{Re}(\tilde{\boldsymbol{\omega}}^* . \frac{i}{k'^2}(k' \times \widetilde{\mathbf{j} \times \mathbf{b}}))) + (\mathbf{Re}(\tilde{\mathbf{b}}^* . i(k' \times \widetilde{\mathbf{v} \times \mathbf{b}})))]$$
$$\underbrace{\phantom{(\mathbf{Re}(\tilde{\boldsymbol{\omega}}^* . \frac{i}{k'^2}(k' \times \widetilde{\mathbf{j} \times \mathbf{b}})))}}_{T_{jb}} \quad \underbrace{\phantom{(\mathbf{Re}(\tilde{\mathbf{b}}^* . i(k' \times \widetilde{\mathbf{v} \times \mathbf{b}})))}}_{T_{vb}}$$
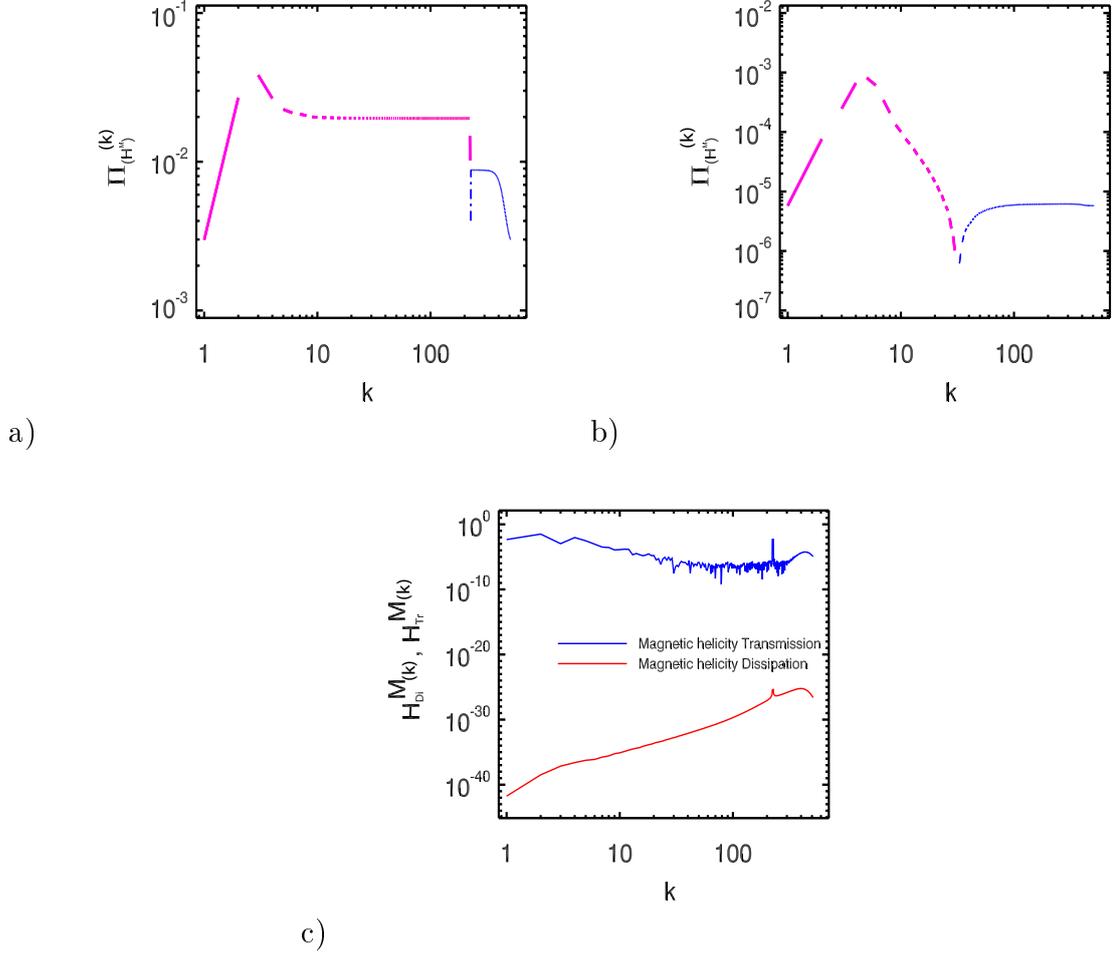
Figure 4.7: Flux of magnetic helicity spectra and comparison of transmission and dissipation terms. a) flux in the forced case b) flux in the decay case and c) comparison of transmission term to dissipation term of magnetic helicity (see eq.(4.4)) (in flux plots, magenta: inverse cascade, blue: direct cascade).

(see Appendix B for derivation) does not remain constant for both the forced and decaying cases (see fig. 4.8 d and e). However, when maximum kinetic helicity is also injected along with maximum magnetic helicity, then the flux turns constant (see fig. 4.8f). This might be because of the kinematic dynamo action coming into play, when kinetic helicity is injected into the system. In this case, the approximate scaling law can be regarded as representing an inertial range. Note that the flux plots have been normalized with energy dissipation rate.[3]

---

[3]Since for magnetic energy, the flux contribution is from both the magnetic and velocity fields, the sum of kinetic and magnetic energy dissipation rates i.e. the total energy dissipation rate is used for the normalization of the spectra.
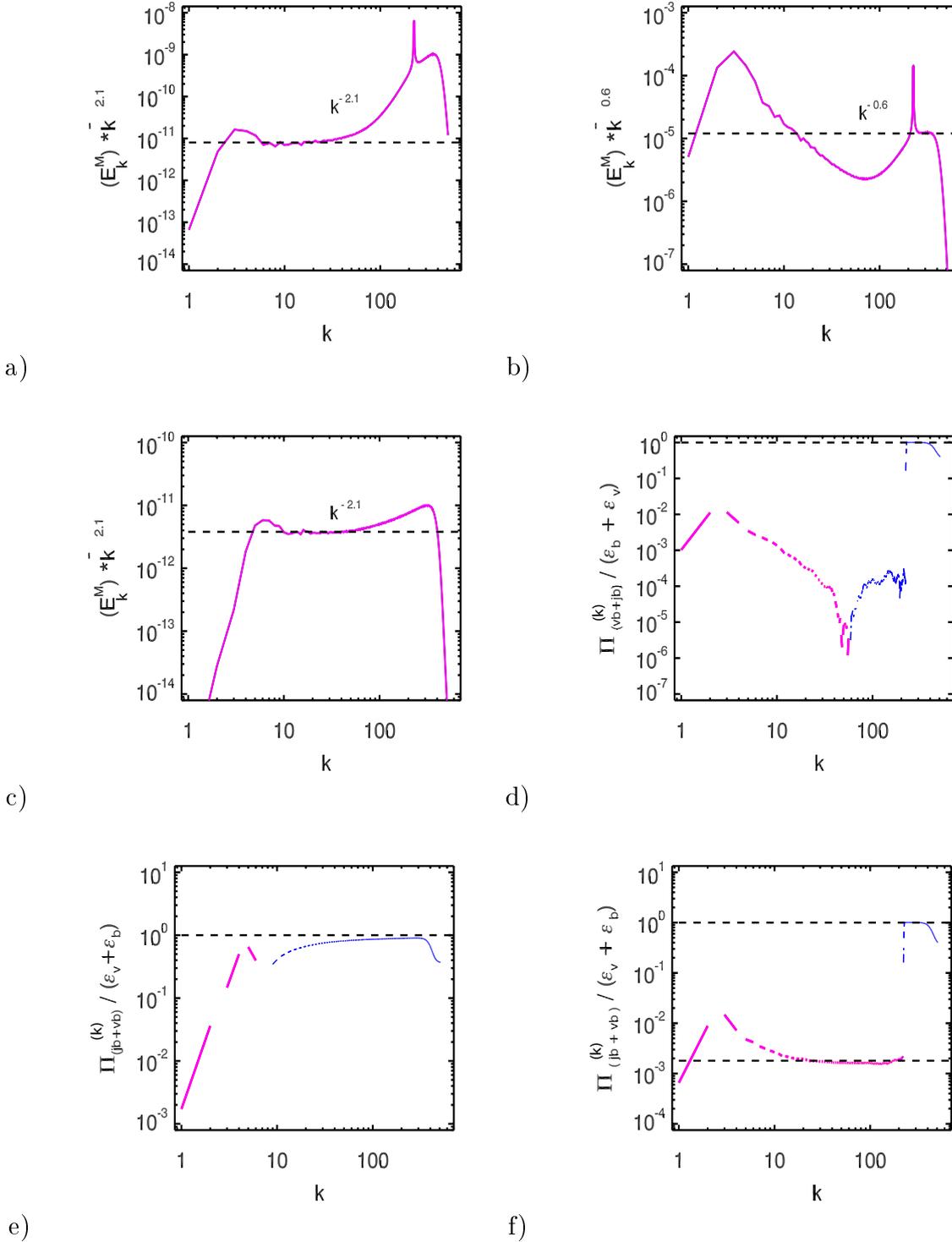
Figure 4.8: Magnetic energy and flux. a) first approximate scaling range in the magnetic energy spectrum in the forced case b) second approximate scaling range in the magnetic energy spectrum in the forced case c) approximate scaling range in the magnetic energy spectrum, decaying case, d) magnetic energy flux in the forced case e) magnetic energy flux in the decaying case and f) magnetic energy flux in the forced case when kinetic helicity is also injected. (in flux plots, magenta: inverse cascade, blue: direct cascade)

4.4.3   Kinetic Energy Spectrum

The next spectrum that is being discussed is of kinetic energy. Here for the first time an inverse spectral transport is reported for kinetic energy, in 3D-MHD turbulence, although it is a common observation in 2D-hydrodynamics. This might arise because of the inverse cascade of magnetic energy. Because the cross helicity is very small, there can be interactions and exchanges between velocity and magnetic fields, through the Lorentz force terms present in both velocity field and magnetic field equations. It was shown in time plots above, that the magnetic energy starts dominating the system after a period of time. This increase in magnetic energy might influence the way the velocity field acts. It appears that the velocity field also has a spectral transfer towards small k, although not with an increase in overall kinetic energy. Thus the inverse spectral transport behavior is seen in the kinetic energy spectrum but the spectral powers are not high. For the forced case, the low k approximate scaling range shows a -1.2 power law, while the high k region shows a -0.6 power law (fig. 4.9 a and b). For the decaying case, the power law is -0.7 (fig. 4.9c). The horizontal lines in the respective spectra represent the corresponding power laws. The flux of kinetic energy $\Pi_{v\omega}(k)$ is given by $\int_0^k d^3k' \, (\underbrace{\mathbf{Re}(\tilde{\boldsymbol{\omega}}^* \cdot \frac{i}{k'^2}(k' \times \widetilde{\mathbf{v} \times \boldsymbol{\omega}}))}_{T_{v\omega}})$ (see Appendix B)

and is plotted similarly for all the cases discussed for magnetic energy flux. Here too the flux plots are normalized. The normalization factor here is kinetic energy dissipation rate only. The most interesting fact in the flux plots is the pure inverse spectral transport nature of the kinetic energy flux. This flux stays constant over a large range of wavenumbers, when kinetic helicity is also injected, in the forced case (fig. 4.9 d and f). For the decay case, the flux shows both the inverse and direct spectral transports (fig. 4.9e).

4.4.4   Total Energy Spectrum

The total energy (sum of the kinetic energy and the magnetic energy) is an ideal invariant in 3D-MHD turbulence. In decaying turbulence, it is known to show a Kolmogorov type power law of -5/3 [13]. Here in this work, it is shown that in the low k regions in the forced case, the same holds too, while in the high k region, a bottleneck is observed (fig. 4.10 a,b and c). The horizontal lines in each of these spectra represent the compensated power law.
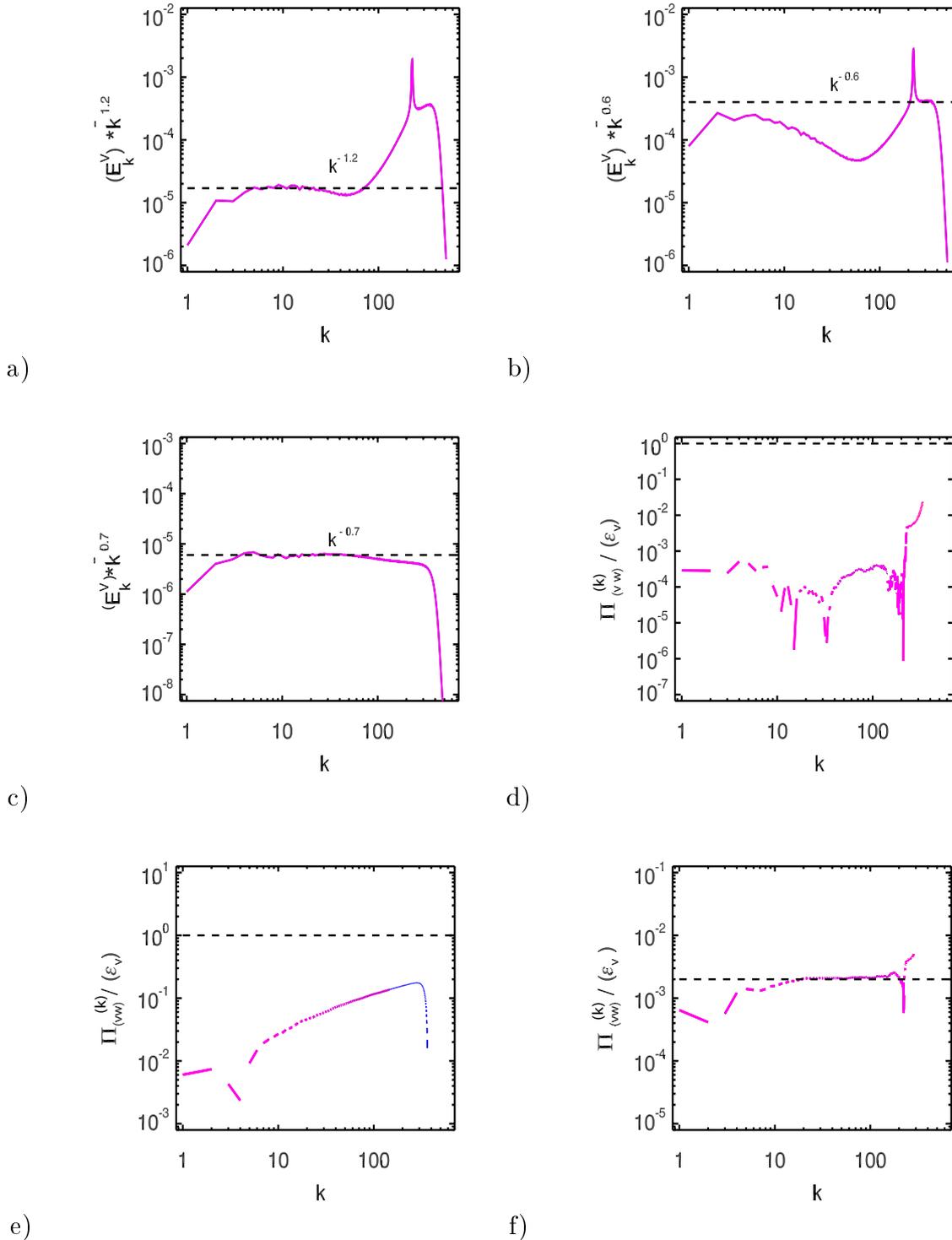
Figure 4.9: Kinetic energy and flux. a) first approximate scaling range in the kinetic energy spectrum in the forced case b) second approximate scaling range in the kinetic spectrum in the forced case c) approximate scaling range in the kinetic energy spectrum, decaying case, d) kinetic energy flux in the forced case e) kinetic energy flux in the decaying case and f) kinetic energy flux in the forced case when kinetic helicity is also injected. (in flux plots, magenta: inverse cascade, blue: direct cascade)

The normalization factor used was $\epsilon^{2/3}$. Here ϵ is the total energy dissipation. The dissipative range in the case of forced case is in the very high k region ($k \sim 400$), similar to that for the decaying case. The flux terms that are obtained in the total energy case are the sums of the fluxes of kinetic energy and magnetic energy, discussed above. The plots are compensated with total energy dissipation rate. The total energy flux is a constant over a band of wavenumbers only in the case when both magnetic and kinetic helicities are injected (fig. 4.10f). Otherwise when only magnetic helicity is injected or the system is purely decaying in nature, this property is not present in the spectra (fig. 4.10 d and e). The turbulence theories normally emphasize on equipartition of energies [7]. But it was observed in both decaying and forced cases that the magnetic energy dominates the total energy budget (fig. 4.11) (the same factor is observed in the time plots), though the starting values for both kinetic and magnetic energies are the same. The magnetic energy is growing at the expense of kinetic energy and this factor needs to be looked at more closely. A possible explanation for the increase of magnetic energy is offered in the next section.

4.4.5   Spectra of Kinetic Helicity and Other Quantities

Kinetic helicity spectra $H_k^V = \frac{1}{2} \int dk^3 \tilde{\mathbf{v}} \cdot \tilde{\boldsymbol{\omega}}$ also shows an approximate power law behavior in both the forced and decaying cases (see Appendix C1 for plots). This too is reported for the first time, for 3D-MHD turbulence. These inertial ranges occur in the same wave number regions as the inertial range of magnetic helicity. In the forced case the power law exponents are -0.4 and 0.3 for low k and high k cases respectively. In the decaying case, the exponent is -0.2.

Residual helicity ($H_k^R = H_k^V - k^2 H_k^M$), the quantity that is significant in the Alfvén effect (see section 3.2.2 and also [7]), also shows an approximate power law behavior, in both the cases, in its spectra (see Appendix C3). Residual energy, was shown to have a power law behavior of $k^{-7/3}$ in decaying case and this result is found to be true in this work also. It also does show two approximate scaling ranges in the forced case (see Appendix C2), but in this case, the spectral relation $E_k^R \sim k E_k^2$ is not satisfied exactly. In the low k range, the obtained power law is away from the value predicted by the theoretical relation by $\sim$ -0.2 and in the high k range it is away from the value by $\sim$ -0.5.

a)   b)

c)   d)

e)   f)
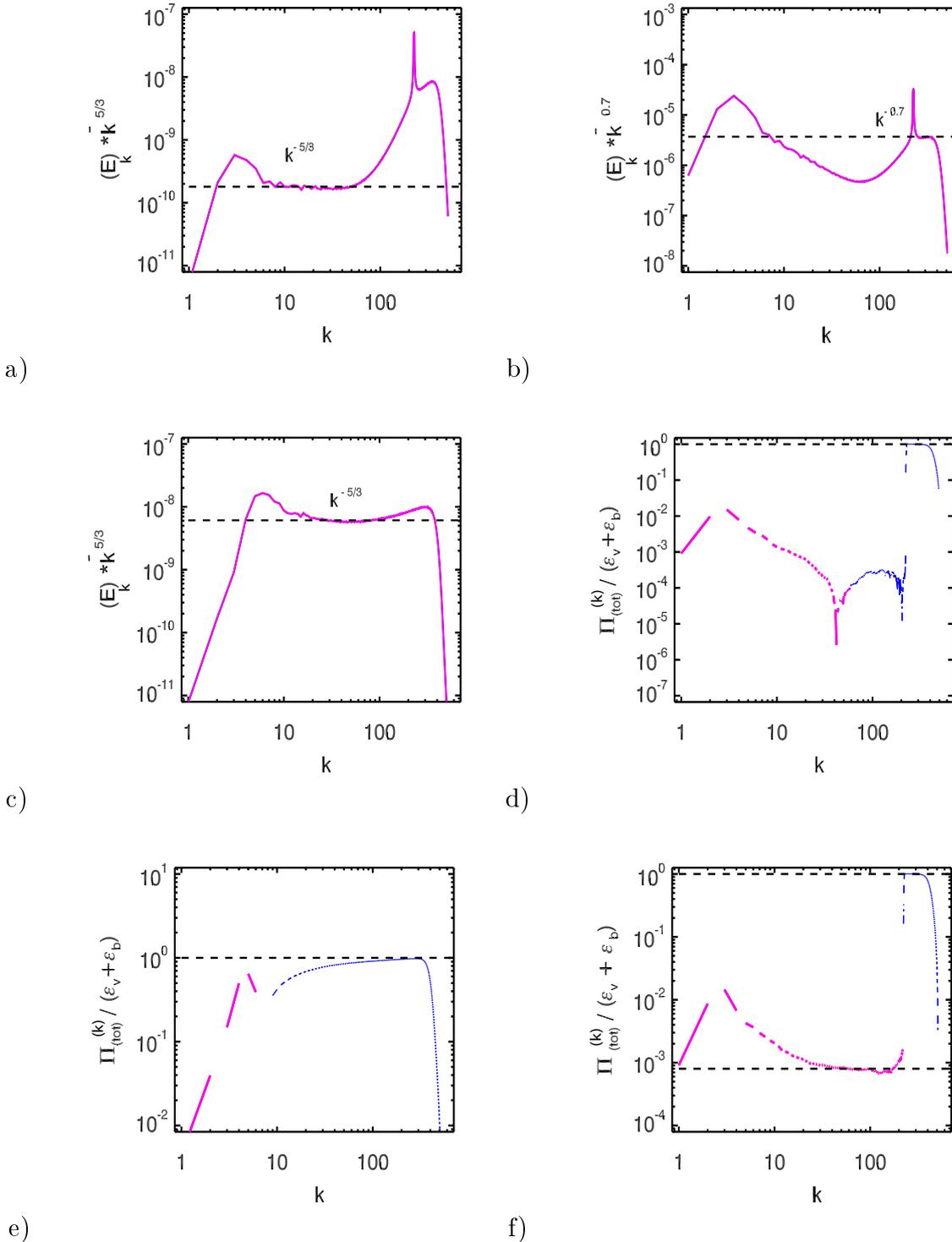
Figure 4.10: Total energy and flux. a) first approximate scaling range in the total energy spectrum in the forced case b) second approximate scaling range in the total energy spectrum in the forced case c) approximate scaling range in the total energy spectrum in the decaying case (note that this scaling range is highly influenced by the bottleneck on the high k region and inverse transfer of the energy in the low k region), d) total energy flux in the forced case e) total energy flux in the decaying case and f) total energy flux in the forced case when kinetic helicity is also injected. (in flux plots, magenta: inverse cascade, blue: direct cascade)
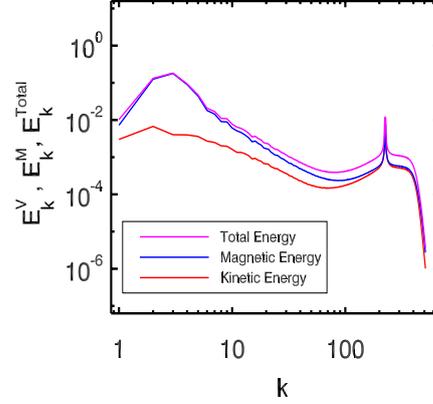
Figure 4.11: Comparison of energies in the forced case. Shown are the normalized plots of total, kinetic and magnetic energies.

Other parameters which show approximate scaling ranges and power law behaviors are the electric current density $\mathbf{j}_k$ (more specifically j_k^2) (see Appendix C5) and the magnetic vector potential (see Appendix C4).

The power law behaviors in current and vector potential are explained on the basis that they are directly related to the magnetic field, in their formulation. The residual helicity, although is a difference of two quantities that show power law behavior, is not expected to, or may not show any power law behavior. But it does show power laws. The kinetic helicity, is an ideal invariant in 3D-hydrodynamic turbulence, but not in MHD. Even then, it shows clear power law behaviors. It is also important to note that, the power laws obtained for these quantities do not exactly satisfy their respective mathematical relations (see [7]) and have significant deviations. For example magnetic vector potential and magnetic helicity, by virtue of the formula ($H^M = 0.5 \int_V \mathbf{A}.\mathbf{b}dV$), are related in the spectral space as ($H_k^M \sim k^2 A_k^2$), but the power laws obtained do not satisfy such a relation. In order to understand these whole set of power laws, it is opined that a new mathematical setup might be needed.

The power law behaviors are summarized below in two tables. This grouping is deliberately done as the power laws in first table are used along with the EDQNM equations, to understand the underlying physics. The second grouping is a report on several other power laws, observed, but are not yet understood fully for their

underlying physics. The power law values in both the tables also show the errors associated in determining them. The way these errors have been determined is explained next with an example of determining the error in the power law for magnetic helicity in the decaying case.

4.4.6 Determining the Error in the Power Laws

The first source of error can be the parallax error in judging the scaling range as it has to be determined with naked eye observations. Although flux spectra give an idea on this range (flux is constant in inertial ranges) but not all spectra show constant flux. Even after time averaging several spectra, to get a more accurate value, the parallax error persists. Only that the time averaging reduces this error. To illustrate this point, magnetic helicity spectrum in the decaying case, which is erroneously normalized with a power law of $k^{-3.5}$ instead of $k^{-3.6}$(the value reported in the table 4.4) after time averaging (the period used was t=8 to 10) is shown in fig. 4.12a. The case taken for illustration is when the judgment in determining the power law is the poorest. This power although appears to compensate the spectrum, clearly is not the correct value (as the spectrum is seen to be under compensated in the low k region and over compensated in the high k region). Such parallax error judgments, though rare, have to be figured into the error estimates, as the ultimate judgment of the power law value is subjective to human error.

The second source of error is the data spread in the scaling range. Ideally, in the scaling range, after normalization and compensation, all the data values should be the same and at each point should be equal to the reference line that is plotted in the spectra (which has a constant value throughout). In order to show that this is not true, the plot is deliberately thinned to the minimum possible thinness permitted by the plotting program as shown in fig. 4.12b. The plot clearly shows the wiggle or fluctuations in the data which are slightly above and below the reference line. This wiggle makes the power law to be determined erroneously with $\sim k^{0.08}$ inaccuracy. This is clear from the spectrum which is compensated with $k^{-3.65}$, that seems to be equally a good compensation as $k^{-3.6}$, as the small fluctuations observed in the data of the spectrum allow for such fluctuations around the correctly obtained power law value. The maximum value of such fluctuations could be $\sim k^{0.08}$ as already mentioned.

Thus for the magnetic helicity spectrum, in the decaying case, the maximum error

in the determination of the power law value could be of the order of $\sim k^{\pm 0.2}$, which is an addition of the two sources of errors, which serves as the worst case scenario.
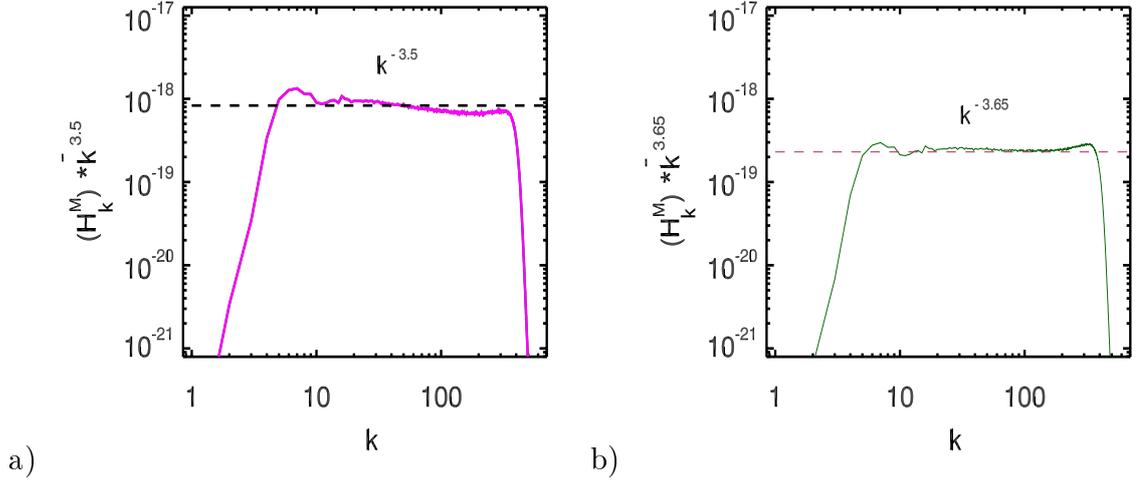
Figure 4.12: Error determination in the spectra. a) magnetic helicity scaling range determined erroneously to a tune of $k^{0.1}$ and b) a close look at the wiggle in the data of magnetic helicity spectrum.

Similarly errors were determined for all other quantities and have been tabulated as seen in tables 4.4 and 4.5. It can been seen that these errors are already very small in many cases and it can be expected that if much higher resolution simulations, with even higher Reynolds numbers are performed then, these errors might get further reduced.

4.5   EDQNM Analysis of the Power Laws

To understand the underlying physics of the power laws obtained in the above section, from earlier experience [14], dimensional analysis of EDQNM equations is applied together with a hypothesis of dynamical equilibrium (see discussion in section 3.2.2.) to these power laws. Here, the EDQNM equation for magnetic helicity, given by equation (3.27) is used, for the analysis of the power laws obtained in table 4.4. This choice of equation is obvious, keeping in mind that the focus of this studies is, on understanding the inverse cascade of magnetic helicity and its influence on other quantities both spatially and spectrally. The

equation is reproduced here.

$$\left(\frac{\partial}{\partial t} + 2\eta k^2\right) H_k^M = \tilde{F}_k^M + \int_{\triangle k} dp dq \theta_{kpq} \left(T_{V\tilde{M}}^{\tilde{M}} + T_{\tilde{V}M}^{\tilde{M}} + T_{M\tilde{M}}^{\tilde{M}}\right). \qquad (4.4)$$

Physical quantity	Power laws in 1024^3 simulations (k^α)		Decaying turbulence
	Forced turbulence		
	low k $(7-30)$	high k $(250-400)$	
Total energy E_k	-5/3±0.2	-0.7±0.3 (bottle neck)	-5/3±0.2
Magnetic energy E_k^M	-2.1±0.3	-0.6±0.3	-2.1±0.2
Kinetic energy E_k^V	-1.2±0.2	-0.6±0.3	-0.7±0.2
Magnetic helicity H_k^M	-3.3±0.2	-1.7±0.3	-3.6±0.2
Kinetic helicity H_k^V	-0.4±0.2	0.3±0.2	-0.2±0.2

Table 4.4: Summary of some of the power laws in forced and decaying 3D-MHD turbulence. α represents the power law exponent. Also shown are the errors in determining these power laws.

Physical quantity	More power laws in 1024^3 simulations (k^α)		Decaying turbulence
	Forced turbulence		
	low k $(7-30)$	high k $(250-400)$	
Residual energy E_k^R	-2.1±0.3	-0.4±0.4	-7/3±0.2
Residual helicity H_k^R	-1.4±0.3	1.1±0.4	-1.8±0.3
Magnetic vector potential A_k	-3.8±0.3	-2.8±0.4	-3.9±0.3
Current j_k^2	0.1±0.2	1.4±0.3	0.1±0.2

Table 4.5: Some more power laws in forced and decaying 3D-MHD turbulence. α represents the power law exponent. Also shown are the errors in determining these power laws.

This is the equation for the magnetic helicity spectrum in EDQNM and it has three terms on the r.h.s.. For using this equation, stationarity is assumed eliminating the partial differential with respect to time on the l.h.s.. If the inertial (scaling) range in the spectra is only considered, then dissipative effects from the second term of the l.h.s. are negligible. The direct effect of the forcing is also not present in this inertial range. Thus it can also be neglected. Hence now, the terms left are the three terms on the r.h.s. The first term $T_{V\tilde{M}}^{\tilde{M}}$ indicates the interaction of magnetic helicity and kinetic energy terms. The second term $T_{\tilde{V}M}^{\tilde{M}}$

indicates the interaction of magnetic energy and kinetic helicity. Finally, the term $T_{M\tilde{M}}^{\tilde{M}}$, represents the interaction of magnetic energy and magnetic helicity, as can be seen from the equations (3.29 - 3.31). The $\triangle$ restricts the integration to wave vectors $\mathbf{k}, \mathbf{p}, \mathbf{q}$, which form a triangle in the $p - q$ plane, defined by $k = |p + q|$. The time θ_{kpq} is the characteristic of the eddy damping of the nonlinear energy flux involving the wavenumbers k, p and q [14, 7]. It is defined phenomenologically, but its particular form does not play a role in the following analysis [14]. From the spectral analysis it is seen that the nonlinear interactions between velocity field and magnetic field are present in the system and that there is an increase in magnetic energy at the cost of kinetic energy (both the time evolution and spectral evolution support this fact). At the same time, it is also seen that the magnetic helicity flux supports an active inverse cascade (spectral transfer) both in the forced and decaying cases. In particular it remains fairly constant in the forced case. Similar things are happening for magnetic and kinetic energies, where spectral transport to low k regions, is seen. Hence to understand the influence of the velocity field on the magnetic field, the terms of the equation (4.4), that contain interaction quantities of both the fields are preferred over the terms containing quantities belonging to the same field. Thus the third term is dropped from the analysis.

Now the two terms left are $T_{V\tilde{M}}^{\tilde{M}}$ and $T_{\tilde{V}M}^{\tilde{M}}$. The triadic interactions of k, p and q can be both local and nonlocal. Hence in principle, all possible triadic interactions are considered. This is in tune with an argument that the nonlinear mode interactions of $\mathbf{v}$ and $\mathbf{b}$ fluctuations on a small scale say $k_0{}^{-1}$, simultaneously generate large-scale Fourier components on all scales [70]. Thus the inverse cascade process may not be a step-by-step process, but may be a long-range spectral process [70].

Hence writing the two terms in their dimensional form yields:

$$kp^{-1}q^{-1}h_{kpq}(k^2 H_p^M E_q^V - p^2 E_q^V H_k^M)$$
$$\sim kk^{-1}k^{-1}k^2 H_k^M E_k^V$$
$$\sim kH_k^M E_k^V \sim T_1, \qquad (4.5)$$

$$kp^{-1}q^{-1}h_{kpq}(k^2 p^{-2} H_p^V E_q^M - p^2 k^{-2} H_q^V E_k^M)$$

$$\sim kk^{-1}k^{-1}k^2 k^{-2} H_k^V E_k^M$$

$$\sim k^{-1} H_k^V E_k^M \sim T_2. \quad (4.6)$$

Here the wavenumbers p and q have been written in the dimensional form of k. Looking at these terms, it can be said that, the first term (equation (4.5)) represents the effect of nonlinear magnetic field line deformations by the turbulent flow as the magnetic helicity tries to inverse cascade, while the second term (equation (4.6)) represents the effect of the twisted velocity field fluctuations in the turbulent flow on the evolution of magnetic helicity, as the velocity of the flow tends to reduce in strength and in turn the strength of the magnetic field tends to increase at its expense. These two processes might have their origins in the Lorentz force terms in the vorticity and induction equations (here equation (4.1) and (4.2) also see section 1.1.2) which represent the nonlinear interactions between the magnetic and velocity fields and are also the terms through which the energy transfers from one field to other can take place. Thus to attain some clear picture on how these two processes are related to each other and show the observed spectral and spatial behaviors (studied in next chapter), in the inertial (scaling) ranges; it is supposed that there exists a dynamic equilibrium between these two processes; allowing the two terms to be equated dimensionally, as:

$$T_1 \sim T_2$$

$$k H_k^M E_k^V \sim k^{-1} H_k^V E_k^M. \quad (4.7)$$

This finally yields:

$$E_k^M \sim k^2 \frac{H_k^M E_k^V}{H_k^V}. \quad (4.8)$$

The terms E_k^V and H_k^V are dimensionally related by a factor of k. That is $E_k^V / H_k^V \sim k^{-1}$. In the forced case, when magnetic helicity is alone injected or in the case when both kinetic and magnetic helicities are injected, the plot of H_k^V / E_k^V appear to satisfy

this relation as seen in the (Appendix fig. C6 a,b and c). But the power laws of these quantities in the table 4.4, for the forced case do not satisfy this relation and tend to deviate as much as 10 and 20%; from dimensional argument; in high k and low k regions respectively. In the decaying case, this discrepancy is seen both in the plot as well as the power laws to as much as 50%. Dimensionally E_k^M and H_k^M are also related by a factor of k by $E_k^M \sim k H_k^M$. If the power laws from table 4.4 are plucked in this dimensional equation, the relation once again shows a deviation of 10 and 20% for the high k to low k regions of the forced case respectively. For the decaying case the deviation is once again 50% (also see the Appendix fig. C7 a,b and c).

But the relation in equation (4.8), on the whole is satisfied in all the three cases (two forced case scaling ranges and one decaying case scaling range), when all the four power laws in table 4.4 are plucked into it, at once without considering the errors. If the errors are also accounted for, then the deviation from the relation could be between 10 and 30 % in the low k region of the forced case and the decaying case, and between 10 and 50% in the bottleneck region (high k region) of the force case. This is an indication of the nonlinear mode interactions between **v** and **b**, which are driving the inverse cascade, while enhancing the magnetic energy at the cost of kinetic energy, thus supporting the analysis.

4.5.1   Interpretation

Writing the equation (4.8), as

$$H_k^V \sim \left(\frac{E_k^V}{E_k^M} \right) k^2 H_k^M.$$

(4.9)

or as

$$E_k^M \sim \left(\frac{k^2 H_k^M}{H_k^V} \right) E_k^V.$$

(4.10)

gives more insights into the system in hand. The equation (4.9) reduces to a simple dimensional relation between H_k^V and H_k^M if there is equipartition of energies (i.e. $E_k^M \simeq E_k^V$). This implies residual helicity ($H_k^R = H_k^V - k^2 H_k^M$) relaxes to zero, giving rise to Alfvén effect (see section 3.2.2).

If the equation (4.8) is now written as equation (4.10), it then states that if there is Alfvén effect, present in the system i.e. $H_k^V \simeq k^2 H_k^M$, then once again the r.h.s. and l.h.s. become equal. This implies residual energy ($E_k^R = E_k^V - E_k^M$) relaxes to zero, giving rise to equipartition of energies, at all scales, as seen in the numerical simulations of the EDQNM equations [7] and the eddy damping rate θ_{kpq} is dominated by the Alfvénic contribution τ_A the interaction time scales of colliding shear Alfvén waves (see section 3.2.1 and [7]).

It is clear from the spectra and the power laws obtained for kinetic energy, magnetic energy, magnetic helicity, kinetic helicity, residual helicity and residual energy, that they do not confer to either the equipartition or give any hint on the Alfvén effect. Hence the best form to write the equation, to truly represent the essence of the observed behavior in the simulations is indeed equation (4.8). Further equations (4.9) and (4.10) also tend to imply that the observed enhancement of magnetic energy, through the inverse cascade of magnetic helicity is a direct consequence of the two drivers residual helicity and residual energy, which are non-zero, here in these simulations.

Thus these simulations also strengthen the physical explanation given for the generation of inverse cascade through a phenomenon called 'helicity or α effect' (see pp.332 and 342 of [7] for a complete explanation). It specifies that residual helicity is the true motor of instabilities, which drive the magnetic energy and magnetic helicity towards the larger scales. The local Alfvén effect (temporary equipartition at a given particular scale), creates the imbalance in helicities, which further drives the magnetic helicity and magnetic energy to larger and larger scales by the 'helicity effect' from that particular scale. This process thus mainly leads to a limited saturation of the spectra at a given large-scale (or small wavenumber), but overall saturation of the spectra can never be obtained, as there is no limit for the large scales that could be achieved, through this process [7].

In the numerical simulations, inverse cascade drives the peak of the spectrum to smaller k. But when this peak reaches close to the boundary (or may even hit it) the system has no more scope to evolve and in such a scenario, saturation of the spectra is observed (here it is only an numerical anomaly). It was reported in [30] that the transfer of magnetic helicity to large scales, is initially quick for certain amount of time and reaches a saturation (because of the saturation in magnetic energy). From then on this movement to large scales proceeds in an extremely slow manner following a $\approx 1 - e$ curve, where e is the exponential function. Thus there are no hard and fast rules on when to stop the numerical simulations, as theoretically, the largest scales obtained

could be infinity. Normally simulations are stopped well before the boundary effects start to dominate and contaminate the spectra with reflections. This slow down of inverse cascade process, after a brisk start, is also seen in this work. But it is not possible to determine any specific time relation for this slow down as the equation mentioned in [30] uses mean magnetic field configuration, while here in this studies, there is no mean magnetic field. It is also emphasized here that sufficient care was taken in order that the spectra are free from boundary effects, by introducing a energy sink at small k values (see section 2.6).

Discussion

Thus from equation (4.8) and the discussion that followed, it can be speculated that, the increase in the magnetic energy might be due to an interaction between the magnetic and kinetic helicities, via the residual helicity route. This interaction might cause more knottedness in the plasma, creating large magnetic structures, whose integrated energy (the quantity generally plotted in the spectrum) shows an increase. Because of the same knottedness, velocity of the flow might reduce and cause a decrease in the kinetic energy (also observed in the spectra). In this process, kinetic energy is transformed at low k into magnetic energy. Hence at low k it is at least an order smaller in amplitude to magnetic energy, while at high k both the energies are almost equal (see fig. 4.11). Since the flow velocity is decreasing, the vorticity also shows the same behavior, which in turn diminishes the value of kinetic helicity. This relation is also supported through the visualization of the spatial structures and structure function analysis, in the next chapter.

Although the tables 4.4 and 4.5, show power law behaviors in several quantities, only four quantities have been found to show an internal relation ship among them selves as seen from the equation (4.8) and the discussion that followed it. Earlier the power law behavior of one of the quantities (i.e. residual energy) was explained in [14]. But there are several other quantities (e.g. residual helicity, magnetic vector potential and current) which have been reported to show power law behaviors for the first time in this work. The underlying physics leading to the power law behaviors in these quantities is not well understood and it also appears that the present models (including EDQNM) are not capable of revealing this physics. It is quite probable that for understanding these power law behaviors and the physics behind them, a new set of approximations or even a new mathematical set up involving the MHD equations, might be necessary. The above mentioned unresolved task, although very interesting, is beyond the scope

of this work.

Chapter 5

Influence of Inverse Cascade of Magnetic Helicity on the Spatial Structures of 3D-MHD Turbulence

Spatial structures are the other aspect of turbulence, studied after spectral properties, to gain further insights into a turbulent flow. Here, in this chapter, the spatial properties of 3D-MHD turbulence are discussed, under the influence of inverse cascade of magnetic helicity. It has been found in this work that forcing at high k does not result in large-scale magnetic structures, but only forms regions of concentrated magnetic field which appear to have structures of fractal dimensions; as suggested by a model curve of structure function exponents. To overcome this and form large magnetic structures, the forcing has to be withdrawn after a certain amount of time and this results in the large-scale structure formation. This issue is discussed in detail, substantiating the claims with structure function exponents. Correlation functions and PDFs are also discussed.

5.1   Structures in Forced Turbulence

Although traditionally first the structure functions, intermittency and then structures are studied in that respective order; here in this work first the structures in the forced turbulence are discussed. This is done because, it is seen that for the type of high k forcing used, the structures formed are not actually the ones, expected but are much different. This difference makes for an interesting study, later in the discussion. When the magnetic field structures in the forced turbulence case are looked at $t = 6$,

they appear as shown in fig. 5.1 a,b,c and d.
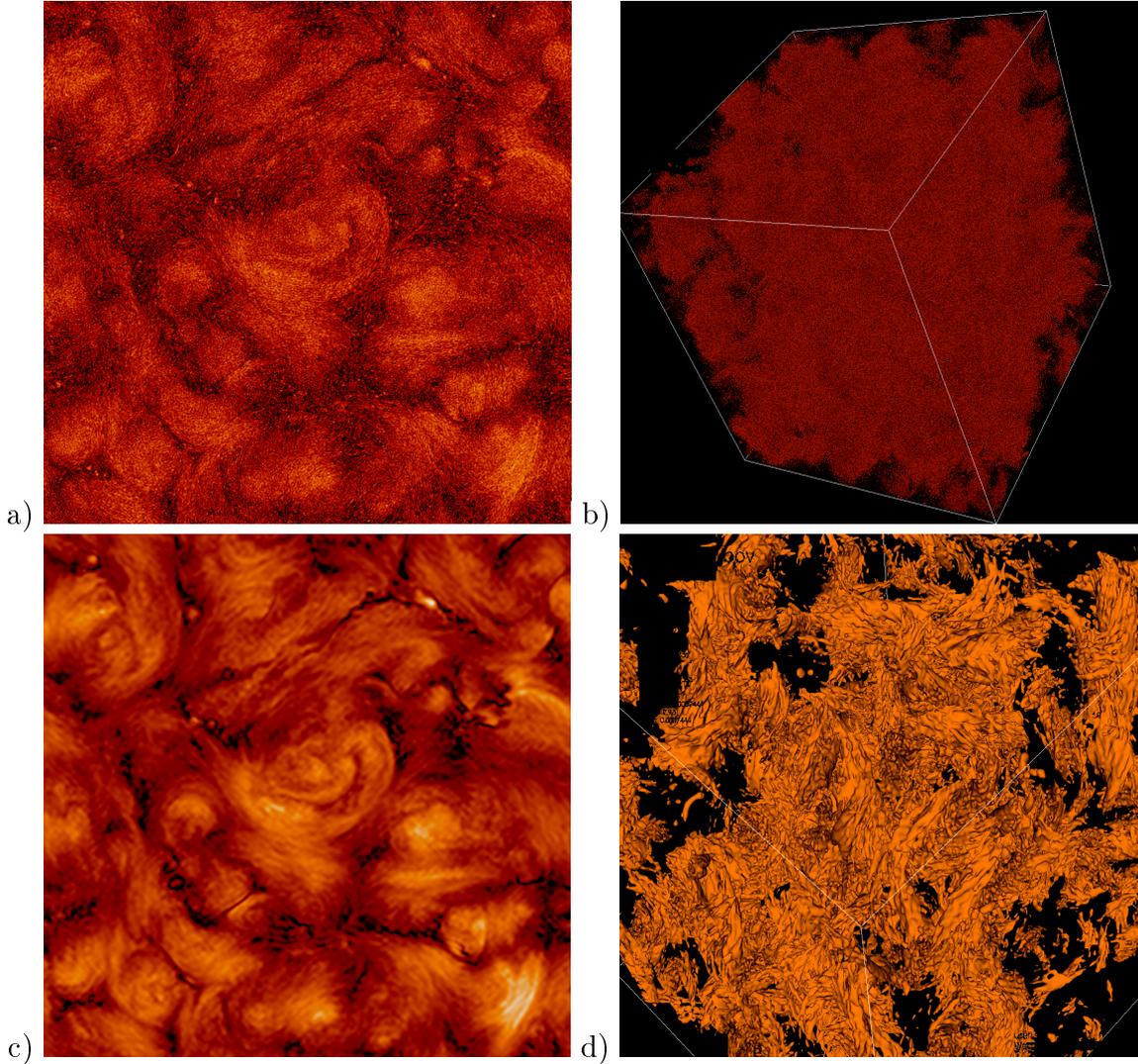
Figure 5.1: Magnetic field structures and iso-surfaces in the forced case. a) cut across the plane of unfiltered magnetic field structure b) iso-surfaces of unfiltered magnetic field c) cut across the plane of cut-off filtered out put of magnetic field structures and d) iso-surfaces of the cut-off filtered out put of magnetic field.

From the pictures in fig. 5.1 a and b, it is clear that the structures in the high k forced turbulence are significantly influenced by small-scale fluctuations. The iso-surfaces seen are also an indication of the small-scale structure present there. But the spectra indicate an increase in the magnetic energy and inverse cascade of magnetic helicity suggests that the structures formed should be larger. To see these large structures

more clearly, a high-k cutoff filter is used. The filter is characterized as follows:

$$f(k) = \begin{cases} f(k) & \text{if} \quad k \leq k_{cutoff}, \\ 0, & \text{otherwise}. \end{cases} \tag{5.1}$$

The filtered output is shown in the picture of fig. 5.1c and iso-surfaces of the same are seen in the picture of fig. 5.1d. The filter cut-off is placed at $k \sim 70$. From these two pictures it can be inferred that the magnetic field has several regions of high concentration. But these regions are like clumps of several small scales and do not show any definite expected large-scale structures. Modeling of the iso-surfaces points to the fact that the inherent features in the field are fractal in nature, as a result of high k random forcing used here (see section 5.3 for the modeling), i.e. the iso-surfaces are neither one-dimensional nor two-dimensional structures but have a co-dimension of 1.5 (see section 5.3). This filtered system is what is studied in the forced case, for understanding the structures, structure functions and other statistical properties of the forced turbulent system. From here on the reference to forced case implies the output obtained from the cut-off filter. Also all these features are studied for the new strategy (termed here as special case) in which the forcing is stopped, allowing decaying turbulence to take charge, to form the large-scale magnetic structures (the idea explained in detail in section 5.5.3). Decaying case is also reported separately.

5.2   Structure Functions and ESS

The definition of a structure function has already been mentioned in section 3.3 (which was arrived at using equations (3.1) and (3.2)). This equation was written there in terms of velocity. For many other quantities, a similar equation could be written. Thus a general form of the equation is now reproduced here as:

$$\delta c_\ell = [\mathbf{c}(\mathbf{r} + \boldsymbol{\ell}) - \mathbf{c}(\mathbf{r})] \cdot \boldsymbol{\ell}/\ell \tag{5.2}$$

$$c_\ell = \left\langle \delta c_\ell{}^2 \right\rangle^{1/2}. \tag{5.3}$$

$$S_p^c(\ell) = \langle \delta c_\ell{}^p \rangle \sim \ell^{\zeta_p}, \tag{5.4}$$

Here ζ_p is a constant, p-dependent scaling exponent and $\mathbf{c}$ is any quantity like velocity or magnetic field or Elsässer variable. Note that the equation (5.4) is only valid in the inertial (scaling) range(s) of the spectra.

Here it is also to be noted that only velocity is Galilean invariant and is the primary quantity that is plotted in the 2D-hydrodynamic case. The Elsässer variable $\mathbf{z}^{\pm}$, represents the total energy which is an ideal invariant in 3D-MHD (not Galilean invariant), under the assumption of negligible cross helicity (i.e. when $H^C \sim 0$, then $(\mathbf{z}^+)^2 \sim (\mathbf{z}^-)^2$ and $E \sim \frac{1}{4}(\mathbf{z}^+)^2$). Magnetic field is not an invariant of any form. However, since total energy is dominated by magnetic energy and also since the interest is on understanding magnetic field structures; here structure functions for magnetic field and $\mathbf{z}^+$, are plotted.

Structure Functions

In general, from the equation (5.1) several orders of structure functions can be plotted. In this work the structure functions of order 1 to 8 are plotted. Convexity and monotonicity constraints ([1]) are not applicable to odd order structure function scaling exponents, so there is a chance that the odd order structure functions can become negative (see [1]). Hence all the structure functions plotted here are calculated from the absolute values of field increments, avoiding cancellation effects, in the averaging process. Considering the fact that higher order structure functions suffer from severe statistical convergence errors, in this work the order of structure functions plotted is limited to eight orders, although it is possible to plot many higher order structure functions. Using the extended self similarity approach (see below) these eight orders of structure functions accurately and adequately represent the scaling behavior in the structures. Figures 5.2a,b and 5.2c,d are the structure function plots of $\mathbf{z}^+$ and $\mathbf{b}$ respectively. Figure 5.2a represents the structure functions at states closer to the initial states of the systems (exact times mentioned in the caption of the figure), for $\mathbf{z}^+$ in all the three cases mentioned in section 5.1. Figure 5.2b is the final state of structure functions of $\mathbf{z}^+$. Figures 5.2c and 5.2d are structure functions of $\mathbf{b}$ at the same instances respectively. On all these graphs the x-axis is from 0 to 2π, the limits of the bounding box. All the four figures show two orders of structure functions S_2 and S_8. The forced case is plotted in red, special case in green and decay case in blue from here-on in this entire section.

In the initial state, the decaying turbulence structure function has the highest magnitude, the forced case comes second and the special case comes last, for both S_2 and S_8. In the decaying case, this plot corresponds to the state of the system which for a short period of time has a large amount of energy before the actual decay process starts (see

fig. 4.2). For the forced case it is the state when turbulence has started (see fig. 4.3). Since the special case has its origin in the forced case, the plot here also corresponds to the case where turbulence has just kicked in. It is in fact at this point in time that the forcing is withdrawn from the system. The shape of the plots show a region over which all of them have a constant value. This trend changes in the final stages of the simulation i.e. fig. 5.2b, where the magnitude of the forced case dominates while the decaying case has the least magnitude of the three. These features in the forced case are a result of sustained input of magnetic helicity through the driving, while for the decaying case the energy is in dissipative phase, without any input. For the special case, it is tending towards the decaying case. The same trend is observed for **b** in fig. 5.2 c and d.

An important property of structure functions is that they exhibit self-similar behavior, in the inertial range as $S_p^c(\ell) = a_p l^{\zeta_p}$. Thus the knowledge of a_p and ζ_p character- ize the statistical distribution of eddies in the inertial range [17, 20]. These scaling exponents are expected to be clearly visible in the logarithmic derivate plots of the structure functions as the derivatives asymptotically form a plateau at inertial-range scales. These plateaux appear in front of a fall-off of the curves at large scales. The log- arithmic derivatives approach a constant value immediately in front of this transition from inertial to large scales.

a)
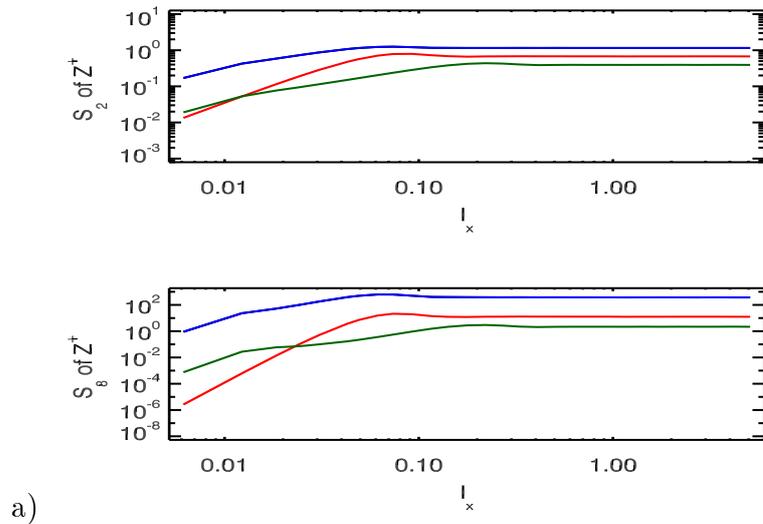
Figure caption on page 93
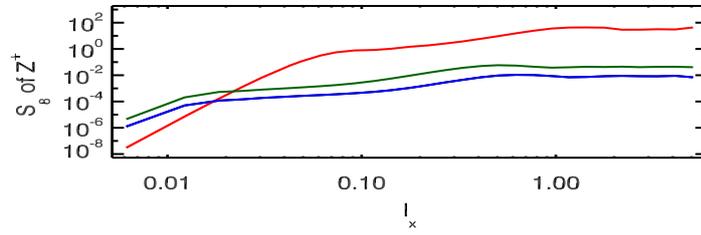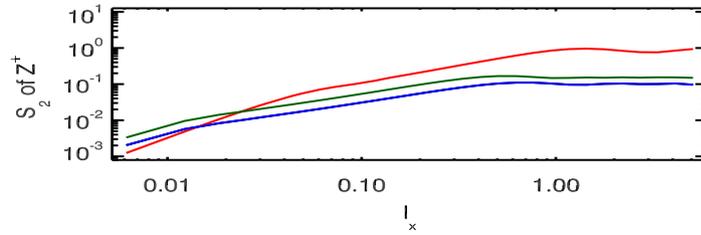
b)
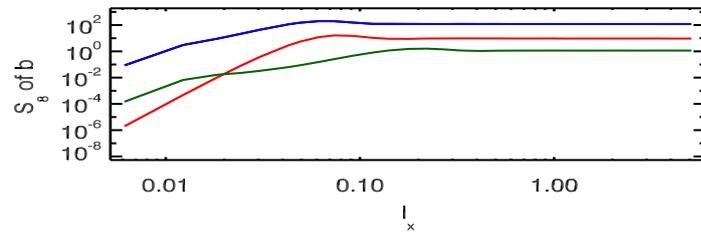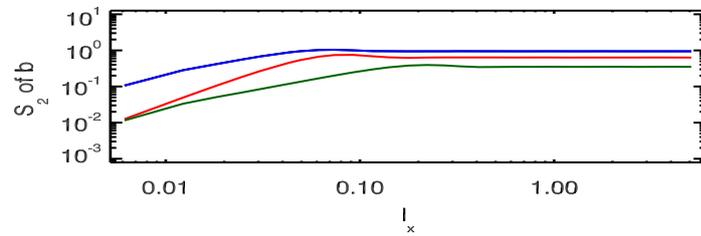
c)

Figure caption on page 93

d)
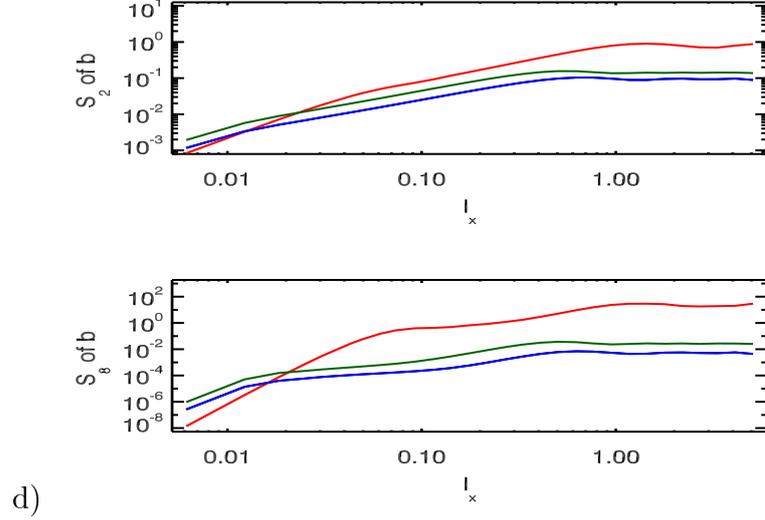
Figure 5.2: Structure Functions of S_2 and S_8 for $\mathbf{z}^+$ and $\mathbf{b}$. a) initial states of all the three cases for $\mathbf{z}^+$, b) final states of all the three cases for $\mathbf{z}^+$, c) initial states of all the three cases for $\mathbf{b}$ and d) final states of all the three cases for $\mathbf{b}$. The three cases: red: forced, green: special and blue: decaying. The initial times are t=1.28, t=0.36 and t=0.18 for forced, special and decaying cases respectively. The final times are t=6.66, t=5.89 and t=9.33 for forced, special and decaying cases respectively.

This value indicates the most probable scaling exponent of the structure functions at inertial range scales.

Logarithmic Derivatives

The logarithmic derivative of the structure functions are given by $dlnS_p^c(\ell)/dln(l)$ and as already mentioned they show a flatness in and around the inertial range. The y-axis value at which this flatness occurs for the second order structure function, is indicated by ζ_2 and it is related to the spectral power of the energy spectrum by $\alpha = 1 + \zeta_2$, where α is the magnitude of the power law [1]. Thus the y-axis component for this logarithmic derivative plot of $\mathbf{z}^+$, at which flatness occurs, serves as one of the confirmation methods for the spectral power law of energy, in turbulent systems. This plot becomes unstable as order increases because of the accumulation of statistical noise at high orders. The next set of plots in fig. 5.3 a-d, show the corresponding logarithmic derivatives of the structure function plots of fig. 5.2 a-d respectively. In the plots of fig. 5.3 a and b, the logarithmic derivative for the structure functions of fig. 5.2 a and b are shown.

a)

b)
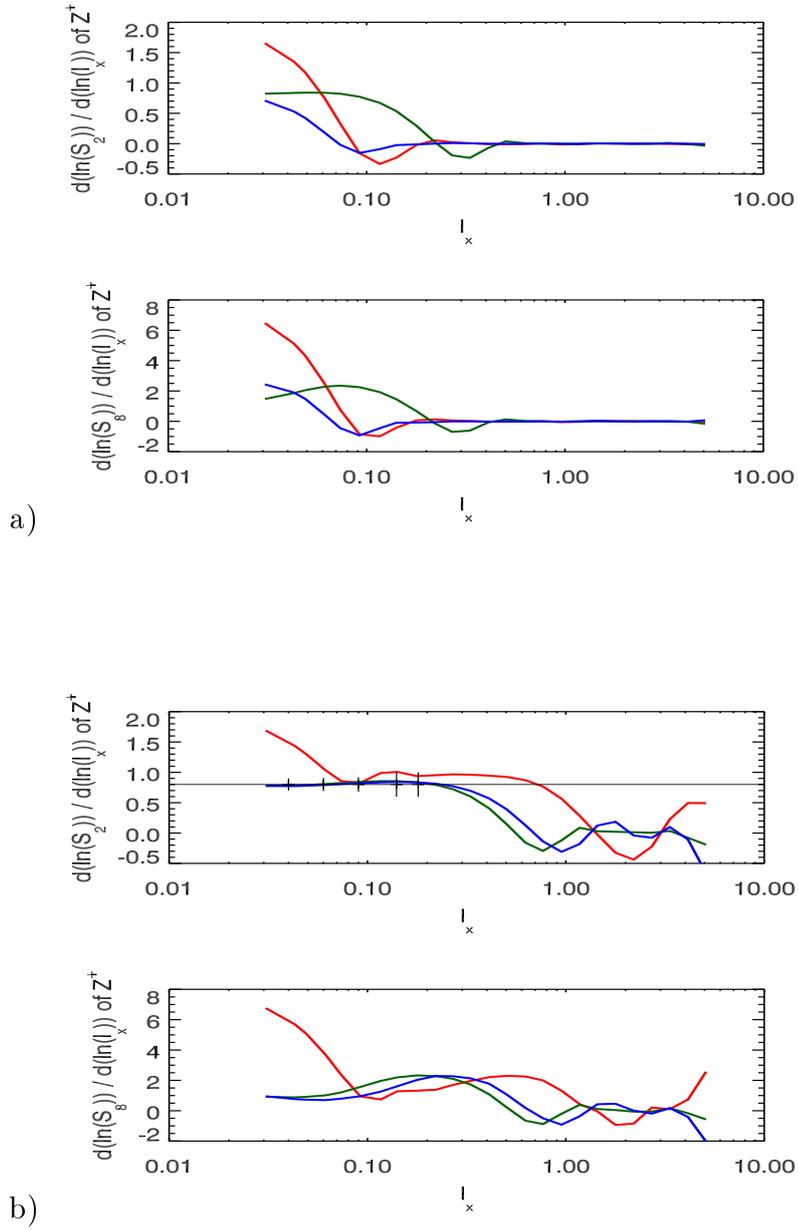
Figure caption on page 95

c)

d)
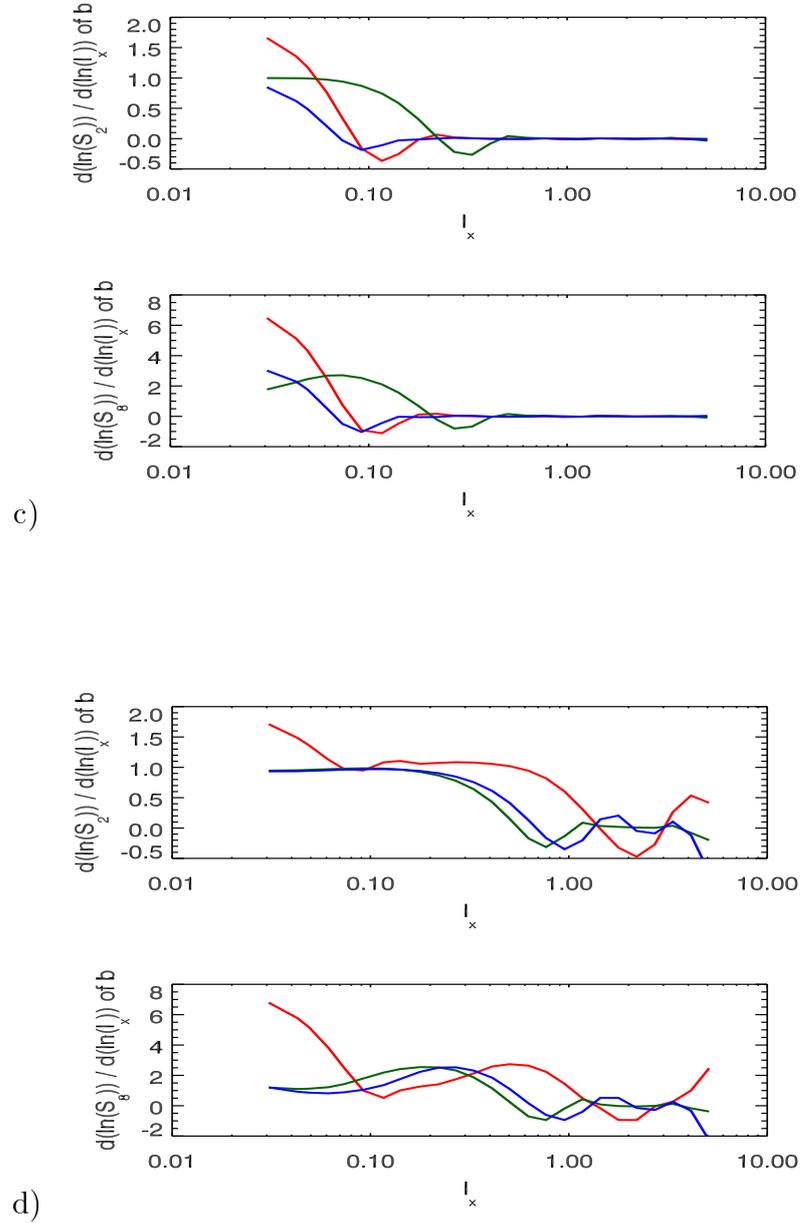
Figure 5.3: Logarithmic derivatives of structure functions of S_2 and S_8 for $\mathbf{z}^+$ and $\mathbf{b}$. a) initial states of all the three cases for $\mathbf{z}^+$, b) final states of all the three cases for $\mathbf{z}^+$, c) initial states of all the three cases for $\mathbf{b}$ and d) final states of all the three cases for $\mathbf{b}$. The three cases: red: forced, green: special and blue: decaying.

The initial plots (fig. 5.3a) do not yield the scaling function exponents as the turbulence in all the three cases is not fully developed. From the final state the scaling exponents

are estimated. For the decay and special cases, a constant value is observed in the logarithmic derivative plot from 0.04 to 0.18 for S_2, which corresponds to the inertial range of $k = 7 - 30$ in the energy spectrum of the decay case (see fig. 4.10c). The exponent value obtained is 0.8 with an error of ± 0.05 in the initial part of the range (at 0.04 of the x-axis) to as high as ± 0.2 (at 0.2 of the x-axis) in the final part of the range, as seen from the horizontal line shown in the top plot of fig. 5.3b. For the forced case, the plateau region starts at 0.15 and extends up to 0.6, but this does not correspond to any inertial range in the energy spectrum. The value of this plateau region is 1. However the plot joins the decay and special case curves briefly between 0.07 to 0.09, which is the closest it gets near the inertial range. The actual expected exponent value is 0.66 but the associated fitting procedure cause measurement errors (shown by the error bars in the plot) which are estimated by the vertical extension of the plateaux. The usage of hyperviscosity in the simulations may also have an effect on the structure formation process [66], probably affecting the determination of the value of the exponent. The higher order plot (S_8) generally shows more irregular behavior owing to accumulation of statistical noise. Although the nature of the curve looks similar for magnetic field, no such exponent estimates are made from its plots of fig. 5.3 c and d as it is not an ideal invariant. It has also been observed that logarithmic derivative plots of lower order structure functions are more orderly than the higher order ones. Thus it is difficult to determine a structure function constant ζ_p, for higher orders, as p becomes larger than 4 [17, 20]. The statistical noise levels are high for the higher order structure functions and errors are also high in this method. Thus an approach called extended self similarity (ESS) is used (see section 3.3.1), to get better understanding of the structure function exponents, principally at higher orders. In ESS, all other structure functions are drawn relative to a lower order structure function, whose structure function exponent is unambiguously known, or known with minimum error.

ESS

The basic idea and equation for ESS was explained in the section 3.3.1 through the equations (3.39) and (3.40). They are reproduced here for further discussions.

$$S_p(S_r(\ell)) \sim (\ell^{\zeta_r})^{\zeta_p} \sim \ell^{\xi_{p,r}}, \tag{5.5}$$

$$\zeta_p = \xi_{p,r}/\zeta_r. \tag{5.6}$$

Here $\xi_{p,r}$ is the relative scaling exponent and equation (5.5) gives the prescription to attain the absolute scaling exponent ζ_p, when any other structure function S_p, is plotted relative to S_r. In this work, S_r is the second order structure function, as it has a strong relation with the energy spectrum. Consistently, for magnetic field too the second order structure function is used as the base.

a)

b)
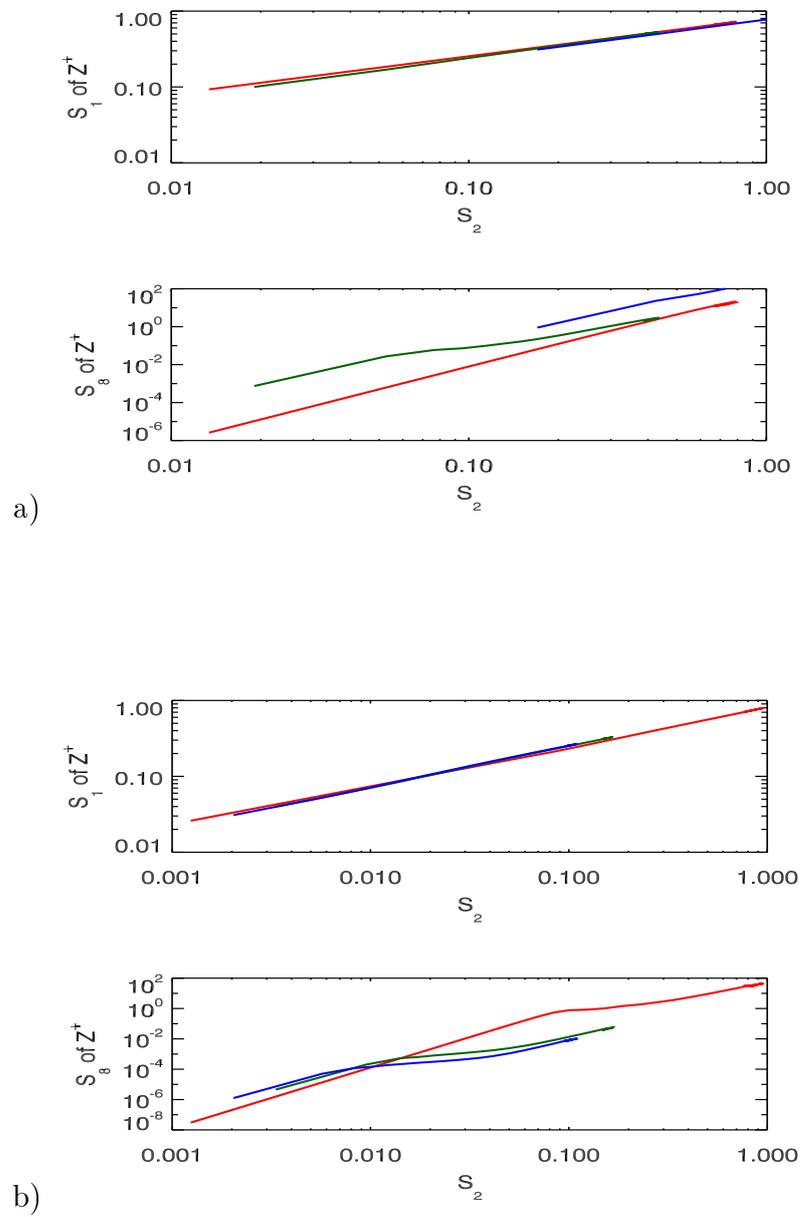
Figure caption on page 98

c)

d)
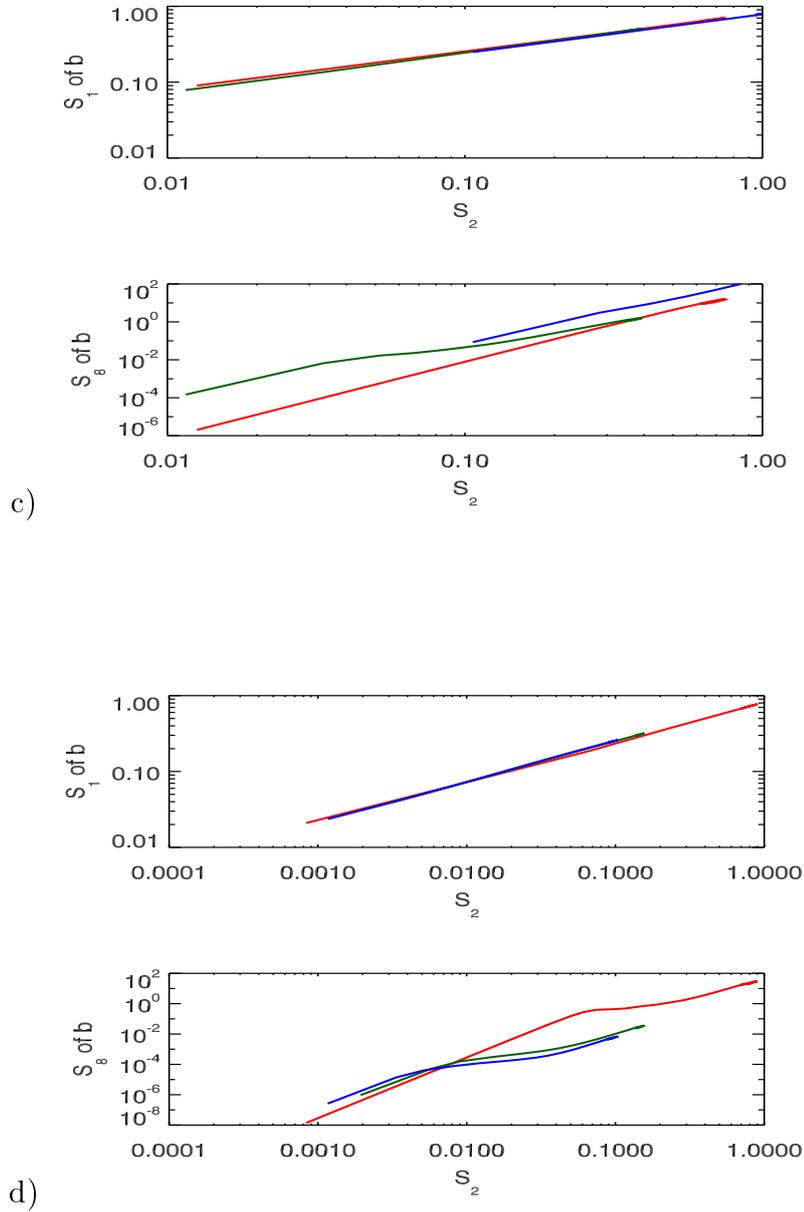
Figure 5.4: Extended self similarity plots for S_1 and S_8 with respect to S_2 for $\mathbf{z}^+$ and $\mathbf{b}$. a) initial states of all the three cases for $\mathbf{z}^+$, b) final states of all the three cases for $\mathbf{z}^+$, c) initial states of all the three cases for $\mathbf{b}$ and d) final states of all the three cases for $\mathbf{b}$. The three cases: red: forced, green: special and blue: decaying.

The advantages of this approach stem from the fact that structure functions of the same field exhibit same kind of features in their shape. Thus when a structure function

is plotted relative to a lower order structure function, the former gets compensated and the noise levels are suppressed well, bringing out the inertial ranges of the structure functions of higher orders more prominently.

For getting the higher order structure function exponent, the plot of any other structure function S_p relative to S_r is plotted. This normally shows up as a straight line (in lower order structure functions) to near straight line (in higher order structure functions). A straight line is fitted through this curve and the slope and y-intercept are calculated. The slope gives the structure function exponent. It is a practice that the same curve is drawn at fairly large intervals of time, so that the structure function exponent is determined to a better accuracy and error is also determined to a greater degree. Care also is taken to choose these different intervals belong to the state of the system where the turbulence is fully developed and the spectra are showing a self-similar behavior. It was found that the minimum error in most of the cases, in this work, was of the order of ± 0.0001 in the lower order exponents to a maximum of ± 0.09. The ESS plots of the $\mathbf{z}^+$ and magnetic field are shown in fig. 5.4 a and b and fig. 5.4 c and d for all the three cases respectively. Here it is seen that at lower order i.e. S_1 Vs S_2, the curves are almost straight lines but for higher order i.e. S_8 Vs S_2, a significant deviation from straight line is observed. All the other curves lie in between these two extreme cases. It can also be seen that the decaying case and special case almost every time go together while the values in the forced case span a large range. This is an indication of presence of both small scales and large scales in the forced case at two extreme ends of these curves (see red curves in the fig. 5.4 a,b,c and d). From these plots, it is seen that indeed the ESS method suppresses the statistical noise and makes the determination of the structure function exponents, a lot easier.

5.3 Intermittency and Modeling

Intermittency is one of the common features of real turbulent systems. Ideally, it is assumed that the dissipative structures of same size are distributed self similarly in a turbulent flow, all over the space [1, 48]. Practical turbulent flows, both in experiments and numerical simulations, show a varied distribution of these dissipative structures. This deviation accounts for the nonlinear behavior seen in the higher order structure function plots. More theoretical back ground on this was discussed in chapter 3 under section 3.3.2.

Following that discussion, and the general formula in equation (3.47), the structure

function exponent is written as:

$$\zeta_p = (1 - x)p/g + C_0(1 - (1 - x/C_0)^{p/g}). \tag{5.7}$$

Here on the l.h.s. is a value that is determined from ESS. On the r.h.s. is the model, whose parameters x, g and C_0 are determined on physical grounds, based on phenomenological models. This equation is in general called the log-Poisson model. Based on phenomenologies, the parameters on the r.h.s. are determined. The two possible phenomenologies used are Kolmogorov and Iroshnikov-Kraichnan (see sections 3.1.2 and 3.1.3). In the first case, $x = 2/g$ where $g = 3$ for isotropic MHD turbulence. p is the order of the structure function under consideration and C_0 is a co-dimension variable that is set to three possible values i.e. 1,2 and 1.5. If $C_0 = 1$, then it represents the two-dimensional structures (sheets), when it is 2, it represents one dimensional structures (filaments) and when it is set to 1.5, it represents fractal dimensions.[1] In case of IK phenomenology, $x = 2/g$ where $g = 4$.

order p	Structure function exponents for $\mathbf{z}^+$					
	ξ_p/ζ_2		ξ_p/ζ_2		ξ_p/ζ_2	
	filtered		stopped forcing		decay	
	t=3.09	t=6.66	t=3.05	t=5.78	t=6.00	t=9.33
1	0.52±1e-3	0.52±1e-3	0.54±1e-3	0.54±1e-3	0.55±1e-3	0.55±1e-3
2	1.	1.	1.	1.	1.	1.
3	1.45±5e-2	1.44±5e-2	1.38±5e-2	1.37±5e-2	1.36±2e-2	1.35±2e-2
4	1.85±0.02	1.82±0.02	1.68±0.02	1.64±0.02	1.63±5e-2	1.59±5e-2
5	2.22±0.04	2.15±0.04	1.90±0.03	1.83±0.03	1.82±0.03	1.76±0.03
6	2.56±0.06	2.44±0.06	2.06±0.05	1.97±0.05	1.95±0.05	1.86±0.05
7	2.88±0.08	2.72±0.08	2.19±0.06	2.07±0.06	2.05±0.06	1.93±0.06
8	3.18±0.09	2.99±0.09	2.29±0.08	2.14±0.08	2.12±0.07	1.97±0.07

Table 5.1: Structure function exponents for $\mathbf{z}^+$. Errors in each case are also shown.

---

[1] From [1], the probability of finding an object of linear size l and dimension d in a D dimensional unit box is $\sim l^{D-d}$. Also $C_0 = D - d$ is the co-dimension of the dissipative eddies as $< \epsilon_l^n > \sim l^{-nx} l^{D-d}$ for order of the exponent $n \gg 1$, where ϵ is the dissipation in the structures and x the scaling exponent. Here it is to be noted that the dissipative structures can have irregular but self-similar shapes, hard to be defined by Eulerian geometry and hence are called fractal. They have dimensions which are not integers but are fractions. In fact any fractional dimension could be used but $C_0 = 1.5$ appears to give the best model curve consistent with the scaling exponent curve.

	Structure function exponents for magnetic field					
order p	ξ_p/ζ_2		ξ_p/ζ_2		ξ_p/ζ_2	
	filtered		stopped forcing		decay	
	t=3.09	t=6.66	t=3.05	t=5.78	t=6.00	t=9.33
1	0.52±1e-3	0.52±1e-3	0.54±1e-3	0.54±1e-3	0.54±1e-3	0.54±1e-3
2	1.	1.	1.	1.	1.	1.
3	1.44±5e-2	1.42±5e-2	1.39±5e-2	1.37±5e-2	1.37±2e-2	1.36±2e-2
4	1.83±0.02	1.78±0.02	1.68±0.02	1.65±0.02	1.63±5e-2	1.60±5e-2
5	2.17±0.04	2.08±0.04	1.89±0.03	1.83±0.03	1.81±0.03	1.75±0.03
6	2.49±0.06	2.35±0.05	2.04±0.04	1.96±0.04	1.93±0.05	1.84±0.05
7	2.78±0.08	2.61±0.06	2.15±0.05	2.06±0.05	2.03±0.06	1.91±0.06
8	3.06±0.09	2.86±0.09	2.24±0.05	2.14±0.05	2.10±0.07	1.95±0.07

Table 5.2: Structure function exponents for magnetic field. Errors in each case are also shown.

Thus a total of 6 models graphs are possible for each set of structure function exponents, on the l.h.s.. From the data plots and the overlapped model plots, a conclusion can be arrived at, on the nature of the structures and phenomenology of the turbulence. Hence first from the ESS analysis, structure function exponents for several orders at different time intervals, are determined. Here this is done for 3 cases a) forced case, b) decaying case and c) special case (stopping the forcing at a certain point of time and allowing system to decay).

a)
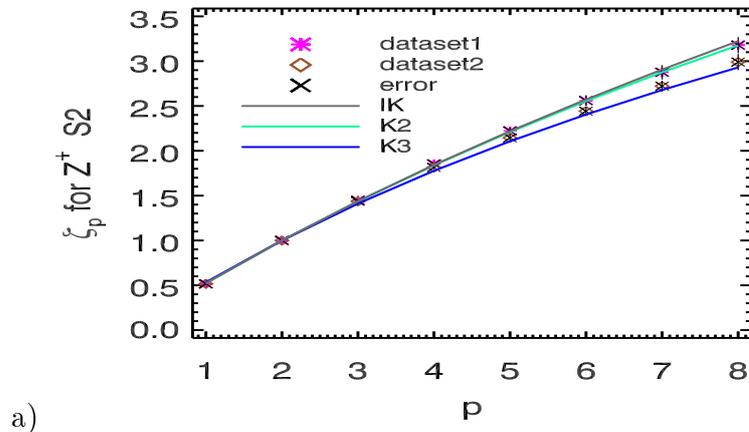
Figure caption on page 103
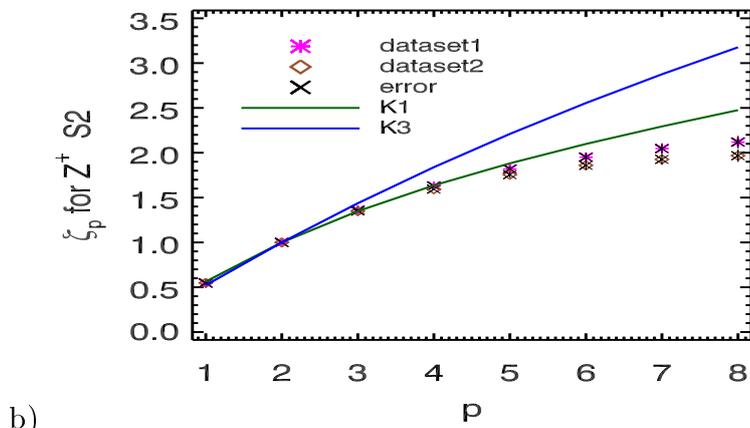
b)

c)

d)

Figure caption on page 103

e)

f)
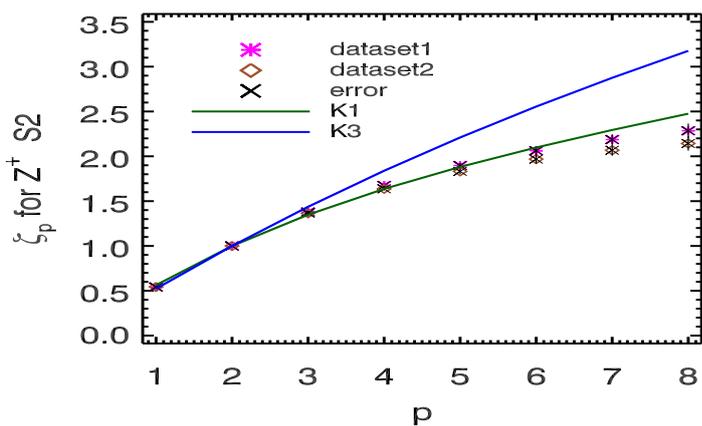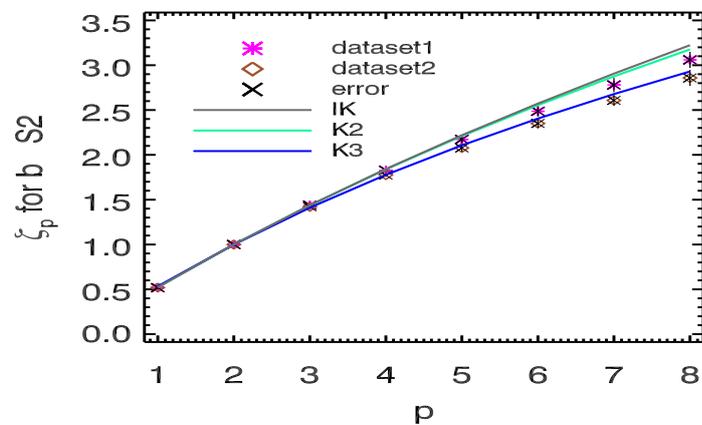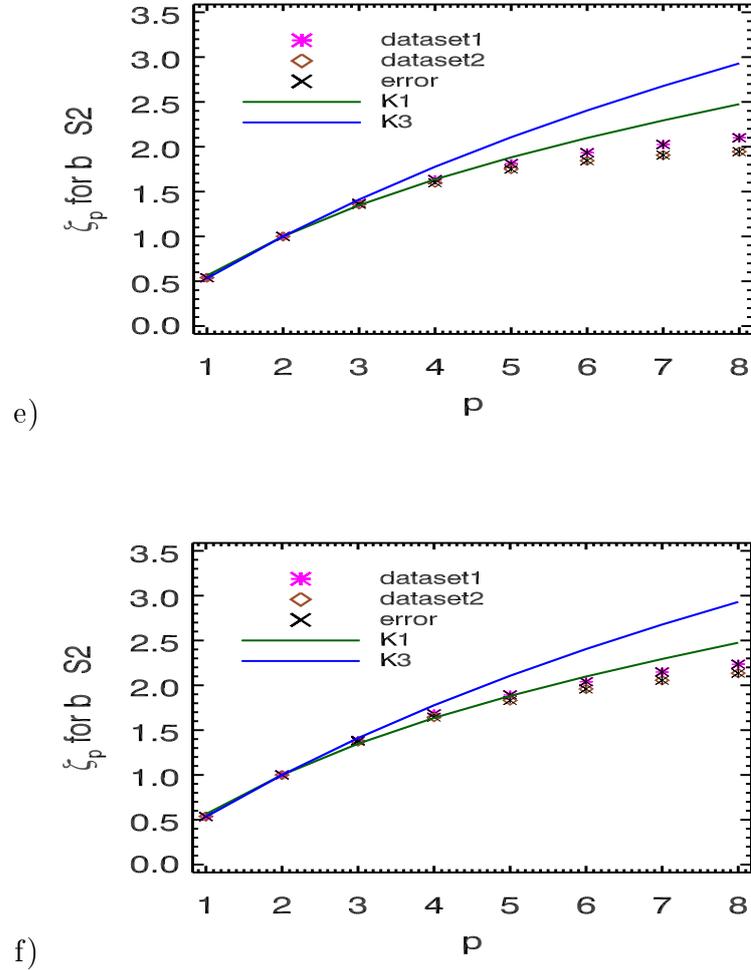
Figure 5.5: Intermittency Modeling a) ζ_p Vs p for $\mathbf{z}^+$ for forced case, b) ζ_p Vs p for $\mathbf{z}^+$ for decaying case, c) ζ_p Vs p for $\mathbf{z}^+$ for special case, d) ζ_p Vs p of $\mathbf{b}$ for forced case, e) ζ_p Vs p of $\mathbf{b}$ for decaying case and f) ζ_p Vs p of $\mathbf{b}$ for special case. (Here K2: Kolomogorov curve with C_0=1.5, K3: Kolomogorov curve with C_0=2, K1: Kolomogorov curve with C_0=1 and IK: Iroshinikov-Kraichnan curve with C_0=1). dataset1 and dataset2 are the data from the table 5.1 and 5.2 dataset1: the first column of each case and dataset2: second column of each case. Note that the estimated error when plotted is within the plotted data symbol size.

The results from this studies are summarized in the table 5.1 and 5.2 for $\mathbf{z}^+$ and $\mathbf{b}$ respectively. Plotting the values in the table, with relevant model plots of the possible 6 combinations of the equation (5.7), for each column, results in figures 5.5 a-f. Figures 5.5 a,b and c represent the structure function exponent curves of $\mathbf{z}^+$ for the three cases discussed here. Figure 5.5a represents the plot for forced case. Here at the first

instance i.e. t=3.09 dataset1 coincides with IK curve completely (hence magenta curve not seen) but as time progresses, the data aligns towards K2 the Kolmogorov type curve with fractal dimension structures. The other two cases decay (fig. 5.5b) and special cases (fig. 5.5c) are virtually indistinguishable at the times chosen here. Both align towards the Kolomogorov type curve with two dimensional structures. Figures 5.5 d,e and f represent the structure function exponent curves for magnetic field. Here in the forced case both the datasets are visible. The dataset1 is in between K3 and K2 i.e. it represents structures with either one dimension or fractal dimensions. The dataset2 moves towards K2 representing fractal dimensional structures. Once again the plots of other two cases are indistinguishable and align towards K1 curve representing two dimensional structures. If an earlier starting point was taken for the special case and the final curve is kept *as is* then the effect of forcing and its removal on the structure formation can be perceived, which will be explained in section 5.5.3. From the plots it can be inferred that in the forced case, the structures lie between IK type curve with two dimensional structures in the early part of the simulation. They get closer to K2 type curve with co-dimension equal to 1.5, with the progress of time, for total energy. In the case of magnetic field, the data sets lie between K3 and K2 curves indicating 1 to 1.5 dimensional structures. For both the decay case and the special case, the curves match closely with K1 in the lower orders and deviate at higher orders. Hence, in both these cases, the structures formed are predominantly two-dimensional.

From these observations, it can be inferred that although there is an inverse cascade of magnetic helicity, taking place from high k to low k, in the high k forced system, the structures formed appear to be either locally anisotropic in nature or of fractal dimensions. In other words, the forced case does not show coherent large-scale structure formation but only forms regions of field concentration. Sub-scale structures are also produced. Which means the inverse cascade progresses and forms large-scale structure, but because of the forcing, these structures break down into fractal dimensioned structures at small k. In the decaying case and the case when forcing is withdrawn at a certain point of time, the structures formed are two dimensional, while here too inverse cascade is active but without any forcing. This observation, is further substantiated with structure studies. From the analysis of the data and its modeling using the phenomenological model curves, an idea about the underlying phenomenology can be obtained, which then would point out to the dynamical processes responsible for the turbulent flow. In this work, the proximity of the data curves to the Kolmogorov type curves in all the three cases, suggest that probably in the MHD turbulent flows studied

here, the ideas from Kolmogorov's phenomenology on turbulence are more valid. This view gains strength by observing the evolution of the magnetic field from very small scales to large scales (see fig. 5.18) where the magnetic field structures grow in a similar manner as the hirarchial eddies in an atmospheric turbulence (2D-hydrodynamic). It is very important to note that in this work, such a behavior is limited to magnetic field structures alone and no such tendency is observed in the velocity field. Thus it can be suggested that the internal dynamics of the turbulent flow which is responsible for the inverse cascade of magnetic helicity (which in turn is responsible for the formation of the large-scale magnetic structures) although, appears to be similar to the hirarchial eddy model of Kolmogorov phenomenology, rest of the quantities in the flow do not strengthen this opinion in totality. Iroshnikov-Kraichnan phenomenology is almost ruled out in both the turbulent flows (decaying and forced) studied here. Hence, the results obtained from this work point to the fact, once again, that there is no proper phenomenological or theoretical model, that can explain the MHD flows entirely (see also section 3.1.4).

5.4 Other Statistical Tools

In the studies of structure functions, only two quantities $\mathbf{z}^+$ and $\mathbf{b}$ were used. $\mathbf{j}$ or current and magnetic helicity structures are also very interesting to study and may also contribute to the understanding of inverse cascade processes. Also since it was found that the trend of both $\mathbf{z}^+$ and $\mathbf{b}$ is almost the same, the quantity $\mathbf{b}$ will no longer be studied while looking at the probability distribution functions (PDFs) and Kurtosis plots.

5.4.1 PDFs

Intermittency is linked to the probability of occurrence of extreme events in the flow. One such measure of occurrence is the probability density function or PDF, of the considered variable. The PDF of any quantity c is $P(\delta c, l) \equiv P(\delta c)$. It depends on two variables, increments in c i.e. δc and the length l. The distribution of any uncorrelated random variable is a Gaussian, as stated by the central limit theorem. If there is any correlation, then deviations from this behavior are observed [1, 71]. Here first the sharpness and spread of the PDFs are discussed and then using Kurtosis plots, their flatness is also considered.

In all the following PDF plots, several length separations (bins) are chosen for plotting the spatial increment of any quantity (here three quantities: $\mathbf{z}^+, H^M$ and j^2) and the

plots are normalized to unit variance for clarity. The plots obtained by dividing the space into minimum number of bins (i.e. the ones which have largest spatial distance between any two sampled points) are the ones with minimum spread (magenta colored curves in each of these plots). As the number of bins increases, i.e. the distance between any two sampled points reduces, the spread increases in the plots (in many of the plots red curves represent this nature). The same trend is observed in the Navier-Stokes turbulence for velocity increments as reported in [71]. Please note that the time to which these PDFs correspond are the final states of the system considered in the structure function analysis in each case (i.e. t=6.66 for forced case, t=5.78 for special case and t=9.33 for the decay case). Also note that the x-axis which is a 'normalized increment' $\delta c/\sigma_{\delta_l} c$ where the term in the denominator points to the standard deviation at the chosen bin length (obtained from the second order structure function as $\sqrt{S_2}$ of any quantity).

Figures 5.6 a,b and c show the PDFs of $\mathbf{z}^+$ for forced, special and decaying cases respectively. Also shown are the reference Gaussian PDFs, with unit variance in each case. From these plots and their reference plots, it is seen that these PDFs are very close to the Gaussians but are not exactly Gaussians (also due to the overlap of several curves all the curves are not clearly seen). The near Gaussian PDFs of the largest length separation (i.e. the magenta colored curve) implies that extremely large scales are uncorrelated with each other. The PDFs with wide tails, which significantly deviate from the Gaussian behavior (e.g. red curve) in their tails, indicate that as the binning distance decreases, the correlations between the small-scale structures increase. The probability value from largest length scale to the smallest length scale at any particular chosen small increment varies over 3 to 5 orders, in each of the figures 5.6 a-c. Which means the probability of observing such an event reduces rapidly. The deviation of the tails of the curves at small length increments (more number of bins) from the Gaussian behavior can be interpreted as the presence of intermittency at small scales. The behavior of these plots also supports the way inverse cascade of magnetic helicity proceeds, and builds up magnetic energy at the cost of kinetic energy (equation 4.8). In the quantity $\mathbf{z}^+$ (which is the proxy for total energy), the dominant contribution is from magnetic energy. So, this quantity can be expected to follow the same trend as that of magnetic field. Hence the observed PDFs of $\mathbf{z}^+$ could be interpreted based on the nature of the structures in the magnetic field alone. The initial state of the system consists of extremely small scales which interact with each other to evolve into large scale structures. While doing so, the small scale structures can be expected to

have strong correlations among themselves, which results in those tails, that deviate from Gaussianity. As the number of large scale structures increases, the correlations among themselves can also be expected to decrease and the PDFs capture this behavior accurately.

In the forced case PDFs the central plot (magenta curve) is the closest curve to a Gaussian indicating small amount of correlation among the large-scale structures, while for the special case and the decay case, this curve is relatively broader, indicating some amount of correlations and even intermittency among the large-scale structures in these two cases. The observed trend in rest of the curves in all the cases is similar (i.e. considerable deviations from Gaussianity).

PDFs for magnetic helicity (fig. 5.7 a,b and c) show completely different trend. They have a sharp central peak (which fits well with a model Gaussian for decay and special cases) and pronounced wings, more like a Mexican hat. This trend is same for forced (with an exception that the model Gaussian does not fit the central peak), special and decaying cases. The important difference is in the sharpness of central peak. It is broader for the forced case. While the sharpness is much higher for the decaying or special cases, with the special case showing the sharpest peak. From these PDFs it can be inferred that there are only few types of distinct scales involved in the flow. One which are extremely large (responsible for sharp central PDFs) and other which are extremely small responsible for the broad but almost uniform tails. A smooth transition between the scales is absent. These features also point to a strong intermittency nature in the small scales.

a)
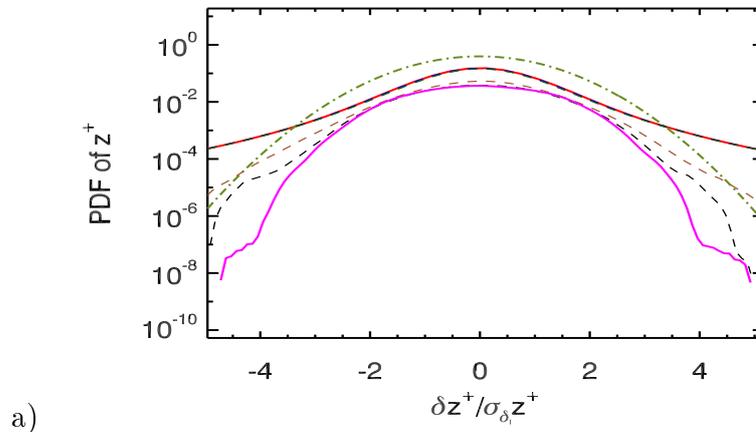
Figure caption on page 108

b)

c)
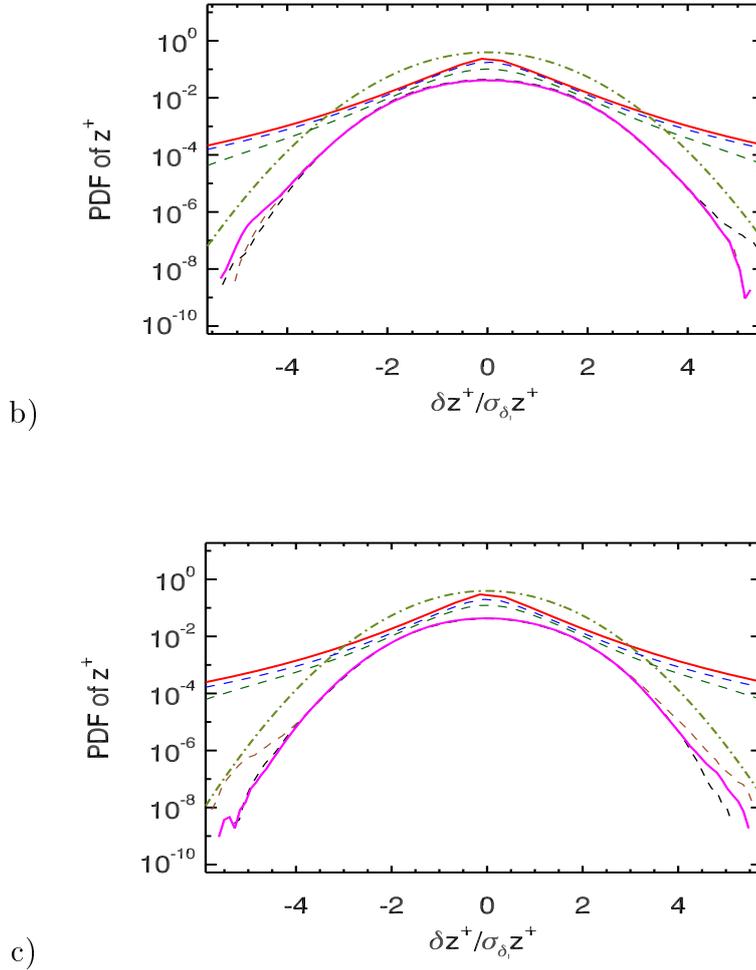
Figure 5.6: PDFs of $\mathbf{z}^+$ a) PDFs for forced case b) PDFs for special case and c) PDFs for decaying case (color code: largest size of the sampling bin: magenta to smallest size of the sampling bin: red and olive green curve : the reference Gaussian).

The nature of correlations among different scales here is very distinct and probably constant for several bin sizes i.e. even though the bin size varies, the nature of PDFs for several length scales remains the same as seen from the over lap of several curves. The PDFs of j^2 (fig. 5.8 a,b and c), show another different trend. They have narrower tops and very broad wings. Here it appears that there are no extremely large scales in the decaying and special cases but in the forced case there appear to be few (uncorrelated) large scale current structures.
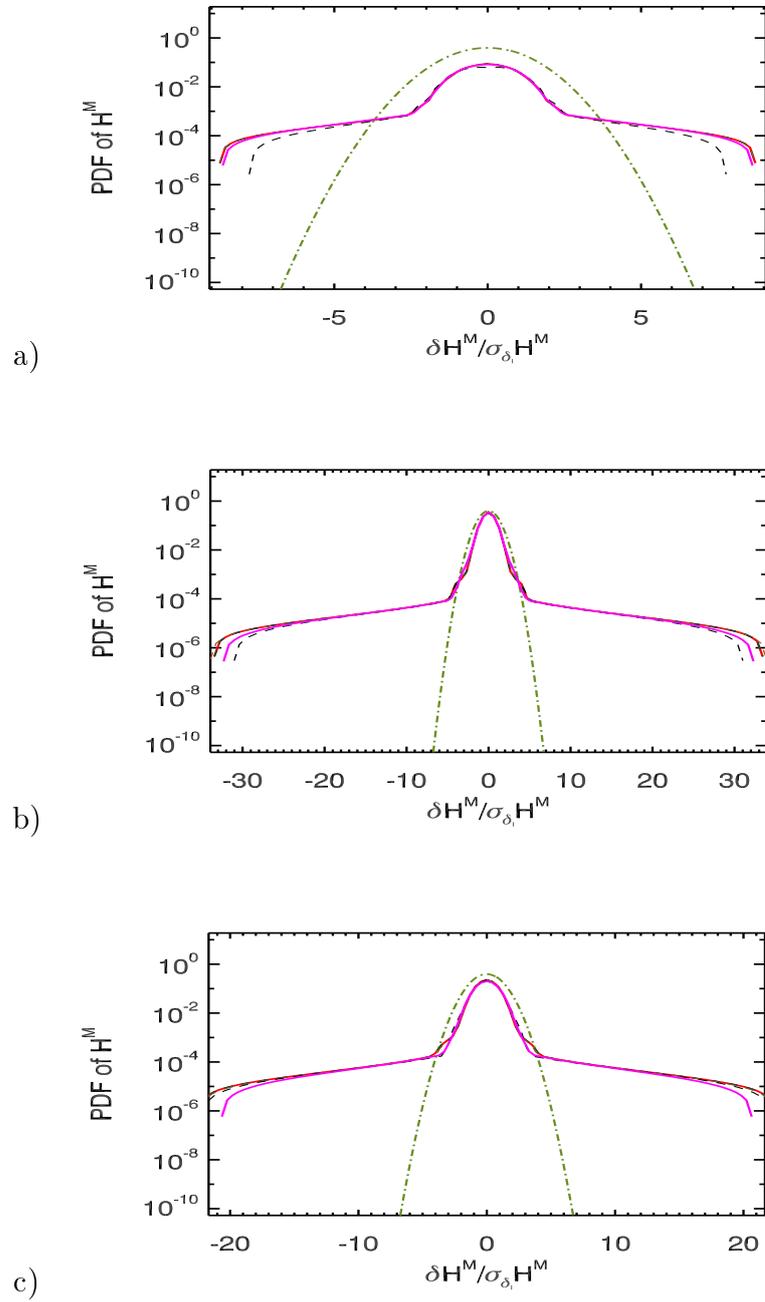
Figure 5.7: PDFs of H^M a) PDFs for forced case b) PDFs for special case and c) PDFs for decaying case (color code: largest size of the sampling bin: magenta to smallest size of the sampling bin: red and olive green curve: reference Gaussian). Here the overlap between the curves is very strong so all the plotted curves are not clearly seen.
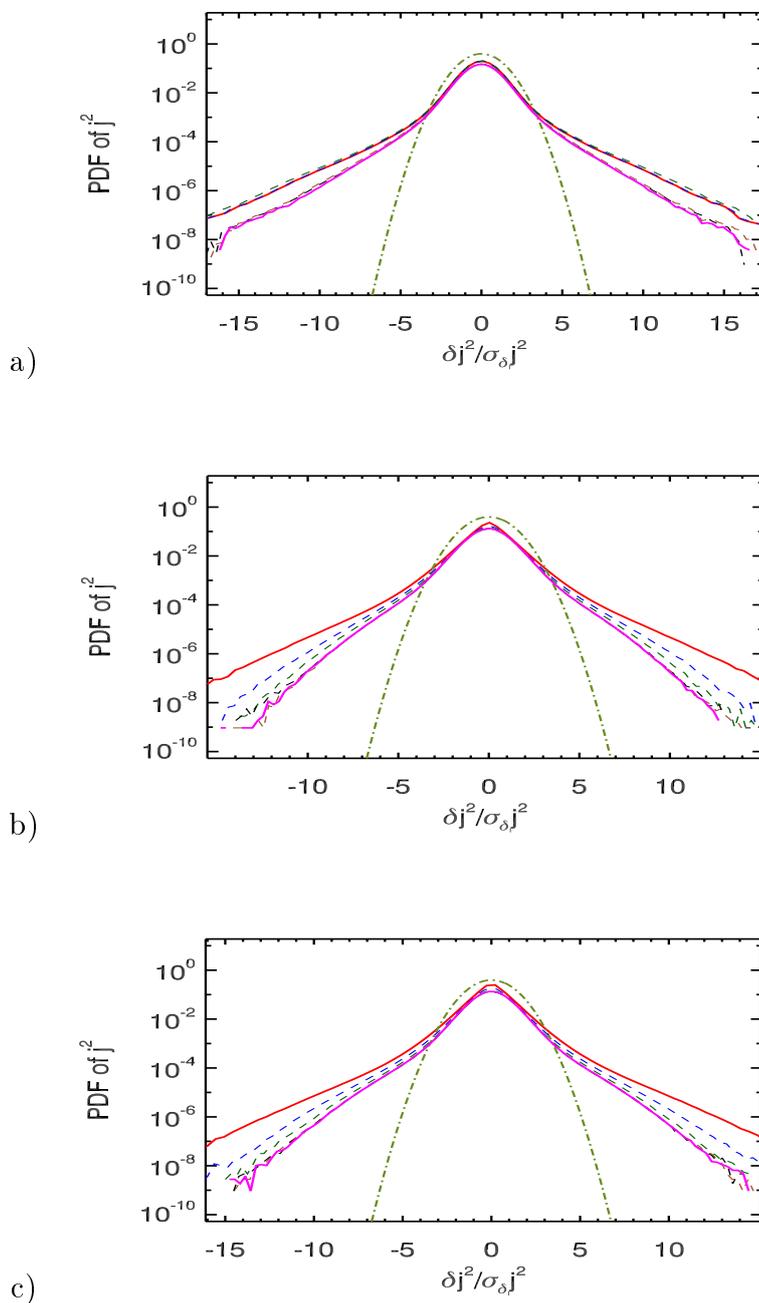
Figure 5.8: PDFs of j^2 a) PDFs for forced case b) PDFs for special case and c) PDFs for decaying case (color code: largest size of the sampling bin: magenta to smallest size of the sampling bin: red and olive green curve: the reference Gaussian).

In these PDFs the wings are extremely long and wide and for several binning sizes. This fact points out to the nature of current structures (generally thin sheet like) which do

not appear to change in length once they are formed and also are strongly intermittent (as seen from the deviation in the tails from the reference Gaussian). From all these sets of PDFs it can be inferred that though there is negligible cross helicity, the nonlinear mode interactions on small scales between **v** and **b** are present in large numbers as seen from the spread of the wings of the PDFs, which deviate from Gaussianity, and have strong correlations among themselves. One more tool which can help in better understanding of the structures is Kurtosis and it is discussed next.

5.4.2 Kurtosis

Kurtosis is a measure of 'peakedness' and 'flatness' of the PDFs. It is defined by:

$$F(l) = \frac{S_4(l)}{S_2^2(l)} \tag{5.8}$$

here S_4 and S_2 are the fourth order and second order moments respectively. The flatness of the Gaussian PDFs is exactly F = 3. High values of F characterize PDFs with sharp peaks and flat tails, where as low values identify PDFs with rounded peaks and broad shoulders. Thus the flatness F is a useful measure of intermittent features. Two sets of kurtosis curves are drawn for all the quantities. These two sets correspond to the initial state and final states of the systems that are used in the structure function analysis (see caption of fig. 5.2) above. From the analysis of the PDFs , some insight into the intermittent behavior of the MHD flows was obtained. Now from the Kurtosis plots at both initial state and the final state of the system, the changes in the intermittent behavior of several quantities in the flow can also be understood, while supporting the PDF analysis.

Figures 5.9 a and b represent the initial and final states of Kurtosis curves of $\mathbf{z}^+$ for all the three cases. It is seen that the value of Kurtosis is very high for the forced case in comparison with the other two cases, initially. The decaying case appears to show a near Gaussian Kurtosis in the initial stages and in the final state it has two regions. A region where the value of Kurtosis is at a peak and the curve showing a fall off and a region where it remains close to Gaussian. This is an manifestation of the same trend that was seen in the PDFs: peak values close to the Gaussian curve and broader tails deviating from the Gaussian. The same argument holds for special case too. For the forced case their is an slight increase in Kurtosis, but it attains a plateau in the small l region and closes towards the Gaussian in the high l regions. From the initial state plots it can be inferred that the initial state of the decaying case is a Gaussian distribution

(as described in the initial conditions in section 4.1). The chosen initial state for the forced case has dominantly small scales which have strong correlations and hence are highly intermittent (i.e. this is a transitionary state) and in the special case, where the forcing was withdrawn after a certain amount of time, it appears that the correlations among the small scales have just begun (since actual initial state of the forced case is also a Gaussian from which this special case has evolved) as does intermittency in its initial state. The final state plots in general, confirm the PDF analysis where strong intermittency in the small scales and very less or no intermittency in the large scales (i.e. strong correlations in the small scales and little or few correlations at the large scales) are observed.
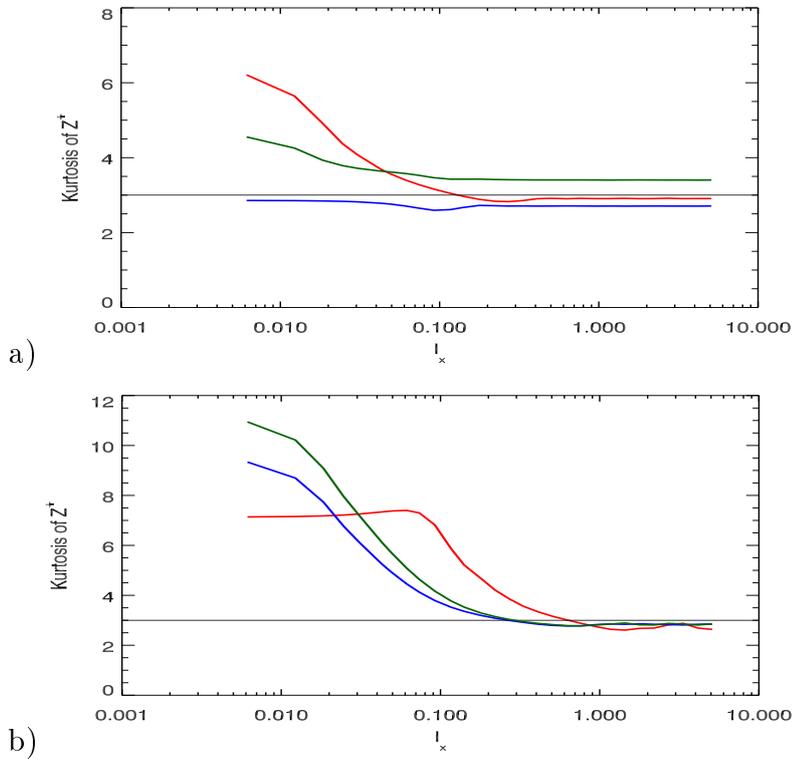
Figure 5.9: Kurtosis curves in the a) near initial and b) final state of the systems for $\mathbf{z}^+$. red: forced case, green: special case, blue: decaying case and black: reference line for Kurtosis of a Gaussian.

Figures 5.10 a and b represent the initial and final states of Kurtosis curves of H^M for all the three cases. All these three plots look alike. In the final state a flat region for almost all of l followed by a small parabola like bend at large scales is seen. This is also consistent with the PDFs seen above for magnetic helicity. They show very few types of structures and the intermediate scales are absent. This transition between the scales is not smooth but abrupt. Thus the two distinct features seen in the PDfs, the Mexican

hat and an abrupt tail , are corroborated. Also true is the strong intermittency seen in the PDFs as the values of the Kurtosis curves range from 200 in decaying case to about 20 in the forced case. Relatively small value of Kurtosis for the forced case may be because of the relatively flatter peak which do not fit with the model Gaussian in the PDFs. The initial state Kurtosis curves also look alike (like three parallel lines almost) but they do represent the dual scale nature of the magnetic helicity structures (seen in the PDFs) with values of the Kurtosis as high as 10^5 to as low as 3500. Since this state is not yet completely turbulent, these values do not make any impact.
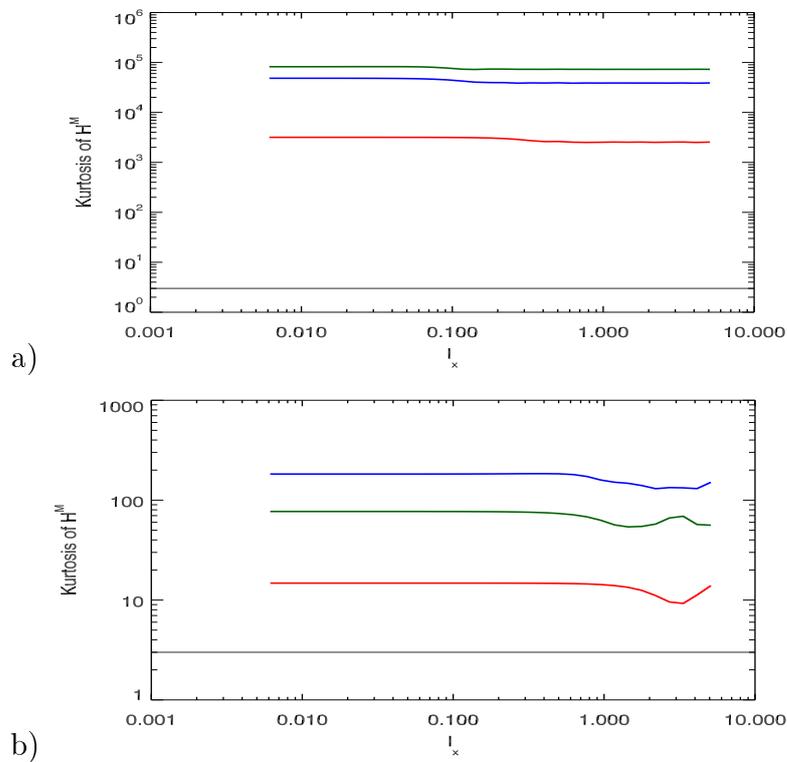
Figure 5.10: Kurtosis curves in the a) near initial and b) final state of the systems for H^M. red: forced case, green: special case, blue: decaying case and black: reference line for Kurtosis of a Gaussian.

Figures 5.11 a and b represent the initial and final states of Kurtosis curves of j^2 for all the three cases. The forced case Kurtosis in the initial stage appears like an exponential (only a shape comparison not a mathematical fit) but changes to a strange shape with two regions where the value shoots suddenly from 8 to 10 and then falls smoothly, close to 6. The special case starts at a value of about 5 but soon reaches to a constant value 4, which is spread over a large l. In the final state, it shows a significant increase in magnitude and a change in curve shape to an exponential like curve (here too only a shape comparison not a mathematical fit). The decay case in the initial state appears

to be close to a Gaussian all the while, but changes to an exponential like curve with a large magnitude as in the special case, in the final state.

j^2 structures once formed do not change in length (hence no change in correlation length) and almost remain the same. But they do show intermittent behavior as was reported in the PDF studies. These two facts once again are reiterated by the Kurtosis curves where the change in Kurtosis from initial state to final state is ~ 3. The shapes of these curves in the final states, do indicate that over the complete scale range, j^2 structures exhibit intermittency, which the PDFs could capture in totality. In the initial state however, only the chosen initial state of the forced case exhibits significant intermittency and the other two cases are close to the Gaussian and hence little or no intermittency.
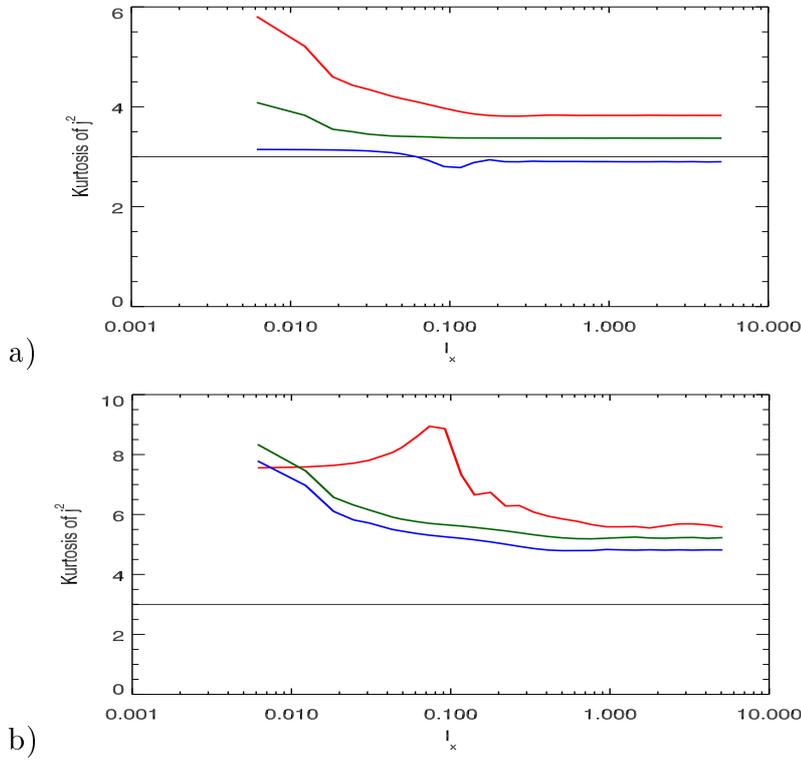
Figure 5.11: Kurtosis curves in the a) near initial and b) final state of the systems for j^2. red: forced case, green: special case, blue: decaying case and black: reference line for Kurtosis of a Gaussian.

5.4.3 Correlation Functions

Correlation function in the context of this work is defined as:

$$\rho(r) = \frac{\int_{-X}^{X} c_x(x) c_x(x+r) dx}{\int_{-X}^{X} c_x{}^2(x) dx} \tag{5.9}$$

where 'X' is taken to be much greater than any characteristic length scale associated with the fluctuations in c_x. Here it represents the boundary of the simulation box. The correlation length is defined in this context as the point where the function $\rho(r)$ falls to $1/e$. More generally, the Fourier transform of the autocorrelation of some one-dimensional function $g(x)$ is referred to as the one-dimensional energy spectrum of that function [1].

The correlation length is also an indication of the length scales. Here the following two plots in fig. 5.7 a and b represent the correlation functions of several quantities of interest in a 3D-MHD turbulent system for forced and special cases respectively. The decaying case correlation functions are exactly similar to that of the special case counterparts and hence are not shown here. The correlation function was chosen to be in the direction of $x - z$ plane but the notation $C(x)$ will continue to be used for this function. Here magnetic helicity falls from unity, crosses zero and goes into the negative side. The fact that it never is zero indicates to the formation of large structures in this quantity. It then starts rising and shows a trend close to periodic behavior. This behavior could also be explained from the presence of only a few type of scales (as was observed in the PDFs) in this quantity. Magnetic energy and total energy show exactly the same trend, giving more support to the fact that in this system magnetic energy is the dominant component of total energy. This function also appears to show long term periodicity. The velocity correlation function shows an exponential fall off. The current correlation function shows a sharp initial fall and from there it oscillates and shows the signs of dampening curve in the forced case, while it falls off smoothly without any oscillations in both special and decaying cases. This behavior of current correlation function may be due to the fact that the current structures do not vary in size once they are formed in the decaying case. In the forced cases however there can be current structures of more than one size as seen from the PDFs but it appears that the size of the structures in these different scale ranges might differ very little and this probably is the reason for the small oscillation seen in its correlation function. For all these correlation functions, a correlation length is estimated. For this purpose, the correlation function for each of these quantities is assumed to follow an exponential curve. In such a case, the correlation length is the value at which the curve falls by $\sim 1/e$. So, for each of these plots, in both the cases, the point where the value of the curve is $\sim 1/e$ of the initial peak value is identified. This is the correlation length in each of the quantities and it is here defined in the length units of the periodic box (also see caption of fig. 5.12). The correlation lengths of several quantities are tabulated as

shown in table 5.3.

a)

b)
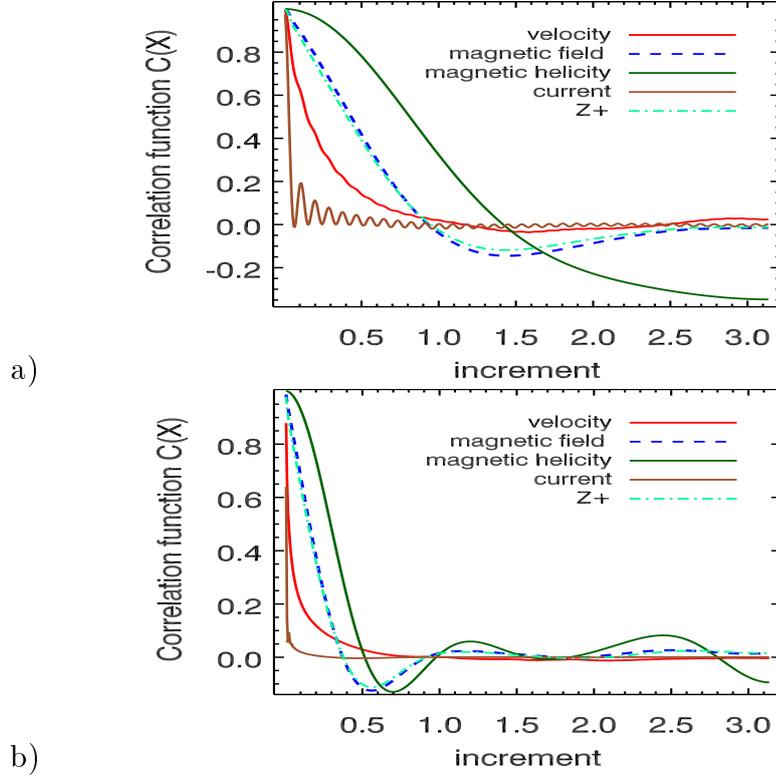
Figure 5.12: Correlation functions. a) Correlation functions from the filtered output for forced case and b) correlation functions for the special case

quantity	Correlation lengths of some quantities					
	filtered			stopped forcing		
	t=2.09	t=4.06	t=6.66	t=2.33	t=4.25	t=5.89
H^M	0.5	0.7	0.84	0.18	0.28	0.31
$\mathbf{b},\mathbf{z}^+$	0.32	0.43	0.5	0.01	0.15	0.17
$\mathbf{v}$	0.18	0.21	0.22	0.035	0.04	0.05
$\mathbf{j}$	0.04	0.04	0.04	0.02	0.02	0.02

Table 5.3: Correlation lengths of some quantities at three instances of time in the flow. The units for correlation length here are the same as units of length for the simulation box. Note that the length was made non-dimensional using a characteristic length scale (see equation (1.7). Hence the values obtained here are to be multiplied with characteristic length scale to get a quantitative value.

The correlation lengths are determined at three different points in time to know how this parameter changes in various quantities over time, in the simulations. From this

table it is clear that the correlation lengths increase for many quantities (which is an indication of increase in integral length scales), while correlation lengths for current remained the same. The other major indication from the increase in correlation length is that there is indeed an evolution from small scales to large scales (e.g. for magnetic field) in the system. The constant value of current correlation length, indicates that the current sheets are formed fairly early in time and remain more or less of the same size. The changes in the correlation lengths for velocity field are smaller indicating that probably the velocity field structures do not differ greatly in size.

5.5 Spatial Structures

The spatial structure in this work is significant in understanding the nature of the turbulent flow and the scales involved in the dynamics. The decaying case structures presented here are at t=9.33. Forced case structures presented are at t=6.66. These are the final states of the system in both the cases. For the special case, the times are mentioned when they are presented in the following section. Also the quantities presented below like magnetic field, velocity, current ($\mathbf{j}$) and vorticity are actually the moduli (absolute values) of their respective fields. Hence from here on if the word magnetic field or velocity is used in the context of the structures, it actually means that the *modulus* of that particular field is being discussed. First the structures for various quantities of interest are shown below for the decaying case.

5.5.1 Decaying Case

The structures of the decaying case discussed here are of a well developed turbulent system, where the inverse cascade of magnetic helicity transported several quantities from the initial small scales at k=70 to large scales at $k\sim3$. This system is expected to show large-scale structures. First the magnetic field structures are shown along with the iso-surfaces of the same in pictures of fig. 5.13 a and g respectively. Figure 5.13a shows the cut across the plane of the magnetic field. This shows strong tangled field structures and some magnetic reconnection regions in the field (explained later). Several intermittent scales (scales over which the field strength shows abrupt changes) are also seen. The iso-surfaces show two-dimensional structure. These are twisted flux tubes which are also the dissipative structures in the field.
Figures 5.13 b and c represent the magnetic helicity structures in three dimensions. Magnetic helicity shows huge structures (magnitude of magnetic helicity is shown in fig. 5.13b), like eyes in some places and column like structures all around. The iso-

surfaces (fig. 5.13c) show possibly the largest structures of any field. These structures are 3 dimensional and some of them extend over the entire box and can be compared to kinetic helicity flux surfaces seen in 3D-HD (see[72]). Figures 5.13 d and h represent the current structures. The current structures by magnitude are very large but are thinly spread over the entire plane. The iso-surfaces of current are thin sheet like. Figures 5.13 e and i represent the velocity field structures. The velocity field is low in magnitude and also thinly spread over the entire plane, but the structures show a strong intermittency. Iso-surfaces show thin sheet like structures. Figures 5.13 f and j represent the vorticity structures. The vorticity structures are also low in magnitude and thinly spread like the current structures. These structures appear to be similar to the ones seen in 2D-HD of [37]. The iso-surfaces show once again thin sheet like structures.

The magnetic field structures seen here are a result of build up of magnetic energy caused by the inverse cascade of magnetic helicity. Although the initial values for kinetic energy and magnetic energy are the same, it is clearly seen that the magnetic field structures are quiet stronger than their velocity field counterparts. Similar is the case for magnetic helicity and vorticity (which is a good proxy for kinetic helicity). Thus the spectral relation that was obtained in the previous chapter i.e. equation (4.8), appears to be valid for the decaying case. The interpretation that the magnetic energy is growing at the cost of kinetic energy is also substantiated. Several of the fields show strong intermittent behavior (e.g. velocity, current and vorticity) thus giving the much needed support to both the structure function and PDF analyses.

5.5.2   Forced Case Structures

Magnetic field structures in the forced case were already discussed in section 5.1. For completeness, shown here is the 3D-magnetic field in fig. 5.14a and iso-surface of the same in fig. 5.14b. The magnetic field structure shows some regions of field concentration and the iso-surfaces represent fractal structure as measured from structure function exponent curve (see previous section). All other fields (not shown here) also correspondingly behave the same way as their decaying counterpart quantities, but form regions of concentrations in their respective structures. Also the structures show a similar trend in their features, making it possible to believe that the relation in equation (4.8) is valid here too. It was observed in [8] that when the forcing was in low k region, large-scale structure was seen to appear. However in the context of this work, the forcing is in high k region.

a)

b)

c)

d)

e)

f)
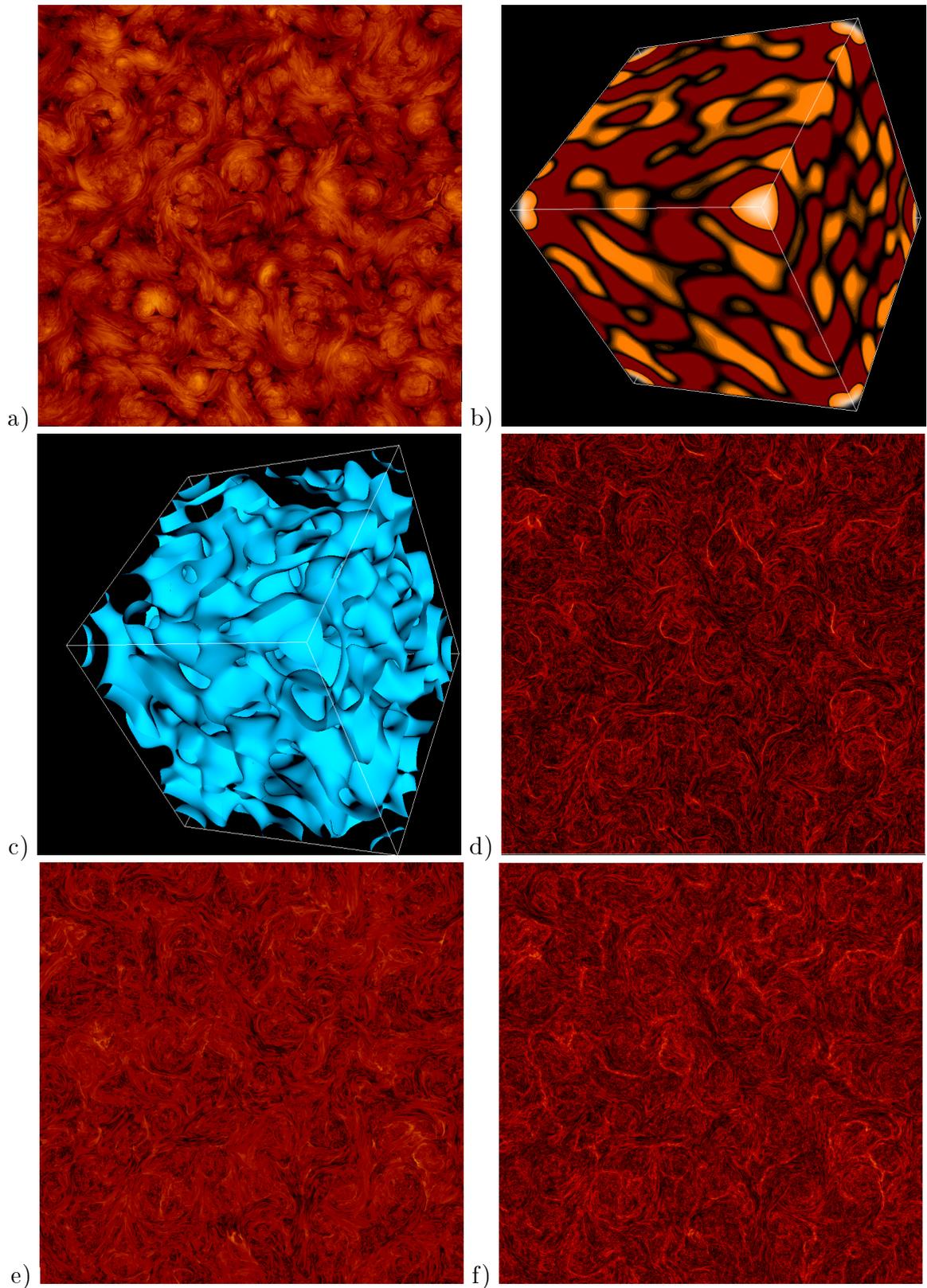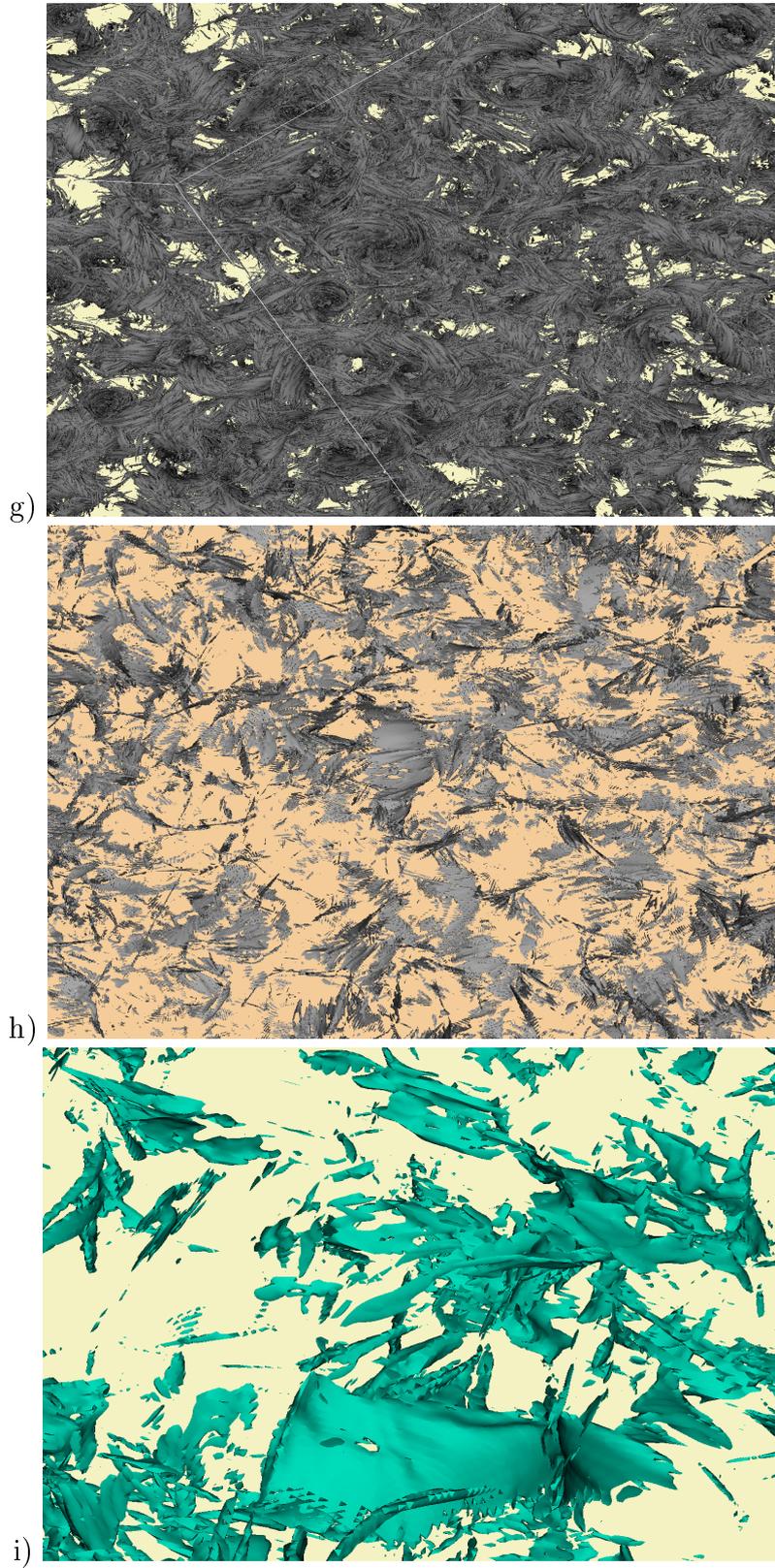
Figure caption on page 121

Figure caption on page 121

j)
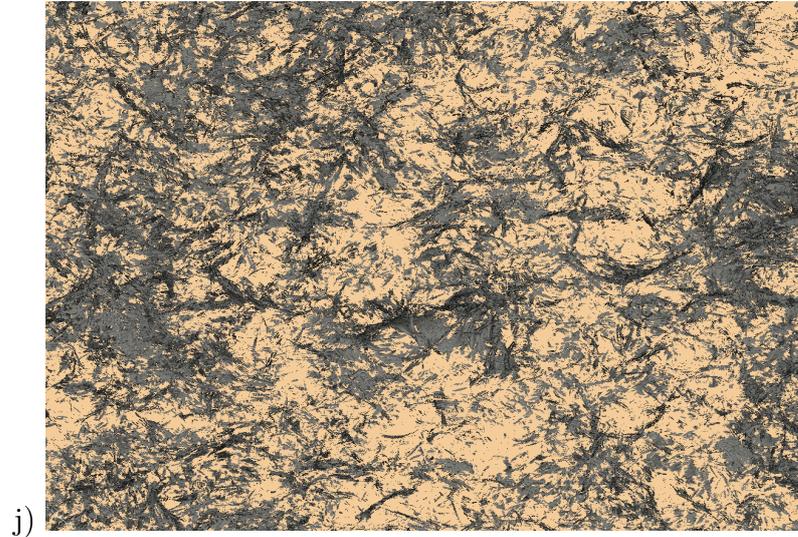
Figure 5.13: Real space structures and iso-surfaces for various quantities in the decaying case. a) cut across the plane of magnetic field structure, b) 3D-view of magnetic helicity structures, c) iso-surfaces of magnetic helicity, d) cut across the plane of current, e) cut across the plane of velocity field, f) cut across the plane of vorticity, g) iso-surfaces of the magnetic field (zoomed by 1.4 times), h) iso-surfaces of current (zoomed by 12 times), i) iso-surfaces of velocity (zoomed by 14.4 times) and j) iso-surfaces of vorticity(zoomed by 12 times). Resolution in all these pictures is 1024^3.

Thus it can be concluded that the initial state of the system and its location has a strong influence on the final structures formed. The forcing mechanism might also have a strong influence on the structures of various other quantities. The aim of this forced case is to see if this method results in large-scale structure formation. But since it only results in regions of field concentration, a new variation is now adapted.

5.5.3   Stop the Forcing

After looking at the structures in the forced case and decaying case, a new strategy is adapted in the forced case. In the evolution of magnetic helicity spectrum (fig. 4.5a), forcing is stopped at a specific point in time and the system is allowed to decay from then on.
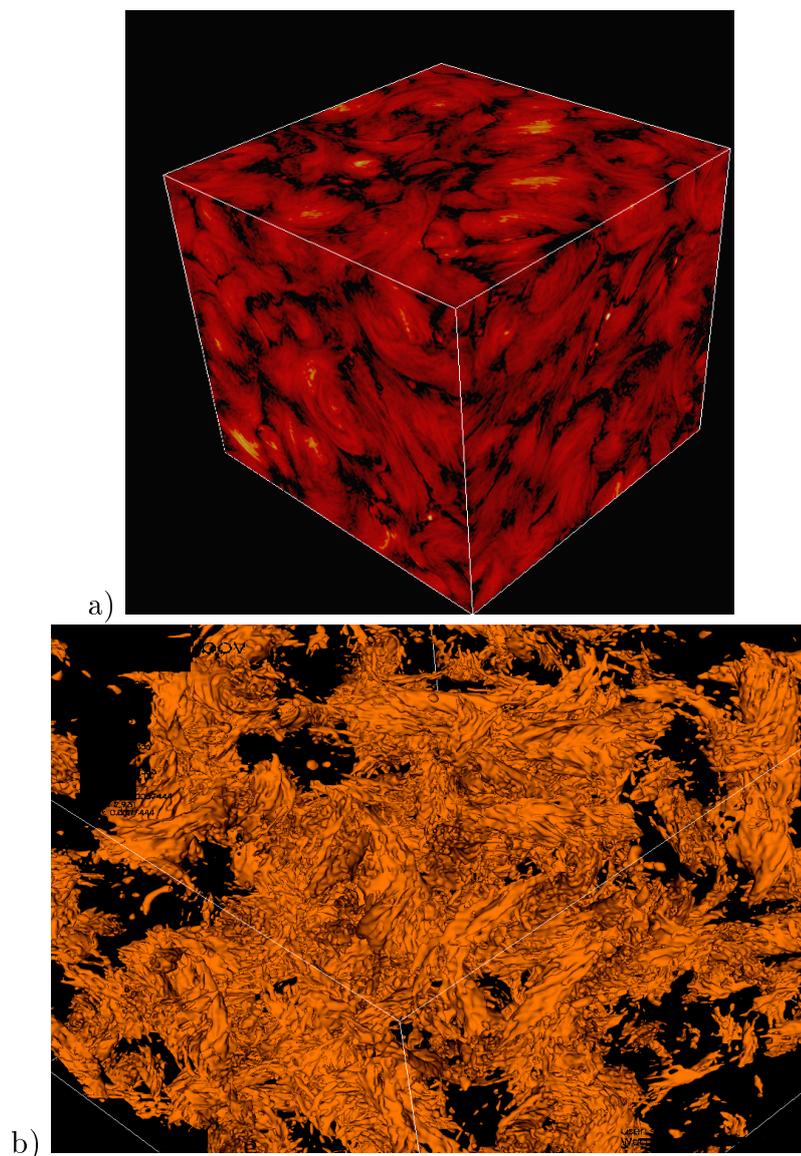
Figure 5.14: Magnetic field structures and iso-surfaces in the forced case. a) 3D-structures of cut-off filtered out put of magnetic field structures and b) iso-surfaces of the cut-off filtered out put of magnetic field .

It would mean that the initial energy is no more at equipartition, among kinetic and magnetic energies, when the decay starts. Three such cases are reported to ascertain the effect of stopping the forcing at various points in time and also to look at the difference in structures formed in each case.

Case I

In this first case, the forcing was stopped at a very late stage when the peak of the magnetic helicity spectra is close to the boundary at $k=2$. (fig. 5.15b). Here if the

forcing is withdrawn and the system is allowed to decay, the spectra severely feel the boundary effect. But the structures are the largest of the three cases (see other two cases also) (see fig. 5.15 a and c). The iso-surfaces seen are twisted flux ropes. The magnetic field structures show some magnetic reconnection regions (see section 5.5.5) either side of which, two oppositely rotating vortices are seen. These structures still have dominant influence of the forcing (the bright regions in the field structure).
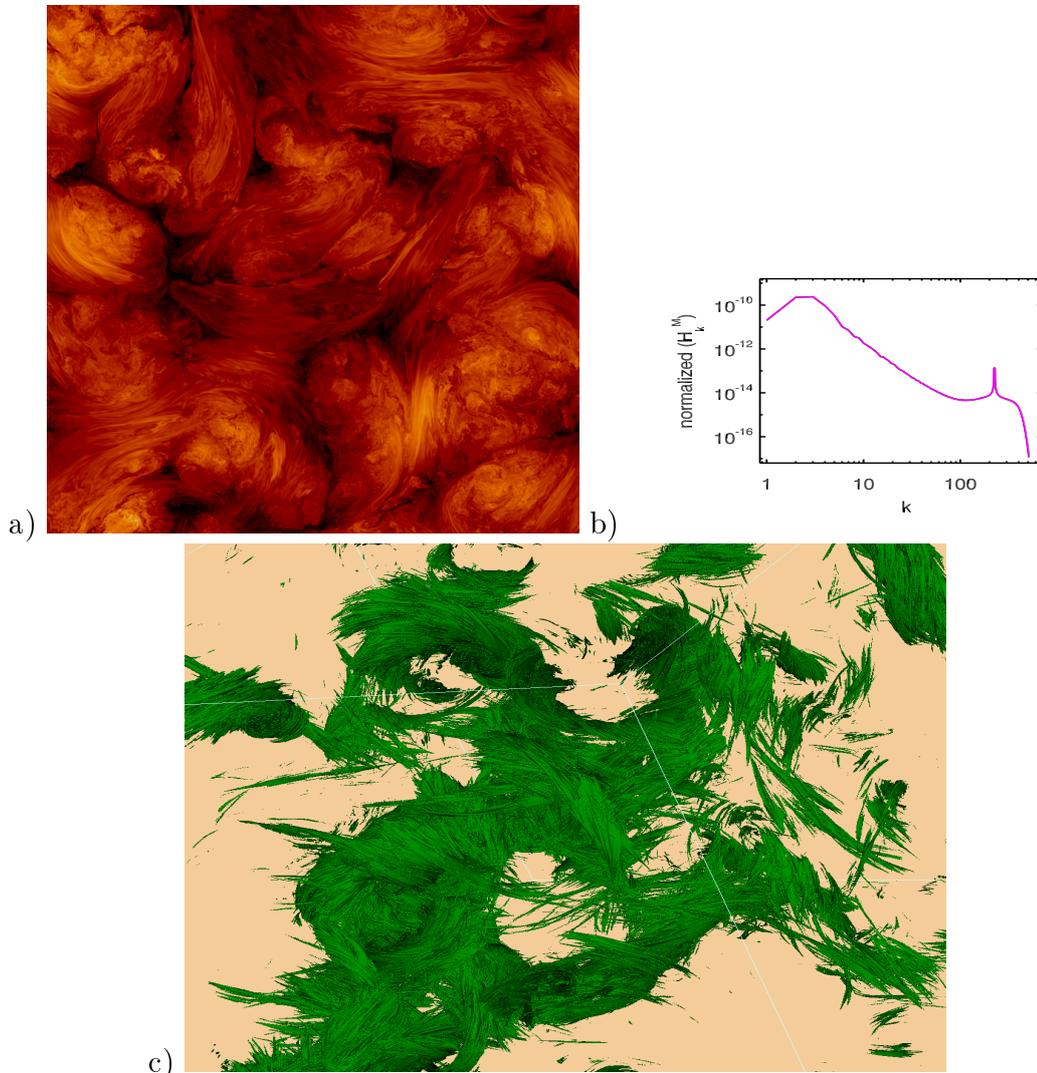
Figure 5.15: Case 1. a) cut across the plane of magnetic field structure b) magnetic helicity spectrum at which the forcing was stopped (t=6.7) and c) iso-surfaces of the magnetic field in this case (zoomed by 1.5 times).

Case 2

In the second case the forcing is stopped at $k = 70$, and the decaying turbulence is allowed to take over (fig. 5.16b). Here the magnetic field structures are much smaller and a lot more magnetic reconnection regions are seen (fig. 5.16 a and c) (see section 5.5.5.). Also can be seen are several scales, in the structure. The iso-surfaces of the magnetic field are twisted flux tubes but very small in size and a lot more than what were seen in the case1. This is the case with similar starting point as the decaying case studied at the beginning of the section.
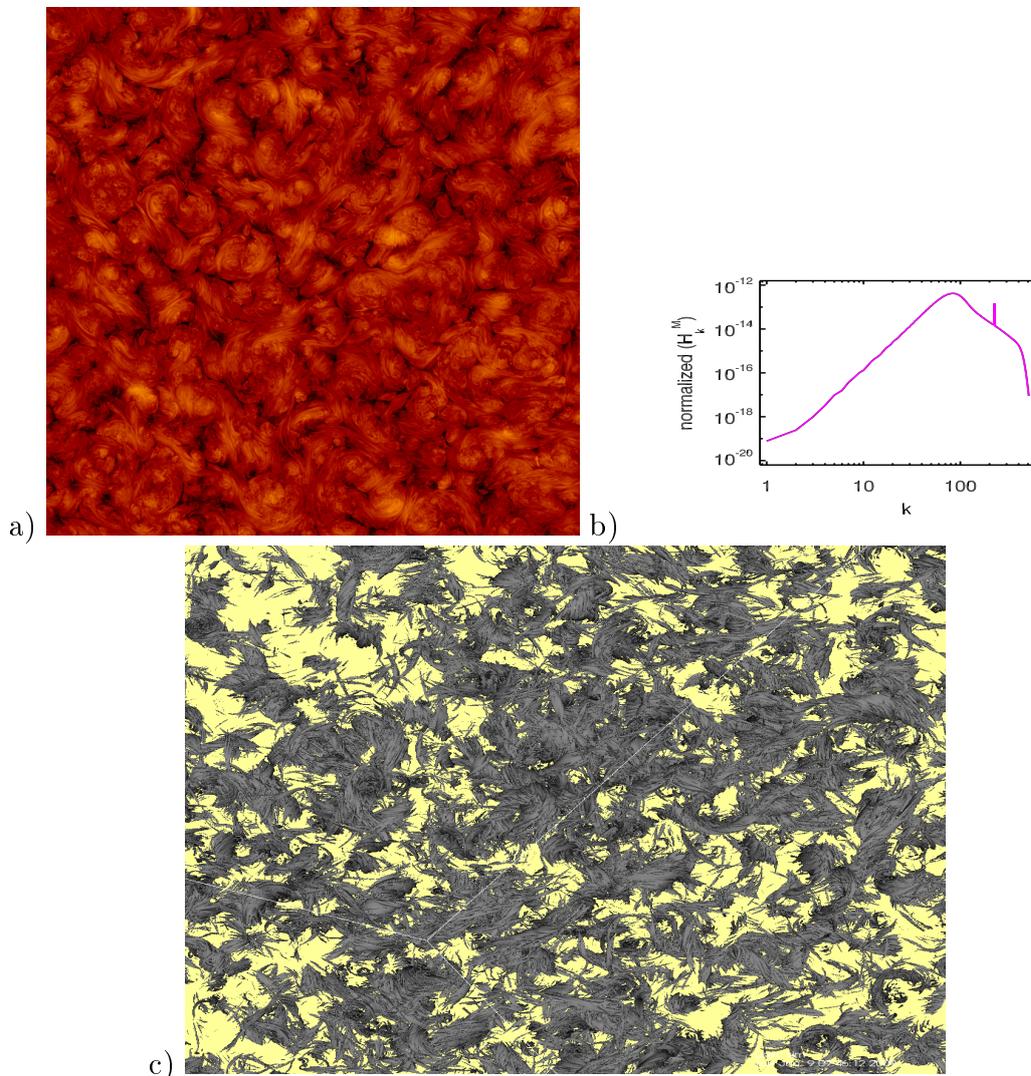
Figure 5.16: Case 2. a) cut across the plane of magnetic field structure b) magnetic helicity spectrum at which the forcing was stopped (t=2) and c) iso-surfaces of the magnetic field in this case (zoomed by 1.5 times)

Case 3

In the third case the forcing is stopped at $k = 40$, and the decaying turbulence is allowed to take over (fig. 5.17b). Here the magnetic field has medium sized structures, with large number of magnetic reconnection regions (fig. 5.17 a and c) (see section 5.5.5). Also can be seen are several scales, in the structure. The iso-surfaces of the magnetic field are twisted flux tubes but very small in size and a lot more than what were seen in the case 1 and considerably less than what are seen in the case 2.
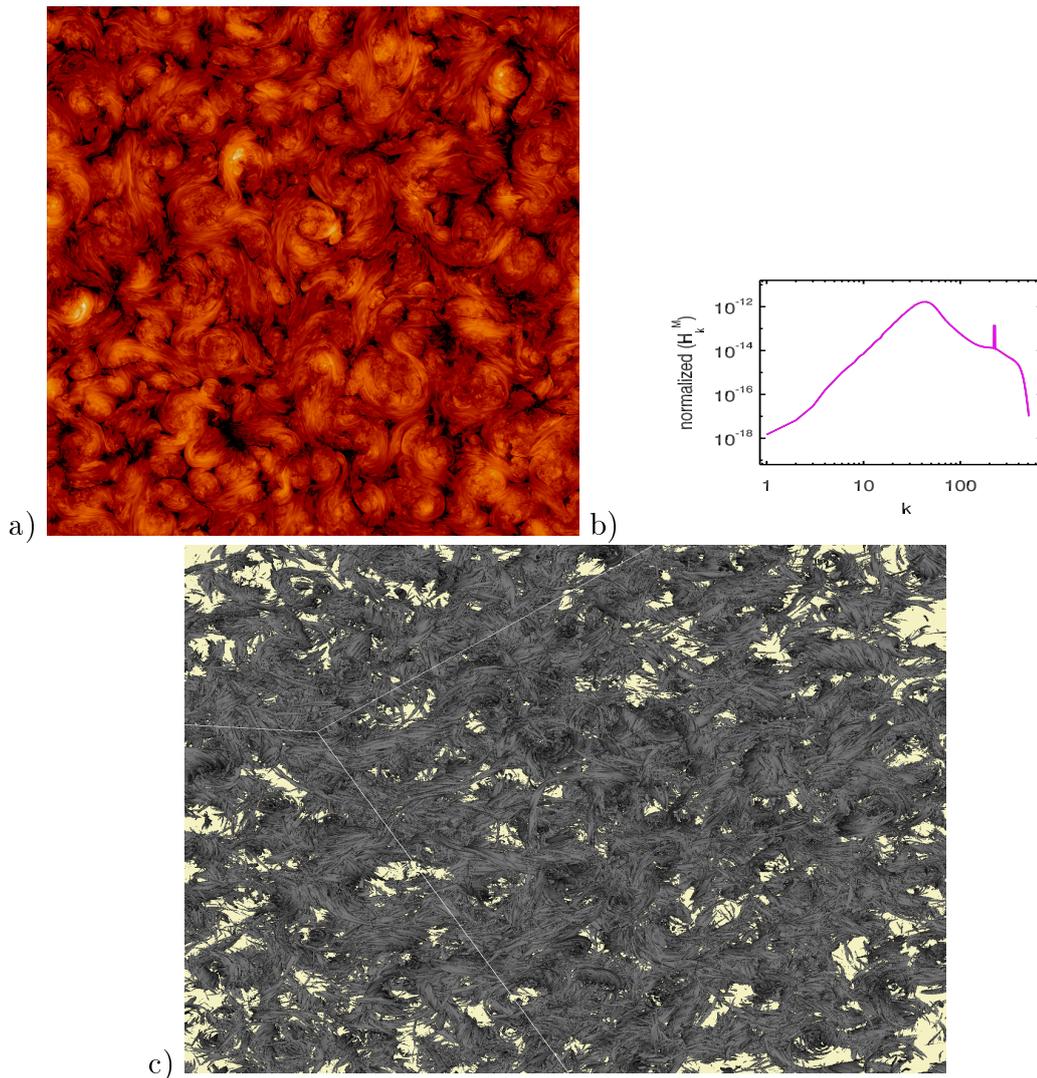
Figure 5.17: Case 3. a) cut across the plane of magnetic field structure b) magnetic helicity spectrum at which the forcing was stopped (t=3.5) and c) iso-surfaces of the magnetic field in this case (zoomed by 1.7 times).

This intermediate case is studied more closely to understand the evolution of magnetic field, because the structures have properties of both case 1 and case 2 which form the

extremities.

5.5.4   Evolution of the Magnetic Field

By looking at the three cases described above, the evolution of the magnetic field in a case where forcing was stopped and decaying turbulence was allowed to takeover, can be understood. Here it is seen that the initial state fig. 5.18a, is dominated by random small-scale structures. As the decaying turbulence takes over, slowly structure appears as seen through the pictures of fig. 5.18 b to e. In these pictures several magnetic reconnection regions are seen which decrease in number as the structures become fewer and larger. Thus, it appears like magnetic reconnection (see section 5.5.5) plays a significant role in structure formation. As decaying turbulence takes over, from the randomness of the initial state, slowly, structure formation is seen, where in the initial, point like, random magnetic field structures grow into small structures with some shape. Here already several magnetic reconnection regions emerge. The process continues further and the structures grow larger, while the magnetic reconnection regions become less in number. As this is happening, through the decaying turbulence, the system is also losing energy. Thus the magnitude of the structures goes on decreasing.

This is the special case that was being mentioned in the structure function analysis and other sections of this chapter. This case closely complies with the decaying turbulence case in its evolution.

Change in Dimensionality of the Structures

It was already mentioned in section 5.3 that in the special case the dimensions will change from fractal dimensions to two dimensional structures as the forcing is withdrawn. Here it is once again emphasized using two plots in fig. 5.19 a and b. The first plot here shows the structure function scaling exponents curve for the forced case. It also shows a model fit which is Kolomogorov type curve with a co-dimension of 1.5 (shown in the legend as K2). The second plot shows the scaling exponents when the forcing is withdrawn and decaying turbulence is allowed to dominate. The model curve that matches with these exponents is Kolmogorov type curve with co-dimension of 2 (shown as K1 in the legend). Also shown is the Kolmogorov type curve with co-dimension 1.5 for reference.

a) b) c) d) e)
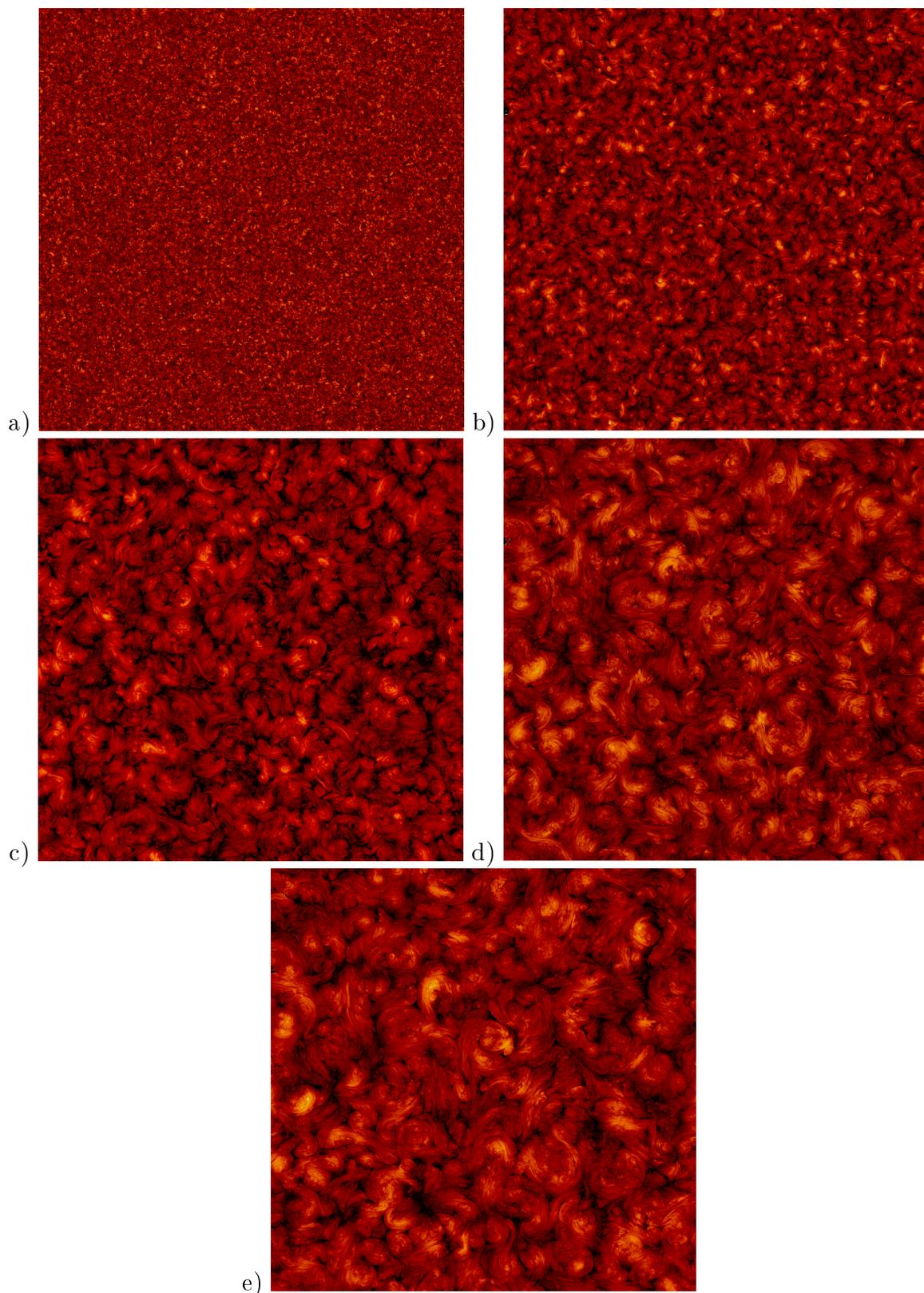
Figure caption on page 128

Figure 5.18: Evolution of the Magnetic Field. a) cut across the plane of unfiltered magnetic field structure (at $t = 3.5$), $b - e$) cut across the plane of magnetic field structures (at $t = 4.5, 5.5, 6.5$ and 8).

From this plot it is can be understood that while in the forcing case the structures have fractal dimensions, in the event of removing the force after some time, and allowing decaying turbulence to take over, they evolve into two dimensional structures. Hence from this discussion it can be inferred that when a high k forcing (of the type used here) stirs small-scale random fluctuations for a particular amount of time, it forms fractal dimensional structures. And as the effect of forcing is waning, the decaying turbulence takes over and the magnetic structures that evolve will be two dimensional. That is in the pictures of the fig. 5.18, from fig. 5.18 a to e, the evolution of magnetic structures also coincides with the changing of their dimensions from fractal to definite two dimensional ones.

Correlation Length Vs Energy Dissipation

Section 5.4.2 discusses the correlation functions and correlation lengths of several quantities. Here if the correlation lengths of magnetic field structures are considered in various stages of evolution and a plot is drawn with correlation length on x-axis and magnetic energy dissipation on y-axis, then an inference on size of magnetic structure that shows minimal dissipation, can be made. For this purpose, the correlation lengths were calculated at three points in the evolution process of the magnetic field as described in 5.4.2 and energy dissipation was obtained for these three points from the simulation data. The data is as shown in the table 5.3.

Time	Length	Dissipation
t=2.33	0.01	0.0285
t=4.25	0.15	0.0155
t=5.89	0.17	0.0063

Table 5.4: Correlation lengths and energy dissipation values at different times for magnetic field structures

a)

b)
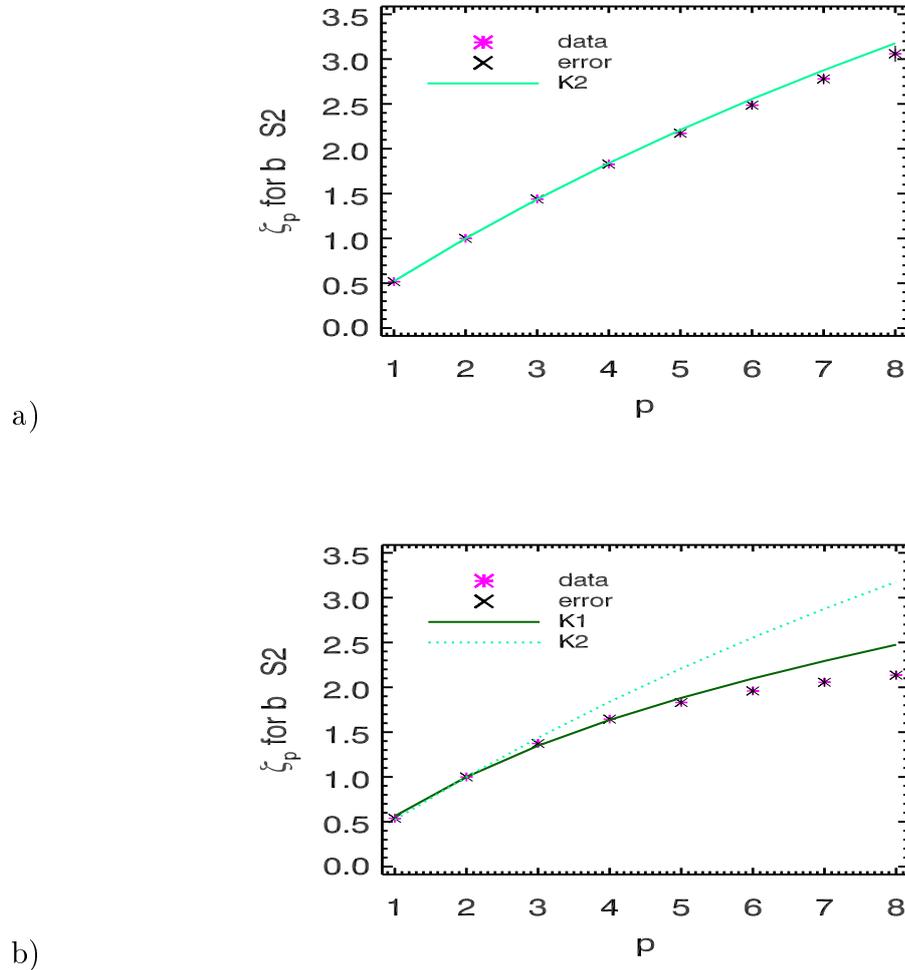
Figure 5.19: Intermittency modeling for evolving magnetic structures. a) structure function exponent curve for initial forced state and b) structure function exponent for finally evolved state due to decaying turbulence. Note that the estimated error when plotted is within the plotted data symbol size.

This data is plotted as shown in fig. 5.20. The magenta colored graph is the data from which it can be observed that as correlation length increases, dissipation decreases. Now if this line in extrapolated to meet the x-axis i.e. to make dissipation tend to zero, an estimate on the size of the structure that shows minimum dissipation can be had. By fitting a line (olive green colored line in the figure) using a linear curve fit, such an estimate is made. It turns out that at a correlation length of 0.22, (that is 22 times the initial size of the structure) the dissipation may tend to zero, forming a stable magnetic structure with minimal dissipation.
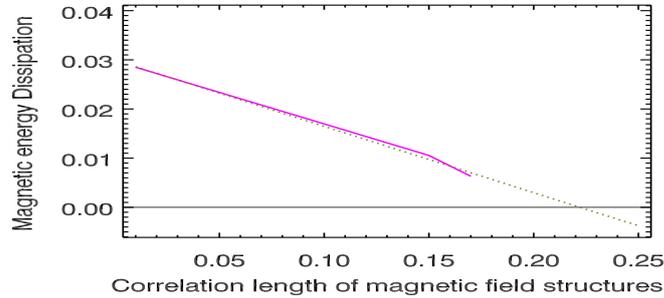
Figure 5.20: Correlation length Vs Dissipation. Data is in magenta color, curve fit is in oliver color and reference x-axis to represent y=0 is in black.

This estimate is valid for only one simulation here. But if this procedure is adapted for several simulations, which use different types of forcing mechanisms, a better statistical estimate on the size of the magnetic structure that dissipates minimally can be achieved. This knowledge may help in understanding stable magnetic structures seen in celestial magnetospheres.

5.5.5   Magnetic Reconnection

Magnetic reconnection or simply reconnection can be defined as a topological re-structuring of a magnetic field caused by a change in the connectivity of its field lines. In a flow when magnetic reconnection happens, the resultant flow direction will be perpendicular to the field lines that caused this magnetic reconnection and the current is also perpendicular to the direction of the resultant flow (if two field lines approached oppositely in z-direction, then the resultant direction can be say x and the current will then flow in y-direction creating a current layer or sheet). There are several types of magnetic reconnections. Collisional and collision-less being the two important among them. Here in this work, the type of magnetic reconnection occurring is collisional. To illustrate that magnetic reconnection indeed is present, and is significant in the case where forcing is stopped and decaying turbulence is allowed to dominate, a 512^3 reso-lution simulation is used. This simulation is almost similar to case 3, described above. The cut across the plane for magnetic field and the magnetic field vectors at the same instant are shown in 5.21 a and b. In fig. 5.21c, a superposition of the previous two figures is done. Some magnetic reconnection regions which are easily recognizable are also pointed in this figure. These reconnection regions are formed between two counter rotating magnetic field structures and in the area between them, perpendicular to both, a current sheet is formed. This is the collisional magnetic reconnection.

To understand the field alignments, refer to fig. 5.21d. This figure shows the iso-surfaces of magnetic field, current and velocity field. From this figure it is seen that the iso-surfaces of magnetic field and current are perpendicular to each other, while velocity field is randomly oriented without showing any specific alignment pattern. Thus from the iso-surface plot of current and magnetic fields, it can be inferred that two counter clockwise moving eddies, which are in the process of large-scale structure formation, move via the magnetic reconnection stage, while the current sheet is formed in a plane perpendicular to these eddies, similar to that seen in [59]. A straight forward classification of the magnetic reconnection picture shown here is not available currently, though it appears to be closer to the Sweet-Parker reconnection model (look in [1]).

5.6 Conclusions

From this studies of statistical and spatial properties of the magnetic fields and other quantities, in the two cases 1) with magnetic helicity injection and 2) natural decay, the following conclusions can be drawn: 1) high k forcing does not allow large-scale structure formation. 2) In the generation of large-scale magnetic field, decaying turbulence plays a significant role.

a)　　　　　　　　　　　　　　　　b)

Figure caption on page 133

c)

d)
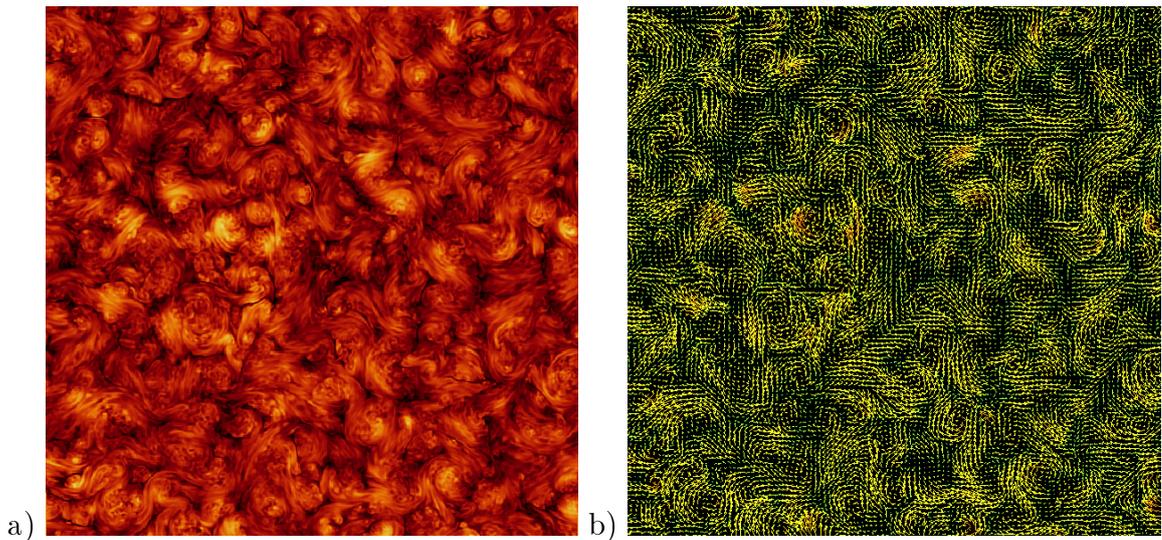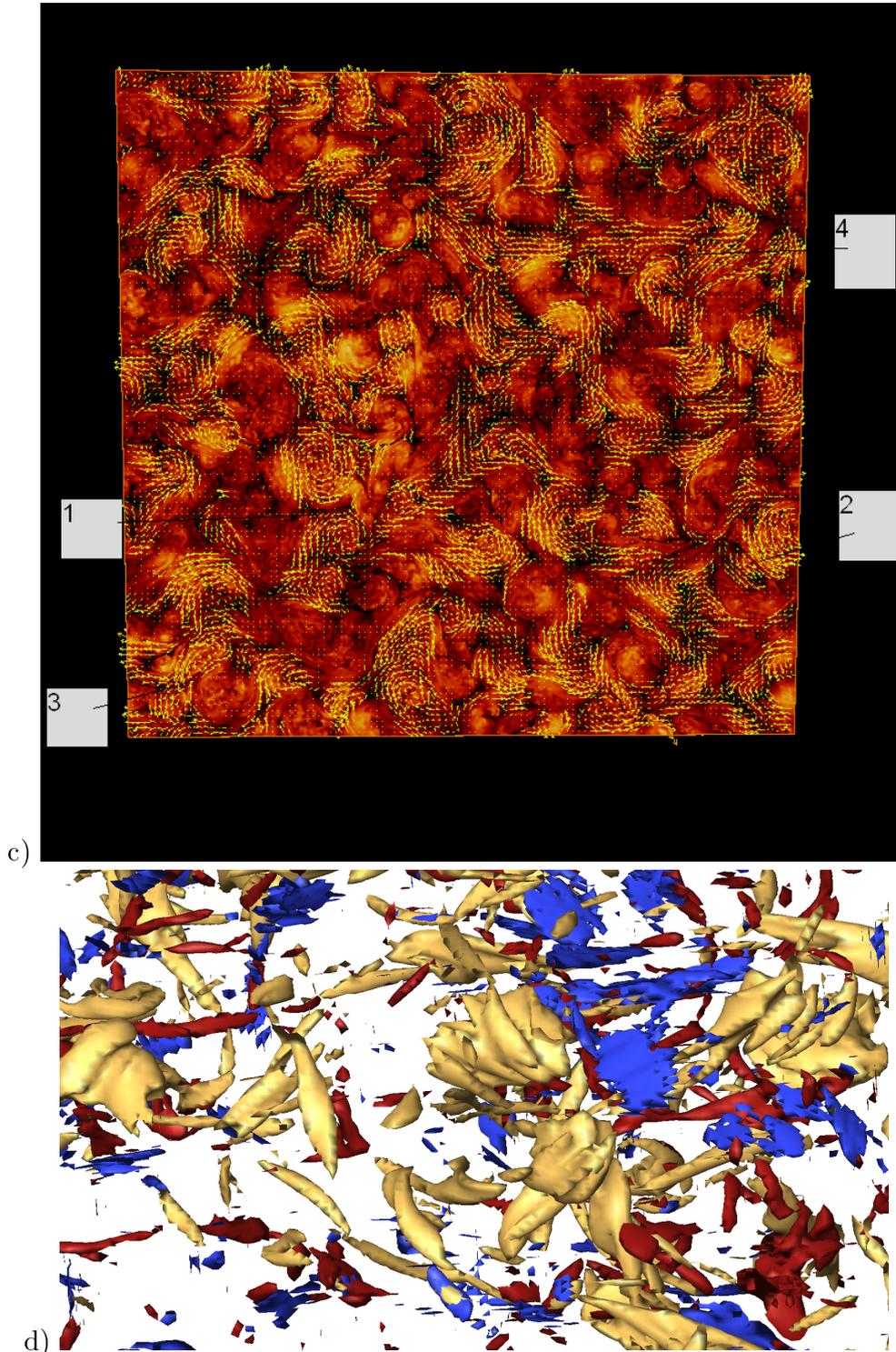
Figure caption on page 133

Figure 5.21: Magnetic Reconnection a) cut across the plane of magnetic field b) vectors of the same plane c) super imposition of figures a and b, 4 magnetic reconnection regions are marked here, and d) iso-surfaces of magnetic field (in gold color), current (in blue color) and velocity (in red color). Resolution 512^3, at t=4. $\hat{\mu}_n = \hat{\eta}_n = $2e-35., forcing withdrawn at t $\sim$ 1.

3) The equation (4.8) has been well supported from the structures perspective as well and 4) The size of the structures formed depends on the point of stoppage of the force.

Interpretation

1) It is believed that the dynamo action by turbulent flows of conducting media in the cores of planets or interiors of the stars is responsible for the generation of their magnetic energy. The generated magnetic energy is generally limited to small scales with large number of turbulent fluctuations. But all these celestial objects show huge magnetospheres which have large-scale magnetic structures with very few turbulent fluctuations. The origin of these large-scale structures is not well understood. A plausible explanation is the inverse cascade of magnetic helicity which can transport magnetic energy into large scales from extremely small scales, as seen in these simulations and thus can result in the formation of large-scale structures with minimum turbulent fluctuations and dissipation. (see section 5.5.4).

2) A prescription for large-scale structure formation from very small scales is proposed using both the forced and decaying turbulences. This proposal is currently restricted to the kind of random helical forcing used in this work only. The steps involved are :first the forcing has to stir the random fluctuations for certain amount of time during which several regions of magnetic field concentration are formed which have fractal dimensional structures. At this stage the forcing is withdrawn allowing the decaying turbulence to dominate the system for long period of time, which changes the dimensions of the structures from fractal to two dimensions, while large-scale magnetic structures evolve from these regions of magnetic field concentration. It appears that magnetic reconnection plays a significant role in this process. This prescription is also termed as special case in this work.

3) The three sub-cases discussed in the special case had three distinct starting points which indicated the amount of time the system was forced. In these three sub-cases, the resultant structures had different sizes. When the forcing acted for long and the decaying turbulence took over, the structures were the largest (see case 1 of section 5.5.3). When the forcing acted for less amount of time before the decaying turbulence took over, the structures were comparatively small (see case 2 of section 5.5.3). When the forcing acted for intermediate amount of time before decaying turbulence took over,

the structures were of intermediate size (see case 3 of section 5.5.3). Thus from this analysis, a speculation on the amount of time the forcing acted on a turbulent system could be made, by analyzing the size of the magnetic structures present in it. If case 2 and decaying case are compared (since they have the same starting point $k=70$), the effect of starting with fields of equal energy as in the decaying case and unequal energies as in case 2 could be understood. It is seen from these two cases that when there was initial equipartition of energies, the structures formed are larger than in the case when there is asymmetrical distribution in initial energies. Also the number of magnetic reconnection regions, whose number seems to have an inverse relation with the size of magnetic structures, could also be a good indicator of the time over which the forcing might have acted on a turbulent system.

4) The time estimate of the forcing mentioned above, can also lead to the source and its physical features, which actually set the initial stirring of the plasma (an investigation beyond the scope of this work). Caution here is that the forcing mechanism used in this work is a very specific one with properties like delta correlation, forcing acting in high k etc. Hence several other forcing mechanisms have to be tried to confirm the results obtained here, to make a good statistical model, which can predict the nature and physics of the source by looking at the large-scale magnetic structures.

Discussion

From the interpretations of the conclusions of the statistical and spatial features, it can be said that through this work, an alternate way of understanding the formation of some of the observed large scale magnetic structures in the celestial bodies, is being established, but with a strong limitation of a one off forcing method. The proposed prescription for large-scale magnetic structure formation has to be valid for several forcing mechanisms (which need to be modified to be used in high k region) before it can be accepted as a general prescription. Hence it is proposed that several forcing mechanisms available in the turbulence theory community ([8, 59, 10, 11]) be modified, for carrying out this verification. If the results from such attempts also tally with the results from this work, then the attempts at building a stochastic model to explain large-scale magnetic structure formation become feasible. When such model studies and observations are performed simultaneously and the results corroborated, it might lead to several interesting conclusions on observed features like magnetic reconnection and the large scale magnetic structures.

In 2D-hydrodynamic turbulence a successful attempt has been made to understand

the energy and enstrophy cascades [45, 46], by filtering the structures in a special manner and using a mathematical approach called multi scale gradient method. In 3D-MHD turbulence, currently such attempts have not been reported , probably because the evolution of the structures have not been studied closely, as has been done in this work. Hence now an attempt can be made at evolving equivalent procedures and necessary mathematics, so as to understand the exact relation between large-scale magnetic structure formation and inverse cascade of magnetic helicity in a quantitative way. It might be possible that magnetic reconnection plays an important role in such a formulation.

Chapter 6

Summary and Conclusions

6.1 Summary

The main objective of this thesis is to understand the influence of the inverse cascade of magnetic helicity on various quantities of 3D-MHD turbulence, using high resolution direct numerical simulations (1024^3 mesh points). For this purpose, to an already existing 3D-MHD pseudo spectral code, a new forcing sub-routine is added. Two cases of 3D-MHD turbulence are studied. In the first case forced turbulence is studied with the initial energy distribution and the forcing localized in the large k region ($k >100$). This set up is unique in the sense that earlier direct numerical simulation setups of forced MHD turbulence, were limited by their resolutions and had forcing terms and initial conditions in the moderate to small wave numbers($k \leq 30$). This setup is also intended to verify or confirm the k^{-2} power law obtained for inverse cascade of magnetic helicity in the numerical simulations of EDQNM approximations of 3D-MHD equations of forced turbulence. In the second case, pure decaying turbulence case is studied to understand the influence of the inverse cascade of magnetic helicity on this system. Here the initial energy distribution is peaked at a moderate wave number ($k =70$). Hyperviscosity is used in the numerical simulations to have scale separation between the inertial range and the dissipation range. This numerical approach used here comes with few drawbacks. The energy spectra show bottle neck and it is not possible to define a definite Reynolds number in the hyperviscous simulations.

The studies on influence of the inverse cascade of magnetic helicity on the spectral properties of several quantities of MHD turbulence is reported next. Two approximate scaling ranges are seen for the first time in 3D-MHD turbulence, one in high k (250 - 400) and other in the low k (7 - 30) regions, for all the quantities, in the forced turbu-

lent system. One approximate scaling range in the low k region is seen for the decaying case. For some of the quantities this scaling range is also the inertial range (i.e. the flux of this quantity is constant in that range). For energy spectrum, already known $k^{-5/3}$ power law (K41) in the inertial range, is confirmed, in the low k regions for both the cases. In the high k region of the forced case, bottleneck is observed. In the spectra it is observed that the magnetic energy is always larger than the corresponding kinetic energy. Power laws obtained in the magnetic helicity spectra for both the decaying and forced cases, do not at all comply with the EDQNM result. Instead a new set of power laws are seen for the two scaling ranges of the forced case and the lone scaling range in the decaying case of the magnetic helicity spectra. Along with magnetic helicity and magnetic energy, several other quantities, some of which have never been known to show any power law behavior, show one, in both the cases described. It is interesting to note that many of these quantities are not ideal invariants in 3D-MHD. These power law behaviors have been analyzed together with the dimensional analysis of EDQNM equations, to obtain a new relation among four of the quantities showing power laws. The new relation relates magnetic helicity (H_k^M) , magnetic energy (E_k^M), kinetic helicity (H_k^V) and kinetic energy (E_k^V), through their spectral powers as $E_k^M \sim k^2 \frac{H_k^M E_k^V}{H_k^V}$. This relation is true for both the scaling ranges of forced case and the single scaling range of the decaying case. This relation implies that there are nonlinear mode interactions between the velocity field ($\mathbf{v}$) and magnetic field ($\mathbf{b}$), over the entire spectral range, that are responsible for the inverse cascade of magnetic helicity and hence the increase in magnetic energy. Already known relation between the power laws of total energy and residual energy is satisfied exactly in the scaling range of decaying case and with some errors in the forced case scaling ranges. The other power laws obtained in this work currently do not satisfy any dimensional or phenomenological relations. To understand them, probably a new mathematical framework is needed.

The influence of inverse cascade of magnetic helicity on spatial structures is studied next. Here first it is shown that the high k forcing does not result in the formation of large-scale structures as was the expectation. In fact, it is seen that formed large-scale structures are being destroyed by this forcing. The structures obtained are significantly influenced by small scales which hide the large scales present in the system. Hence a cut-off filter (placed at $k = 70$) is used to overcome the influence of the small-scale structures. Plotting of structure functions, extended self similarity (ESS) and intermittency modeling of the structure function exponents curves, is the first analysis that is performed to understand the nature of the spatial structures. Structure function

analysis and intermittency modeling of cut-off filtered output of the forced case emphasize the fact that the magnetic structures formed are neither one-dimensional nor two-dimensional but have fractal dimensions. A similar analysis of the decaying case shows two-dimensional structures. As one of the objectives of this work was to look for large-scale structure formation in the magnetic field, a new strategy is adapted. In this new strategy, the forcing is withdrawn at three different points in the evolution of the magnetic helicity spectrum and decaying turbulence is allowed to take over (referred to as special case). In this setup from the initial fractal type structures, the structures slowly evolved into two dimensional ones. PDFs and correlation functions are also studied, which indicate the intermittent nature of the magnetic field and the velocity field, in forced, decaying and the special case. The shapes of the structure function exponent curves and the PDFs, suggest that there is dominant sub-structure present in the forced case. In the decaying case, dominant coherent structure nature is suggested, from the same analysis. In the special cases, from dominant sub structure nature of the structures at the beginning of the simulations, the transformation of the structures to dominant coherent structures at the end of the simulations, is portrayed by this analysis. Correlation lengths in all the three cases increase for many quantities, with time, indicating the formation of larger structures, with the progress of time.

Real space structures are visualized using tools like AMIRA (commercial software) and Visit (free ware from LLNL,USA). The visualization of the structures confirms and supports the structure function analysis. In the forced case, the iso-surfaces of the magnetic field are neither one dimensional nor fully two dimensional, confirming their fractal dimensional nature, as seen from the structure function analysis. There are large number of regions of magnetic field concentrations without definite structure formation, indicating the effect of the high k forcing of the type employed here on the system. In the case of decaying turbulence, large-scale magnetic structures form and evolve with the progress of time. As the system is decaying, the magnitude of these structures decreases while their size is increasing. In the special case, the size of the structures and their evolution depends on the point of stoppage of the force. Hence, in the three sub-cases studied under this special case, very large magnetic field structures (when the forcing was stopped very late in time i.e. t=9), medium size structures (when the forcing was stopped at a moderate time i.e. t=3.3) and much smaller structures (forcing stopped very early in time i.e. 1.1), are reported. The common feature of these three sub-cases and the decaying case is the presence of a number of magnetic reconnection regions. The number of magnetic reconnection regions increases as the

structures are many and smaller, and they are pronouncedly few if the structures are few and very large.

6.2   Conclusions

Thus from the spectral and spatial analysis of the influence of inverse cascade of magnetic helicity, on various quantities of 3D-MHD turbulence the following points could be concluded:

- Power law behaviors in several quantities including many non- ideal invariant quantities are observed

- New relation based on EDQNM with a possible explanation for large-scale magnetic structure formation in 3D-MHD turbulence is obtained

- High wave number forcing destroys magnetic structures

- Decaying turbulence is important for large-scale structure formation. Magnetic reconnection plays a significant role in this structure formation

Interpretation

These results could be interpreted in the astrophysical context as follows:

[1] **Large−Scale Magnetic Structure of a Planet**: It is believed that the dynamo action by turbulent flows of conducting media in the cores of planets or interiors of the stars is responsible for the generation of their magnetic energy. The generated magnetic energy is generally limited to small scales with a large number of turbulent fluctuations. But all these celestial objects show huge magnetospheres which have large-scale magnetic structures with very few turbulent fluctuations. The origin of these large-scale structures is not well understood. A plausible explanation is the inverse cascade of magnetic helicity which can transport magnetic energy into large scales from extremely small scales, as seen in these simulations and thus can result in the formation of large-scale structures with minimum turbulent fluctuations.

[2] **Formation of Large−Scale Magnetic Structures**: The new spectral relation obtained suggests that the nonlinear mode interactions between velocity and magnetic fields, cause a rise in the magnetic energy at the cost of kinetic energy. Thus the magnetic field structures should become large, as inverse cascade of magnetic helicity is in action. The visualization of these structures suggests

that high k forcing (of the type used here) of the turbulent flow alone is not sufficient for large-scale structure formation. It has also been seen that decaying turbulence has an important role in the large-scale structure formation. Thus if an initial plasma configuration consisting of random magnetic fluctuations in the small scales, is forced in those small scales and the system is let to evolve, it will only form concentrated regions of magnetic field in the plasma. Large-scale magnetic structures will evolve from this configuration only if the forcing is withdrawn at a certain point of time, allowing the decaying turbulence to dominate. This statement is currently specific only to the type of the forced system studied here. Generalization would require further studies.

[3] **Speculating the Source of Forcing**: It was seen in the special case that the size of structures formed depended on the point of stoppage of the force. Thus if in any part of the universe, an isolated large-scale magnetic structure is detected, then a plausible explanation could be given from the point mentioned above, bearing in mind the limitation, that any such explanation is currently only specific to the kind of forcing and decaying turbulent flows discussed in this work. It is also possible to speculate on the nature or source of the forcing, from the size of the structures. It was seen that very large structures formed if the forcing acted for longer time with few (but large) magnetic reconnection regions observed in the structure. As the time of action of the force on the system became smaller and smaller, the size of the structures also became smaller and smaller, with an increase in the number of magnetic reconnection regions. This suggests that if the influence of the forcing was there for a short time, the size of the structures will be small and if its influence is longer, the observed structures are large. Thus a kind of direct relation between the time of influence of the forcing and the size of the structures is what these arguments point to. Also it is interesting to note that these arguments point to an inverse relation between the time of influence of forcing and the number of magnetic reconnection regions. Thus if these two facts are stochastically modeled then the time of influence of forcing can be estimated from the size of the observed structures or magnetic reconnection regions. From this information the nature and physics of the source that caused this forcing on the isolated plasma could also be predicted. But for building a stochastic model, just one off forcing methods is not sufficient (as was done here) and would need several possible samples obtained from different forcing methods. The work in

this dissertation thus offers to be a good starting point for further such studies, which might culminate in the envisaged stochastic model.

Appendix A

Normalization Factor for Magnetic Helicity Spectra using Dimensional Analysis

In the spectral domain, the magnetic helicity $(\tilde{H}^M)$ is given by the volume integral of dot product of vector potential and magnetic field as:

$$\tilde{H}^M(k) = \int \tilde{\mathbf{A}} \cdot \tilde{\mathbf{b}}^* d^3k \qquad \text{where} \qquad \tilde{\mathbf{A}} = \frac{i}{k^2}\mathbf{k} \times \tilde{\mathbf{b}} \qquad (A.1)$$

Since the equations are all in Alfv́en wave units, the units of magnetic field are that of velocity i.e. L/T where L is the length and T is the time.

In the inertial range magnetic helicity shows a power law, which means it is proportional to some power of wavenumber k^α, where α is the power law exponent. The proportionality constant is the dissipation coefficient raised to some power of its own $\epsilon_{H_d}^\beta$, where β is its exponent.

To determine the value of these power law exponents, α and β, the following equation is used:

$$\tilde{H}^M(k) = \epsilon_{H_d}^\beta k^\alpha \qquad (A.2)$$

Dimensional analysis is now used to determine the values of the exponents .

Dimensions of magnetic helicity: $L^4 T^{-2}$

Dimensions of ϵ_{H_d}: $L^3 T^{-3}$ as $\epsilon_{H_d} = \frac{dH^M}{dt}$

Thus from the above equation:

$$L^4 T^{-2} \sim (L^3 T^{-3})^\beta L^\alpha \tag{A.3}$$

$$L^4 T^{-2} \sim L^{3\beta} T^{-3\beta} L^\alpha$$

$$L^4 T^{-2} \sim L^{3\beta+\alpha} T^{-3\beta}$$

Now equating the powers of r.h.s. and l.h.s.:

$$3\beta + \alpha = 4$$

$$3\beta = 2$$

Which means:

$$\beta = 2/3 \qquad\qquad \beta = (4 - \alpha)/3 \tag{A.4}$$

Thus the values of α and β are uniquely obtained from this dimensional analysis as 2 and 2/3 respectively. The numerical simulations of EDQNM equations studying forced 3D-MHD turbulence also suggest a power law behavior or k^{-2} for the inverse cascade of magnetic helicity. But it is seen in this work that this power law may not be the same for various cases of turbulence like decaying and forced 3D-MHD turbulences and shows a significant deviation from the value obtained from EDQNM equations. Hence the magnetic helicity spectra will not be normalized with this normalization factor.

Appendix B

Flux of Energy

Equations (1.39) and (1.40) represent the vorticity and induction equations in the spectral space. The ideal invariant total energy is given by equation (1.43). The first goal is to write this equation in terms of vorticity. For this velocity is written in terms of vorticity, in the spectral space as shown below

$$\tilde{\mathbf{v}} = \frac{i}{k^2}\mathbf{k} \times \tilde{\boldsymbol{\omega}}. \tag{B.1}$$

from which:

$$|\tilde{\mathbf{v}}^2| = \frac{1}{k^2}|\tilde{\boldsymbol{\omega}}|^2$$

Substituting this equation in equation (1.43), leads to:

$$E(\mathbf{k}) = \frac{1}{2}\left(\frac{1}{k^2}|\tilde{\boldsymbol{\omega}}|^2 + |\tilde{\mathbf{b}}|^2\right) \tag{B.2}$$

This equation is now modified for the flux as:(

$$\dot{E}(\mathbf{k}) = \frac{1}{2k^2}\left(\dot{\tilde{\boldsymbol{\omega}}}^*.\tilde{\boldsymbol{\omega}} + \tilde{\boldsymbol{\omega}}^*.\dot{\tilde{\boldsymbol{\omega}}}\right) + \frac{1}{2}\left(\dot{\tilde{\mathbf{b}}}^*.\tilde{\mathbf{b}} + \tilde{\mathbf{b}}^*.\dot{\tilde{\mathbf{b}}}\right)$$

Substituting the equations (1.39) and (1.40) in the above (from here writing only the r.h.s.):

$$= \frac{1}{2k^2}(-i\tilde{\boldsymbol{\omega}}.\left\{\mathbf{k} \times [\widetilde{\mathbf{v} \times \boldsymbol{\omega}} - \widetilde{\mathbf{b} \times \mathbf{j}}]^*\right\} - \hat{\mu}k^2|\tilde{\boldsymbol{\omega}}|^2 + i\tilde{\boldsymbol{\omega}}^*.\left\{\mathbf{k} \times [\widetilde{\mathbf{v} \times \boldsymbol{\omega}} - \widetilde{\mathbf{b} \times \mathbf{j}}]\right\} - \hat{\mu}k^2|\tilde{\boldsymbol{\omega}}|^2) + (-i\tilde{\mathbf{b}}.\left\{\mathbf{k} \times \widetilde{\mathbf{v} \times \mathbf{b}}\right\}^* - \hat{\eta}k^2|\tilde{\mathbf{b}}|^2 + i\tilde{\mathbf{b}}^*.\left\{\mathbf{k} \times \widetilde{\mathbf{v} \times \mathbf{b}}\right\} - \hat{\eta}k^2|\tilde{\mathbf{b}}|^2)$$

Rearranging the r.h.s.:

$$= \tfrac{1}{2}(\tfrac{i}{k^2}\tilde{\boldsymbol{\omega}}^*.\left\{\mathbf{k}\times[\widetilde{\mathbf{v}\times\boldsymbol{\omega}}-\widetilde{\mathbf{b}\times\mathbf{j}}]\right\}+i\tilde{\mathbf{b}}^*.\left\{\mathbf{k}\times\widetilde{\mathbf{v}\times\mathbf{b}}\right\}+C.C.)-\hat{\mu}|\tilde{\boldsymbol{\omega}}|^2-\hat{\eta}k^2|\tilde{\mathbf{b}}|^2,$$

where $C.C.$ is the complex conjugate.

Hence at a particular mode $\mathbf{k}$, the flux terms would be the real part of the r.h.s. above and is read as

$$\int_0^k d^3k'\dot{E}(\mathbf{k}') = \mathbf{Re}\left\{\tilde{\boldsymbol{\omega}}^*.\frac{i}{k^2}(\mathbf{k}\times[\widetilde{\mathbf{v}\times\boldsymbol{\omega}}-\widetilde{\mathbf{b}\times\mathbf{j}}])+\tilde{\mathbf{b}}^*.i(\mathbf{k}\times\widetilde{\mathbf{v}\times\mathbf{b}})\right\}$$
$$-(\hat{\mu}|\tilde{\boldsymbol{\omega}}|^2+\hat{\eta}k^2|\tilde{\mathbf{b}}|^2) \tag{B.3}$$

Thus the equation representing the total flux, is the integrated value of all terms over the entire spectral volume, giving:

$$\dot{E}(\mathbf{k}) = T_{vw}^E(\mathbf{k}) + T_{jb}^E(\mathbf{k}) + T_{vb}^E(k) - D^E(\mathbf{k}) \tag{B.4}$$

Here

$$T_{vw}^E(\mathbf{k}) = \int_0^k d^3k'(\mathbf{Re}\left\{\tilde{\boldsymbol{\omega}}^*.\frac{i}{k'^2}(\mathbf{k}'\times[\widetilde{\mathbf{v}\times\boldsymbol{\omega}}])\right\}) \tag{B.5}$$

$$T_{jb}^E(\mathbf{k}) = \int_0^k d^3k'(\mathbf{Re}\left\{\tilde{\boldsymbol{\omega}}^*.\frac{i}{k'^2}(\mathbf{k}'\times[\widetilde{\mathbf{j}\times\mathbf{b}}])\right\}) \tag{B.6}$$

$$T_{vb}^E(\mathbf{k}) = \int_0^k d^3k'(\mathbf{Re}\left\{\tilde{\mathbf{b}}^*.i(\mathbf{k}'\times[\widetilde{\mathbf{v}\times\mathbf{b}}])\right\}) \tag{B.7}$$

$$D^E(\mathbf{k}) = \int_0^k d^3k'(\hat{\mu}|\tilde{\boldsymbol{\omega}}|^2+\hat{\eta}k'^2|\tilde{\mathbf{b}}|^2) \tag{B.8}$$

The terms T_{vw}^E, $T_{jb}^E + T_{vb}^E$ and D^E represent the flux of kinetic energy, magnetic energy and the dissipation terms respectively, for the total turbulent energy E. When hyperviscosity (here of the order 8) is also accounted for, the dissipation term D^E will have some product terms of k and will look as :

$$D^E(\mathbf{k}) = \int_0^k d^3k'(\hat{\mu}k'^6|\tilde{\boldsymbol{\omega}}|^2+\hat{\eta}k'^8|\tilde{\mathbf{b}}|^2),$$

with no changes in the transmission terms.

Appendix C

Additional Plots for Chapter 4

In this Appendix, plots of other quantities that show approximate power law behaviors in the simulations (which were only mentioned but not shown through figures in chapter 4) are presented. Also plotted are the quantities E_k^V/H_k^V and E_k^M/H_k^M which are important for the discussion of the new relation obtained in the section 4.5. The data sets used for plotting these spectra are at t=6 for forced case and t=10 for the decaying case.

C.1   Kinetic Helicity

The quantity plotted below is Kinetic helicity in both forced and decaying turbulence cases. It is defined by the equation $H_k^V = \frac{1}{2} \int dk^3 \tilde{\mathbf{v}} \cdot \tilde{\boldsymbol{\omega}}$. The power law obtained from these plots is used in the relation of equation (4.8) of chapter 4.
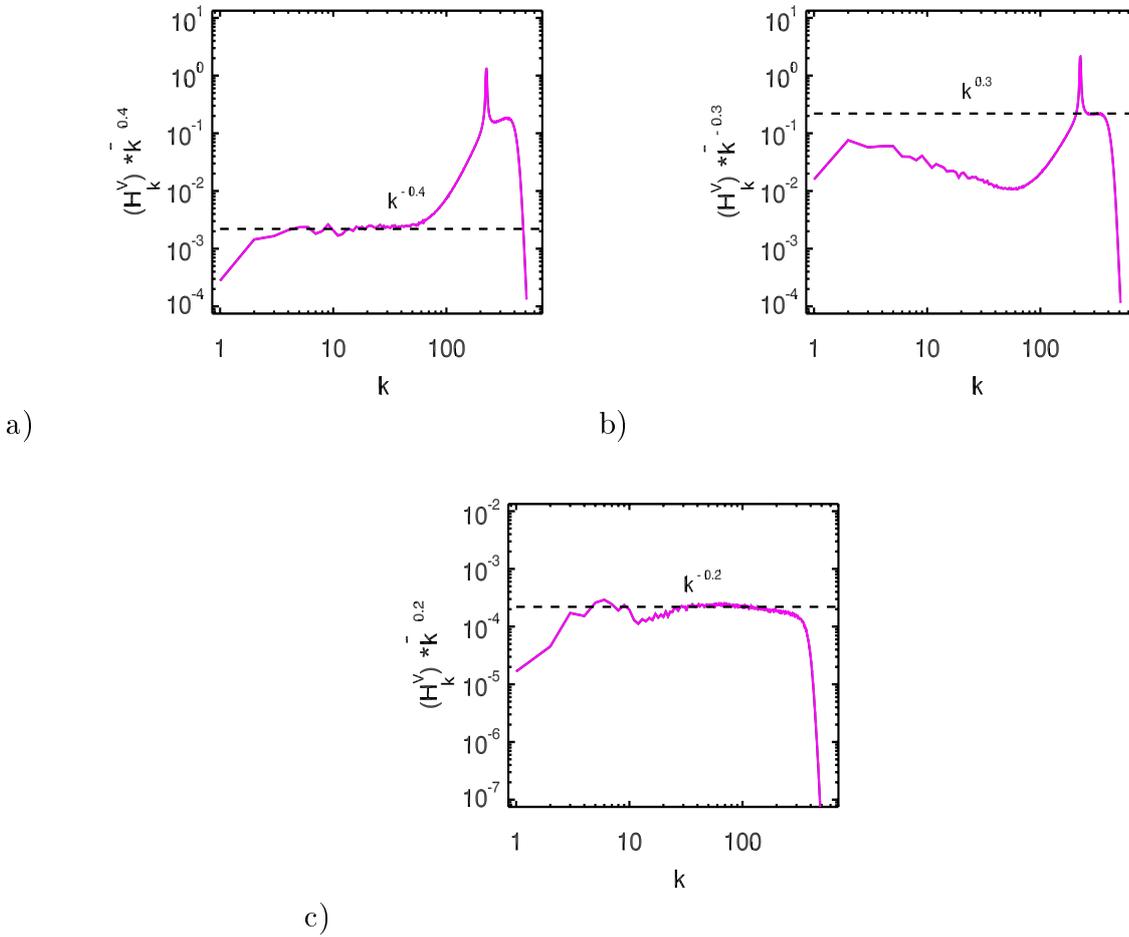
Figure C.1: Compensated kinetic helicity spectra in a 1024^3 simulation. a) low k approximate scaling range for forced case b) high k approximate scaling range for forced case and c) approximate scaling range for decay case.

C.2   Residual Energy

Residual energy is defined as: $E_k^R = |E_k^M - E_k^V|$. It was shown in [14] that it shows a power law relation with total energy as $E_k^R \sim k E_k^2$. (see tables 4.4 and 4.5 of chapter 4, for the exact power law values). Also see section 4.4.5 for a brief description on the power laws shown by the residual energy spectra in both the cases.
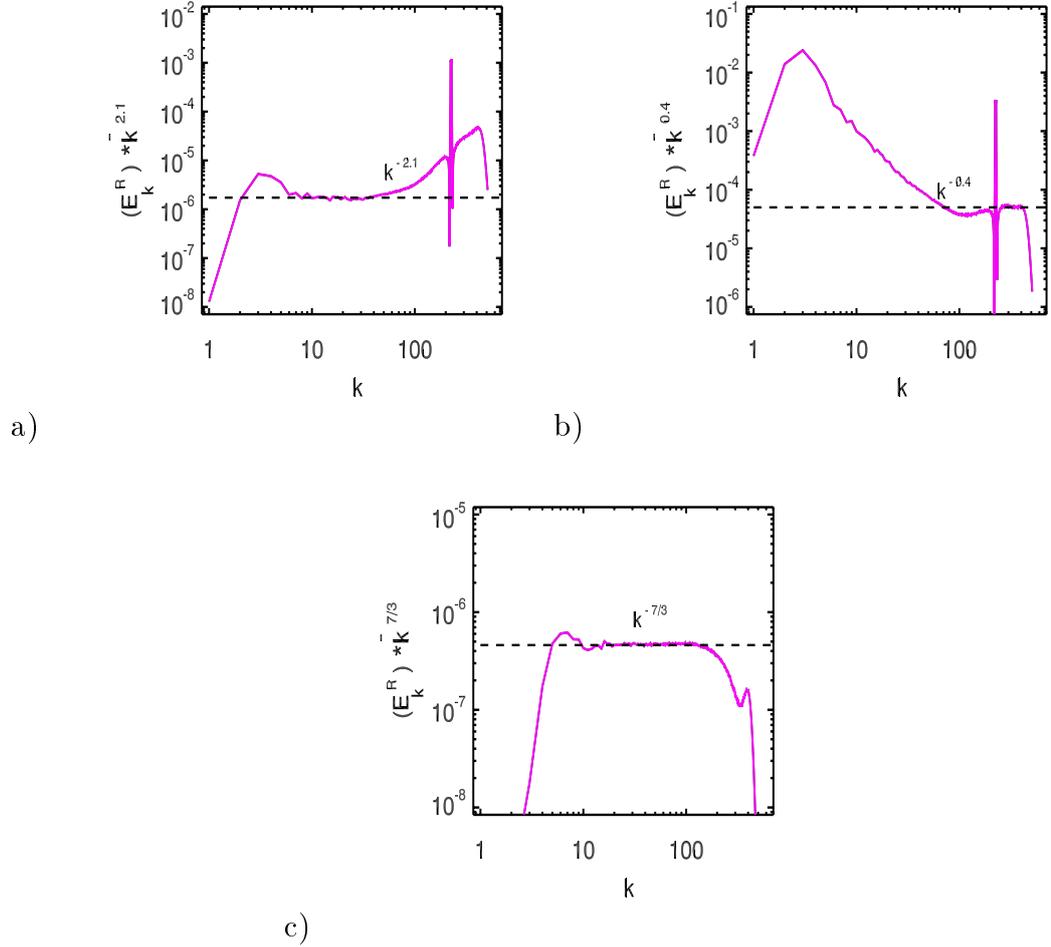
Figure C.2: Compensated residual energy spectra in a 1024^3 simulation. a) low k approximate scaling range for forced case b) high k approximate scaling range for forced case and c) approximate scaling range for decay case.

C.3   Residual Helicity

Residual helicity is the difference of kinetic and magnetic helicities related as shown $H_k^R = H_k^V - k^2 H_k^M$. This quantity was not known to show a power law behavior earlier. This is the first such reported instance. This quantity has significance in explaining the movement of inverse cascade to large scales (see section 4.5.1).

a)   b)

c)
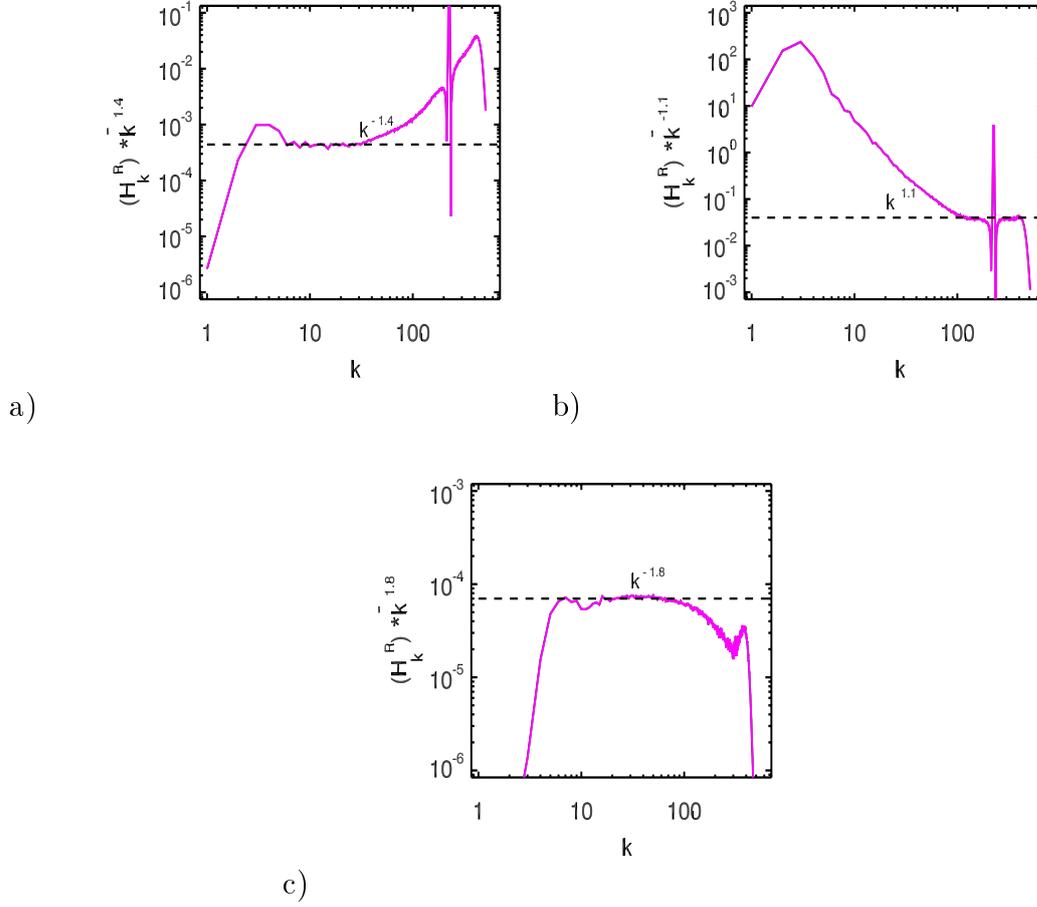
Figure C.3: Compensated residual helicity spectra in a 1024^3 simulation. a) low k approximate scaling range for forced case b) high k approximate scaling range for forced case and c) approximate scaling range for decay case.

C.4 Magnetic Vector Potential

Magnetic vector potential is defined as $\tilde{\mathbf{A}} = \frac{i}{k^2}\mathbf{k} \times \tilde{\mathbf{b}}$ in the Fourier space. This quantity was never expected to show a power law behavior but shows one as is seen from the figures below.
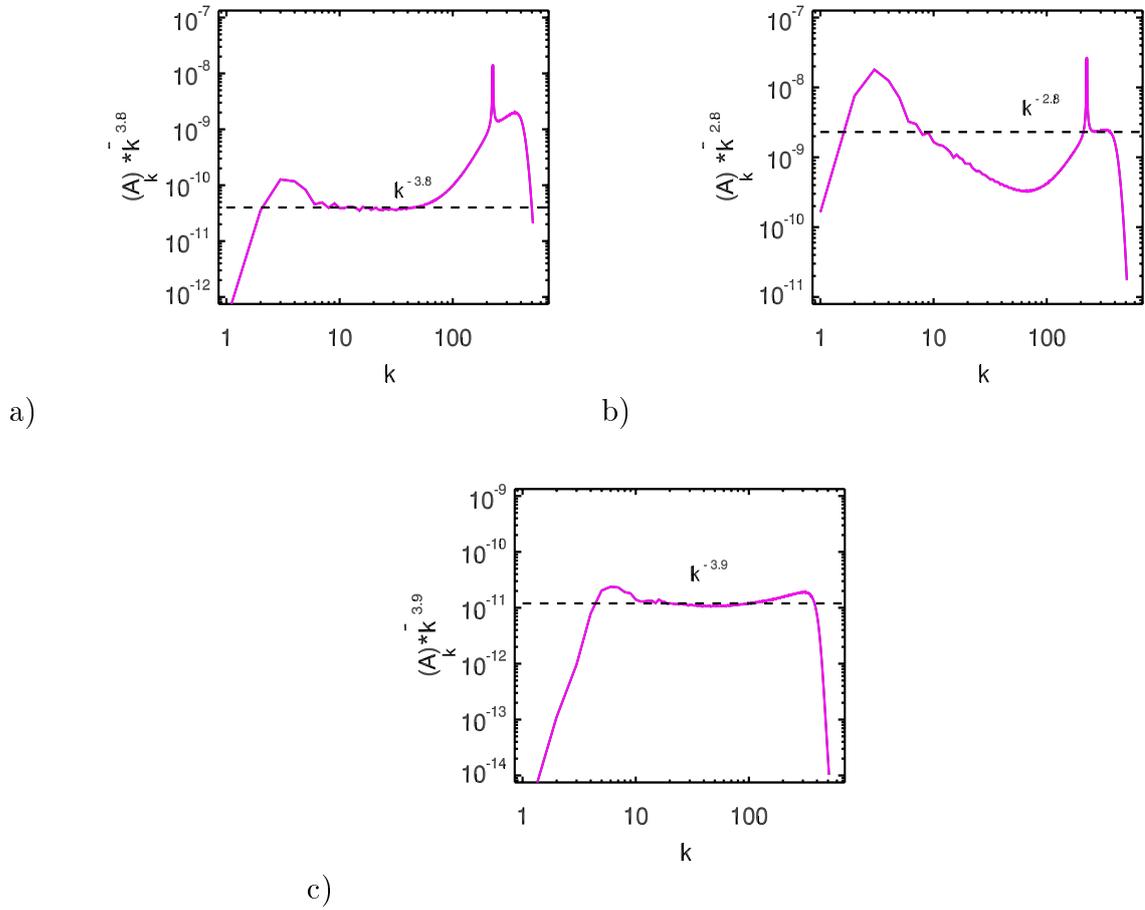
Figure C.4: Compensated magnetic vector potential spectra in a 1024^3 simulation. a) low k approximate scaling range for forced case b) high k approximate scaling range for forced case and c) approximate scaling range for decay case.

C.5 $j^2 Spectra$

Current defined by $\mathbf{j} = \nabla \times \mathbf{b}$, shows a power law spectrum, which is also for the first time reported here. The significance and physics of the power laws of current and magnetic vector potential are currently not well understood.

a)   b)

c)
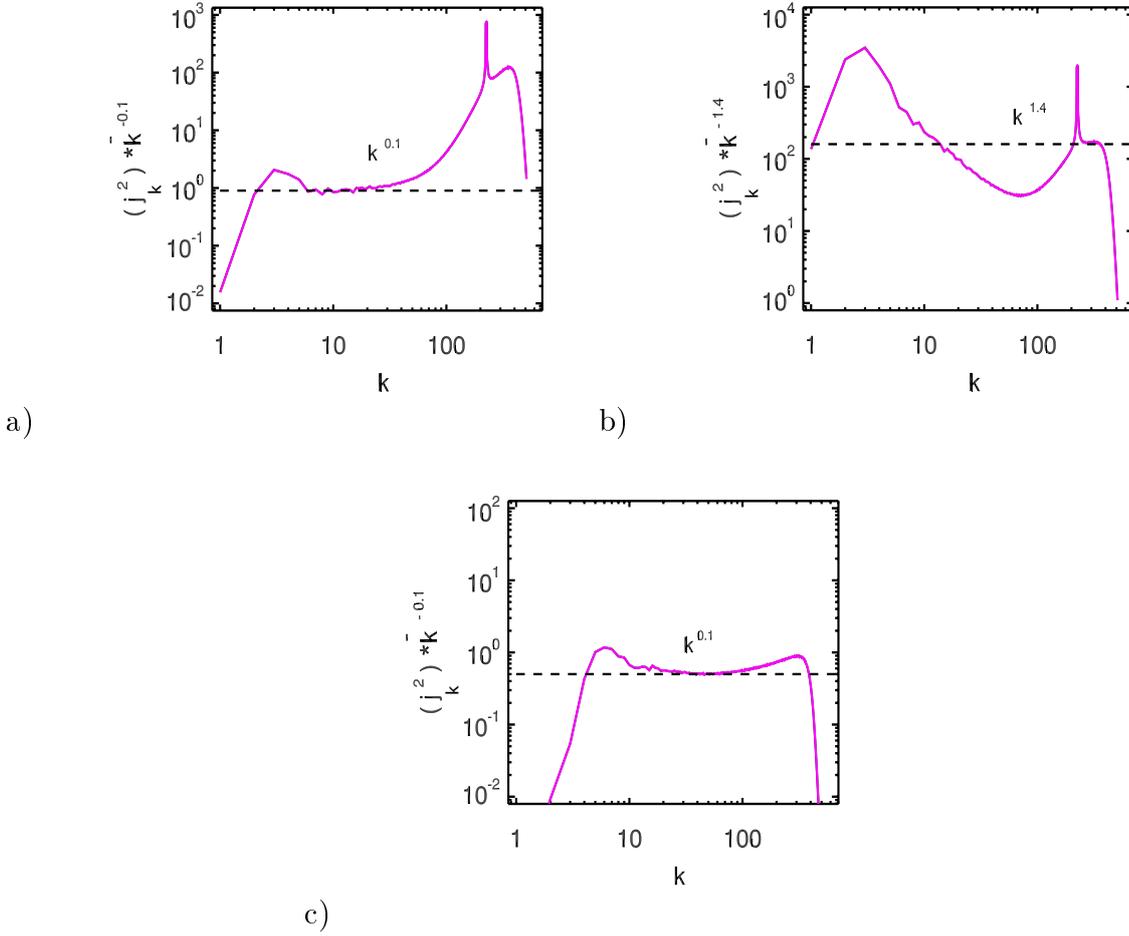
Figure C.5: Compensated j^2 spectra in a 1024^3 simulation. a) low k approximate scaling range for forced case b) high k approximate scaling range for forced case and c) approximate scaling range for decay case.

C.6 $\mathbf{E}_k^V/H_k^V$

This quantity is plotted to check the validity or otherwise of the relation $E_k^V/H_k^V \sim k$. It is discussed in section 4.5.1. The quantity plotted here is H_k^V/E_k^V which should behave as $\sim k^{-1}$.

a)   b)

c)
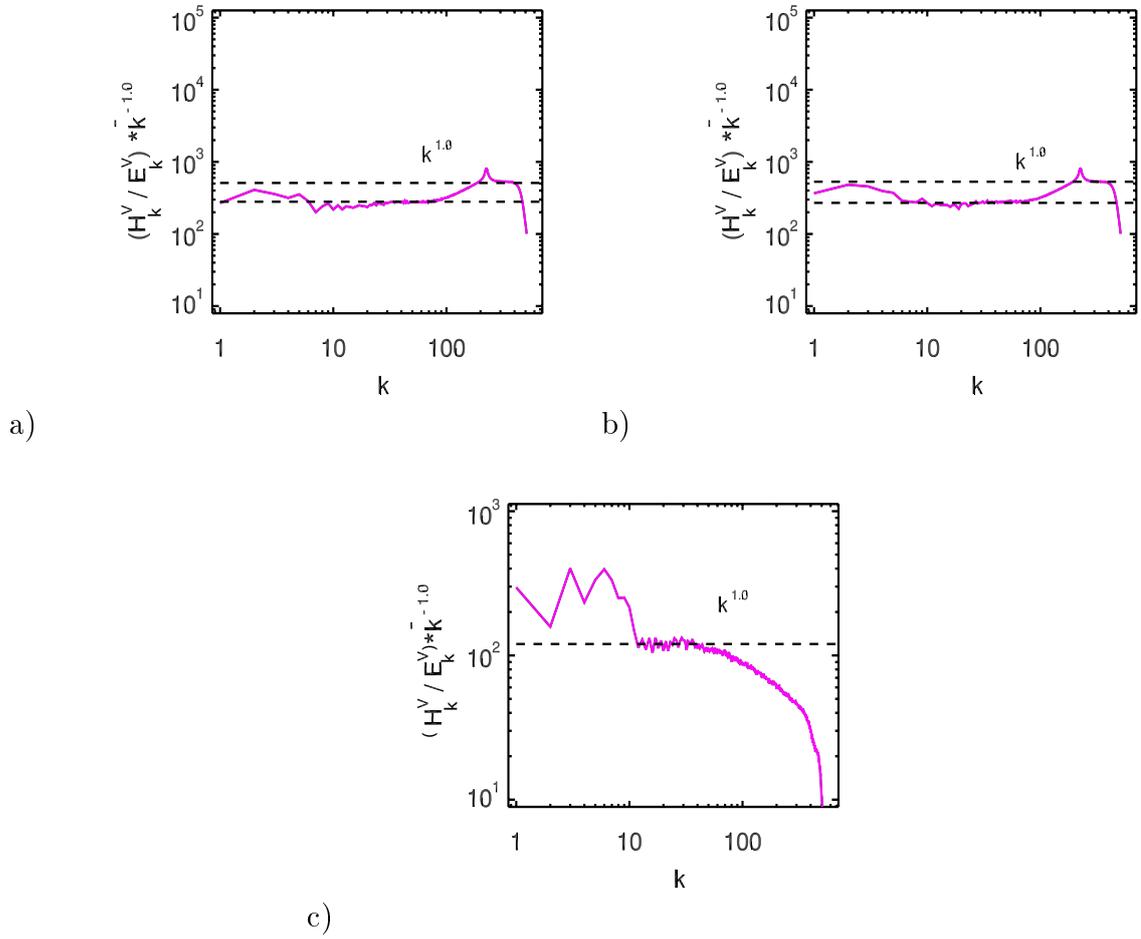
Figure C.6: Compensated E_k^V/H_k^V spectra in a 1024^3 simulation. a) $k^{-1.0}$ power law valid in both the approximate scaling ranges for magnetic helicity injection b) $k^{-1.0}$ power law valid in both the approximate scaling ranges for magnetic helicity and kinetic helicity injection and c) $k^{-1.0}$ approximate scaling range for the decay case.

C.7 E_k^M/H_k^M

This quantity is plotted for checking the validity of the relation $E_k^M = kH_k^M$. This relation does not comply at all with the spectral relations as is observed from figures below and text in section 4.5.1.

a)   b)

c)
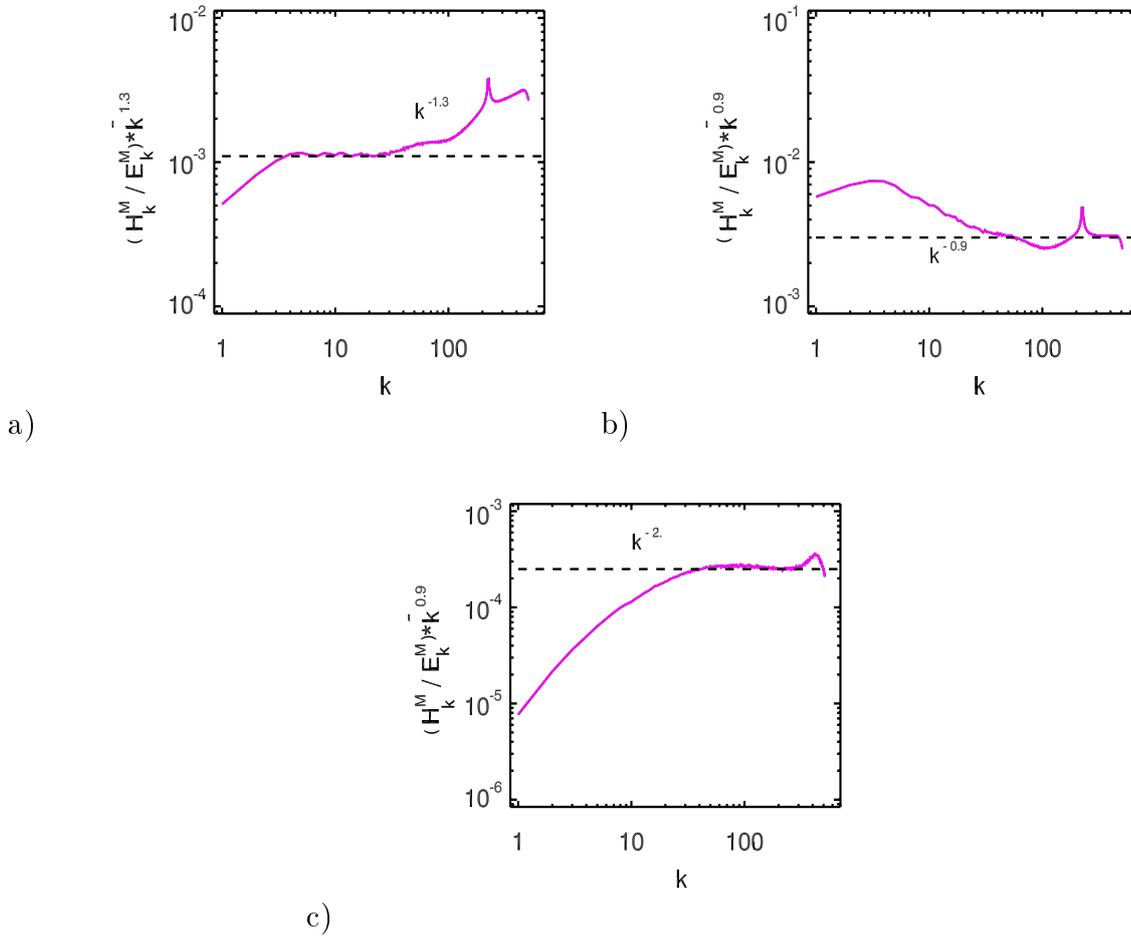
Figure C.7: Compensated E_k^M / H_k^M spectra in a 1024^3 simulation. a) $k^{-1.3}$ power law valid for the first approximate scaling range in the magnetic helicity injection case b) $k^{-0.9}$ power law valid for the second approximate scaling range in the magnetic helicity injection and c) $k^{-2.0}$ approximate scaling range for the decay case. Note that the kinetic helicity injection case also follows the same plots as a and b shown here. Hence they are not plotted separately.

Bibliography

[1] D. Biskamp. Magnetohydrodynamic turbulence. *Cambridge University Press*, (2001).

[2] Z.-S. She, S. Chen, G. Doolen, R.H. Kraichnan, and S.A. Orszag. Reynolds number dependence of isotropic Navier-Stokes turbulence. *Phys.Rev.Lett.*, 70(21):3251, (1993).

[3] H.K. Moffatt. The degree of knottedness of tangled vortex lines. *J. Fluid Mech.*, 35(1):117, (1969).

[4] S. Ortolani. Reversed field pinch confinement physics. *Plasma Physics and Controlled Fusion*, 31(10):1665, (1989).

[5] U. Frisch, A. Pouquet, J. Léorat, and A. Mazure. Possibility of an inverse cascade of magnetic helicity in magnetohydrodynamic turbulence. *J. Fluid Mech.*, 68(4):769, (1975).

[6] R.H. Kraichnan. Inertial ranges in two-dimensional turbulence. *Phys. Fluids*, 10(7):1417, (1967).

[7] A. Pouquet, U. Frisch, and Léorat. Strong MHD helical turbulence and the nonlinear dynamo effect. *J. Fluid Mech.*, 77(2):321, (1976).

[8] A. Brandenburg. The inverse cascade and nonlinear alpha-effect in simulations of isotropic helical hydromagnetic turbulence. *Astrophys. J.*, 550:824, (2001).

[9] P.D. Mininni, D.C. Montgomery, and A.G. Pouquet. Numerical solutions of the three-dimensional magnetohydrodynamic alpha-model. *Phys.Rev.E*, 71:046304, (2005).

[10] A. Alexakis, P. Mininni, and A. Pouquet. On the inverse cascade of magnetic helicity. *Astrophys. J*, 640:335, (2006).

[11] A. Brandenburg, W. Dobler, and K. Subramanian. Magnetic helicity in stellar dynamos:new numerical experiments. *Astron.Nachr./AN*, 323(2):99, (2002).

[12] W.-C. Müller and D. Biskamp. Scaling properties of three-dimensional mag-netohydrodynamic turbulence. *Phys.Rev.Lett*, 84(3):475, (2000).

[13] D. Biskamp and W.-C. Müller. Scaling properties of three-dimensional isotropic magnetohydrodynamic turbulence. *Phys of Plasmas*, 7(12):4889, (2000).

[14] W.-C. Müller and R. Grappin. Spectral energy dynamics in magnetohydro-dynamic turbulence. *Phys.Rev.Lett.*, 95:114502, (2005).

[15] M. Lesieur. Turbulence in fluids. *Springer*, (2008).

[16] M. Goossens. An introduction to plasma astrophysics and magnetohydrody-namics. *Kluwer Academic Publishers*, (2003).

[17] D. Škandera. Statistical properties and structure of turbulent convection. *PhD thesis, Fakultät für Physik, Technischen Universität München*, (2007).

[18] W.-C. Müller. Magnetohydrodynamic turbulence. *Lecture Notes in Physics 756, Hillebrandt,W. and Kupka,F. (eds.)*, Springer, (2009).

[19] D.J. Tritton. Physical fluid dynamics. *Clarendon Press, Oxford*, (1998).

[20] W.-C. Müller. Makroskopische und statistische Eigenschaften dreidimension-aler magnetohydrodynamischer Turbulenz. *IPP-Report, Max-Planck-Institut für Plasmaphysik*, IPP 5/90, (2000).

[21] U. Frisch, M. Lesieur, and A. Brissaud. A markovian random coupling model for turbulence. *J. Fluid Mech.*, 65(1):145, (1974).

[22] M.A. Uddin, N. Taniguchi, M. Tanahashi, T. Miyauchi, and T. Kobayashi. GS and SGS coherent structures in homogeneous isotropic turbulence. *Suchi Ryutai Rikigaku Shinpojiumu Koen Ronbunshu*, 15:70, (2006).

[23] S. Oughton and R. Prandi. Kinetic helicity and MHD turbulence. *J.Plasma Physics*, 64(2):179, (2000).

[24] A.F. Rañada. On the magnetic helicity. *Eur.J.Phys.*, 13:70, (1992).

[25] M.A. Berger. Introduction to magnetic helicity. *Plasma Phys.Control.Fusion*, 41:B167, (1999).

[26] T. Forbes. Magnetic reconnection MHD theory and applications. *Cambridge University Press*, (2000).

[27] P. Démoulin. Recent theoretical and observational developments in magnetic helicity studies. *Advances in Space Research*, 39:1674, (2007).

[28] A.A. Pevtsov. What helicity can tell us about solar magnetic fields. *J.Astrophys.Astr*, 29:49, (2008).

[29] A.H. Boozer. Magnetic helicity and dynamos. *Phys. Fluids B*, 5(7):2271, (1993).

[30] A. Brandenburg. Importance of magnetic helicity in dynamos. *Importance of magnetic helicity in dynamos,Lect.Notes Phys.*, 664:219, (2005).

[31] A. Brandenburg and K. Subramanian. Astrophysical magnetic fields and nonlinear dynamo theory. *Physics Reports*, 417:1, (2005).

[32] P. Frick and D. Sokoloff. Cascade and dynamo action in a shell model of magnetohydrodynamic turbulence. *Phys.Rev.E*, 57(4):4155, (1998).

[33] A. Brandenburg. Computational aspects of astrophysical MHD and turbulence. *Advances in nonlinear dynamos (The Fluid Mechanics of Astrophysics and Geophysics) eds. A.Ferriz-Mas and M.Nunez, Taylor & Francis, London and New York*, 9:269, (2003).

[34] M.Y. Hussaini and T.A. Zang. Spectral methods in fluid dynamics. *Ann.Rev.Fluid Mech.*, 19:339, (1987).

[35] M. Thiele. Struktur und statistische Eigenschaften hydrodynamischer und magnetohydrodynamischer Turbulenz unter Rotation. *Diploma Thesis,Theoretische Physik II, Universität Bayreuth*, (2005).

[36] D.O. Go'mez, P.D. Mininni, and P. Dmitruk. Parallel simulations in turbulent MHD. *Physica Scripta*, T116:123, (2005).

[37] G. Boffetta. Energy and enstrophy fluxes in the double cascade of two-dimensional turbulence. *J. Fluid Mech.*, 589:253, (2007).

[38] M. Chertkov, C. Connaughton, I. Kolokolov, and V. Lebedev. Dynamics of energy condensation in two-dimensional turbulence. *Phys. Rev. Lett.*, 99:084501, (2007).

[39] T. Nishimura and M. Matsumoto. http://www.math.keio.ac.jp/matumoto/emt.html. (2002).

[40] N.L. Haugen. Energy spectra and scaling relations in numerical turbulence with laboratory and astrophysical applications. *PhD thesis,Faculty of Natural Sciences and Technology, Department of Physics,Norwegian University of Science and Technology*, (2004).

[41] V. Borue and S.A. Orszag. Forced three-dimensional homogeneous turbulence with hyperviscosity. *Europhys.Lett.*, 29(9):687, (1995).

[42] A.A. Schekochihin, N.E.L. Haugen, A. Brandenburg, S.C. Cowley, J.L. Maron, and J.C. Mcwilliams. The onset of a small-scale turbulent dynamo at low magnetic Prandtl numbers. *Astrophys. J.*, 625:L115, (2005).

[43] http://www.mpi-forum.org/docs/mpi-20-html/mpi2-report.html.

[44] A. Tsinober. An informal introduction to turbulence. *Kluwer Academic Publishers*, (2001).

[45] S. Chen, R.E. Ecke, G.L. Eyink, X. Wang, and Z. Xiao. Physical mechanism of the two-dimensional enstrophy cascade. *Phys. Rev. Lett.*, 91(21):214501, (2003).

[46] S. Chen, R.E. Ecke, G.L. Eyink, M. Rivera, M. Wan, and Z. Xiao. Physical mechanism of the two-dimensional inverse energy cascade. *Phys. Rev. Lett.*, 96:084502, (2006).

[47] P. Sagaut, S. Deck, and M. Terracol. Multiscale and multiresolution approaches in turbulence. *Imperial College Press*, (2006).

[48] U. Frisch. Turbulence:the legacy of A.N.Kolmogorov. *Cambridge University Press*, (1995).

[49] A. Brandenburg. Numerical simulations of turbulent dynamos. *The origins of galactic magnetic fields,Moss,D. and Beck,R. and Shukurov,A. (eds.)*, ASP conference series vol.JD14, (2000).

[50] P. Goldreich and S. Sridhar. Toward a theory of interstellar turbulence II. strong Alfvénic turbulence. *Astrophys. J.*, 438:763, (1995).

[51] S. Sridhar and P. Goldreich. Toward a theory of interstellar turbulence. I. weak Alfvénic turbulence. *Astrophys. J.*, 432:612, (1994).

[52] W.-C. Müller, D. Biskamp, and R. Grappin. Statistical anisotropy of magnetohydrodynamic turbulence. *Phys.Rev.E*, 67:066302, (2003).

[53] S. Boldyrev. On the spectrum of magnetohydrodynamic turbulence. *Astrophys. J.*, 626:L37, (2005).

[54] G. Gogoberidze. On the nature of incompressible magnetohydrodynamic turbulence. *Phys.Plasmas*, 14:022304, (2007).

[55] R.H. Kraichnan. Inertial-range spectrum of hydromagnetic turbulence. *Phys. Fluids*, 8:1385, (1965).

[56] R. Grappin, U. Frisch, J. Léorat, and A. Pouquet. Alfvénic fluctuations as asymptotic states of MHD turbulence. *A&A*, 105:6, (1982).

[57] R. Grappin, J. Léorat, and A. Pouquet. Dependence of MHD turbulence spectra on the velocity field-magnetic field correlation. *A&A*, 126:51, (1983).

[58] W.-C. Müller and R. Grappin. Nonlinear cascades and spatial structure of magnetohydrodynamic turbulence. *Theory of relaxation processes in magnetised plasmas-from astrophysics to fusion devices,Sarazin,Y. and Ghendrih,Ph, and Garbet,X. and Diamond,P.(eds.)*, IOP publishing, in press, (2005).

[59] P.D. Mininni, A.G. Pouquet, and D.C. Montgomery. Small scale structures in three-dimensional magnetohydrodynamic turbulence. *Phys.Rev.Lett.*, 97:244503, (2006).

[60] N.E.L. Haugen and A. Brandenburg. Inertial range scaling in numerical turbulence with hyperviscosity. *Phys.Rev.E*, 70:026405, (2004).

[61] A. Brandenburg and G.R. Sarson. Effect of hyperdiffusivity on turbulent dynamos with helicity. *Phys. Rev.Lett.*, 88(5):055003, (2002).

[62] V. Borue and S.A. Orszag. Self-similar decay of three-dimensional homogeneous turbulence with hyperviscosity. *Phys.Rev.E.*, 51(2):R856, (1995).

[63] M.K. Verma and D. Donzis. Energy transfer and bottleneck effect in turbulence. *J.Phys.A:Math.Theor.*, 40:4401, (2007).

[64] M.K. Verma, D.A. Roberts, M.L. Goldstein, S. Gosh, and W.T. Stribling. A numerical study of the nonlinear cascade of energy in magnetohydrodynamic turbulence. *J. Geophys. Res.*, 101(A10):21619, (1996).

[65] W. Dobler, N.E. Haugen, T.A. Yousef, and A. Brandenburg. The bottleneck effect in three-dimensional turbulence simulations. *Phys.Rev.E*, 68:026304, (2003).

[66] U. Frisch, S. Kurien, R. Pandit, W. Pauls, S.S. Ray, and J.-Z. Wirth, A.and Zhu. Hyperviscosity, galerkin truncation and bottlenecks in turbulence. *Phys. Rev. Lett.*, 101:144501, (2008).

[67] J.P. Graham, P.D. Mininni, and A. Pouquet. The Lagrangian-averaged model for magnetohydrodynamics turbulence and the absence of bottleneck. *arxiv:0806.2054v2[physics.plasm-ph]*, (2008).

[68] C.V. Tran and J.C. Bowman. Robustness of the inverse cascade in two-dimensional turbulence. *Phys.Rev.E*, 69:036303, (2004).

[69] M. Christensson, M. Hindmarsh, and A. Brandenburg. Inverse cascade in decaying three-dimensional magnetohydrodynamic turbulence. *Phys.Rev.E*, 64:056405, (2001).

[70] H.K. Moffatt. *Magnetic field generation in electrically conducting fluids*, Cambridge University Press, 1978.

[71] H. Homann. Lagrangian statistics of turbulent flows in fluids and plasmas. *PhD thesis,Fakultät für Physik und Astronomie, Ruhr-Universistät Bochum*, (2006).

[72] Q. Chen, S. Chen, and G.L. Eyink. The joint cascade of energy and helicity in three-dimensional turbulence. *Phys. Fluids*, 15(2):361, (2003).

Acknowledgments

This work would not have been possible without the support of my thesis supervisor, Priv.-Doz. Dr. Wolf-Christian Müller. I thank him from the bottom of my heart, for giving me an opportunity to work in his group at the Max-Planck-Institut für Plasmaphysik (IPP), Garching, Germany. I also thank him for being so patient with my numerous doubts and mistakes. His easy availability whenever a student needs him and the easy and comforting manner he treats his students, makes working with him a pleasant experience. I must also thank Max-Planck society and specially IPP for having started the 'Independent Junior Research Groups', under which,my supervisor could give opportunities to students like me. Dr. Angela Busse, my colleague, was of great help in every stage of my thesis and I remain thankful to her, for all the co-operation, compassion and sympathy (mainly on my language barrier) she had shown. I benefited a lot because of the discussions I had with her on subject matters and also on German way of life from the non-subject discussions. I am also thankful to Dr. Dan Škandera who was my senior, whose Ph.D thesis has helped in several ways while writing this thesis. I am thankful to Mr. Christian Vogel, my junior, for his help on issues like manuscript reading towards the end of my thesis and other subject and non-subject matters. I also wish to thank all other members of my group for their understanding and support.

I felt very fortunate to receive few but subtle comments from Prof. Dr. D.Biskamp, in the final stages of this thesis, which helped me enormously in improving the text. His book 'Magnetohydrodynamic Turbulence' was almost the Bible which I looked up to for clearing any conceptual doubt. I wish to thank him both for his comments on this work and also for the book, which I referred to in this work countless times.

I wish to thank the super computing team at the RZG, especially Dr. Mrs. In-